ARGON LASER OXIDATION OF SILICON

Francesca Micheli
Thesis submitted for the degree of Ph.D,
University of London

March 1990

ProQuest Number: 10797758

All rights reserved

INFORMATION TO ALL USERS
The quality of this reproduction is dependent upon the quality of the copy submitted.

In the unlikely event that the author did not send a complete manuscript
and there are missing pages, these will be noted. Also, if material had to be removed,
a note will indicate the deletion.

ProQuest 10797758

Published by ProQuest LLC (2018). Copyright of the Dissertation is held by the Author.

All rights reserved.
This work is protected against unauthorized copying under Title 17, United States Code
Microform Edition © ProQuest LLC.

ProQuest LLC.
789 East Eisenhower Parkway
P.O. Box 1346
Ann Arbor, MI 48106 – 1346

ABSTRACT

The growth of high quality silicon dioxide layers of thicknesses between a few 10's and a few 100's Å is a fundamental step in the development of present and future VLSI technology. The use of optical radiation allows very fast heating times compared to a classical quartz furnace and is therefore well suited to the formation of very thin layers.

Our investigation aimed at isolating and quantifying a possible photonic enhancement to the mainly thermal oxidation process, as was suggested in recent years. This could mean lower fabrication temperatures and, therefore, reduced unwanted side effects. Furthermore, laser processing gives the opportunity of very fine scale pattern production either by direct writing or projection imaging.

C-Si samples of various orientations and doping levels were oxidized in dry oxygen with an Argon laser as the sole source of energy.

By exploiting the thin film interference effect, we succeeded in amplifying small differences in the growth rates induced by the two strongest laser spectral lines and arising by non-thermal effects, thereby confirming the existence of a photonic effect related to incident photon flux.

To further improve our technique and measurement facilities, we devised an in-situ, non-invasive, computer controlled monitor capable of measuring oxide thickness and temperature on the irradiated sample.

An estimate of the absolute value of this photonic component to the reaction was provided by experiments with double-side polished silicon, which acted as a sort of 'filter' for this non-thermal effect. An empirical mathematical model was obtained for the photonic component of the growth rate. Oxidation of heavily doped samples gave further backing to suggested scenarios of photoexcited carriers induced effects.

Our results were finally discussed in the light of the vast amount of literature available in the field of silicon oxidation.

TABLE OF CONTENTS

Abstract 2

Acknowledgements 5

Introduction 6

Chapter I, Brief Review of Thermal Oxidation of Silicon 12

I.1 Introduction 12
I.2 Deal and Grove model 12
I.3 Oxidant transport studies 15
I.4 Parallel oxidation 16
I.5 Oxygen dissociation 17
I.6 Space-charge and field-related effects 18
I.7 Stress, stress relaxation and viscous flow 25
I.8 Reaction layer 28
I.9 Summary and modelling 29

Chapter II, Experimental Apparatus and Procedures 31

II.1 Introduction 31
II.2 Experimental apparatus 31
II.3 Experimental procedure 33
II.4 Reflectometer 34
II.4.1 Principle of operation 36
II.4.2 Instrument background 39
II.5 Hardware description 44
II.5.1 Introduction 44
II.5.2 System requirements and accuracy considerations 45
II.5.3 Photoreceiver 46
II.5.4 Synchronous demodulator 48
II.5.5 Switched integrator module 48
II.5.6 A/D conversion 52
II.5.7 Global performance tests 53

Chapter III, Thermal Modelling and Oxidation Results 54
III.1 Introduction 54
III.2 Modelling of silicon temperature 54

III.3 Initial experiment 58
III.4 Experimental work 62
III.4.1 Lightly boron doped <100> Si 62
III.4.2 Double-side polished Si 65
III.4.3 Pre-oxidized substrate 70
III.4.4 Lightly phosphorus doped <111> Si 70
III.4.5 Heavily doped Si 72
III.4.6 Low temperature oxidations 75
III.5 SiO_2 films characterization 79
III.5.1 Infrared characterization 79
III.5.2 Electrical characterization 85

Chapter IV, Computer Modelling and Discussion of Results 87
IV.1 Computer modelling of growth process 87
IV.1.1 514nm versus 488nm 87
IV.1.2 Photonic versus thermal growth 93
IV.1.3 Low temperature oxidation 99
IV.2 Comparative evaluation of experimental results in the light of previous laser oxidation experiments 101
IV.3 Oxygen interaction with electrons 111
IV.4 Discussion of laser enhancement mechanisms 117
IV.4.1 Electron tunnelling and thermoionic emission 117
IV.4.2 Photogenerated electrons 120
IV.4.3 Experimental verification 123
IV.4.4 Photonic enhancement and oxidation models 125
IV.4.5 Fixed positive charge and its effects on electronic and ionic fluxes 127
IV.4.6 Summary and comments on orientation dependence 132

Conclusions 135

Appendix I, SiO_2 bulk and interface properties 138

Appendix II, Photo-enhancement and electronic effects 147

References 154

List of publications 174

ACKNOWLEDGEMENTS

I would like to acknowledge receipt of a two year grant from SERC and a one year postgraduate studentship from IEE. I am also very grateful to Prof Ron Lawes of Rutherford Labs. for his support.

I would also like to thank Dr Robin Thompson of Hughes Microelectronics, Dr John Wilkes of Mullard, Dr Alison Hodge of RSRE, Prof E. Lightowlers of King's College (London) and Mr D. Pryor of Wacker Chemicals (UK) for the very generous supply of a variety of silicon wafers. I also wish to acknowledge the invaluable contribution of Chris Brown of GTM, Dr John Wilson of Heriot-Watt University and Dr Alison Hodge of RSRE for ellipsometric measurements of oxide thicknesses. I am especially grateful to Prof Mino Green of Imperial College for the use of the ellipsometer and to Drs Judith Milledge and Monica Mendelsshon of the Dept. of Geology at University College London for the use of the infrared spectrometer.

Many students and members of staff at UCL deserve my gratitude, if nothing else for patiently tolerating me for so long. First of all, my collegue Vishal Nayar (now at RSRE), whose constant support and unfailing encouragement have been essential to the actual completion of this, at times, daunting task (not to mention the endless technical discussions and a great help with the electrical characterization, for which I am also indebted to Parthiv Patel).

Tony Overbury has, at all times, kept a brave face to the vagaries of the Argon laser (though he looked a bit shaken when the tube exploded in front of him) and has been always of great help to me, while Mark Abbott has, with his helpful suggestions, prevented me (and many others) from resorting to violence towards the computer.

I am very grateful to the clean room staff for help and advice and to the mechanical workshop staff for succeeding in decoding my terrible drawings without complaints.

Finally, I would like to thank my supervisor, Dr Ian Boyd, for help, encouragement and challenge over these long years. As his first student, probably I haven't been the easiest one.

INTRODUCTION

Silicon dioxide is utilized throughout modern integrated circuit fabrication processes, as a mask, as surface passivation, to provide isolation between devices or multilayer metallization systems and, most important of all, as an essential active component in MOS structures. In fact, planar processing silicon technology owes its success to the properties of silicon dioxide.

The major reason behind the explosive growth of integrated circuit technology has been the constantly falling cost per function. This has resulted primarily from a phenomenal increase in the number of components per chip, forecast to reach the 100 million mark around the year 2000 (Fig 1), which has been achieved by simultaneously decreasing the feature size (Fig 1), increasing the die (and wafer) size and improving the packing efficiency. Smaller device dimensions are also required to decrease MOSFETs' intrinsic time delay (thereby increasing speed of operation). Another benefit of miniaturization is the reduction of power consumption.

This scaling down of device lateral dimensions has brought about a corresponding decrease in oxide thicknesses: high quality oxides with precisely controllable thicknesses in the region of a few 100's of Ångstroms are required and the trend is rapidly approaching the sub-100Å range for the next generation of gate dielectrics or tunnelling heterojunctions.

Traditionally device quality SiO_2 has been, and still is, grown in quartz tube furnaces at temperatures around 1000 °C and in dry oxygen. However, extended high temperature processing can generate dislocations and stacking faults in the silicon, hillock formation in metals such as Al, warping in large diameter wafers and change in previously formed dopant profiles (Fig 2), all of which lead to degradation in both yield and performance of VLSI devices. Furthermore, the standard furnace, with its long heating and cooling times, is not best suited for the fabrication of the thinnest layers.

Other methods for producing device quality silicon dioxide have

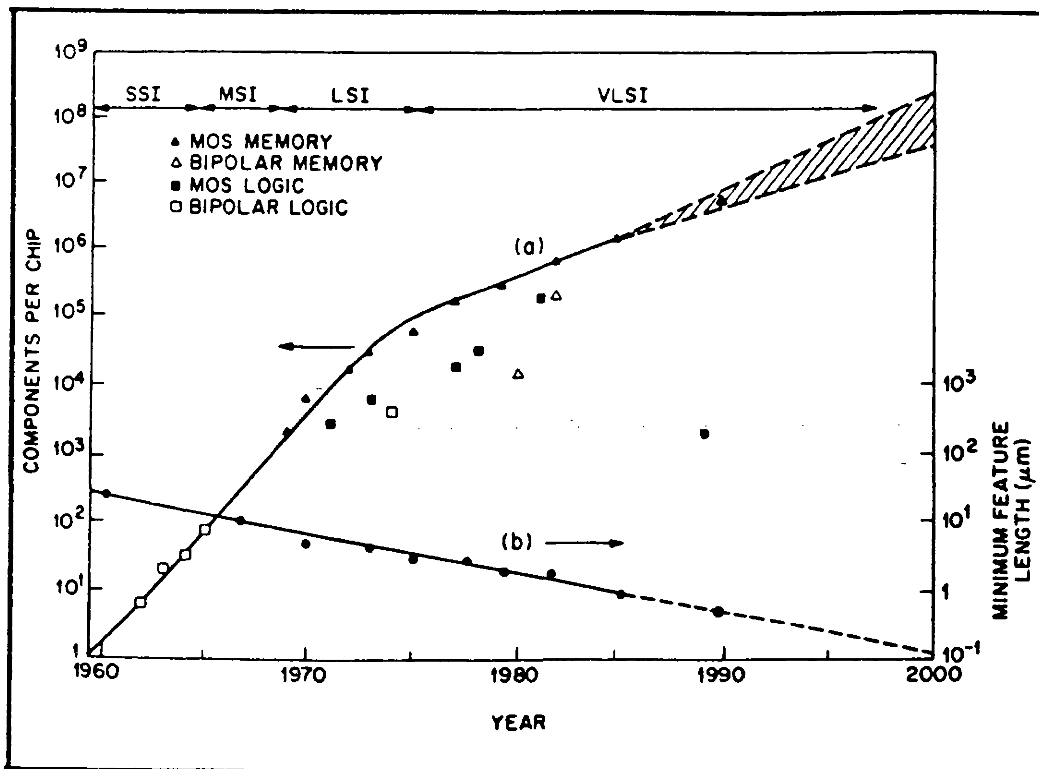

Fig 1: (a) Exponential growth of the number of components per IC chip. (b) Exponential decrease of the minimum device dimensions [SZE, 1988].

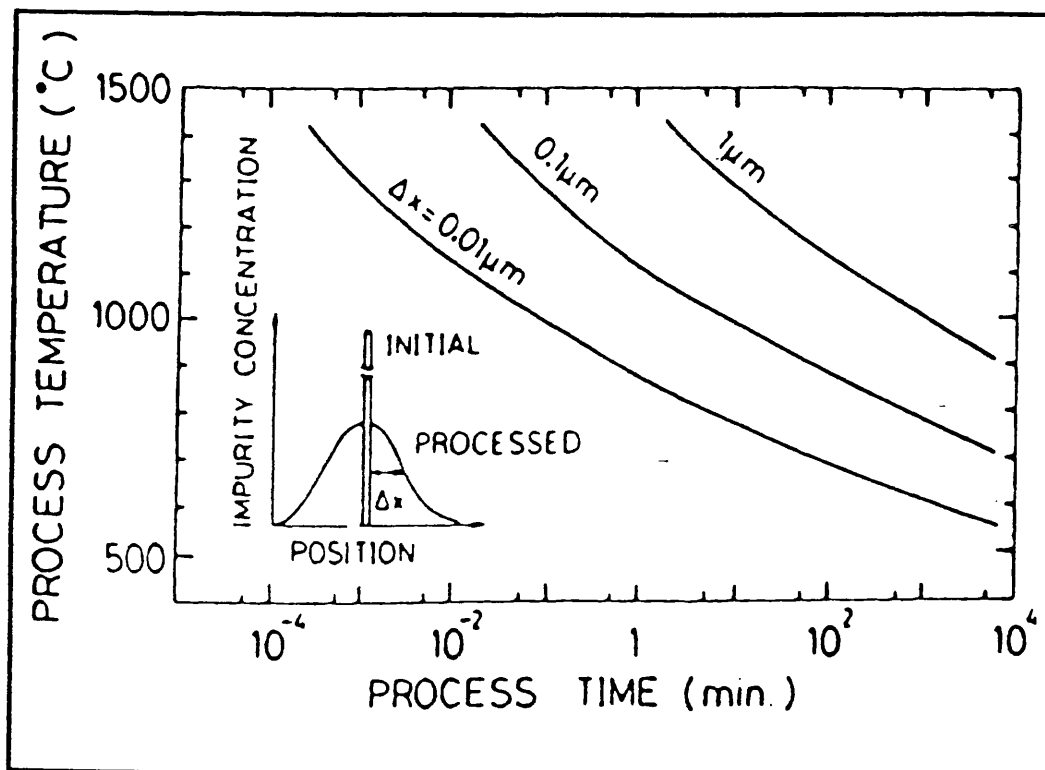

Fig 2: Broadening of impurity profiles in c-Si by thermal processing [HIROSE,1988].

been investigated in the last few years. Most of these aim to achieve the film quality of thermal oxides using low temperature fabrication processes. Alternatively, rapid thermal oxidation (RTO) techniques exploit the extremely high temperatures obtainable in silicon with optical radiation furnaces to limit the processing time to a few 10's or 100's of seconds (see, for instance, [SINGH, 1988; MOSLEHI, 1988]).

A large number of low temperature processes ($25\ ^{\circ}C \leq T \leq 700\ ^{\circ}C$) have been recently reported in the literature, such as various forms of plasma-enhanced [HERAK et al., 1989; LUCOVSKY et al., 1989] and photo-enhanced [SHIRAFUJI et al., 1988] chemical vapour deposition (CVD), plasma oxidation [KIMURA et al., 1988] and anodization [TAYLOR et al., 1988], oxidation in plasma afterglows [VINCKIER et al., 1987], sputter deposition [SUYAMA et al., 1987], electron beam enhanced oxidation [COLLOT et al., 1985], low [TODOROV et al., 1988] and very low [HECHT et al., 1989] energy ion beam oxidation, catalytic oxidation [OELLIG et al., 1987] and ozone-enhanced oxidation [RUZYLLO et al., 1987]. In most cases, however, the structural and, most crucially, the electrical properties achievable in dry thermal oxides have not been attained yet.

In 1971 Oren and Ghandhi [OREN et al., 1971] reported an enhancement in the silicon oxide growth rate when the sample was simultaneously subjected to classical thermal oxidation and UV incoherent radiation. Similar suggestions of a non thermal enhancement were later proposed by Schafer and Lyon [SCHAFER et al., 1981, 1982], Boyd [BOYD, 1983], Young and Tiller [YOUNG et al., 1983], Fiori [FIORI, 1984] and Orlowski and Richter [ORLOWSKI et al., 1984]. In all these studies CW or pulsed laser sources were used, in the visible or UV ranges. The introduction of tungsten halogen or arc lamps into the field of semiconductor processing has brought new (and often contrasting) evidence to the subject of photonic enhancement in silicon oxidation. Some authors have reported various degrees of enhancement in the growth rate with respect to standard thermal oxidation [HODGE et al., 1986; MOSLEHI et al., 1985; TUNG et al., 1986] and even mentioned the possibility of a photonic effect [PONPON et al., 1986].

The use of optical radiation allows very fast heating (and cooling) rates compared to a classical quartz furnace and is therefore well suited to the formation of very thin layers. Besides, the use of a

laser beam allows strict localization of the heat in all dimensions. The photonic enhancement reported was high enough to offer the prospect of considerably reducing the processing temperature whilst still obtaining high quality, repeatable, thin oxides in reasonably short times.

The catalyst of interest in this project was the considerable number of research studies addressing the various aspects of coherent and incoherent light processing of semiconductors in the fields of microelectronics and optoelectronics. The attractions of laser processing are manifold. Laser beams are localized and can, in theory, image to the ultimate optical resolution achievable (the diffraction limit). The directionality of laser beams means that they can be easily manoeuvred using present day control technology. As sources of intense monochromatic, yet occasionally tunable light, they provide unique, never previously achievable, processing conditions for novel production procedures. Since laser radiation can be coupled into matter in virtually any state, it also enables a wide variety of traditional and novel low-temperature chemical reactions to be investigated. The capabilities of laser processing are best appreciated in the 'direct writing' process (the production of patterned features directly on the substrate by very localized chemical reactions initiated by the focused laser beam), but projection imaging techniques are also extensively used for large area processing, especially utilizing excimer lasers.

A variety of physical mechanisms and chemical reactions (homogeneous and heterogeneous) are involved in laser assisted processing. There are broadly two main categories of operation, although often they both contribute to the reaction. In pyrolytic processes the main effect of the laser beam is thermal. In this case, the laser wavelength is chosen so that it is strongly absorbed by the substrate (initially through electronic excitation and finally converted into heat), but not by the surrounding atmosphere; any reactant molecules in the vicinity of the heated substrate decompose by collisional excitation with the surface and react with it.

In photolytic processes the wavelength must be appropriately chosen to be strongly absorbed by the reactant gas either in the surrounding environment or adsorbed onto the surface; excitation of these molecules occurs by a single (or multi-photon) process and photodissociation follows. The generated products react thence on the

surface.

Incoherent light sources and CW/pulsed lasers, with wavelengths ranging from the 157 nm of the F_2 laser to the 10 μm of the CO_2 laser have all found a variety of applications.

All the traditional steps required in the fabrication of integrated circuits have been successfully demonstrated with laser techniques, in addition to a variety of novel microfabrication processes in the fields of optics, optoelectronics and microwave technology [BOYD, 1987; MICHELI et al., 1986; BÄUERLE, 1988; HAIGH et al., 1988; and ref. therein].

In the last few years lasers have been used to initiate the formation of high temperature superconducting thin films by induced evaporation and the patterning of such films by induced structural or chemical transformations [BÄUERLE, 1989]. However, even less fashionable materials and processes have been attracting renewed research effort, such as **annealing** of semiconductors (the most recent studies have concentrated mainly on thin film transistors [MORITA et al., 1989], SOI technology and its application to 3D IC design [DASGUPTA et al., 1988]; excimer laser annealing of SiC has also been reported [CHOU et al., 1990]); **oxidation** of semiconductors and metals; silicon **nitradation**; general thin film deposition by **laser evaporation** (ranging from dielectrics to epitaxial compound semiconductors [SANKUR et al., 1988, 1989], polymers [HANSEN et al., 1988], magnetic films [OGALE et al., 1988, 1989]; and optical coating materials [GLUCK et al., 1989]); **deposition** (process optimization has been carried out for the deposition of a large variety of metals, dielectrics and semiconductors, while novel applications include photo-assisted epitaxial growth of II-VI and III-V semiconductors [IRVINE et al., 1987; SUDARSAN et al., 1989; KARAM et al.,1988], p-n junctions on GaAs [KARAM et al., 1988], deposition of amorphous superlattice structures [LOWNDES et al., 1988], silicone polymers [ALEXANDRESCU et al., 1988] and transparent and conducting films such as SnO_2 [KUNZ et al. 1989]; **doping** and **alloying** in silicon and compound semiconductors (junctions as shallow as ≈ 0.1 μm can now be obtained [SAMESHIMA et al., 1988]); **silicide formation** for interconnections; vapour-phase **synthesis** of ceramic powders [CASEY et al., 1987]; wet or dry **etching** of all commonly used metals, dielectrics, polymers and semiconductors (the most common recently being photolytic etching with excimer lasers; novel applications of laser etching include etching of ceramic materials

[EYETT et al., 1986; LU et al., 1988], silicate glasses [BRAREN et al., 1988] and bilayer etching of GaAs surfaces [MAKI et al., 1989]); **wafer bonding** [GEYSELAERS et al., 1989] and selective **via-hole filling** [MUKAI et al., 1987; SPIESS et al., 1989].

While from an engineering point of view these practical considerations justified the enterprise of studying the laser oxidation of silicon, from a physics point of view we were motivated by the curiosity of examining this simple though still ill-understood process from a different angle, in the hope of making a small contribution towards clarifying some of the many unanswered questions.

Chapter I is a synopsis of the present knowledge on dry thermal oxidation of silicon: starting with a classic phenomenological model dating back to 1965, the highlights of the last few decades of modelling efforts are briefly presented.

In Chapter II a description of the experimental apparatus and procedures adopted is presented. The need for an in-situ thickness and temperature monitor is explained and the reflectometer's principle of operation, hardware and software described.

Chapter III reports experimental data of oxide growth as a function of time for a variety of <111> and <100> c-Si samples, both lightly and heavily doped, single-side or double-side polished. While most oxidations were performed at temperatures > 780 °C, a few low temperature experiments are reported. A preliminary structural and electrical characterization of the laser oxides is also presented.

In Chapter IV we present the results of extensive computer modelling of the oxidation data and the empirical mathematical model for the photonic component of the growth rate which resulted from this study. Our results are compared with previously published work on laser oxidation of silicon and finally discussed in the light of the oxidation models presented in Chapter I.

Brief Review of Thermal Oxidation Of Silicon

I.1 Introduction

Thermally formed silicon dioxide has been used in the fabrication of silicon devices since the late 1950's. Following the pioneering work of Frosch and Derick [FROSCH et al., 1957], Atalla et al. [ATALLA et al., 1959] and Ligenza and Spitzer [LIGENZA et al, 1960], over thirty years of intense research on the subject have passed and yet many questions are still unanswered. In the following paragraphs we will describe the oxidation model which most has influenced the field in the last twenty five years, its limitations and a few of the principal (innumerable) suggestions aimed at answering these open questions. Our interest is mainly on the growth of thin oxides in dry oxygen environments, at atmospheric pressure and temperatures in the range 750 to 1100 °C.

I.2 Deal and Grove model

This phenomenological model was first proposed in 1963 [DEAL, 1963] and characterized in detail in 1965 [DEAL et al., 1965] and constitutes the backbone of most of the following work. It had been already established at the time that oxygen, not silicon, is the primary transported species during the oxidation process [ATALLA, 1960; LIGENZA et al., 1960; JORGENSEN, 1962; PLISKIN et al., 1964].

The model is based on the assumption that the thermal oxidation of silicon proceeds by (a) the adsorption of an oxidizing species at the outer surface of the growing oxide, (b) Fickian diffusion of that species through the oxide and, finally, (c) the reaction of the oxidizing species with the silicon at the Si/SiO_2 interface to form new SiO_2. It is also assumed that the oxidation process reaches steady state very rapidly and that, under this condition, the fluxes characterizing each stage (a) to (c) are equal. A schematic

representation of the oxidation process is shown in Fig I.1.

The mathematical expression for the whole process was found to be of a linear-parabolic form:

$$x^2 + Ax = B\,(t + \tau) \qquad (1.1)$$

where x is the oxide thickness at time t and

$$A = 2\,D\,(1/k + 1/h) \qquad (1.2)$$

$$B = 2\,D\,C^{*} / N \qquad (1.3)$$

$$\tau = (x_o{}^2 + Ax_o)/B \qquad (1.4)$$

with

D = diffusion coefficient of oxidizing species;

C^{*} = oxidant equilibrium concentration in the oxide;

N = number of oxidant molecules in a unit volume of oxide;

k = rate constant at Si/SiO_2 interface;

h = rate constant at outer oxide surface;

x_o = effective thickness at the start of an oxidation. A finite thickness is always required to fit the experimental data.

Two limiting cases of the oxidation process result in either a parabolic expression for thicker oxides ($x^2 = Bt$, the diffusion controlled regime), where B is the parabolic rate constant, or a linear expression for thinner oxides ($x = B/A\,(t + \tau)$, the interface reaction controlled regime), where B/A is the linear rate constant.

The linear and parabolic rate constants B and B/A can be represented by Arrhenius-type expressions of the form:

$$C \exp(-E/kT) \qquad (1.5)$$

where E is the activation energy, k Boltzman's constant, T the temperature and C a constant. For <111> Si, dry oxygen and a pressure of 760 torr, the activation energy for B was found to be 1.24 eV, close to the value of 1.17 eV for the diffusivity of oxygen in fused silica [NORTON, 1961] (no detailed data are available, as yet, on the oxygen diffusivity through thin, i.e. ≤ a few 100's of Ångstroms, thermally grown, oxide films), while an activation energy of 2 eV was measured for B/A, similar to the energy required to break a Si-Si bond (1.83 eV [PITZER, 1948]).

The model was found to be in good agreement with a large number of experimental data for both dry and wet oxidations, the main exception being for dry oxides thinner than approximately 300Å, where an anomalously high growth rate was noticed with respect to the model (and accounted for by the parameter τ). At the time, most oxides used in IC applications were above ≈ 1000 Å and this didn't provoke much concern. In the years that followed, though, as interest shifted towards ever thinner oxides, a great deal of research effort tried to explain this 'fast' initial growth rate (and its dependence on Si orientation, contrary to the model expectations at small thicknesses).

Another anomalous trait (with respect to the linear-parabolic expression) was shown by the pressure dependence of the linear rate constant B/A, which should have been a direct proportionality, as was for the parabolic rate constant B. But further experimental investigations showed that the linear rate constant for dry O_2 has a sub-linear dependence on oxygen partial pressure, not explainable in the context of Deal and Grove phenomenological model [van der MEULEN, 1972; LIE et al., 1982].

Still another departure of the oxidation kinetics from the linear parabolic model is provided by the presence of a break (at ≈ 900-1000 °C) in the Arrhenius plot of the parabolic rate constant, both in dry oxygen and steam environments [RAZOUK et al., 1981; DEAL, 1978; IRENE et al, 1978; IRENE, 1982] and of a similar, though considerably reduced, effect in the linear rate constant [IRENE et al., 1978].

These were the main initial discrepancies which prompted a large numbers of studies that soon expanded to a variety of related issues which included the diffusion mechanisms of the oxidant, the type of diffusing oxidant, effects of the type and level of doping, pre-oxidation cleaning effects, the influence of ambient additions, oxide network and interface structural effects and optical, electrical and radiation excitation.

In the light of the most recent developments, we will briefly present some of the principal milestones of these last 25 years of intense research on silicon oxidation.

I.3 Oxidant transport studies

Doremus [DOREMUS, 1976] modelled the diffusion process as resulting from interstitial diffusion of neutral molecular oxygen through the amorphous silica layer. This was later supported by radioactive tracer experiments [ROSENCHER et al., 1979] on SiO_2 layers of thicknesses ranging between ≈ 150 and 3000Å. By performing successive oxidations in $^{16}O_2$ and $^{18}O_2$ and examining the final profiles, they confirmed that oxygen is mostly transported interstitially across the oxide with little or no exchange with the pre-existing network, in contrast to steam oxidation, where a large exchange rate dominates the water diffusion (the difference is so striking that has prompted suggestions that anomalies in the dry oxidation kinetics could be explained by water-enhanced oxygen transport [WOLTERS et al., 1987]). The fixing of the heavy isotope at the internal silicon/oxide interface was interpreted as the motion of $^{18}O_2$ molecules oxidizing silicon at, or near, this interface. Further similar studies soon confirmed these early findings [CRISTY et al., 1981; PFEFFER et al., 1981; MIKKELSEN et al., 1980], opening the way to a considerable amount of research with higher and higher resolution radioactive tracers techniques, which are proving very important in the effort of unravelling the oxidant transport process(es) in ever thinner oxide films [COSTELLO et al., 1984; ROCHET et al.,1984; 1986; 1987; TRIMAILLE et al., 1989; HAN et al., 1985; 1987; 1988; CAWLEY et al., 1987; and references therein].

Most of the experimental results are in good agreement and the different techniques used and environmental conditions (especially water content) could easily account for any minor discrepancy. The evaluation of the results, though, is still very much at the ' tentative suggestion' stage. While the pile-up of heavy isotope at the Si/SiO_2 interface is in agreement with Deal and Grove model, a few percent of all the ^{18}O fixed by the second oxidation was repeatably found near the external gas/oxide interface (for oxides ≥ ≈ 200Å), clearly showing signs of exchange with the network. This percent varied considerably with oxidation temperature, oxygen pressure and especially oxide thickness. In the limiting case of ultra-dry oxides grown at low pressure and fairly high temperature up to thicknesses of ≈ 60Å, almost all the heavy isotope was found fixed near the external surface. In this regime clearly the transport of

oxygen molecules as interstitials is no longer the dominant process and movement of network oxygen has been suggested [ROCHET et al., 1986; MOTT et al., 1989].

The proposed mechanisms invoked to explain the external surface concentration of ^{18}O involve oxidant transport via diffusion of silica network defects as oxygen vacancies, peroxy defects (equivalent to an interstitial oxygen) or valence alternation pairs (see Appendix I for details), with atomic oxygen diffusion as a less likely possibility. Isotopic exchange between the $^{18}O_2$ gas molecules and the ^{16}O atoms in the oxide, followed by diffusion of network atoms by an interstitial defect mechanism involving O_2 molecules was suggested by Revesz et al. [REVESZ et al., 1987].

I.4 Parallel oxidation

Han and Helms [HAN et al., 1987; 1988] proposed a parallel oxidation mechanism with O_2 diffusion to the interface and oxygen vacancy diffusion to the surface. A mathematical model, an extension of Deal and Grove model, was proposed and tested. This formulation fits experimental data from thick films down to native oxide levels, thus seemingly eliminating the x_o problem previously mentioned. Unfortunately, this model fails to provide for less than first power O_2 pressure dependence and a modified version has been recently proposed by Helms and de Larios [HELMS et al., 1989]. According to this new model, O_2 dissociates at the interface into atomic oxygen and reacts with Si, thereby creating oxygen deficient defects which then diffuse to the surface and react with adsorbed O_2.

The original idea of the oxidation of silicon occurring via two parallel mechanisms can be found in the work of Jorgensen [JORGENSEN, 1962] and Raleigh [RALEIGH, 1966] who suggested the importance of the diffusion of both ionic as well as molecular species. Further suggestions involving ionic species are reported in par.I.6.

Ghez and van der Meulen [GHEZ et al., 1972] proposed a parallel mechanism involving one diffusing species (O_2) and two interfacial reactions with Si, one involving O_2 directly and the other involving O atoms (from O_2 dissociation at, or near, the interface). The model was devised in order to explain the origin of the sub-linear pressure

dependence of the linear growth rate B/A.

The addition of two exponentially decaying components to the oxide growth rate expression in D-G model (par.I.2) was found to fit very satisfactorily the growth data from the first few Ångstroms of native oxide [MASSOUD et al., 1985; 1987]. These two components, acting in parallel to the main mechanism (as described by the linear-parabolic model) during the initial stages of the oxidation, were described in terms of Si self-interstitials injected into the oxide and atomic oxygen (generated in the bulk SiO_2 or at the interfaces through O_2 dissociation) diffusing to the oxidizing interface.

A different type of parallel formulation can be found in the work of Irene [IRENE, 1978; 1983], Revesz et al.[REVESZ et al., 1986] and Samalam [SAMALAM, 1985]. They proposed parallel diffusion models for oxygen transport during oxidation which involve a single oxidant which can diffuse through two separate paths in the oxide. According to these models, one component of the oxygen flux reflects the usual diffusion of oxygen and is thickness dependent, while the other is thickness independent and is attributed to transport through 'structural channels' in the oxide. This followed an early suggestion by Revesz and Evans [REVESZ et al., 1969], while some direct evidence for the existence of ≈ 10Å 'micropores' or 'microvoids' (with a density of $\approx 10^{12}cm^{-3}$) has been provided by the high resolution TEM work of Gibson and Dong [GIBSON et al., 1980], later confirmed by Srivastava and Wagner [SRIVASTAVA et al., 1984] and, very recently, by Nielsen et al. [NIELSEN et al., 1989], who used a variable energy positron to study device quality thermal oxides.

It has meanwhile been argued [ORLOWSKI et al., 1988] that the existence of these micropores is more likely to enhance oxygen solubility rather than oxygen transport (though the description of solubility in terms of an equilibrium bulk quantity becomes questionable at oxide thicknesses smaller than the average spacing between the solute molecules, which is approximately 270Å for oxidation in dry oxygen).

I.5 Oxygen dissociation

The issue of a possible O_2 dissociation into atomic oxygen as a (perhaps necessary) intermediate step in the reaction of oxygen with

Si, first raised by Ghez and van der Meulen, was later taken up by numerous authors [BLANC, 1978; CRISTY et al., 1981; HU, 1983; 1984; MASSOUD et al., 1987; MOHARIR et al., 1989; HELMS et al., 1989], though not necessarily in the context of a parallel oxidation mechanism (though the aim was again to try to justify the experimental pressure dependence and/or the initial excess growth rate). Hu [HU, 1984] showed, from first-principles analysis, how an intermediate step of oxygen chemisorption (dissociative or not) on silicon can lead to a power-law pressure dependence of the linear rate constant; the power-law exponent was shown to vary with temperature in a way totally consistent with experimental observations. A similar approach was proposed by Moharir and co-workers, though they suggested that a weaker quasichemical bonding precedes the final oxidation reaction.

Irene and co-workers [IRENE et al., 1987], following the work of Hu [HU, 1983] and Young and Tiller [YOUNG et al., 1987] proposed that the dissociation of oxygen requires the thermionic emission of electrons from the silicon and provided some evidence that this could represent the rate limiting step in the initial stages of oxidation.

I.6 Space-charge and field-related effects

A debate has been going on for more than twenty years over whether silicon oxidation is controlled by the diffusion of charged or neutral species and, consequently, on the importance of electric fields within the oxide. As this will prove of considerable relevance to our work, we will review some of the more relevant results in more detail than we have done for other aspects of kinetics of silicon oxidation.

A study by Jorgensen [JORGENSEN, 1962] has been of great importance in the discussion over neutral versus charged oxidant species. He found that an applied electric field enhanced the oxidation rate when the Si was made positive with respect to the oxide/gas interface while it retarded it (or even stopped it) when the Si was made negative. Oxygen ions were suggested as the predominant diffusing

species. In particular, from the relationship between the experimental stopping voltage and the free energy of formation of the oxide, he concluded that O^{--} was the dominant ionic species [JORGENSEN, 1968].

But Raleigh [RALEIGH, 1966] showed that the effect of the applied potential, in Jorgensen's experiments, in accelerating or retarding SiO_2 thermal growth was due to an electrolytic cell process, brought about by the platinum electrode, superimposed on the normal thermal growth. It was, therefore, an artificial effect caused by the external circuit and, with no such circuit present, polarization fields would develop to inhibit ionic transport.

More recently, Modlin and Tiller [MODLIN et al., 1985] used a corona-discharge to study the effect of electric fields on silicon oxidation. They concluded that neutral molecular oxygen is very likely to be the diffusing species in the bulk (≥ 300Å) of the oxide but O (or even O^-) could possibly be produced in the vicinity of the Si/SiO_2 interface layer.

Studies on electrical conductivity of SiO_2 in the temperature range 0-700 °C [MILLS et al., 1973] concluded that the most likely species responsible for ionic conduction in these conditions was the interstitial O^{--}.

Recent measurements [SRIVASTAVA et al., 1985] of AC and DC SiO_2 conductivity between 25 and 1100 °C suggested that, above 450 °C, conduction takes place via charged oxygen species (as well as electrons, though $\sigma_{ion} > \sigma_{el}$, where σ is the conductivity). These ionic species are likely to be oxygen interstitials at higher oxygen pressures and oxygen vacancies at lower pressures.

In 1948 Cabrera and Mott [CABRERA et al. ,1948] put forward a model for the low temperature oxidation of metals. This theory, although modified and adjusted through the years by various authors, is still considered a reference point in Si oxidation under appropriate processing conditions. A review of the theory [Fehlner et al., 1970] envisaged the possibility that the anions (oxygen anions), rather than the (metal) cations, might move (we have seen that oxygen is the mobile species in silicon oxidation).

The first assumption made in the theory is that electrons can freely pass from the metal to ionize adsorbed oxygen atoms or molecules at the oxide/gas interface, so that the electrons' electrochemical potential (Fermi level) is equal in the metal and the adsorbed layer. The electrons could tunnel through films up to ≈ 30Å thick or could be excited by thermionic emission into the oxide conduction band (travel distances of up to a maximum of ≤ 300Å were suggested by Fromhold [FROMHOLD, 1976]). There is thus a uniform field in the film (zero space charge) created by a positive surface charge on the metal and a negative one from excess oxygen ions (either O_2^-, O^- or O^{--}) on the oxide/gas interface. It is this field that drives the slow ionic transport across the film to the oxide/metal interface.

When the ionic species is injected at the metal-oxide interface, the rate equation takes the form originally devised by Cabrera-Mott [ATKINSON, 1985; 1987] and known as the Cabrera-Mott (C-M) equation:

$$dx/dt = 2\Omega N\nu \exp(-W/kT) \sinh(qaV_s/2kTx) \qquad (1.6)$$

where N is a number of potentially mobile ions, Ω the oxide volume per ion, ν the vibrational frequency of atoms at the interface and 2a the ion hopping distance.

For very thin oxides (strong field and non-linear ionic conductivity), following the approach of Ghez [GHEZ 1973], the C-M equation can be expressed as:

$$dx/dt \approx a\nu \exp(-W/kT) \exp(qaV_s/2kTx) \qquad (1.7)$$

The potential difference V_s depends on the energetics of adsorption of oxygen onto the oxide surface, the details of which are still unknown. When the defects are injected at the oxide/gas interface the predicted kinetics are slightly different [ATKINSON, 1985, 1987]:

$$dx/dt = (5\epsilon V_s a\nu/qN_s x) \exp(-W/kT) \sinh(qaV_s/kTx) \qquad (1.8)$$

where N_s is the number of potential adsorption sites per unit area and ϵ the oxide dielectric constant. For thin films the growth rate can be approximated by:

$$dx/dt \; \alpha \; 1/x \; \exp(-W/kT) \exp(qaV_s/kTx) \qquad (1.9)$$

Integration leads to logarithmic-type kinetics in both cases.

For thick oxides (low field approximation, linear ionic conductivity) the expressions give parabolic and cubic growth kinetics, respectively.

Defects, such as charged non-bridging oxygens or charged silicon vacancies [MOTT, 1981, 1982, 1986] or oxygen vacancies [ATKINSON, 1987] are also possible candidates for the ionic species (see Appendix I for more on defects in SiO_2). In this model there is no need to suppose neutral and charged species in thermodynamical equilibrium; if electrons can get through the film, the charged defect is formed; if not, O_2 is the predominant mobile species [MOTT, 1982]. It may be remarked that in the C-M range no great sensitivity to crystal surface or doping level is expected [MOTT, 1981, 1982].

From extensive studies on low temperature oxidation, Fehlner [FEHLNER, 1984] concluded that, in oxygen at atmospheric pressure, the temperature of transition from ionic to molecular movement is ≈ 500 °C (low temperature is defined as the relative magnitude of thermal to electrostatic energy available to drive the reaction).

But Taft [TAFT, 1984] postulated that the C-M mechanism can be prevalent even at much higher temperatures (i.e. 821 °C in his experiments), though the charged oxygen species involved would rapidly diminish with film thickness (≈ 25Å at 821 °C, ≈ 50Å at 612 °C).

Kamigaki and Itoh [KAMIGAKI et al., 1977] found Cabrera-Mott type of oxidation kinetics for low oxygen partial pressures ($\leq 10^{-2}$atm) and high temperature, for oxide thicknesses between 22 and 207Å. While the C-M and D-G mechanisms appear to be mixed for oxidant pressures between $\approx 10^{-2}$ to 1atm, there is a shift in the relative importance of the two mechanisms at $\approx 10^{-1}$atm.

In an attempt to explain the rapid initial oxidation regime in dry oxygen, Deal and Grove [DEAL et al., 1965] proposed it to be the result of space charge effects. In their interpretation, the oxidizing species is ionic and oxidation is enhanced until the oxide thickness becomes larger than the extent of the space charge region within the oxide, this thickness being of the order of the Debye

length in the oxide:

$$L = \sqrt{(kT/q)(\epsilon_{ox}\,\epsilon_o/2qC^*)} \qquad (1.10)$$

where C^* is the oxygen concentration in the oxide. L is of the order of 150Å at 1000 °C, in reasonable agreement with the oxide kinetics. Based on Jorgensen's results and on their own results of linear pressure dependence of the parabolic rate constant, they concluded that the ionic species was O_2^-.

It was later suggested [GROVE, 1967] that an oxygen molecule, on entering the oxide, could dissociate into O_2^- and a hole. The hole would move faster towards the interface and drag the slower ion by the built-in electric field resulting from the motion of two charged species with different mobilities.

Lora-Tamayo et al. [LORA-TAMAYO et al., 1978], following Jorgensen's results, proposed a growth model where the oxidizing agents are O^- and O_2^{--}, obtained from collisions between O^- ions. The relative importance of each oxidant would depend on the processing temperature. Emphasis is placed on an 'interphase' of ≈ 50Å between Si and SiO_2, where diffusion and reaction of oxidant occur.

In Tiller's very comprehensive study on aspects of Si oxidation [TILLER, 1980] both O^{--} and, possibly, molecular neutral oxygen are considered as diffusing species, with O^{--} being formed at the surface according to a Cabrera-Mott mechanism. In a later paper [TILLER, 1983], he was the first to suggest the possibility that a build up of positive charges at the interface (whatever their origin) would impede the motion of these ionic species towards the interface (see Appendix I for more information on these charges).

Studying the oxidation kinetics of thin oxide films (20-200Å) at various temperatures and oxygen pressures, Hopper et al. [HOPPER et al., 1975] concluded that oxidation of silicon in this regime might be proceeding by two parallel paths and suggested that the existence of both molecular and ionic motion could be the reason for their observed rate data.

A parallel flux of negatively ionized atomic oxygen (O^-), becoming more important for small thicknesses, was Hu's [HU, 1983] tentative

explanation for the extra growth rate in the thin regime, though this could only be possible if there was a substantial electronic conduction through the oxide by tunnelling or thermionic emission. O^- was considered more probable than the neutral O atom due to the considerable difference in the energy of formation (2.5eV at 1200 K for O atoms against 1.1eV for O^-). This mechanism will clearly become less relevant for thicknesses ≥ ≈ 150Å.

Atkinson's [ATKINSON, 1987] detailed kinetic studies also confirm the view that both molecular and ionic transport may contribute to film growth as two parallel processes. The prevalence of one over the other may be dictated by processing conditions (such as oxidant pressure and temperature). O^{--} and oxygen vacancies were considered.

The ionic contribution is described by the Cabrera-Mott mechanism for oxides up to ≈ 50Å (strong field assumption, electronic equilibrium possible) and by Wagner's electrochemical mechanism [WAGNER, 1933] for much thicker films.

In Wagner's theory, originally proposed for the growth of thick metal oxides, the transport of species is governed by the gain in free energy of the system. The growth rate is controlled by transport down the gradient of the thermodynamic potential of oxygen, which becomes smaller as the film thickness increases [ATKINSON, 1985; WOLTERS et al. 1989]. There must be both electronic and ionic transport in order to ionize the metal and oxygen atoms at the interfaces and provide material transport across the film (no net charge transport). When ionic and electronic conductivities are not equal, the smallest determines the overall transport. Since the diffusing species are electrically charged, their fluxes will be determined both by gradients in chemical potential and by electric fields, which arise from ambipolar diffusion in the oxide. The theory is generally considered valid for small fields, i.e. in bulk conditions. Usually, the assumption of charge neutrality will be valid for oxide thicknesses much greater than the Debye-Hückel screening length. We have seen that Deal and Grove considered it to be around 150Å for a growing oxide at 1000 °C, but the number of charges per unit volume near the interface can be considerably higher than the value in the bulk and, therefore, the extent of this region might be of the order of only a few tens of Ångstroms. The growth kinetics predicted by Wagner theory are parabolic.

The idea of parallel oxidizing fluxes was reproposed (including a full mathematical model) by Wong and Cheng [WONG et al., 1988]. Unspecified charged oxygen species injected at the outer surface are suggested as possible principal candidates for the ionic transport.

As in Deal and Grove's model, O_2^- is the diffusing species also in the oxidation model proposed by Hamasaki [HAMASAKI, 1982]. In the initial stages of oxidation a Cabrera-Mott type of mechanism is assumed. For oxides ≥ 30Å he considered it unlikely that tunnelling or thermionic emission (over a barrier increased by the presence of a constant potential) could provide enough electrons to justify the experimental oxidant flux. By assuming that a net fixed positive charge is progressively generated during oxidation, they could justify a reduced barrier for electron injection. This field, though, opposes the transport of negatively charged oxygen towards the interface, thereby limiting the phase of rapid growth, as Tiller had originally suggested.

A similar model (and similar conclusions) but with a constant interfacial retarding potential was proposed by Naito et al. [NAITO et al., 1986].

Using both Grove's diffusing O_2^-/hole pair and Hamasaki's exponential distribution of net positive charge at the interface, Lu and Cheng [LU et al., 1984] devised a mathematical model valid for both thin and thick regimes of oxidation.

Remaining on the subject of fixed positive charges, a model was recently proposed [SCHAFER et al., 1985] to explain the high initial oxidation rate. According to the model, the accumulation of this positive charge during oxidation acts to reduce the concentration of holes at the Si/SiO_2 interface thereby reducing the density of broken Si-Si bonds, which is believed to be the controlling factor in the growth rate during the reaction-limited phase of oxidation.

The exclusive ionic character of the oxide growth and the retarding effects of the fixed positive charge are the ingredients of a very recent and detailed work by Wolters and Zegers-van Duynhoven [WOLTERS et al., 1989]. The ionic transport mechanism proposed by Wagner is the starting point of the new model (as Atkinsons's suggestion for

thicker films). But this time the growth kinetics are not presented in the usual terms of linear and parabolic rates (Deal and Grove model), but as a power-of-time law [REISMAN et al., 1987].

Following Jorgensen, Mills and Kroger, Srivastava and co-workers (see above), they assume that the diffusing ions are O^{--}, though this doesn't need to be constant during growth and no assumption is made on the species present on the outer surface of the oxide. Electronic current is shown to be available in quantity more than sufficient to compensate the ionic current. The fixed positive charges, generated (and annihilated) during oxidation, create a strong opposing field for the ions, thereby retarding the growth. It is therefore this high field region close to the interface that determines the ionic transport and, finally, the rate (as opposed to the reaction-limited phase in Deal and Grove model).

Robertson's model for thin film growth [ROBERTSON, 1987] discounted mechanisms based on oxygen interstitials as O^{--} (because of their very high creation energy), O^{-} (since, being paramagnetic, it would have been experimentally detected) and O_2^{-} (as it is a network defect, not an interstitial species). He proposed instead a threefold co-ordinated oxygen centre, O_3^{+} (this defect is discussed more in detail in Appendix I) injected at the silicon/oxide interface, swept to the surface by an electric field according to a Cabrera-Mott type of mechanism and there reacting with adsorbed oxygen. Tunnelling electrons would set up this field. The electrons are suggested to come from quasi-localized states in the oxide and their release is shown to inject also the appropriate charged defect into the oxide.

I.7 Stress, stress relaxation and viscous flow

In the last decade, the stress developed during the thermal oxidation of silicon has received increasing attention, following the initial studies by Eernisse [EERNISSE, 1977, 1979] who demonstrated the existence of stress in SiO_2 during growth at oxidation temperatures [TAFT, 1978, 1980, 1985, 1987; TILLER, 1980; IRENE et al., 1982; FARGEIX et al., 1983, 1984; GHIBAUDO, 1987; DOREMUS, 1984, 1987, 1989; DOREMUS et al., 1987; HAMASAKI, 1982; IRENE, 1982, 1987; HAN et al., 1985; SRIVASTAVA et al., 1985; KOBEDA et al.,1986, 1987,

1988, 1989; LANDSBERGER et al., 1986, 1987; CAMERA et al., 1985; FITCH et al., 1989; LEROY, 1987; MACK et al., 1989].

Taft [TAFT, 1978, 1987] demonstrated a relationship between growth temperature and refractive index of the SiO_2 film and reported a decrease in its value with increasing temperature until a constant value is reached at ≈ 1150 °C. This was assumed to be a result of an decreased oxide density. Irene et al. [IRENE et al., 1982] related refractive index to density of the oxide, finding a definite decrease in both with increasing processing temperature; the density variation with temperature is taken as an indication of the existence of residual stresses in the SiO_2 network.

An intrinsic stress σ_i originates from the molar volume change when converting Si to SiO_2, and a thermal expansion stress σ_{th} arises from the thermal contraction mismatch which results upon cooling down from the oxidation temperatures. Traditionally the total stress has been measured at room temperature [KOBEDA et al., 1986], but recently an in-situ measuring technique has been described which allows uncoupling of the total stress into the two components [KOBEDA et al., 1989].

From extensive infrared spectroscopy measurements on dry oxides, there seems to be always a substantial residual intrinsic interfacial stress of a value ≈ $4.6 \times 10^9 dyn/cm^2$, independent of growth temperature [FITCH et al., 1989]. This value was confirmed by theoretical calculations [MURRAY et al., 1989].

The stress is such that the oxide layer is under compression in the direction parallel to the interface (while unconstrained displacement can take place in the direction of oxidation); correspondingly, the underlying silicon is under tension along the same direction. Stress and strain levels are maximum at the Si/SiO_2 interface and decrease with distance from it. The intrinsic stress increases with decreasing oxidation temperature. It also shows a marked orientation dependence, especially at the lowest temperatures (<110> ≥ <311> ≥ <100> > <111> [IRENE, 1987]).

Under the implicit assumption that the oxide behaves like a simple Maxwellian (viscoelastic) fluid, it was shown [EERNISSE, 1977; IRENE et al., 1982; IRENE, 1983] that at temperatures lower than ≈ 960 °C the oxide density varies with time during the oxidation and

eventually relaxes towards a final value (which depends on processing temperature and duration); at higher temperatures, however, the relaxation rate through viscous flow is so high that no relaxation response was observed. This value of temperature (which correlates very well with the breakpoint noticed in the Arrhenius plot of the parabolic rate constant of the Deal and Grove model) plays the role of transition temperature separating regions of practically instantaneous response from regions of viscoelastic response.

A variety of stress-related models have been proposed, according to the differing views on how, and to what extent, stress (and stress relaxation) are considered to affect silicon oxidation. There is a vast amount of published literature on the subject, from very theoretical, first-principles, analyses to simpler, more phenomenological, representations. The subject is an extremely complex one but, for our purposes, we only need to mention those models which consider how stress alters the interface reaction [TILLER, 1980; IRENE, 1983; KOBEDA et al., 1987; IRENE et al. 1986], or affects the transport of oxidant through the oxide [DOREMUS, 1984; FARGEIX et al., 1983, 1984; CAMERA et al., 1985].

While all the models in question, relating the viscous properties of the oxide or stress in the oxide to the oxidation kinetics, do so in the context of the linear- parabolic kinetics, the model by Nicollian and Reisman [NICOLLIAN et al., 1988] presents the kinetic data in the novel form of a power-of-time law (a similar mathematical formalism had been previously suggested [REVESZ et al., 1986], but later abandoned for lack of a physical explanation). The key concept of this model is that newly formed oxide undergoes a structural reconfiguration from an initially ordered to an amorphous structure at the oxidation temperature, accompanied by a continuing increase in the average oxide viscosity. Contrary to the previously mentioned assumptions that the growing oxide is a viscoelastic medium, Nicollian and co-workers explicitly treated it as a viscoplastic medium (a viscoelastic material elastically deforms and relaxes by viscous flow, while a viscoplastic medium permanently deforms by viscous flow). Most of the 'dry' oxidation data published since 1965 have been analysed with this model and have all shown a remarkably good fit [REISMAN et al., 1987].

The power law model was later adopted by Wolters et al. [WOLTERS et

al., 1989], but based on a completely different physical explanation (see par.I.6).

Mott [MOTT, 1987; MOTT et al., 1989] points out that the measured intrinsic stresses of the order of 10^9dyn/cm² are nowhere near the theoretical value of 10^{10}–10^{11}dyn/cm² that could be produced by the difference of volumes. It seems, then, at least a possible hypothesis that macroscopic strains are not a major influence on the rate of oxidation, although it is quite possible to envisage the presence of a region, next to the interface, in which the Si–Si and Si–O–Si bonds are strained.

I.8 Reaction layer

The introduction, in the oxidation kinetics, of a transition layer at the Si/SiO_2 interface, characterized by the presence of Si interstitials and/or dislocations in order to reduce the interface strain energy, was initially proposed by Tiller [TILLER, 1981, 1983] (Tiller's 'blocking layer' and two-layer film approximation). Fargeix et al. [FARGEIX et al., 1983] proposed the idea of a reduced oxidant diffusivity layer (extending perhaps up to a few hundred Ångstroms), while Stoneham et al. [STONEHAM et al., 1987] introduced a qualitative model of silicon oxidation based on an interfacial 'reactive layer', stabilized by stress generated with the underlying silicon and with composition and electronic properties that differ from those of bulk silica. This concept of a 'reaction zone' has been recently developed in a more comprehensive picture [MOTT et al., 1989] which takes into account all the wealth of information obtained from the radioactive tracer experiments. This region of different structure is composed of SiO_x (with $x<2$ at least in the first few atomic layers); the zone is ≤ 60Å and is opaque to interstitial O_2. Oxidant transport must proceed therefore in a different way and diffusing oxygen is likely to exchange with the network.

A rather different approach to a 'reaction zone' is the central point in Murali and Murarka's oxidation model, aimed at explaining the initial rapid growth [MURALI et al., 1986]. They postulate the rapid creation of an oxygen-diffused zone (a few tens of Ångstroms

wide) in the silicon substrate during the initial exposure to the oxidizing environment; as a consequence, the initial reaction occurs over a zone and not just at the interface. Recent studies on rapid thermal oxidation suggested this thickness to be of the order of 10-25Å for temperatures in the 1050-1200 °C range [PAZ DE ARAUJO et al., 1989].

I.9 Summary and modelling

The aim of the preceding rapid overview was to show how, after 25 years of research, still there isn't unanimous agreement over many aspects of this apparently simple, but in practice quite complex, chemical reaction, the uncertainties being especially pronounced in the area of thin oxide growth. The possibility that different mechanisms may predominate under different processing conditions is now widely accepted.

At a superficial glance it appears that, at present, the relevance of macroscopic stress in the growth kinetics has been somewhat reduced from an initial widespread enthusiasm, while the effect of internal electric fields is being revalued and atomic oxygen and network defects still attract much research interest. Only the ever increasing accuracy and sophistication of experimental in-situ techniques will, in due course, unravel the fine details of the process.

From a purely mathematical point of view, a large selection of oxidation models is available in the literature. For our modelling purposes we have chosen the work of Massoud and co-workers [MASSOUD et al., 1985, 1987] (see par.I.4 and I.5), though the choice doesn't imply any automatic acceptance of the physical explanation behind it. This oxidation model is an extension of Deal and Grove's, corrected to take into account the initial regime of growth and seems to be generally accepted at present as one which best fits most published data and can be given some physical explanation. The very extensive data were collected with an in-situ ellipsometer. Fig I.2 shows the Arrhenius plots for the linear and parabolic rate constants.

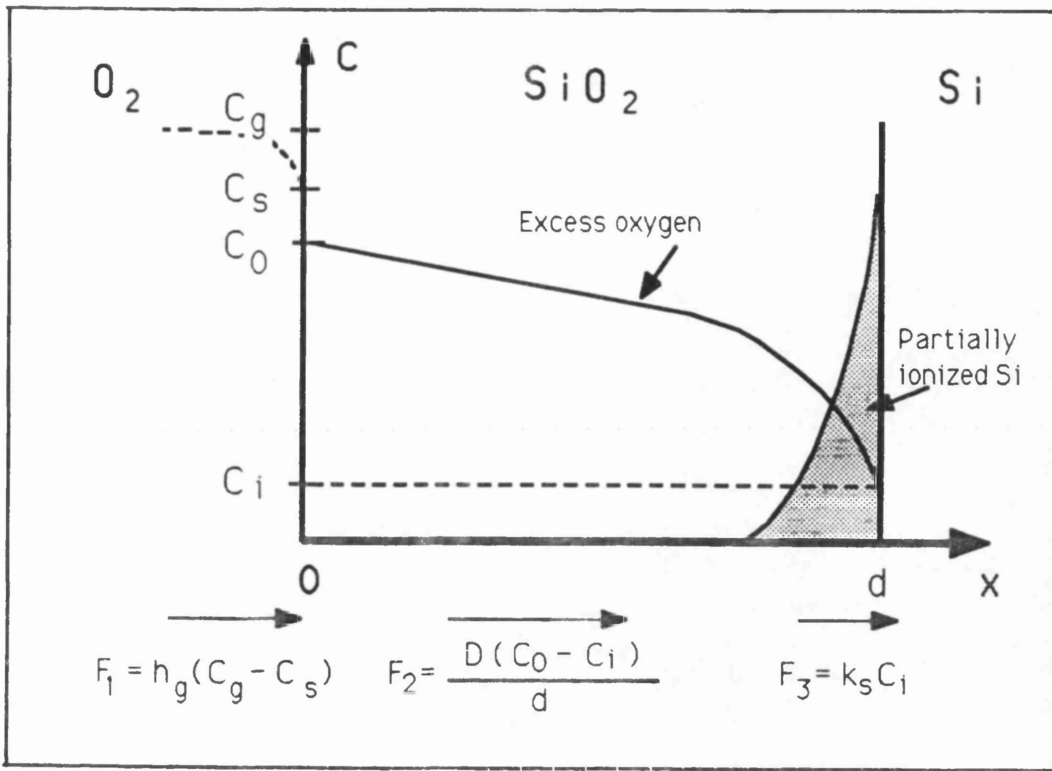

Fig I.1: Basic model of thermal oxidation of silicon (from [DEAL et al., 1965]). The vertical axis represents oxidant concentrations: in the bulk of the gas (C_g), adjacent to the oxide surface (C_s), at outer surface of the oxide (C_o), adjacent to oxide/silicon interface (C_i); h_g: gas-phase mass-transfer coefficient; D: oxidant diffusion coefficient; k_s: reaction constant at Si/SiO_2 interface [SZE, 1988].

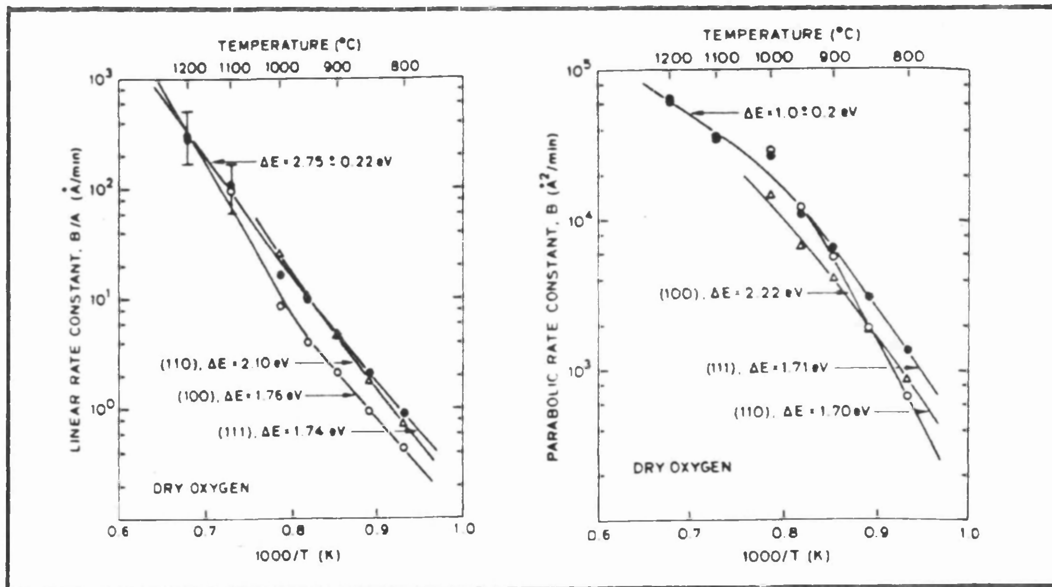

Fig I.2: Linear and parabolic rate constants for <100>, <111> and <110> oriented Si, lightly doped, in dry oxygen [MASSOUD et al., 1985].

CHAPTER II

Experimental Apparatus and Procedures

II.1 Introduction

In this chapter the experimental apparatus used during these investigations is presented together with an outline of the main experimental procedure followed.

Practical and theoretical details which guided or, occasionally, dictated the particular choice of experiments or solutions to specific problems are also presented: this will enable a better understanding of the discussion and evaluation of results in the following chapters.

II.2 Experimental apparatus

The laser used in our experiments was a Coherent Innova 100-20 CW argon laser with a maximum multiline output power in excess of 20W. In single line operation, it could provide over 9W at 514.5nm (green) and over 7W at 488nm (blue) plus smaller powers at intermediate wavelengths. Approximately 3W of multiline UV light (≈ 350nm) were also available.

The Gaussian beam emitted had a diameter ($1/e^2$ of the intensity) of 1.9mm in the visible and 1.6mm in the UV. The laser power stability was specified to be 0.5% over a half an hour period (after the initial warm-up); the power was, nevertheless, constantly monitored during all irradiations as stability was a crucial parameter in all the experiments.

Some experiments have also been carried out with the laser in its mode-locked configuration: pulses 85-90psec wide (half power) were obtained, in the visible range, with a repetition frequency of 76 MHz; the average power achievable was ≈ 1W with a peak power per pulse of ≈ 150W.

The reaction chamber was a stainless steel vessel with input and output valves for connection to a vacuum pump and to the appropriate gas line. The light beam entered the chamber through an anti-reflection coated fused silica window.

An electrical feed-through allowed for use of a thermocouple, a Peltier cooler or a resistive heater inside the chamber while under vacuum or oxidation conditions.

The sample was mounted independently inside the chamber. To reach the high temperatures required for our experiments (i.e. approximately 700 °C to 1200 °C) with the laser light as the only source of energy, the sample needed to be quite small and in thermal isolation (further details of the sample temperature will be given in the next chapter); the holder, therefore, consisted of a firmly held quartz cylinder especially modified to accommodate the sample with minimal contact area, whilst preventing any undesired displacement.

Following a variety of imaginative and rather impractical attempts, an alternative holder was also designed for oxidation of double-side polished samples, where the oxide thickness of both sides is of interest. A C-shaped section of stainless steel clamped two tiny tubes, of either quartz or alumina, between which the sample was held, at diagonally opposite corners, under a slight pressure. The whole assembly was resting on an insulating quartz cylinder. The design provided a better thermal isolation but, being very awkward, was confined to a limited set of experiments.

The gases used (oxygen and nitrogen) were electronic grade (BOC Electra II grade). A further filtering and drying stages were used before introduction into the reaction vessel.

Dielectric mirrors were used throughout the work to avoid possible changes in reflectivity due to surface degradation which could be present with metallic mirrors.

An optical pyrometer monitored the temperature of the sample, though it lacked the spatial resolution required in our case and provided, therefore, only an average value of the surface temperature which was used as a useful guide.

The silicon samples, eihter Czochralski or float zone Si, were 3x3

mm, with thicknesses ranging between 250 and 525μm. Both n and p type, <100> and <111> orientation, with doping concentrations in the range $\approx 10^{14}cm^{-3} - 4x10^{19}cm^{-3}$ were used.

Various cleaning procedures were tried; the technique ultimately used was determined by external recommendations and good repeatability in the experimental results.

The silicon was first cleaned with a sequence of trichloroethylene, acetone and methanol baths followed by rinsing in de-ionised H_2O; the native oxide was then etched off in a 7:1 solution of H_2O and HF, followed by 10 min rinsing in de-ionised H_2O. The sample was then left for a period of $\approx$ 10min in a 1:1 solution of H_2SO_4 and H_2O_2, rinsed again in de-ionised water, re-etched in a very weak solution of water and HF (to remove the oxide formed during the dip in sulphuric acid and hydrogen peroxide), re-rinsed and, finally, blow dried with N_2.

It is now commonly recognized [DE LARIOS et al,1989; OLSEN et al., 1989] that silicon oxidation kinetics are dependent, especially for the thin oxides in which we are interested, on the type of pre-oxidation surface cleaning: in order to ensure consistency, our experiments were performed on samples subjected to an identical cleaning procedure.

II.3 Experimental procedure

The stainless steel vessel was routinely baked and evacuated to ensure that only minimal traces of water vapour were adsorbed on the walls.

The silicon samples were positioned on the quartz holder, inside the vessel, immediately after cleaning. A native oxide of 8-12Å was usually present at this stage. The chamber was evacuated to a pressure of less than 10^{-5} torr. The sample was then irradiated in a N_2 environment to minimize any possible water absorption and re-evacuated.

The positioning of the laser beam was performed at very low incident power and with the reaction chamber filled with N_2 (to avoid any possibility of oxidation at this stage). The beam was incident on

the sample just off normal.

The N_2 was then substituted with 760 Torr of O_2 and the laser power set to a predetermined level (which was monitored for the entire duration of the experiment). The laser power was always ramped (up or down) in order to avoid the possible formation of slip dislocations on the substrate. At the end of the desired oxidation time, the laser was turned off and the chamber flushed with N_2 to cool the silicon rapidly.

The oxide grown was roughly Gaussian in extent, the peak being more or less pronounced according to the thickness achieved (see Figs II.1 and II.2). The thickness was often measured with an ellipsometer which, for thicknesses above approximately 450Å, would also give the oxide refractive index. For thinner oxides (a very large set in our experiments) the refractive index must be assumed and a value 1.458 was used throughout. The sampling beam diameter of the focused ellipsometer was $\approx 50\mu m$.

II.4 Reflectometer

It became apparent, as the project developed, that the inevitable experimental tolerances and, on occasions, errors, could play a significant role in the determination of the wavelength dependence of the silicon oxidation rates. One of the primary causes of errors was the technical impossibility of measuring the reflectivity of silicon, at the two wavelengths of interest, with the accuracy required (possibly the third or fourth decimal place). As the power absorbed by the sample at each wavelength is P(1-R), it is obvious that the error in setting the initial temperature, even if it was possible to set the laser power to any desired value with the desired accuracy, could be significant. As oxidation is very much temperature-dominated, the initial conditions were clearly very important. For instance, an increase of 18 °C at ≈ 880 °C and 50Å of oxide would cause in increase in the growth rate of almost 35% (oxidation model from [MASSOUD et al., 1987]). A simple, non-invasive method of determining the processing temperature with good spatial resolution was therefore essential.

Furthermore, it was considered to be of great benefit to have in-

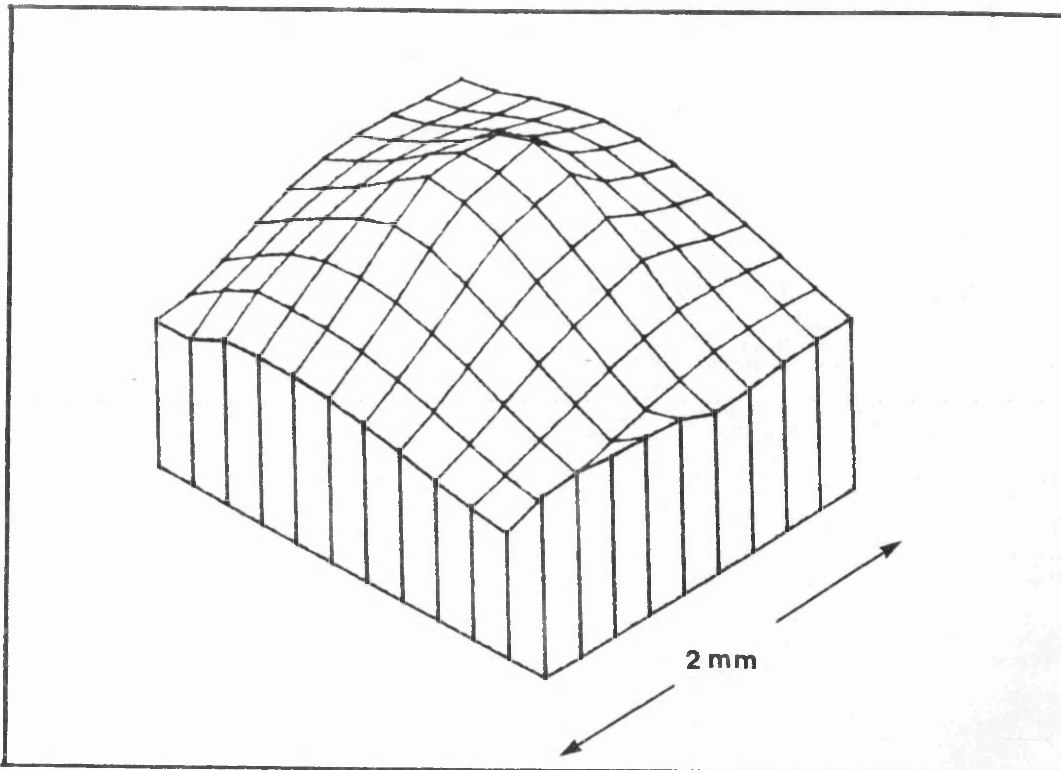

Fig II.1: Three-dimensional profile of $4mm^2$ area of laser oxidized silicon (peak thickness: 810Å, average thickness at the edge of plot: 450Å) [BOYD & MICHELI, 1987].

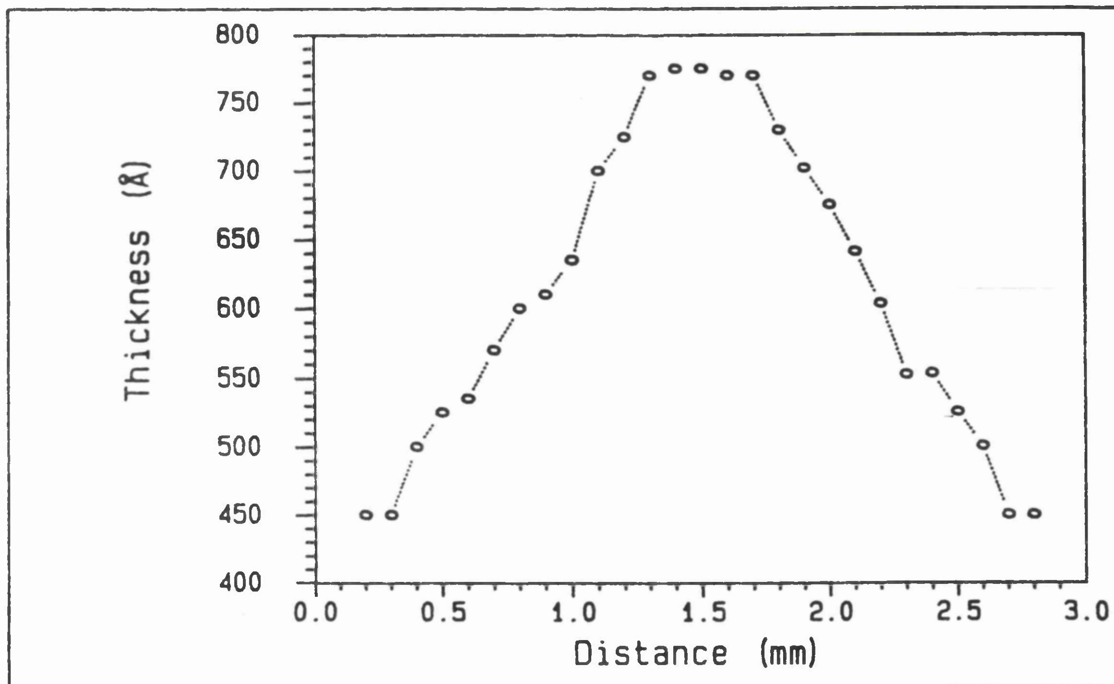

Fig II.2: Thickness profile of laser grown oxide.

situ measurement of the thickness of the growing oxide. This would avoid another external source of error because of positioning the very small samples, which could also have an effect on conductive heat losses from the sample and, ultimately, the temperature induced.

To the best of our knowledge, such an instrument capable of fulfilling these requirements did not, and still does not, exist on the market. The system was designed and built at UCL with the additional requirement that it had to be very cheap and reasonably quick to devise and assemble [MICHELI et al., 1988]. The instrument is described in the following sections.

II.4.1 Principle of operation

A schematic diagram of the oxide growth monitor is shown in Fig II.3.

A 7mW Helium Neon laser beam (Melles Griot 05LHP 171) was chopped at around 500Hz to provide an AC signal (thus enabling the rejection of DC drift and 1/f noise); a beam splitter divided the beam between a reference detector and the main path to the sample being processed.

This beam was expanded and focused onto the silicon surface at almost normal incidence. In all initial experiments the probe beam was passed through the dielectric mirror which deflected the Argon laser beam; subsequent results demonstrated that this arrangement was not sufficiently stable as the mirror expanded with temperature and altered the transmission loss.

To avoid undesirable back-reflections, normal incidence was avoided along the path of both lasers. The HeNe and Argon laser beams were therefore almost collinear and concentric on the Si surface so that the probe beam sampled the hottest spot on it. The focusing lens (after the beam expander) was a best-form lens with a 50cm focal length and produced, in this case, a spot approximately 30μm in diameter (at the $1/e^2$ points), though the choice of lens and focal spot size was a fairly arbitrary one and could easily be adapted to different requirements. An OG 550 Schott colour glass filter was used to stop any Argon light from entering the receiver along the reflected path (although the DC light was not detected as a signal, it could still reduce the detector dynamic range). A BBC

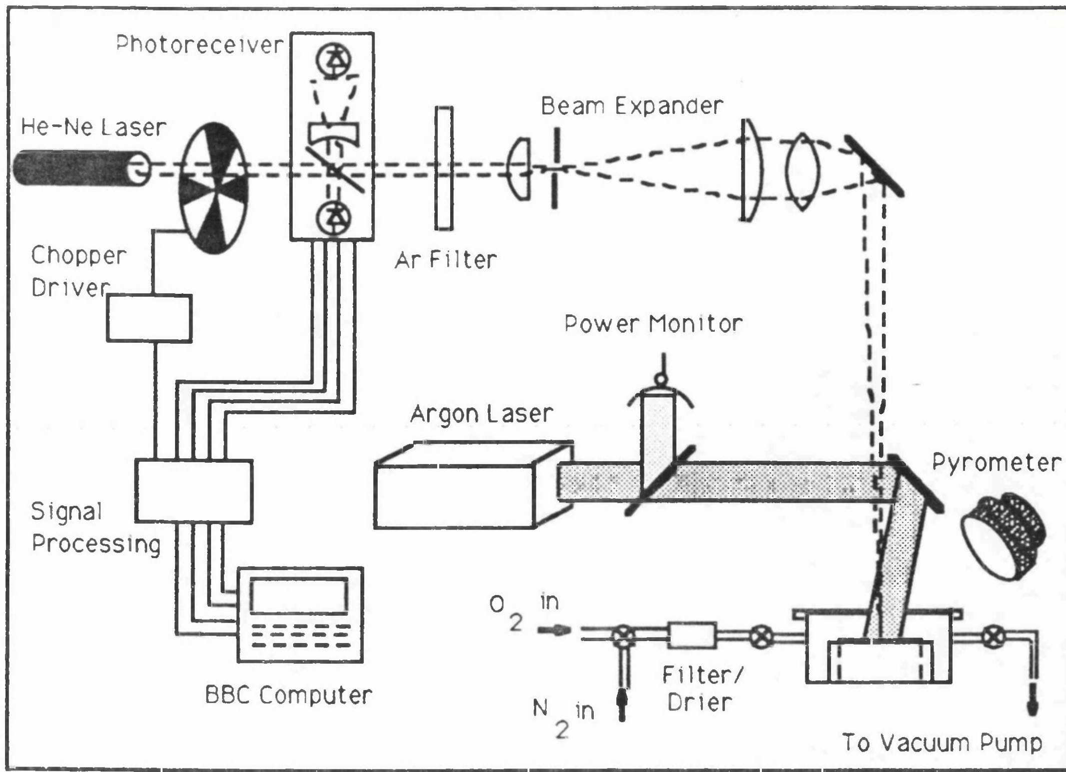

Fig II.3: Experimental set-up for in-situ monitoring of silicon oxidation [MICHELI et al.,1988].

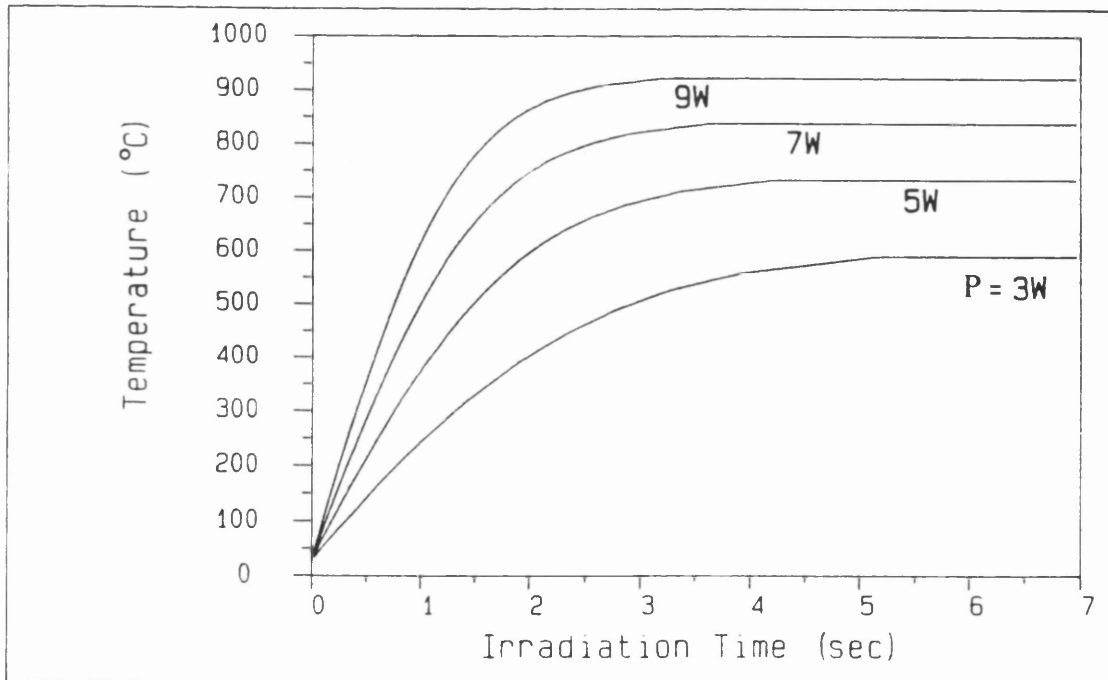

Fig II.4: Temperature as a function of irradiation time in Si for different incident laser powers.

microcomputer controlled the data collection and performed all calculations.

After an initial system calibration, the sequence of events was as follows: when the silicon is at room temperature, the computer collects data from the two detectors and calculates the reflectivity as the ratio of the two signals, R_0, which is a function of the refractive indices of the silicon (real and imaginary parts, $n_s(T=T_0)$, $k_s(T=T_0)$) and of the oxide (assumed real, $n_{ox}(T=T_0)$) and is also a function of the oxide thickness x. The thickness of the oxide can then be determined (the mathematical formulation is presented in next paragraph).

However, when the Ar laser irradiates the silicon and the temperature rises by hundreds of degrees (to a value which we can only very roughly predict or measure at this stage), the thickness can no longer be computed directly since it is well known that the refractive indices of the film and the substrate are functions of the unknown temperature. Thus, a modified approach is required.

The reflectivity is first measured at high temperature, $R[n_{ox}(T), n_s(T), k_s(T), x]$. The Ar laser beam is blocked and the silicon allowed to cool to room temperature. The reflectivity R_0 is measured again and the new film thickness is calculated.

Measurements with the thinnest thermocouple available determined the cooling times (with and without forced ventilation) to $T=T_0$ for different quartz holders and have shown them to be of the order of a few minutes. It has also been determined that only a few seconds are required to cool the silicon to ≈ 100 °C from ≈ 800-1000 °C or to heat it to these temperatures (Fig II.4). Hence, the heating and cooling times for the silicon are extremely short compared with the oxidation process which, because of the typical growth rates concerned, is unaffected by this operation.

With the knowledge of the reflectivity at high temperature, $R(n_{ox}, n_s, k_s, x)$, the oxide thickness, x, and the three expressions for $n_{ox}(T)$, $n_s(T)$ and $k_s(T)$ the unknown processing temperature can finally be computed.

The process is repeated at various intervals during the oxidation process to provide a curve of growth as a function of time and calibrated in temperature.

A flow chart describing the controlling software is shown in Fig II.5.

II.4.2 Instrument background

The thickness monitor exploits the optical properties of a film covered absorbing substrate. Assuming the oxide to be fully transparent, the Fresnel coefficients for the air/oxide, r_1, and oxide/silicon, r_2, interfaces are given by [ANDERS,1967]:

$$r_1 = (n_o - n_{ox}) / (n_o + n_{ox}) \tag{2.1}$$

$$r_2 \exp(i\delta) = (n_{ox}-n_s+ik_s)/(n_{ox}+n_s-ik_s) \tag{2.2}$$

where

$$\tan \delta = (2\, n_{ox}\, k_s) / (n_{ox}^2 - n_s^2 - k_s^2) \tag{2.3}$$

and n_o, n_{ox}, n_s-k_s are the refractive indices of air, silicon dioxide and silicon, respectively. The expression for the normal incidence reflectivity from a plane parallel, homogeneous, non-absorbing film on an absorbing substrate can be written as [ANDERS, 1967]:

$$R = \frac{r_1^2 + r_2^2 + 2r_1r_2 \cos(\Delta + \delta)}{1 + r_1^2r_2^2 + 2r_1r_2 \cos(\Delta + \delta)} \tag{2.4}$$

where $$\Delta = (4\pi/\lambda)\, n_{ox}\, x \tag{2.5}$$

and x is the film thickness.

The variation of normal incidence reflectivity, at the helium-neon laser wavelength of 632.8nm, as a function of oxide thickness is shown in Fig II.6, for two substrate temperatures and in the range of interest for our experiments, using n_{ox}=1.458 (at room temperature).

The formulae can be readily modified to account for oblique incidence and different types of polarisation. The hardware included a separate identical receiver which could be used in experiments requiring, for instance, multiple angular readings.

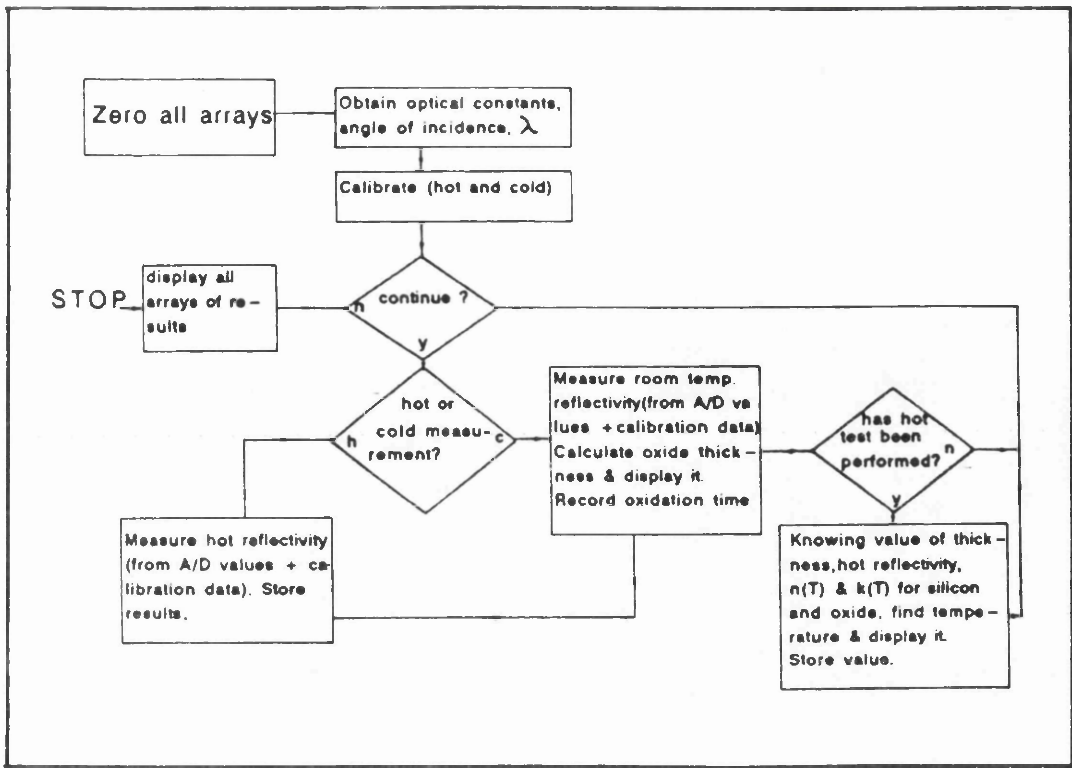

Fig II.5: Flow-chart of monitor controlling software [MICHELI et al.,1988].

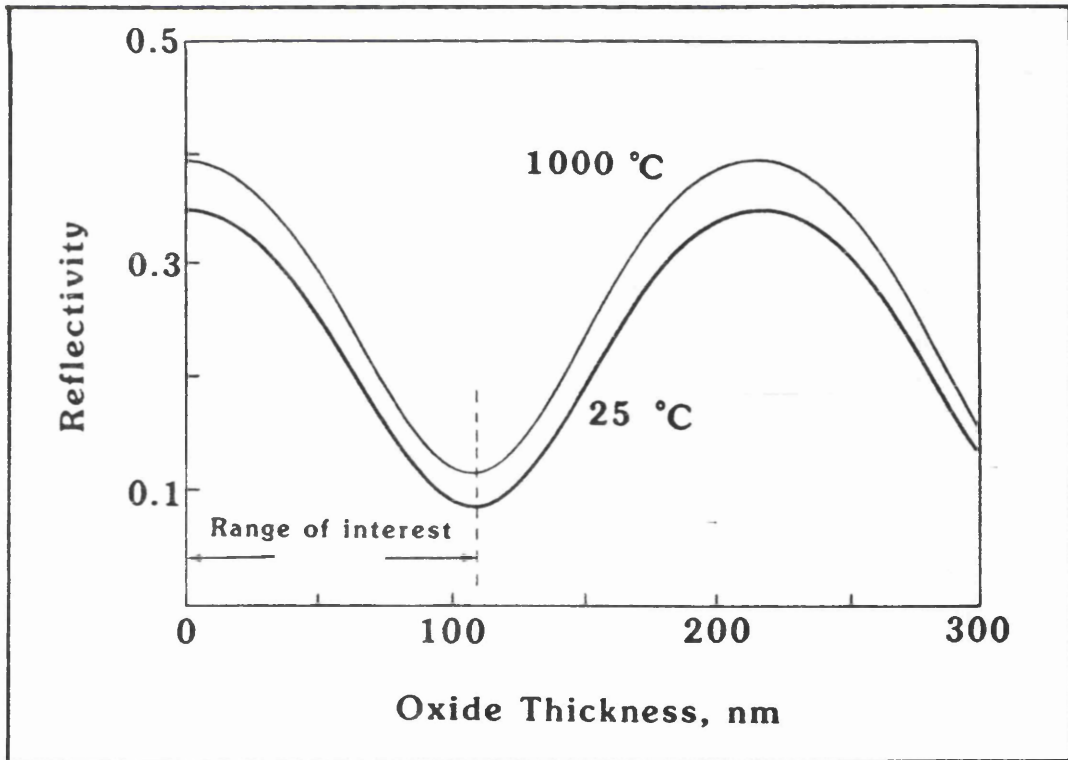

Fig II.6: Reflectivity of oxidized silicon as a function of oxide thickness at λ=632.8nm (T=25 °C and T=1000 °C) [MICHELI et al., 1988].

It is therefore clear that, if we could measure the reflectivity (normal or oblique incidence) accurately enough, we would be able to determine the thickness of the oxide, with the assumption that the optical parameters of silicon and silicon dioxide are known at the wavelength(s) and temperatures of interest.

This latter requirement can be considered satisfied as both materials have been widely studied optically and a vast amount of literature is available. It is worth noting at this stage that ellipsometry also uses a pre-fixed value of n and k for silicon and, for the thin oxides in which we were mostly interested, the refractive index of silicon dioxide is usually specified, as previously mentioned.

Similar techniques, based on reflection, or reflection / transmission, measurements for transparent, partially absorbing and opaque materials, have been widely used for a long time in a variety of applications covering many different examples of thin films or bulk materials. Some recent work contains extensive references on the subject [ANDREW,1986; ELIZALDE et al.,1986; SCHIROKY et al,1987; SU et al,1987; MILLER et al.,1988; OHLIDAL et al,1988; SIQUEIROS et al.,1988; FOULON et al.,1988; TIMANS et al.,1988; ZOLLER et al.,1988; SCHERRER et al.,1988; DILHAC et al., 1989].

Our next requirement was the knowledge of the variation of the real and imaginary parts of the refractive index of silicon and silicon dioxide with temperature, up to the very high temperature used in furnace oxidation (1100-1200 °C). For this purpose, we have used the results obtained by Van der Meulen and Hien [VAN der MEULEN et al.,1974] using high-temperature ellipsometry. A helium-neon laser with a wavelength of 632.8nm was used in their experiments, as in our oxide monitor (though the availability of data at other wavelengths would open up the attractive possibility of performing spectroscopic measurements).

Van der Meulen and Hien calculated the temperature dependence of the real and imaginary parts of the complex refractive index of silicon through a series of ellipsometric measurements carried out on pre-oxidized silicon resting in a N_2 filled furnace heated up to a maximum of 1350 K; pairs of values for the ellipsometric parameters Δ and ψ were calculated as a function of temperature. Room temperature

measurements gave the oxide thickness and the real part of the refractive index n_s at 298 K.

The absorption coefficient k_s (at 298 K) was obtained from transmission data [DASH et al.,1955]. Independent bulk transmission experiments [PHILIPP,1972] confirmed these values.

Very good agreement is shown between data taken for different oxide thicknesses and, although there is some scatter of the values for k_s measured at the lowest oxide thicknesses, the results are quite satisfactory. Very similar discrepancies in the values of k_s for thin oxide films have been reported also by Hopper et al. [HOPPER et al., 1975] and tentatively ascribed to the composition of thin oxide layers (their own measurements showed the films to be closer to SiO than SiO_2). But, on the whole, the behaviour of both n_s and k_s with temperature reported by the two groups are remarkably similar; these data are also consistent with infrared measurements [LUKES, 1959] and emissivity data [SATO,1967], though they disagree with the ellipsometric results of Ibrahim and Bashara [IBRAHIM et al.,1972] (but this last experiment could have suffered by an overestimation of the temperature). Recent work by Jellison and Modine [JELLISON et al., 1983] again confirmed the validity of these data.

There is a general consensus on the value of the imaginary part of the complex refractive index of SiO_2, which appears to be negligible at all temperatures investigated.

The shift, as a function of temperature, of the real part of the refractive index of silicon dioxide, n_{ox}, was calculated quite accurately by Van der Meulen and Hien, though they couldn't obtain an accurate value for n_{ox} at room temperature due to the ellipsometer and their particular choice of oxide thicknesses. Hopper and co-workers calculated a value of 1.458 at 23 °C and a temperature dependence very close to Van der Meulen and Hien's results. We have therefore assumed these values to be correct.

Fig II.7 shows best fit curves for the temperature dependence of the silicon and silicon dioxide refractive indices obtained by van der Meulen and Hien.

As the thermal expansion of SiO_2 is $5x10^{-7}$ [GROVE, 19867], its effect on the measurements will be negligible.

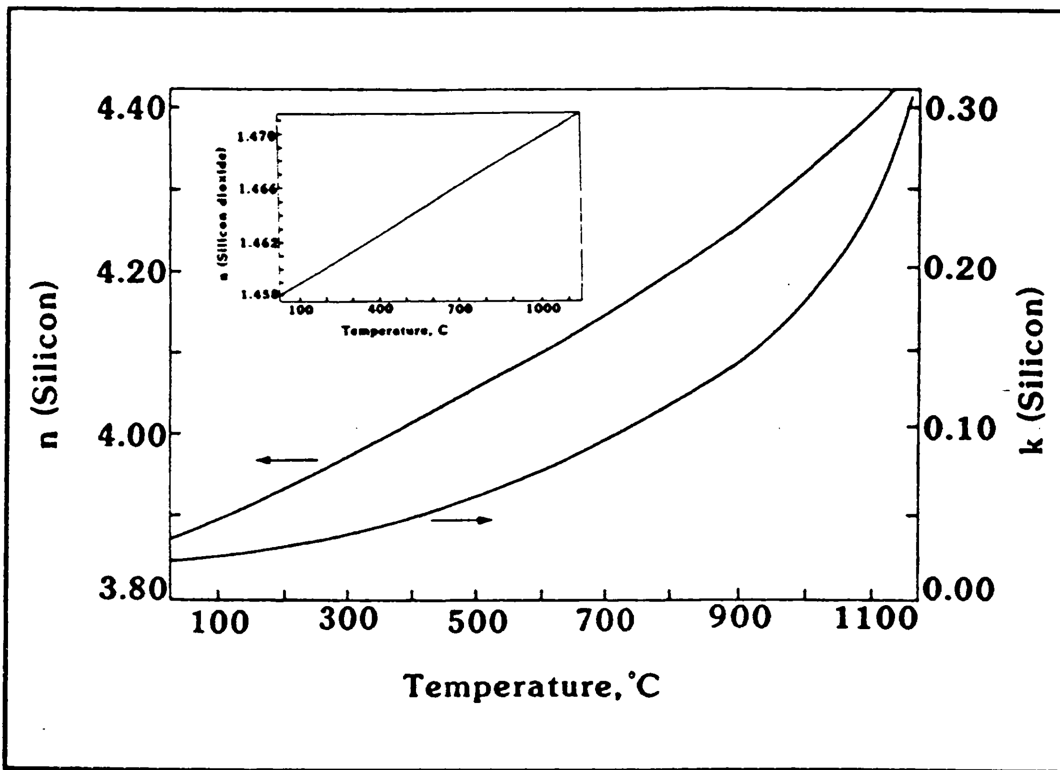

Fig II.7: Temperature dependence of real and imaginary part of refractive index of Si and of real part of refractive index of SiO_2 [VAN DER MEULEN et al., 1974].

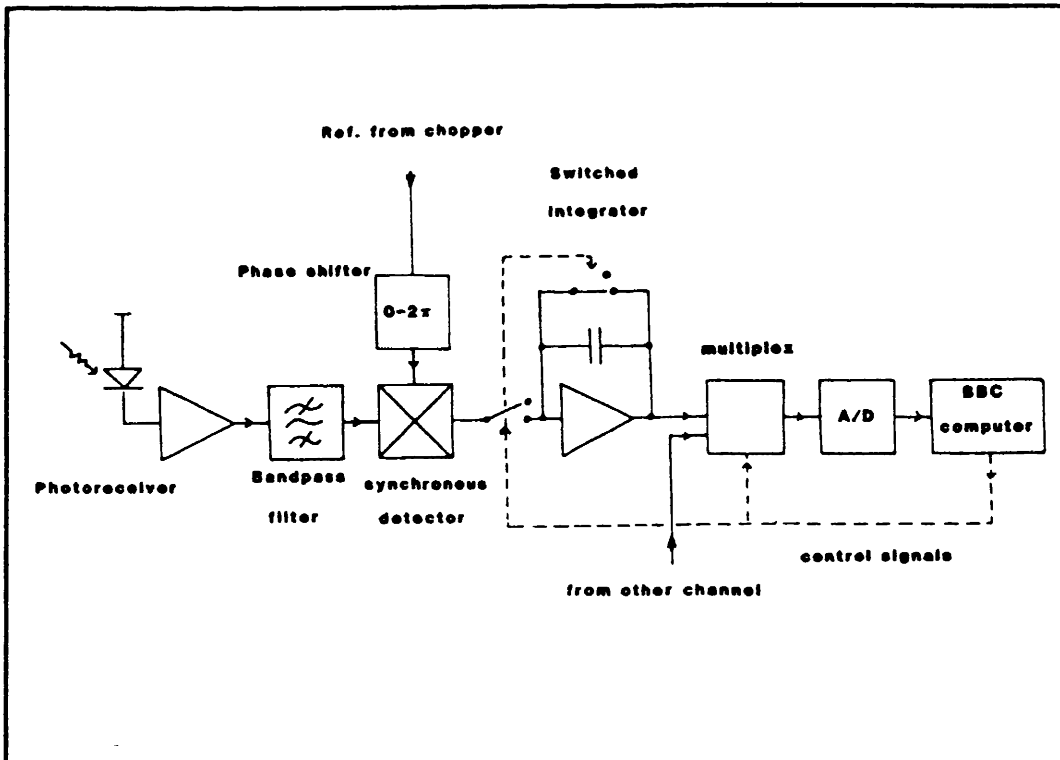

Fig II.8: Block diagram of monitor electronics.

In our work, the possible presence of a Si/SiO_2 interface layer with a different (or graded) refractive index has been neglected. Though the subject is still a matter of heated debate, we have assumed it to be abrupt, as suggested by Grunthaner and Grunthaner [GRUNTHANER et al., 1986] for device quality thermal oxides .

Likewise, we have neglected possible energy loss due to scattering from a rough Si/SiO_2 interface [CARIM et al., 1987; NIWA et al., 1989]. Using Bennett's analysis [BENNETT et al.,1961], we have deduced that the maximum error due to such effects would not significantly affect the specular reflectivity (see Appendix I for a more detailed discussion on the Si/SiO_2 interface).

Finally, following the analysis of Opsal et al.[OPSAL et al.,1987] the effect of the carrier density on the optical parameters n and k was investigated. Assuming negligible plasma relaxation and n >> k at 633nm, we can write:

$$\delta R/R = \frac{-2 \quad \lambda^2 e^2}{\pi n(n^2 - 1) m c^2} N_0 \qquad (2.6)$$

where e is electronic charge, c the speed of light, N_0 the plasma density and m the effective carrier mass ($m = 0.15\ m_o$, where m_o is the free electron mass).

For a carrier density of $10^{18}cm^{-3}$, $\delta R/R$ is approximately -10^{-4}, and $\delta R \approx -3.5x10^{-5}$ at room temperature, where R=0.347. As will be shown later, this is below the limit of the resolution achievable with our present equipment and its influence was neglected in the analysis.

II.5 Hardware description

II.5.1 Introduction

A schematic diagram of the the electronic processing circuitry is shown in Fig II.8.

It consists of two identical channels including a band-limiting photoreceiver, a synchronous detector and a switched integrator

module which outputs a DC signal proportional to the rms value of each input. Both these signals feed, in turn, a multiplexed 13 bit A/D converter providing data to the BBC computer.

Clearly this instrument was only a prototype and some modifications (which became apparent only at the end of the design/test stage) would be necessary if a fully engineered version was required.

II.5.2 System requirements and accuracy considerations

The unambiguous thickness range of the monitor was limited to approximately 1083Å by the 633nm radiation because of the already described Fabry Perot effect.

High linearity and signal-to-noise ratio (S/N) were major considerations in the design of the circuits, while speed was not an important requirement in this application, nor was, to a certain extent, the HeNe laser power stability (due to the ratiometric measurement).

The A/D converter had an intrinsic S/N (quantization noise) which depended on the number of bits available and the receiver design aimed at achieving at least this value (in the pre-quantization stage): this implied that the system could then be easily upgraded by choosing a higher precision A/D. For a full scale signal this S/N is 89dB, but in the reflected channel the signal can experience a worst case drop of approximately 13.8dB, thereby reducing the S/N to 75.2dB.

Resolution is 0.0122% of full scale for a 13-bit A/D converter. In our experiments, the upper end of the signal handling range was determined by the maximum reflectivity expected, i.e. $\leq$ 45%, corresponding to an oxide-free silicon sample at T > 1300 °C. Therefore, for a full scale reading corresponding to R=0.45, the minimum <u>theoretical</u> δR was $\approx 5.5\ 10^{-5}$. From expression (2.4), this implied a <u>theoretical</u> thickness resolution (minimum detectable δx) of:

$<$ 1 Å at oxide thicknesses $\approx$ 660-670Å, or an error $<$ 0.15% ;

$\approx$ 4Å for a native oxide of 15Å, or an error of 26.5% ;

$\approx$ 9Å for an oxide 1083Å thick, or an error of 0.85% .

As expected, the percentage error for extremely thin oxides could be considerable, but, in our experience, the actual error of ≈ 4Å was very similar to that encountered in expensive ellipsometers in the same thickness range.

The theoretical minimum δT detectable was again determined by the minimum δR measurable (reflectance under irradiation, in this case). For very thin oxides, the effect of errors in the thickness calculation must be added, but we calculated that they constituted only a minor contribution to the final count. In the temperature range encountered in silicon oxidation (≥ 500 °C), the minimum <u>theoretical</u> resolvable δT decreased from ≈2 °C at 500 °C to ≤ 1.5 °C at 1000 °C.

II.5.3 Photoreceiver

The circuit is shown in Fig II.9. The first stage of each channel of the photoreceiver is a transimpedance amplifier with the input current provided by a reverse biased p-n photodiode. The diode in the reflected channel has a much larger active area to allow for possible fluctuations in the position of the beam due to sample thermal expansion, thermal lensing effects or refraction in the growing oxide mound during a complete experiment (the beam, as mentioned, was not perfectly normal to the surface). To further decrease sensitivity to beam steering, the reflected beam is appropriately diverged on to the diode surface so that an 'averaging' effect is introduced.

Both photodiodes are linear in the light intensity range of interest.

The transimpedance gain of the reflected channel can be switched between two values to optimize dynamic range according to the mode of operation (after-processing thickness only measurement or in-situ thickness and temperature measurement). The gain of this first stage is kept high to minimize system noise figure.

The frequency response is rolled off to reduce high frequency contributions while preserving the chopped waveform fundamental component. The amplifier output is then high pass filtered to remove DC offset and 1/f noise. Fine gain adjustment is provided by the following buffer.

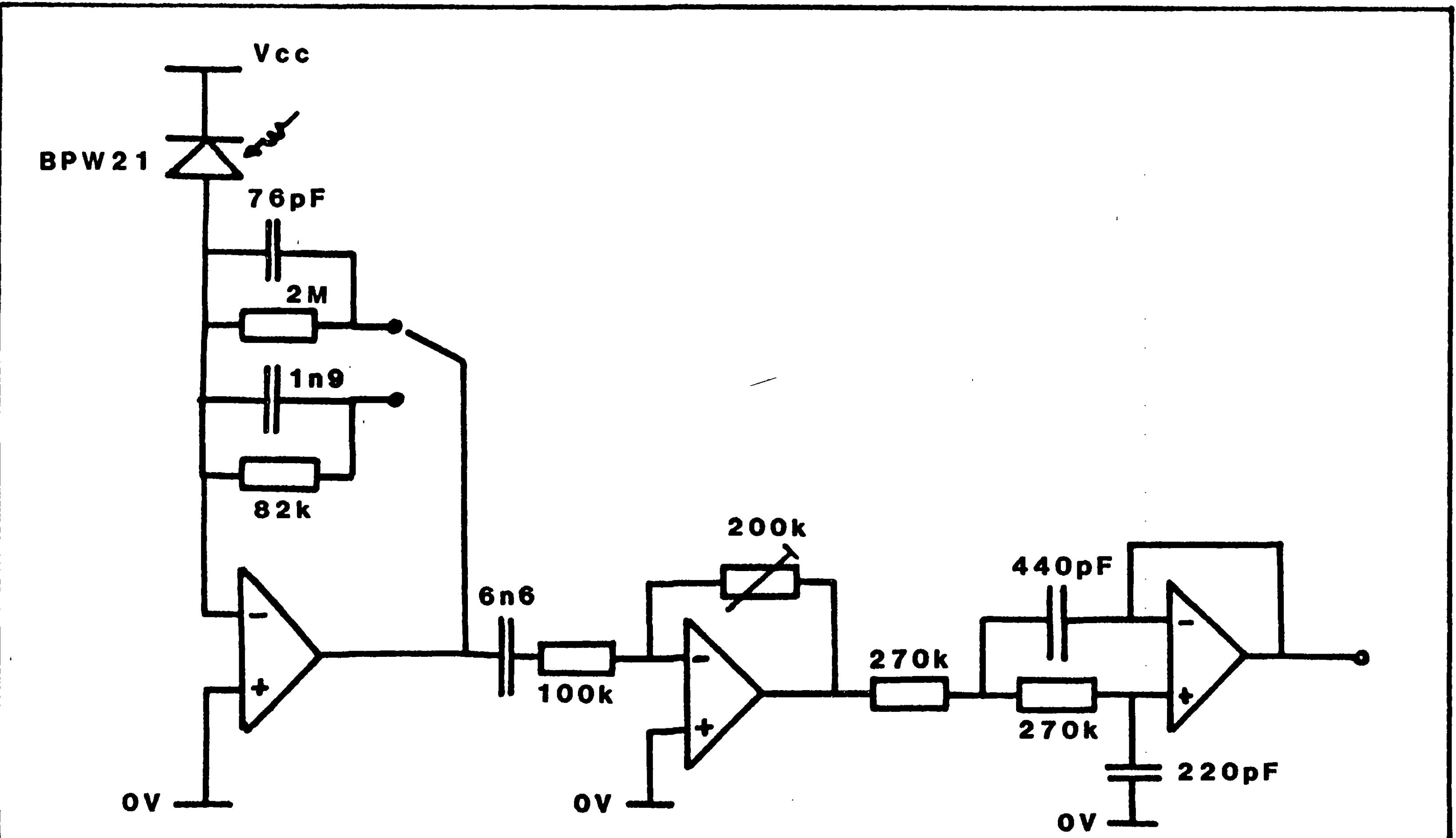

Fig II.9: Photoreceiver circuit diagram (one channel).

Noise measurements at the receiver output for different light levels showed it to be dominated by shot noise in the photocurrent. The S/N at the reference channel photoreceiver output has a constant value of ≈ 65.6dB, while at the reflected channel receiver output the S/N varies from a maximum of 62.8dB (for a full scale output obtained with a cold, clean, sample) to a minimum of 54dB at the low end of the expected signal dynamic range (obtained with a cold sample covered by ≈ 1085Å of oxide).

After the elimination of quadrature noise in the synchronous detector and the S/N improvement due to the switched integrators, the specified aim for S/N was satisfied.

III.5.4 Synchronous Demodulator

A channel of the synchronous demodulator is shown in Fig II.10. The reference signal for the synchronous detector is derived from the chopper reference output and is opto-isolated to avoid any interference or ground loop signals being introduced into the low level analogue channels. The square wave fundamental is then extracted with a low pass filter (LPF) and passed through a variable phase shifter (approximately 0-2π rads), followed by amplification and conversion into a square wave drive signal for the demodulators.

Both demodulator channels consist of a high pass filter (HPF), the synchronous detector itself and a final LPF to remove any fast switching transients.

II.5.5 Switched integrator module

The circuit lay-out is shown in Fig II.11. This module performs the two distinct functions of providing S/N improvement and a DC level proportional to the rms value of the inputs.

The switching sequence of the integrator is computer controlled via the BBC Printer Port. The signals are buffered via digital opto-isolators to avoid digital interference from the computer, thus enabling complete isolation of digital and analogue power supplies.

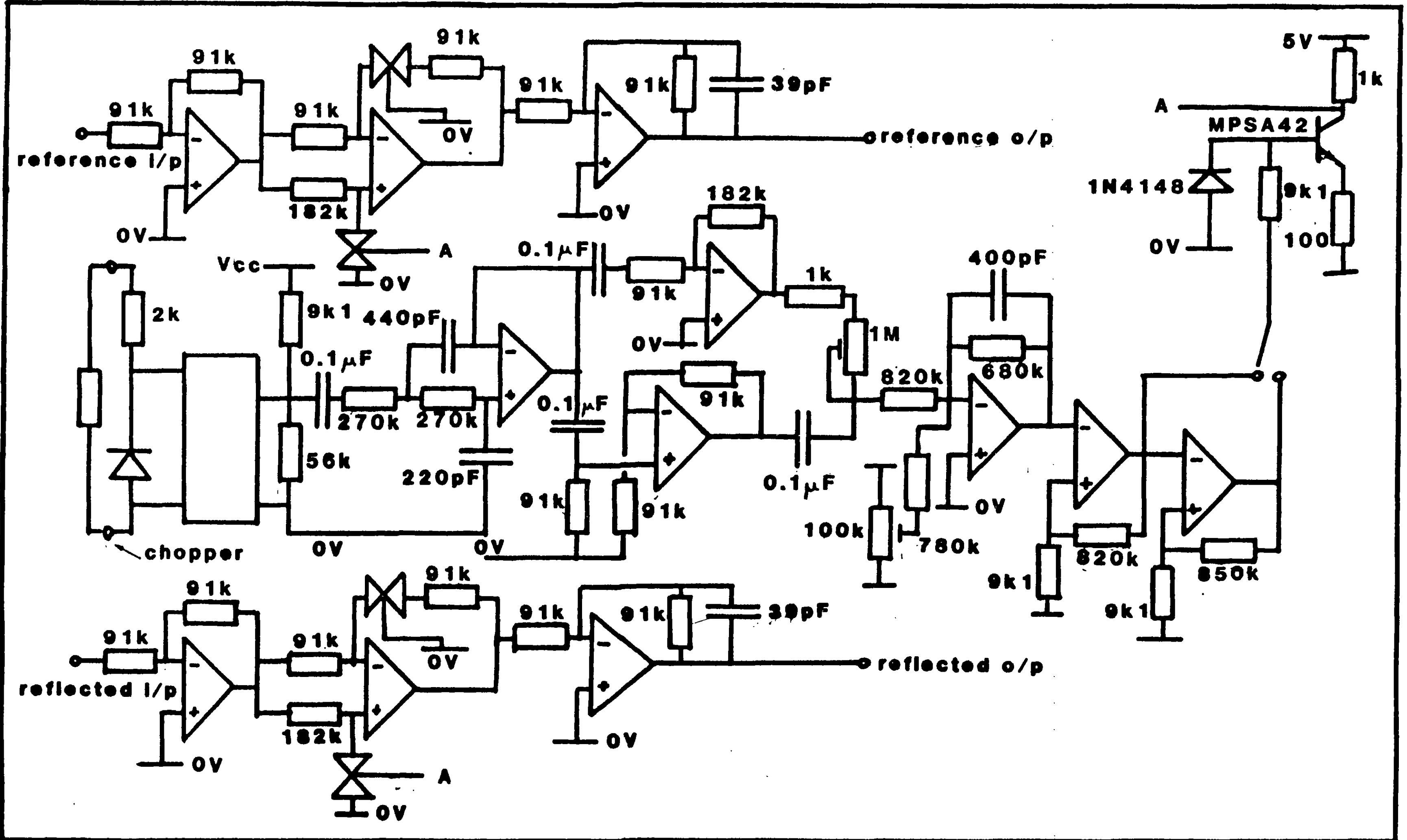

Fig II.10: Synchronous demodulator circuit diagram.

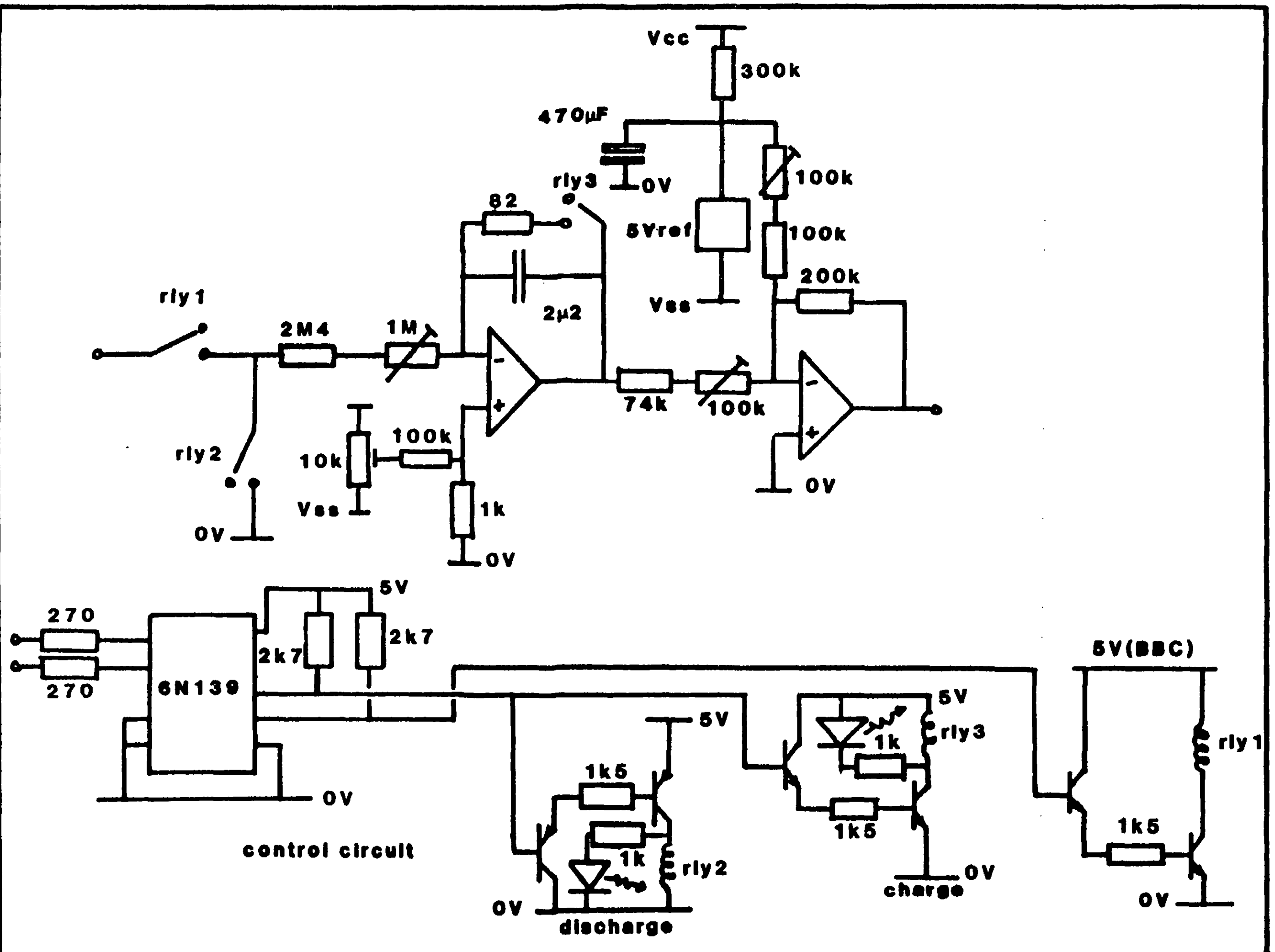

Fig II.11: Switched integrator circuit diagram (one channel).

Each sequence stage is indicated by LEDs in the box for ease of testing. Four preset adjustments are provided:

a-b) course and fine gain adjustment of integrator to optimize signal handling capacity ;

c) 'droop correction', which compensates for the input offset voltage of the op amp (which could result otherwise in output drift);

d) offset adjustment, to set module minimum output voltage at the bottom of the A/D range. This adjustment is derived from a highly stable band gap reference device to avoid temperature and power supply derived drifts.

In practical integrators a major source of errors are input offset voltage (V_{io}) and bias current (I_B). Referring the integrator offset errors to the output voltage V_0, we have:

$$dV_0/dt \text{ (due to offset)} = \pm V_{io}/CR + I_B/C \qquad (2.7)$$

As the op amps have JFET input stages, I_B is rather small (≈ 5 pA) and can be neglected in our application.

The input offset voltage is of the order of 1mV, large enough to be a problem (A/D resolution is approximately 0.5mV). The quantity 1/CR is the integrator "gain" and cannot be increased arbitrarily, but V_{io} can be minimized with simple circuit considerations. The actual nulling of the voltage offset can then be performed (via the droop correction pot) by converting the integrator to a high gain amplifier at the temperature of operation.

When, at the end of each integration, the input voltage of the integrator is switched to zero (open circuit), the output should ideally 'hold' at any value it may have reached, but finite open loop gain A_0 and finite input resistance R_d, in addition to amplifier offsets and capacitor dielectric leakage currents, contribute errors in HOLD mode:

$$dV_0/dt \text{ (hold mode)} = V_{start} / [C(A_0 R_d) \mathbin{//} R_{cap}] + I_B/C \qquad (2.8)$$

With $A_0 \approx 106dB$ and $R_d \approx 10^{12}ohm$, the losses in the capacitor are probably the dominant factor and a very low leakage capacitor must be used. Tests have been performed on the integrators and the drift has been found to be negligible for the HOLD time during which the A/D is collecting data.

The repeatability of the integrator was tested with a primary cell input, resulting in consistency to +1 (or -1), which is the fundamental count inaccuracy of the A/D (separately checked); therefore, there is no degradation in the response due to integration errors.

The integrator linearity has been confirmed by testing with a potentiometer and a high accuracy digital voltmeter.

II.5.6 A/D Conversion

Our original intention had been to use the internal A/D converter of the BBC computer. This proved impossible when initial tests showed that the, theoretically, 12-bit converter was limited to 8 bits of accuracy due to digital interference within the computer affecting the A/D reference circuitry. As a result, it was decided to construct an external A/D converter using a 12-bit + polarity dual slope integrating A/D type INTERSIL ICL 7109 CPL. These devices are guaranteed monotonic and accurate to one LSB (Least Significant Bit). The linearity is specified as ± 0.2 LSB. The maximum conversion rate is of the order of 30 conversions/sec.: this is not a problem in this application and results in a low price.

An extremely useful property of this class of devices is its ability, with an appropriate clock frequency, to reject 50 Hz interference.

The input signals from the two channels (while in HOLD mode) are sequentially presented to the A/D via a relay multiplexer controlled from the computer. Being in practice a 13-bit machine the output data has to be transferred into the 8-bit byte user port of the BBC as a pair of sequential 8-bit bytes. LEDs in the box indicate the channel being converted.

Analogue and digital grounds are isolated to avoid interference (ground current loops are also minimized by using a star grounding

configuration between the various boxes).

The A/D 'driver' software (and A/D chip-bus wiring) have been checked in situ by using an accurate voltage source to cause A/D to generate codes corresponding to boundary conditions (i.e. 0, 1, 4094-5-6, 8191).

II.5.7 Global performance tests

We have compared thickness data obtained by ellipsometry on thermally or laser-oxidized silicon samples with readings from our monitor and have found an excellent agreement in the range examined (≈ 35 Å to ≈ 875 Å), as shown in the insert in Fig III.10. In both cases n_{ox} was fixed to 1.458.

A resistive heater and a thermocouple have been used to perform comparative tests on temperature readings, though the upper value available of ≈ 400 °C clearly limited somewhat the validity of the measurement.

The large increase in reflectivity which follows melting of silicon has often been used as a calibration point for temperature at 1412 °C. The limited bandwidth of our monitor prevented us from seeing this effect. However, we could easily monitor the sudden loss of signal due to scattering which immediately follows the onset of the liquid phase. By measuring the temperature as a function of increasing laser power, the extrapolated value of the melting temperature obtained was always close to 1410 °C (all these measurements were performed under vacuum to enable such high temperatures to be reached and also to avoid oxide growth).

Since there is not yet any established technique for reliable, in situ, temperature measurement with high spatial resolution, we could not completely verify our predicted accuracy in the determination of the temperature over the whole range of interest. Nevertheless, the limited set of experimental confirmations obtained allows us a certain degree of confidence and, hence, these present measurements remain the first to be achieved in-situ.

CHAPTER III

Thermal Modelling and Oxidation Results

III.1 Introduction

A brief description of the thermal model for the irradiated Si sample is first presented. The remainder of the chapter introduces the main experimental results obtained. A more complete analysis and comparison with similar type of work is described in the next chapter. Only one or two representative examples for each set of data will be presented here. The next chapter will indicate the statistical significance achieved with the more complete picture.

III.2 Modelling of Silicon Temperature

It has been already shown here that silicon oxidation is a strong function of processing temperature and that one of the reasons for building the reflectometer was the need of knowing the surface temperature with the desired accuracy.

The problem of temperature monitoring during various forms of laser processing is well known. A large amount of theoretical modelling has appeared in the literature in the last ten years, in contrast to the shortage of reliable, all purpose, experimental techniques.

Most available heating models deal with the more common situation where a semi-infinite heat sink assumption is valid, i.e. where the condition

$$t \ll L^2/4D$$

applies, with L being the substrate thickness, D the thermal diffusivity of the material and t the irradiation time. This was patently not the case for our experimental conditions, where the sample was almost in thermal isolation and uniformly irradiated by a CW laser.

A simple model was generated to obtain a rough estimate of the

processing temperature. Under conditions of perfect thermal isolation the only heat losses present would be radiative. It became apparent though, through comparison of our theoretical simple approximation with a set of experiments performed under different pressure and irradiation conditions, that both conductive losses through the quartz holder and convective losses in the oxygen atmosphere could not be neglected [CARSLAW et al., 1959].

The same experiments provided enough data to build an approximate model of these losses (an accurate prediction would have required the solution of an extremely cumbersome 3D heat flow equation and the precise knowledge of a variety of physical and geometrical parameters for which we could only assume approximate values).

Finally, the simplified heat balance equation could be written as:

$$P[1-R(T)] - A\epsilon(T)\sigma(T^4-T_0^4) - K(T)S(T-T_0)/l - GA(T-T_0)^{5/4} = CV\rho\,\delta T/\delta t \tag{3.1}$$

where

P: incident laser power;

R(T): temperature dependent silicon reflectivity;

$\epsilon(T)$: temperature dependent silicon emissivity; a constant value of 0.65 has been used in the model [SATO, 1967];

A,V: sample surface area and volume;

σ : Stefan's constant;

K(T): temperature dependent quartz thermal conductivity;

S,l: geometric parameters of quartz holder;

G: convection coefficient in still air;

ρ : density of silicon (2.33 g/cm^3);

C: specific heat/unit mass of silicon (0.95 J/g K);

T_0: background temperature.

The expression for quartz thermal conductivity was obtained by curve fitting data found in the literature [AIP Handbook, 1973] and in data sheets provided by quartz suppliers. An empirical relationship between silicon reflectivity and temperature for photon energies below approximately 3eV was found by Jellison [JELLISON, 1984]:

$$R(T) = R(T=300\ K) + 5\times10^{-5}(T-300) \quad (3.2)$$

and was used in our model.

The sample was assumed to be uniformly irradiated (we ignored, therefore, the Gaussian shape of the beam) and to uniformly heat up throughout. Thus no consideration was paid to the temperature dependence of silicon thermal conductivity (K_{Si}) which is of considerable importance in the semi-infinite heat sink case. A comprehensive collection of data for K_{Si} as a function of temperature has been published [HO et al.1974]. In fact, K_{Si} decreases by over 80 % passing from room temperature to 1200 °C and it is possible that, at very high temperatures, there could be a more pronounced 'heat confinement' on the silicon surface than at lower temperatures.

In Fig II.4 was shown an example of the rapid heating times, calculated with the model, for a 3x3mm, 400μm thick, silicon sample, for various laser powers, at λ= 514.5nm.

An example of computed equilibrium temperature as a function of laser power at λ=514.5 nm is also shown in Fig III.1 (dotted line). A check on the validity of the model was performed with a disappearing filament pyrometer, starting from approximately 700 °C (also shown in Fig III.1). The very satisfactory agreement between the values obtained by modelling, with the pyrometer and, finally, the reflectometer (Fig III.1), confirmed the validity of this simplified model (needed for the oxide growth computer simulation presented in next chapter) and also the suitability of the instrument for this particular type of measurement.

Every time a new batch of Si samples was cleaned, a plot similar to Fig III.1 was obtained in order to feed the appropriate parameters to the growth simulation program.

A maximum δT of approximately 2% was measured with the reflectometer between the centre and the edge of the 3x3mm sample, when covered only by native oxide and at temperatures 820-870 °C. This confirmed the validity of our uniform irradiation approximation.

Even greater uniformity was obtained with the alternative sample holder mentioned in paragraph II.2, confirming the lower thermal losses obtainable with this, rather impractical, configuration.

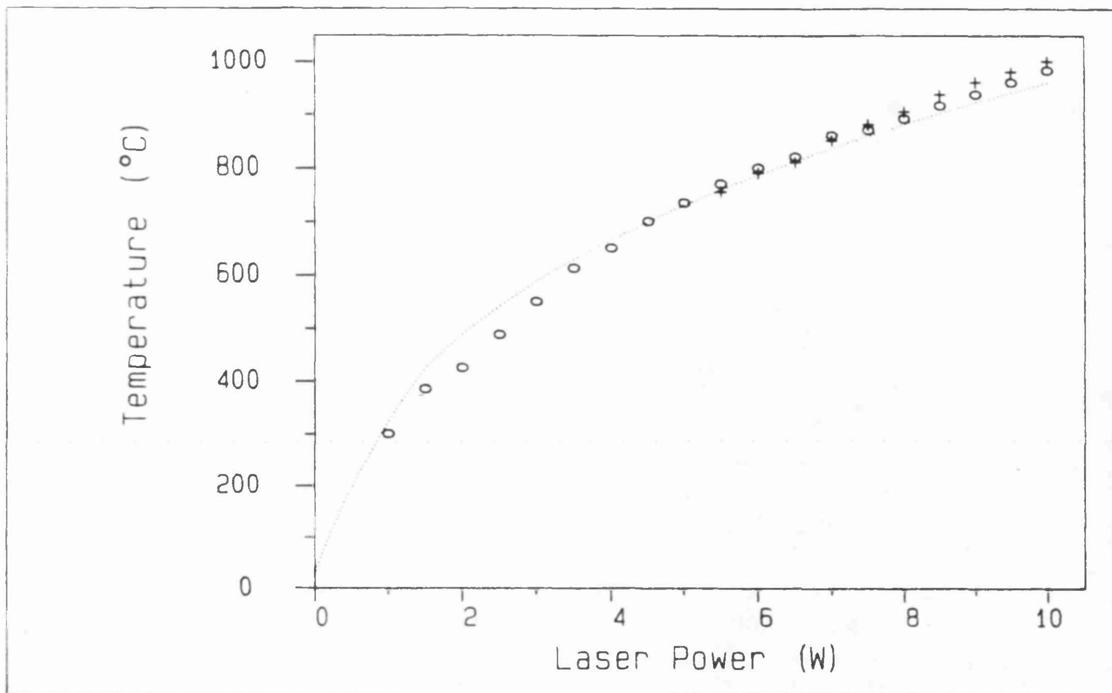

Fig III.1: Silicon temperature as a function of laser power (514nm).
Dotted line: computer model;
o: experimental data (reflectometer);
+: experimental data (pyrometer).

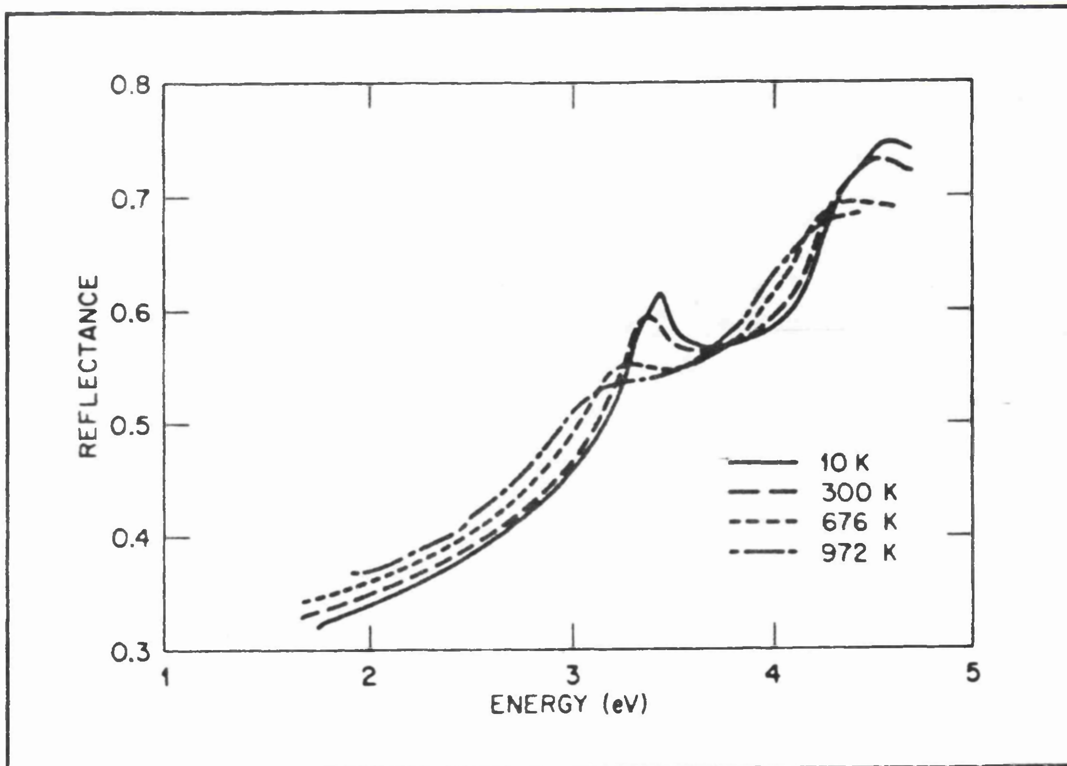

Fig III.2: Normal incidence reflectivity of silicon as a function of photon energy (at several temperatures) [JELLISON, 1984].

III.3 Initial experiment

Following the initial investigations [SCHAFER et al., 1981; BOYD et al., 1981; YOUNG et al., 1983] on silicon oxidation with visible light, we carried out some experiments in order to explore possible photonic effects on the growth rate.

Our work intended not only to reduce the thermal contributions to the oxidation induced by the photons, but also to amplify the photonic enhancement that these previous groups of researchers had noticed. Contrary to most previous work, the only source of energy for our oxidation process was the laser and, as a consequence, much higher power densities (and, therefore, photon fluxes) than ever before were involved.

The aim was to examine the oxide growth kinetics induced by the two most powerful lines of the Ar laser and deduce any possible difference which couldn't be ascribed to thermal factors [MICHELI et al.,1987]. The reflectometer was not developed at this initial stage.

The incident beam power was adjusted so that the same power of $\approx$ 4W was absorbed at each wavelength at the beginning of the oxidation. The optical pyrometer indicated an approximate temperature of 800-830 °C. Fig III.2 shows the Si normal incidence reflectivity as a function of photon energy, while Figs III.3 and III.4 show, respectively, the curves for reflectivity and power absorbed by the sample as a function of oxide thickness at 514.5 and 488nm and at room temperature, where values for n_s, k_s and n_{ox} have been taken from the literature [JELLISON, 1984]. It is clear that a growing oxide will decrease the sample reflectivity which, in turn, will increase the laser power absorbed by the surface. This will lead to an increase in the sample temperature, giving rise to an accelerated oxide growth and to thicker layers, in a classical positive feedback loop arrangement, until a thickness of approximately 900Å is reached. In these experiments we limited the film thickness to 850Å.

From these data alone it was not possible to extract quantitatively any photonic influence to the process. However, by carrying out the experiment at two different wavelengths under essentially identical irradiation conditions, any initial difference in the growth rate would be amplified by this positive feedback mechanism.

Fig III.5 shows the oxide thickness as a function of exposure time for the two wavelengths considered. For short exposure times, the

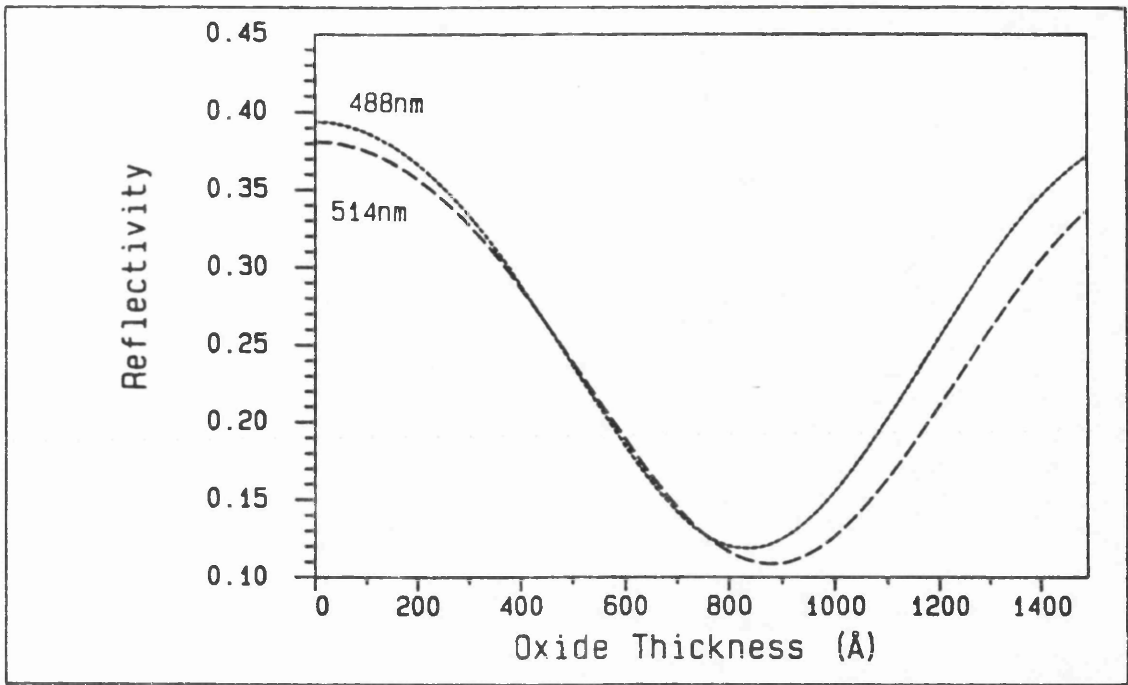

Fig III.3: Normal incidence silicon reflectivity (at 514nm & 488nm) as a function of oxide thickness.

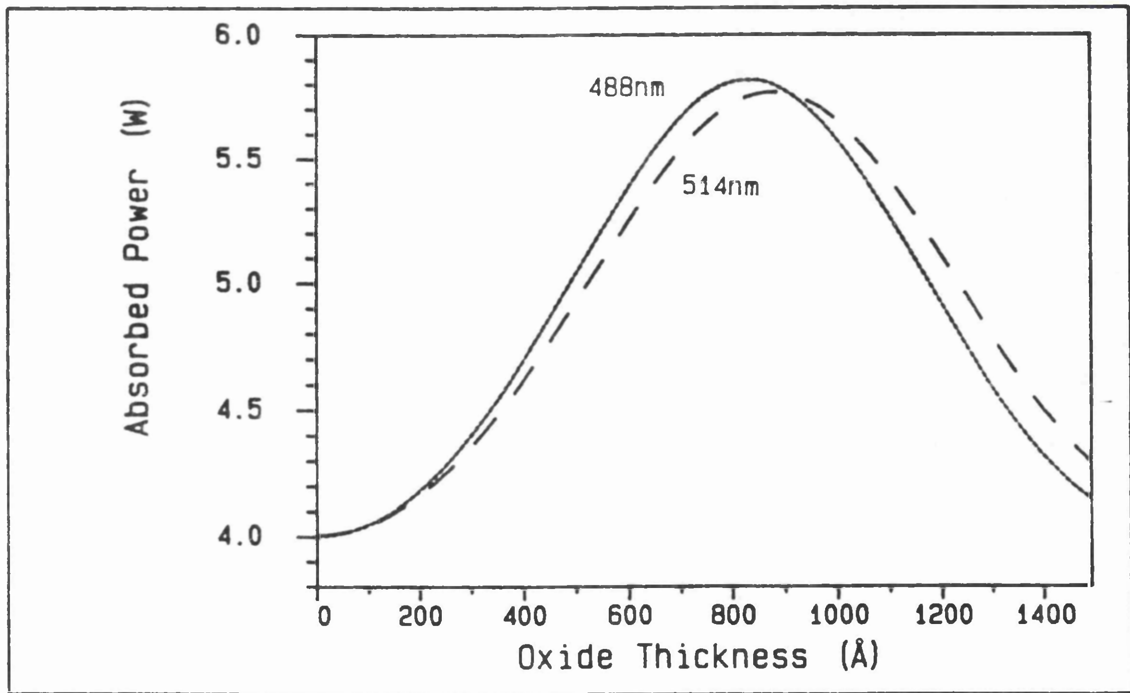

Fig III.4: Power absorbed by sample (at 514nm & 488nm) as a function of oxide thickness [MICHELI et al., 1987].

oxide thicknesses produced were very similar, while at longer exposures there was an obvious increase in oxide thicknesses grown by the longer wavelength. Thus, the reaction rate at 514.5nm was consistently faster than the corresponding rate at 488nm.

The absorption coefficients at 514 and 488nm are approximately $8x10^4$ and $1.2x10^5 cm^{-1}$ at 800 °C, respectively [JELLISON, 1984, and references therein] (Fig III.6). It may be argued, therefore, that if any difference was to be expected from thermal considerations only, the shorter wavelength radiation, with its shorter absorption length, would induce higher surface temperatures and thus faster oxidation rates. Moreover, it can be seen from Figs III.3 and III.4 that, at the thicknesses under consideration, the 488nm radiation could again be expected to produce a faster growing oxide from the faster change in sample reflectivity and, therefore, absorbed power during growth. It is also well known that neither O_2 nor SiO_2 absorbs preferentially one of the two wavelength used here. The laser beam waist was measured in both cases and found to be the same. We can conclude, therefore, that some photonic effect must be at the origin of this difference in growth rate.

Such a wavelength dependence of the oxidation rate has been reported in previous work [SCHAFER et al., 1982; YOUNG et al. 1983], but given the close proximity of the wavelengths in question and the uncertainties still present in the accurate evaluation of the absolute value of the temperature, any difference present has traditionally been too small to see with any degree of confidence without the amplification technique employed here.

By using an initial version of Massoud's model for dry oxidation of silicon [MASSOUD et al.,1985], we loosely quantified the degree of photonic difference in the growth rate induced by the two wavelengths, in terms of our representative thermal model. We found that, based on these preliminary results, an increase of approximately 20-25% in the equivalent thermal oxidation rate, when simulating the 514nm radiation processing, could account for the differences in growth rate due to photonic effects. It should be pointed out, though, that Massoud's model was strictly valid only for oxide thicknesses greater than ≈ 350Å; it was nevertheless used at the time as a first approximation.

In conclusion, by amplifying small differences in the oxide growth

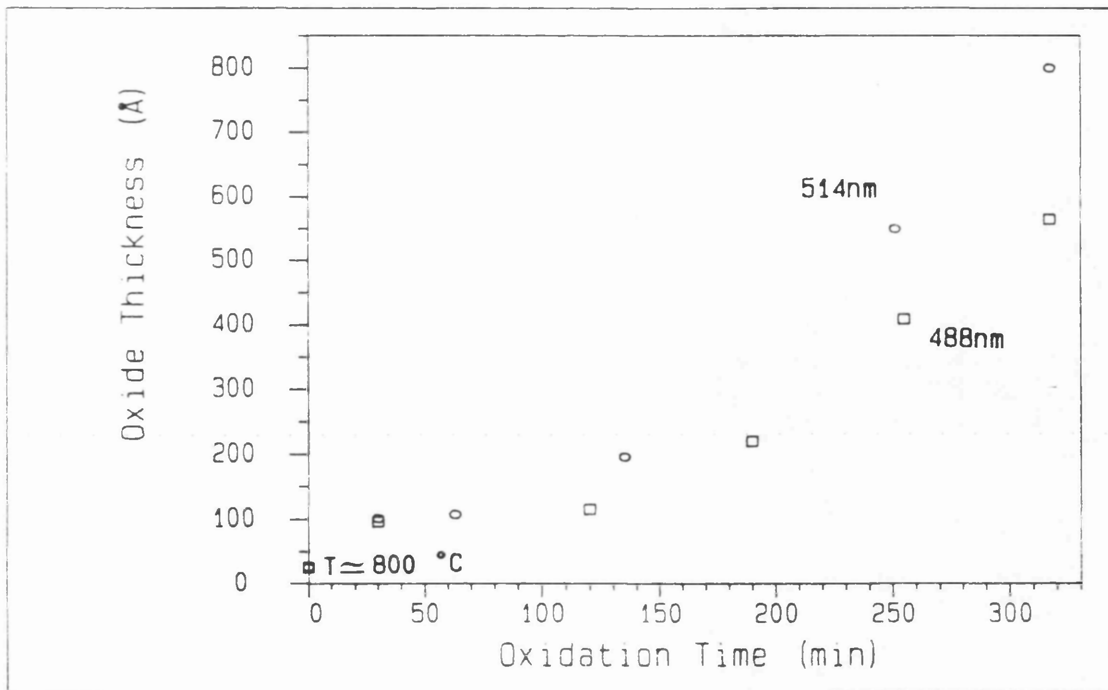

Fig III.5: Oxide thickness as a function of exposure time for <100> Si.

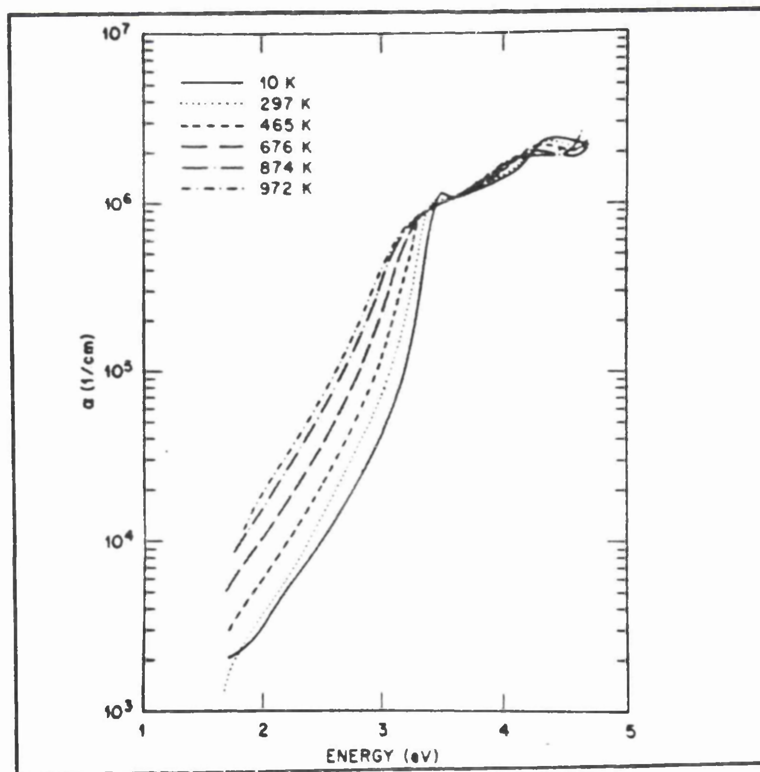

Fig III.6: Absorption coefficient of silicon at several temperatures as a function of photon energy [JELLISON,1984].

rate arising from some non-thermal effects, we initially succeeded in confirming the existence of a photonic effect in the visible light range. The experimental difficulties encountered during the collection of oxidation data clearly demonstrated that a great advantage could be achieved with the realization of an in-situ monitor for oxide thickness and temperature.

As a consequence, all the experimental work reported in the following pages was carried out with the instrument in position, leading to a much higher degree of accuracy and repeatability.

III.4 Experimental work

To obtain a statistically meaningful set of data, the original experiment was repeated a very large number of times with a range of laser powers (and, therefore, initial temperatures). The effects of <100> and <111> orientations and lightly and heavily doped samples have been explored.

III.4.1 Lightly boron doped <100> Si

Being one of the most commonly used silicon types, we decided to study <100> boron doped (p-type) silicon with a resistivity of 15 to 30 Ωcm. Some typical results are shown in Figs III.7 to III.9. The initial temperatures shown here represent the extremes of our range of interest. As can be seen, these considerably more accurate results qualitatively confirmed our original findings that the 514nm line induces an enhanced growth rate with respect to the 488nm, though this difference is very much reduced from what it was originally thought to be. Any discrepancies between the corresponding data in the original and present experiments have obviously to be ascribed to the tentative experimental approach used in the preliminary set up.

The dotted curves in Figs III.7 to III.9 (and in all following figures in this chapter) were obtained by polynomial least square curve fitting of the data.

To better visually appreciate this enhancement effect, Figs III.7 to III.9 also show the final oxide thicknesses obtained (for both

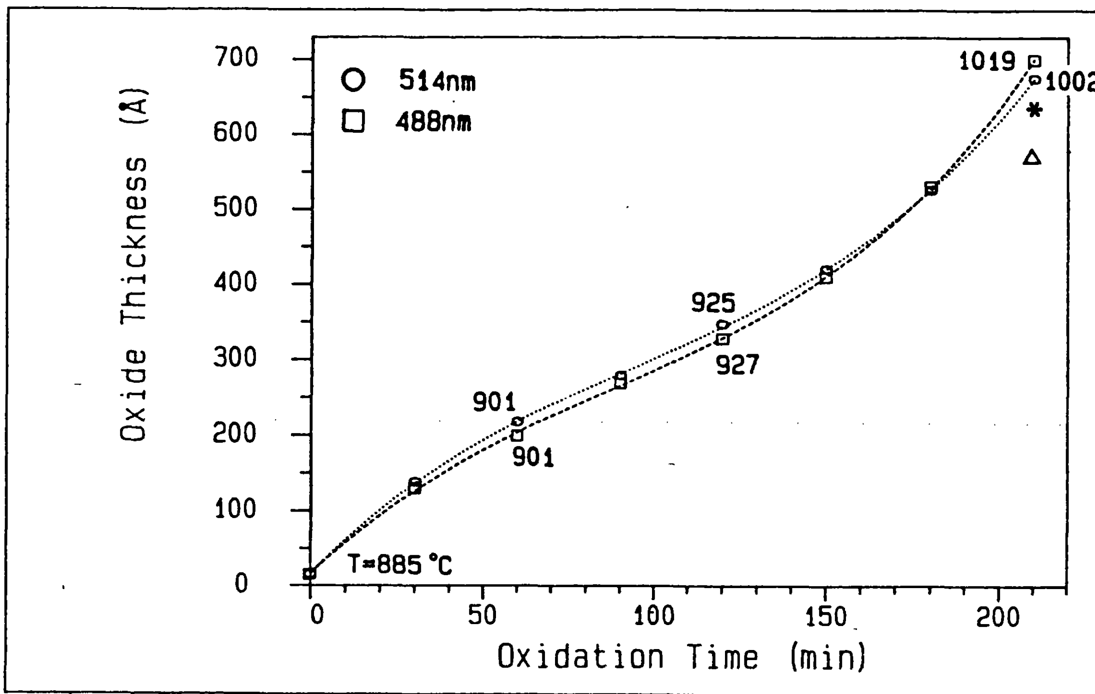

Fig III.7: Oxide thickness as a function of exposure time for <100> Si. Final thicknesses from a purely thermal oxidation model: △ : 514nm; * : 488nm. Error bars are of the order of the dimensions of the symbols.

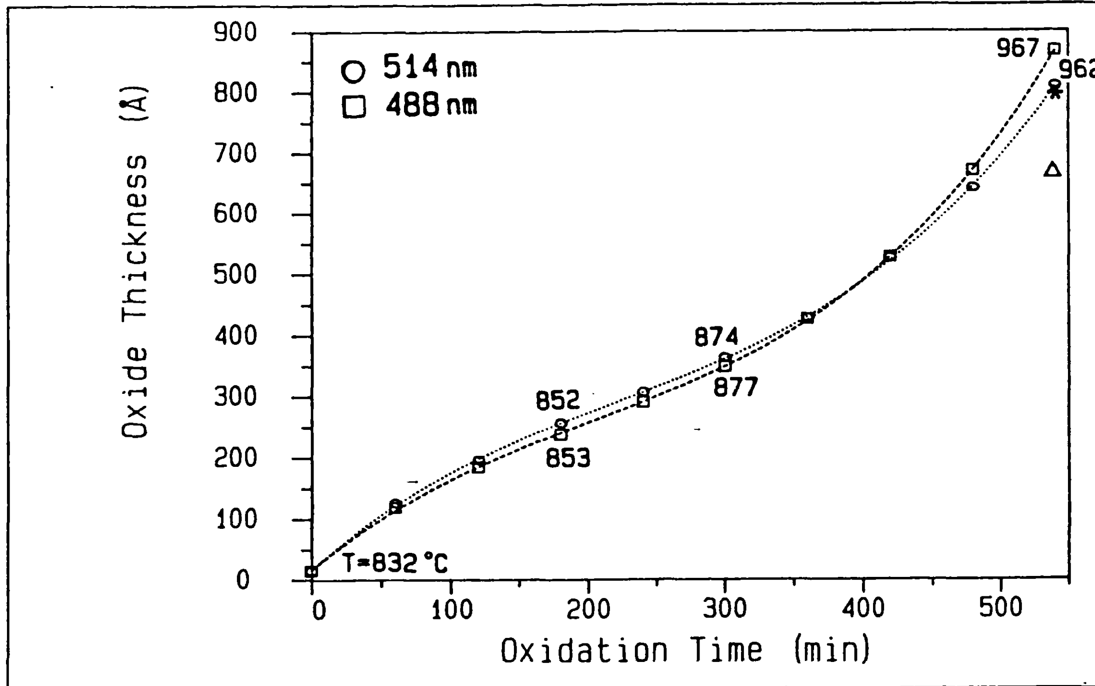

Fig III.8: Oxide thickness as a function of exposure time for <100> Si. Final thicknesses from a purely thermal oxidation model: △ : 514nm; * : 488nm. Error bars are within the dimensions of the symbols.

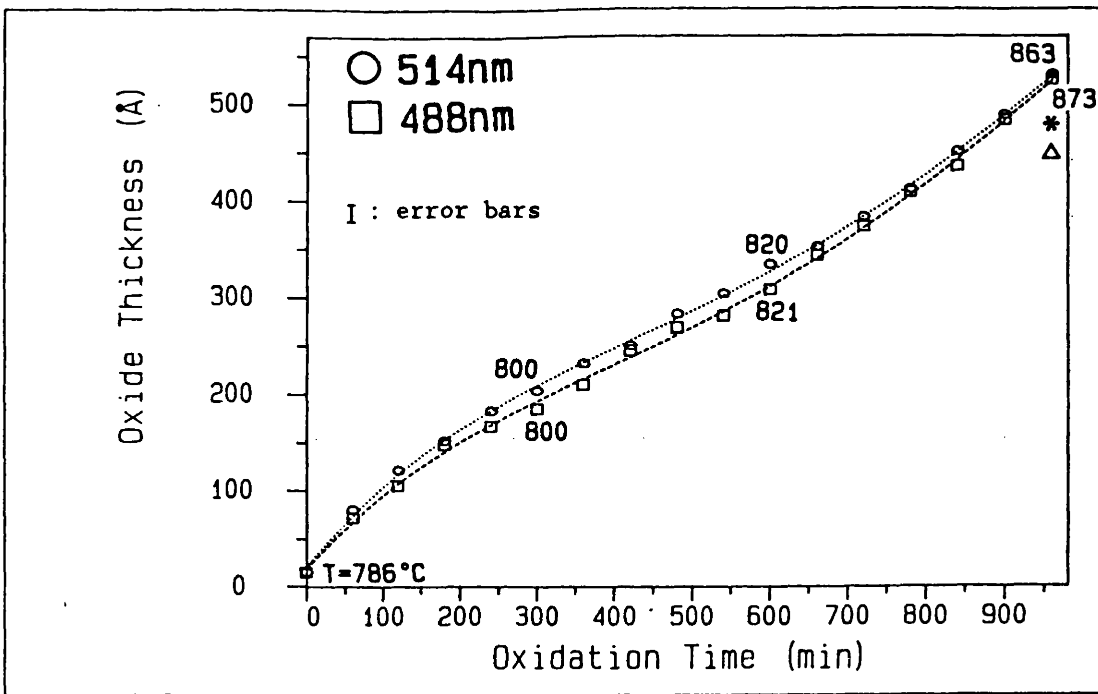

Fig III.9: Oxide thickness as a function of exposure time for <100> Si. Final thicknesses from a <u>purely thermal</u> oxidation model: △ : 514nm; ✱ : 488nm.

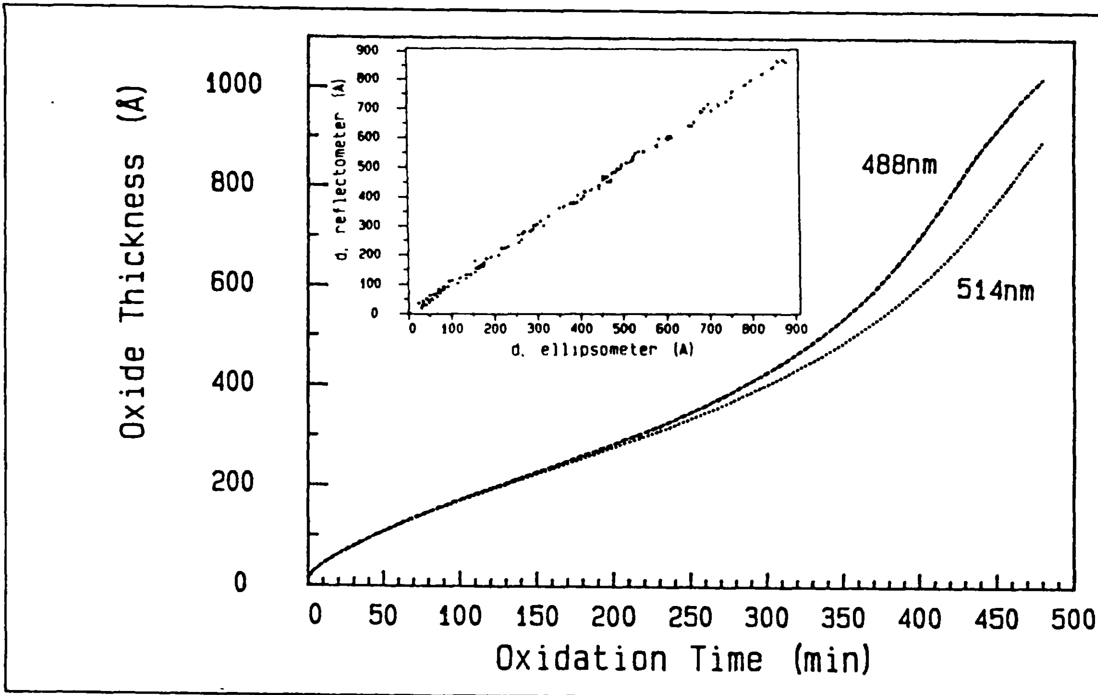

Fig III.10: Oxide-thickness as a function of exposure time for <100> Si (computer model with a purely thermal oxidation rate). The insert shows the correlation between thickness measurements performed on the ellipsometer and on the reflectometer.

wavelengths) with Massoud's most recent model for Si thermal oxidation in dry O_2 [MASSOUD, 1987], adapted to our laser processing situation and thermal configuration. Fig III.10 shows complete curves of thickness as a function of oxidation time obtained with the same purely thermal model. Independent of the shape of the two set of curves (experimental data or models), it is apparent that there has been a relative shift between the 514nm and 488nm oxidation curves, indicating a relative increase in the growth rate induced by the longer wavelength (514nm).

This differential enhancement was confirmed by a large number of experiments carried out at various temperatures.

III.4.2 Double-side polished Si

The encouraging results obtained in previous experiment suggested a simple follow-on experiment: to repeat the 514nm and 488 nm oxidation as before, but on double-side polished (DSP) silicon samples (<100>, lightly boron doped). For DSP silicon, the oxide growth rate (and, therefore, the thickness) on the silicon underside is determined by the temperature differential with the front surface. This value is unknown and rather difficult to calculate accurately at every temperature during the oxidation process, though it can be roughly estimated by a simple one dimensional heat flow model to be of the order of 1.0–3.0 °C with our silicon thicknesses and processing temperatures (similar values were found by Young and Tiller [YOUNG et al, 1987] in a different, but somewhat related, experiment). The oxidation of the silicon underside is always a purely thermal process as no photons impinge upon this surface and the absorption length in Si at 800 °C at these wavelengths is of the order of 0.1 μm, orders of magnitude smaller than the silicon thickness.

In Fig III.11 we have a qualitative example of 514nm and 488nm thermal growth curves together with the final values of the oxide thickness on both the undersides. As the average temperature during growth is greater for the 488nm than for the 514nm (because of the effect shown in Fig III.4) there will be a thicker oxide on the back surface of the 488nm sample than on the back surface of the 514nm sample. Since the final front temperatures are fairly close, the ratio between the two front oxide thicknesses (F_{514}/F_{488}) must be the

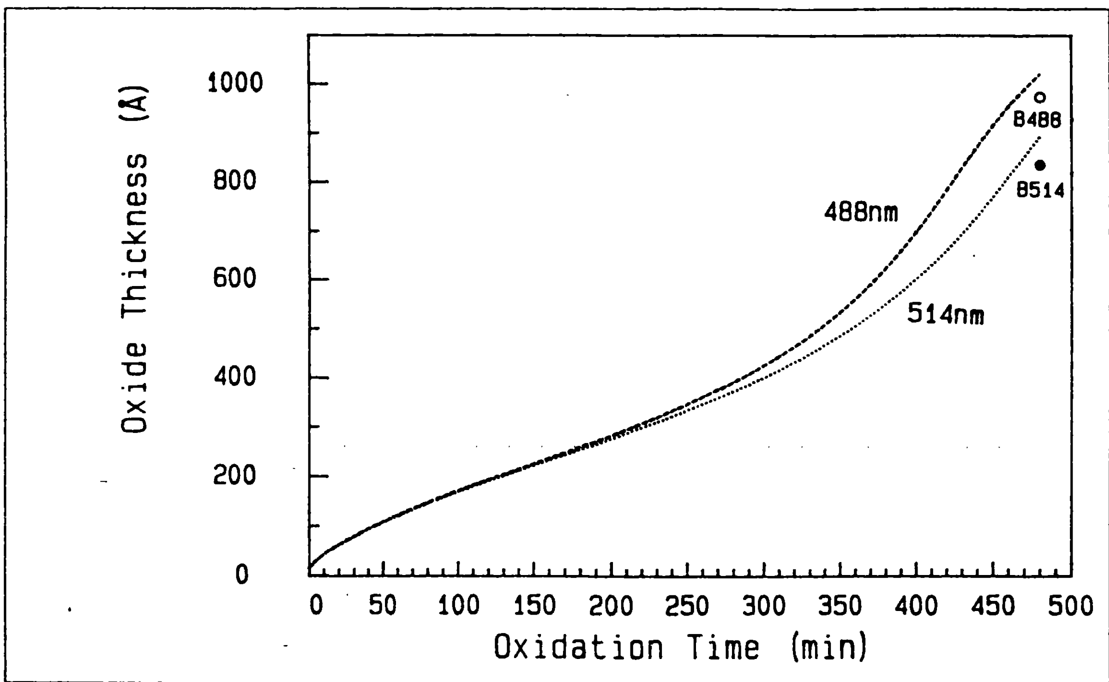

Fig III.11: Oxide thickness as a function of exposure time for <100> Si (computer model with a purely thermal oxidation rate). The points are examples of back surface oxide thicknesses.

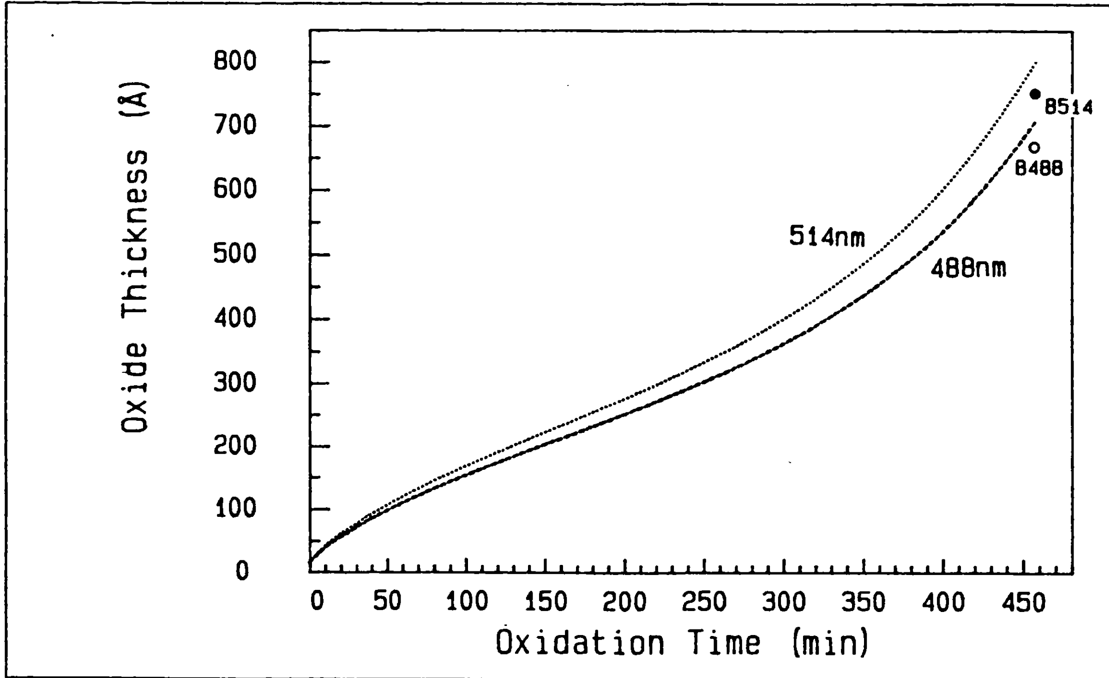

Fig III.12: Oxide thickness as a function of exposure time for <100> Si (computer model with a purely thermal oxidation rate as in Fig III.11, but with the 488nm growth rate reduced by 9%). The points are examples of back surface oxide thicknesses.

same as the ratio between the two oxides grown on the back surfaces (B_{514}/B_{488}).

If there was a photonic enhancement on the growth rate of the front oxides which was considerably larger for the 514nm than for the 488nm, the resultant picture would be as shown in Fig III.12. Here the 514nm average temperature will be higher than the corresponding 488nm and it is now clear that:

$$F_{514}/F_{488} > B_{514}/B_{488} \text{ (and both > 1)}$$

as the back oxides reflect only the temperature differential while the front oxides show the double effect of temperature differential and photonic effects on the growth rate. The relative enhancement in the growth rate can be estimated from the difference of the two ratios (always assuming the final temperatures to be quite close).

Therefore, the DSP Si acts as a filter for the relative photonic effects on the growth rate.

Figs III.13 and III.14 show the results for high temperature and low temperature oxidations, respectively. In both graphs, the results of four experiments are actually presented. From Fig III.13, for thin oxides and temperatures around 900 °C, we have:

$$F_{514}/F_{488} - 1 \approx 0.079$$

i.e. a relative enhancement of approximately 7.9%.

For thicker oxides, at temperatures around 1030 °C:

$$F_{514}/F_{488} - B_{514}/B_{488} \approx 0.0143$$

i.e. a relative enhancement of approximately 1.4%.

To examine further the effect of the processing temperature on this growth rate differential, a much reduced value for the initial temperature was chosen in the experiment whose results are shown in Fig III.14.

The smallest thickness considered at these temperatures (≈ 800 °C) was chosen very close to the thinner case in the previous example. We

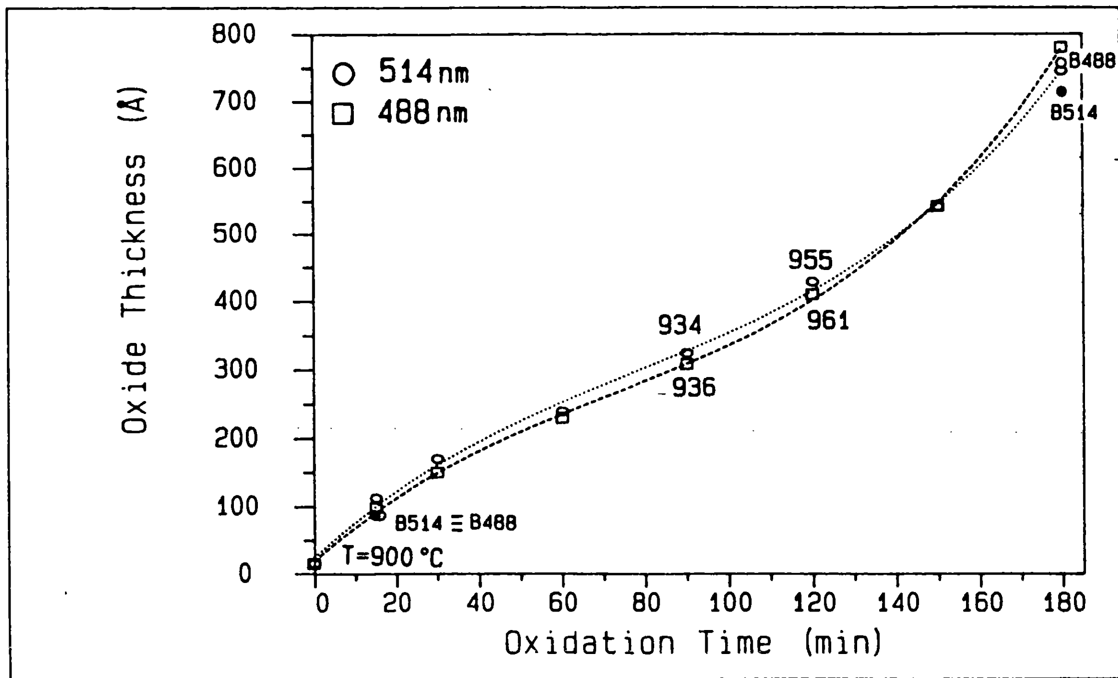

Fig III.13: Oxide thickness as a function of exposure time for <100> DSP Si and high oxidation temperature. Error bars are of the order of the dimensions of the symbols.

- • : oxide thickness on the back Si surface (514nm);
- o : oxide thickness on the back Si surface (488nm).

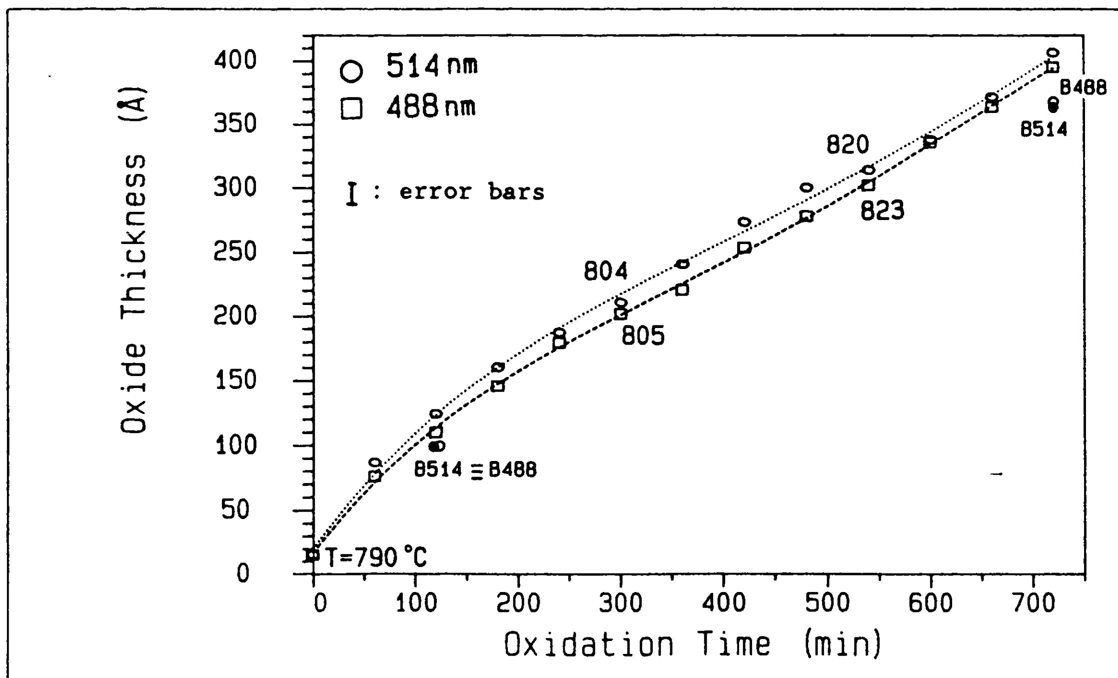

Fig III.14: Oxide thickness as a function of exposure time for <100> DSP Si and low oxidation temperature.

- • : oxide thickness on the back Si surface (514nm);
- o : oxide thickness on the back Si surface (488nm).

can see that:

$$F_{514}/F_{488} - 1 \approx 0.09$$

i.e. a relative enhancement of ≈ 9%.

For the thicker oxides, at temperatures around 840 °C:

$$F_{514}/F_{488} - B_{514}/B_{488} \approx 0.0316$$

i.e. a relative enhancement of ≈ 3.2%.

As we can see from the data, the relative 514/488 enhancement ($\Delta g_{514/488}$) appears to have a slight dependence on thickness and temperature: the highest values are obtained at the smallest thicknesses and temperatures.

The great advantage, though, in the use of DSP silicon is that it gives direct information on the absolute enhancement in the growth rate obtained by either laser line (in the form of an upper limit for the non thermal enhancement).

From Fig III.13, at the lowest end of the 514nm curve, the ratio between the top and bottom oxide thicknesses, $(F/B)_{514}$, is approximately 1.27–1.28, i.e. the oxide thickness on the front surface is ≈ 28% higher than the oxide thickness on the underside of the same sample. Intuitively, this difference cannot be totally justified by a δT of a few degrees. Though this contribution cannot be exactly quantified, it is reasonable to assume it to be of a few percent and the computer modelling confirmed it. Furthermore, at the top end of the thickness range in the same curve, the ratio $(F/B)_{514}$ is approximately 1.08, giving a ≈ 8% total enhancement to the front side oxide. We notice therefore that the enhancement is considerably higher at small thicknesses. Since the temperature differential between the two sides, δT, is likely to increase slightly with the absolute value of T, so the ratio F/B should likewise increase, contrary to our findings. This clearly demonstrates that the difference in the two ratios cannot be simply justified in terms of thermal effects and that, whatever the origin of this enhancement, it is most effective at small oxide thicknesses.

Very similar considerations can be made by examining the 514nm

curve in Fig III.14. We obtain values of ≈ 31.4% and 13.4% for the total irradiated-side enhancement for thinner and thicker oxides, respectively. The photonic-versus-thermal enhancement at 514nm is higher at the smaller thicknesses and lower temperatures, the same trend noticed for $\Delta g_{514/488}$.

In conclusion, the DSP Si experiments have clearly shown the presence of a photonic enhancement in the oxidation rate in the range of laser powers and wavelengths used. The relative enhancement between the two laser lines could be calculated with a reasonable accuracy, while the absolute value with respect to thermal could only be assigned an upper limit as the instantaneous values of the temperature differentials between front and back surfaces are unknown.

III.4.3 Pre-oxidized substrates

Following the discovery of this thickness related enhancement, experiments were performed on a <100> Si substrate which had been previously thermally oxidized to 820Å.

Fig III.15 shows plots of the results obtained. The oxidation could not be extended any further as the instrument can only measure correctly thicknesses up to approximately 1080Å, as mentioned in Chapt.II.

At these thicknesses, the relative behaviour of the curves shown is quite similar to what would be obtained in the purely thermal case, i.e. the 514nm doesn't show an appreciable enhancement in its growth rate with respect to the 488nm line (obviously within the boundary of our experimental error and the applicability of our computer model to the real case).

III.4.4 Lightly phosphorus doped <111> Si

The 514/488 experiment was carried out also on a <111> n-type silicon (16 Ωcm ± 25%).

A typical plot is shown in Fig III.16. The thermal growth rate for <111> Si is generally known to be higher than for <100> Si, with

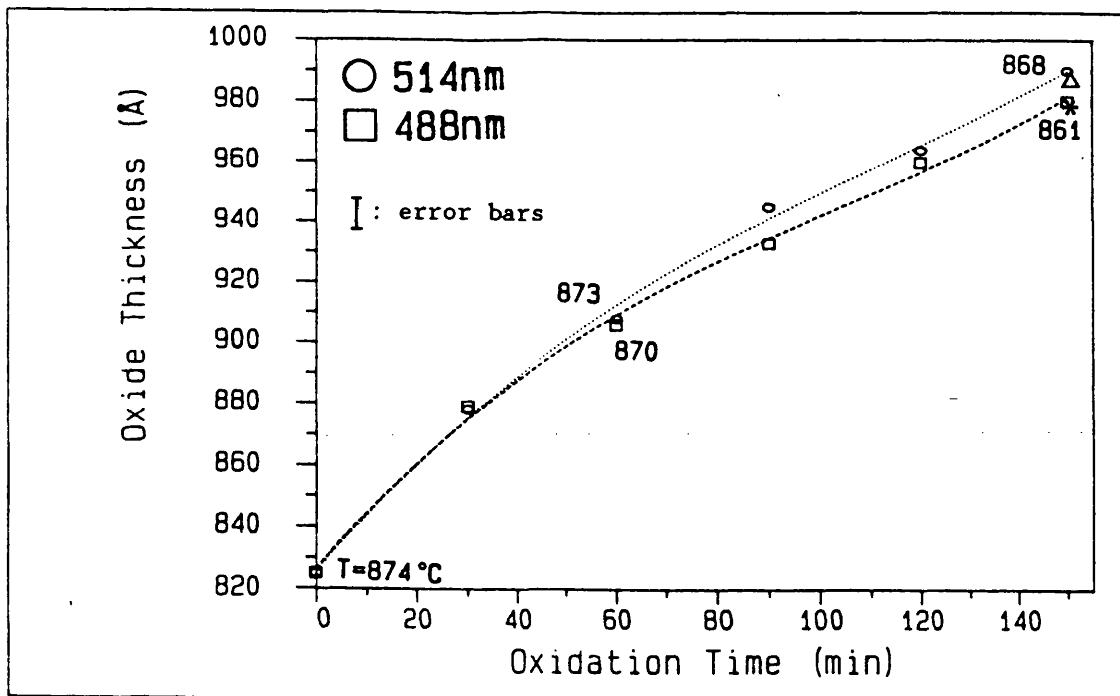

Fig III.15: Oxide thickness as a function of exposure time for a pre-oxidized <100> Si substrate. Final thicknesses from a purely thermal oxidation model: △ : 514nm; ✱ : 488nm.

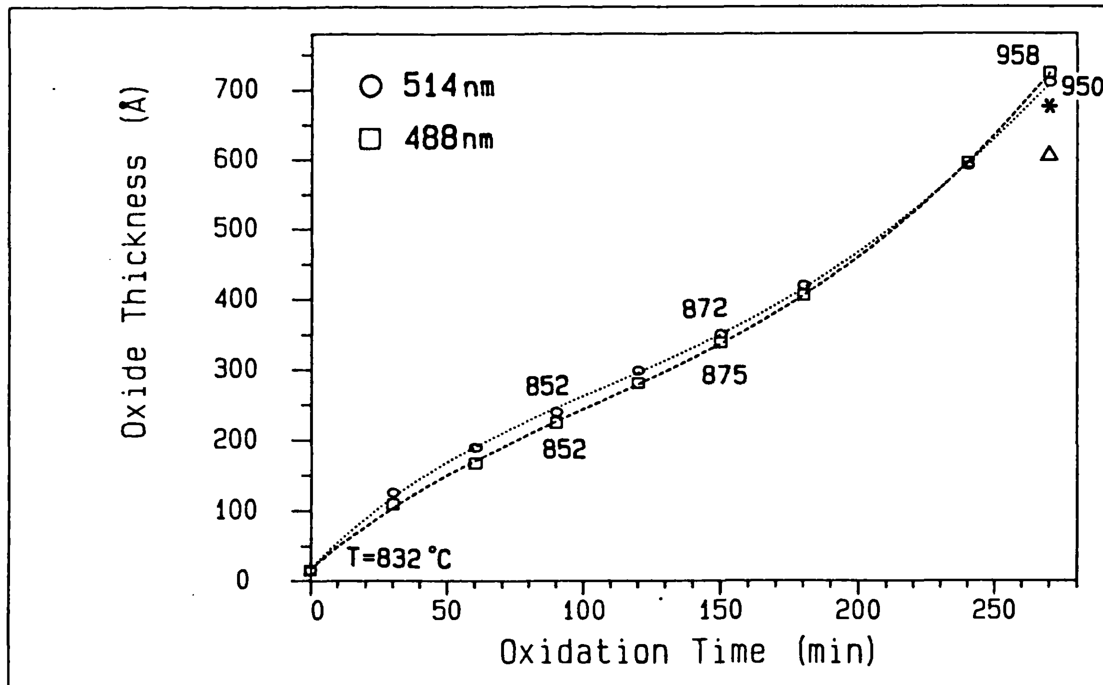

Fig III.16: Oxide thickness as a function of exposure time for <111>Si. Final thicknesses from a purely thermal oxidation model: △: 514nm; ✱ : 488nm. Error bars are of the order of the dimensions of the symbols.

effective density of surface atoms, atomic steps and stress considerations being mentioned as possible explanations of this behaviour [LEWIS et al.,1987]. Our data are in agreement with this general view, as can be seen by comparing the <111> results with the previous <100>. From this comparison we can also see that, as far as the relative 514/488 behaviour is concerned, this silicon orientation provided very similar results to the <100> case, i.e. the 514nm rate showed an enhanced value with respect to the 488nm. One should note that, although the two orientations used here were of a different doping type (light doping), at the high oxidation temperatures used silicon is essentially intrinsic.

It should also be pointed out that the same laws for $n_s(T)$, $k_s(T)$ and $n_{ox}(T)$ at 633nm were used for <100> and <111> Si, as they are embedded in the monitor program. At the temperatures used here, though, n_{ox} might not be identical in the two cases, as shown, for instance, by Landsberger and Tiller [LANDSBERGER et al.,1987]. However, such small differences will not affect the relative <100>/<111> results in any serious way.

III.4.5 Heavily doped Si

We repeated the 514/488 experiment with heavily doped samples. Boron doped <100> Si with dopant concentration $N \approx 3\times10^{19}cm^{-3}$ and phosphorus doped <100> Si with $N \approx 1.5\times10^{19}cm^{-3}$ were used.

The variation of the refractive index of silicon with doping gives a relative variation in reflectivity [OPSAL et al., 1987]:

$$\delta R/R \approx -10^{-22}\ N;$$

for $N \approx 1\text{–}3\times10^{19}cm^{-3}$, $\delta R/R \approx -\ 1\text{–}3\times10^{-3}$ or $\delta R \approx -0.35\text{–}1\times10^{-3}$ for R=0.347. Though the top range of δR could just be detectable with the reflectometer, it was nevertheless assumed that no significant error would be made by using the usual $n_s(T)$ and $k_s(T)$ expressions for the real and imaginary part of the refractive index of Si at 633nm.

Published results from furnace oxidation, in the temperature range we are interested in, indicate that the order of the overall oxidation rate is

$n^+ > p^+ \geq$ low doping

for P or B doping levels $\geq 10^{19}cm^{-3}$ [IRENE et al.,1978; HO et al.,1979; MASSOUD et al.,1985]. Different segregation coefficients and redistribution of impurities or enhanced generation of vacancies or interstitials at the Si/SiO_2 interface have been suggested to explain this effect.

This order was also broadly confirmed in our experiments, but due to the scarcity of data available for the thermal growth of either heavily doped material, it was not possible to separate the effects of possibly different types of enhancement in our data.

We have, however, confirmed that the n^+ samples showed consistently a thicker native oxide than p or p^+.

Jellison [JELLISON,1984] found a minor increase in the absorption coefficient α with B or P doping. However, it was not substantial and was practically the same for the two dopants at our two wavelengths. This could be due to a band gap shrinkage of less than $\approx$ 0.1eV (room temperature), which was also found to be independent of doping type (for P and B dopants [WAGNER, 1987]).

Considerable uncertainties exist over the values of the recombination time τ and the carriers' mobility μ for electrons and holes under our experimental conditions (heavy doping material under laser irradiation). At the doping levels and temperatures in question, we can assume an Auger recombination process to take place [SZE, 1981; PASSARI et al., 1983; DZIEWIOR et al., 1977; HULDT et al., 1979; FOSSUM et al., 1983]. From [WILLANDER et al., 1988] and the aforementioned papers we concluded that the diffusion lengths were in all cases of the order of a few μm and therefore much greater than the absorption length ($\approx$ 0.05-0.1 μm). No influence on the results was therefore expected.

Fig III.17 and III.18 show two examples of growth curves obtained for n^+ and p^+, respectively. One obvious difference stands out immediately from the graphs: while the p^+ 514/488 relative growths show great similarities to the lightly doped Si case (i.e. the 514nm is visibly somewhat enhanced), the n^+ samples' purely thermal growth behaviour is hardly affected by the change in wavelength (see qualitative picture in Fig III.10). Whatever mechanism is increasing the 514nm rate more than the 488nm rate, it is not so effective, or is somehow masked, in heavily doped n samples.

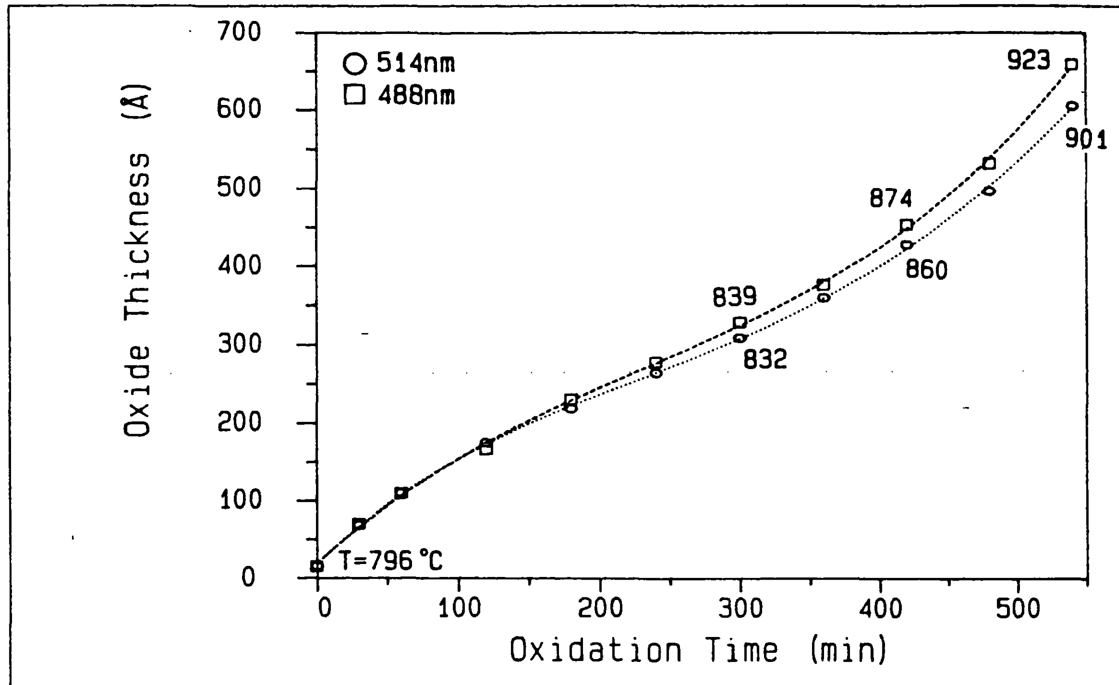

Fig III.17: Oxide thickness as a function of exposure time for <100> n^+ Si. Error bars are of the order of the dimensions of the symbols.

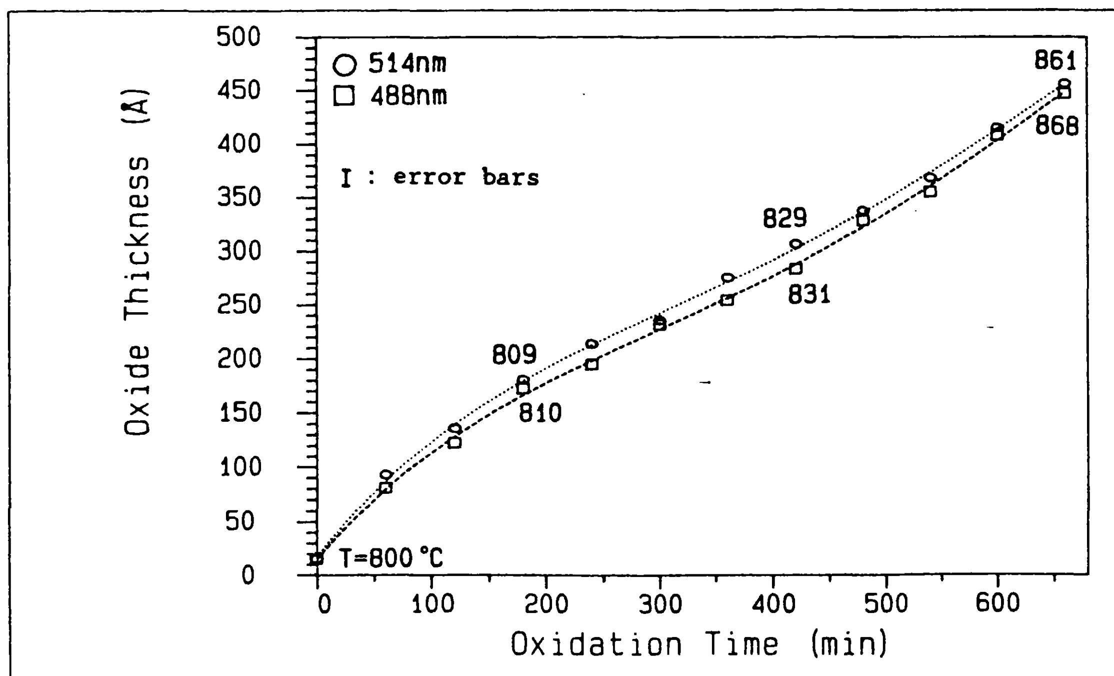

Fig III.18: Oxide thickness as a function of exposure time for <100> p^+ Si.

III.4.6 Low temperature oxidations

It has been repeatedly mentioned that silicon oxidation is a strongly temperature dependent process. Below ≈ 600 °C the thermal growth rate is exceedingly low.

In order to try to minimize the thermal contribution to the reaction and instead exalt the possible photonic aspects, some experiments of approximately room temperature oxidation were attempted in the blue/green range.

A Peltier cooler and a copper block were used to maintain the temperature of the 6x6mm samples (<100>, light doping) around 60 °C, while being irradiated with either 488nm or 514nm at approximately 7.5W. The initial oxide thickness was ≈ 13Å. In all cases an extra sample was positioned in the same O_2 environment but off the Peltier device and laser light to act as a background reference.

At the end of an 8 hour oxidation, the 514nm and 488nm oxide thicknesses were ≈ 24Å and ≈ 21Å, respectively. Since the reference oxides were 16-17Å, this meant we had obtained ≈ 45% and 25% enhancement, respectively. A microspot ellipsometer confirmed ≈ 40% thicker oxide for the 514nm and a ≈ 24% thicker oxide for the 488nm with respect to the reference sample.

A further experiment was carried out with 22W of multiline visible Argon light. The sample was again <100>, p-type, 6x6mm and positioned, as before, on a Peltier cooler dissipating the laser power through a copper block. The stainless steel chamber was also fan cooled. The sample temperature was approximately 110 °C.

The native oxide was ≈ 14-16Å and the oxidation lasted 8 hours. Two extra samples were placed inside the box, out of the laser beam, to act as reference thicknesses. At the end of the period, the irradiated sample oxide had grown to approximately 30-32Å, while the reference samples measured ≈ 18 and 19Å.

An identical sample was oxidized in the same container filled with pure dry O_2 and thermally heated to 135 °C. After 8 hours the oxide thickness was measured to be ≈ 19-20Å, considerably less (in relative terms) than the laser irradiated sample, confirming again the presence of a non thermal contribution to the reaction.

It could be argued at this point that, as a fixed value of n_{ox} is

always used when measuring such thin oxides with the ellipsometer, if irradiation does somehow modify this value considerably (by varying the oxide density), this would result in an error in the thickness reading for the irradiated sample. Even assuming a considerable increase in oxide density of ≈ 10% [NAYAR (RSRE), priv. comm.], this would correspond to a value of $n_{ox} \approx 1.504$ (as compared to the standard 1.458 at the HeNe wavelength). At these thicknesses, such a small variation in n_{ox} could hardly modify the value of the parameter Δ in the ellipsometer and, therefore, would not result in any significant thickness error. This is shown in Fig III.19, where the variation of Δ as a function of thickness is presented, with the refractive index as parameter (details of the calculations can be found in [McCRACKIN et al.,1963]).

Even though this study is limited to the effects of visible radiation on the oxidation of silicon, a brief experiment was carried out with the near UV light available from the laser (≈ 350nm, 3.54eV) and the 514nm radiation.

As the available power in the UV was quite low (not higher than ≈ 2 W at the time of the experiment), a quartz resistive heater was used to raise the processing temperature. The samples were 6x6mm <100>, p-type, lightly doped Si, with a native oxide of approximately 13-15Å. Using the same incident spot-sizes, the power was adjusted to give the same initial temperature in both cases (≈ 510 °C). The oxidations lasted 8 hours and the results are shown in Fig III.20. The significant pre-heating load limited the use of the reflectometer in the usual way as it would have taken too long for the sample to cool down to room temperature at every measurement. It was therefore assumed that the temperature was constant all through the oxidation, in both cases (this was confirmed at the end of each experiment). The driving program could then be modified to read the thicknesses directly from the high temperature data.

Both SiO_2 and O_2 were assumed to be transparent at 350nm. The 350nm absorption length in Si (≈ 100Å) is shorter than the corresponding one at 514nm (≈ 0.4μm), but the equilibrium temperature was measured to be the same in both cases. At these low doping and injection levels (and temperature), the carriers diffusion length in Si is much greater than both absorption lengths and, therefore, any <u>relative</u> effect could be neglected.

Within the obvious limits of our accuracy assessment, the 3.5eV

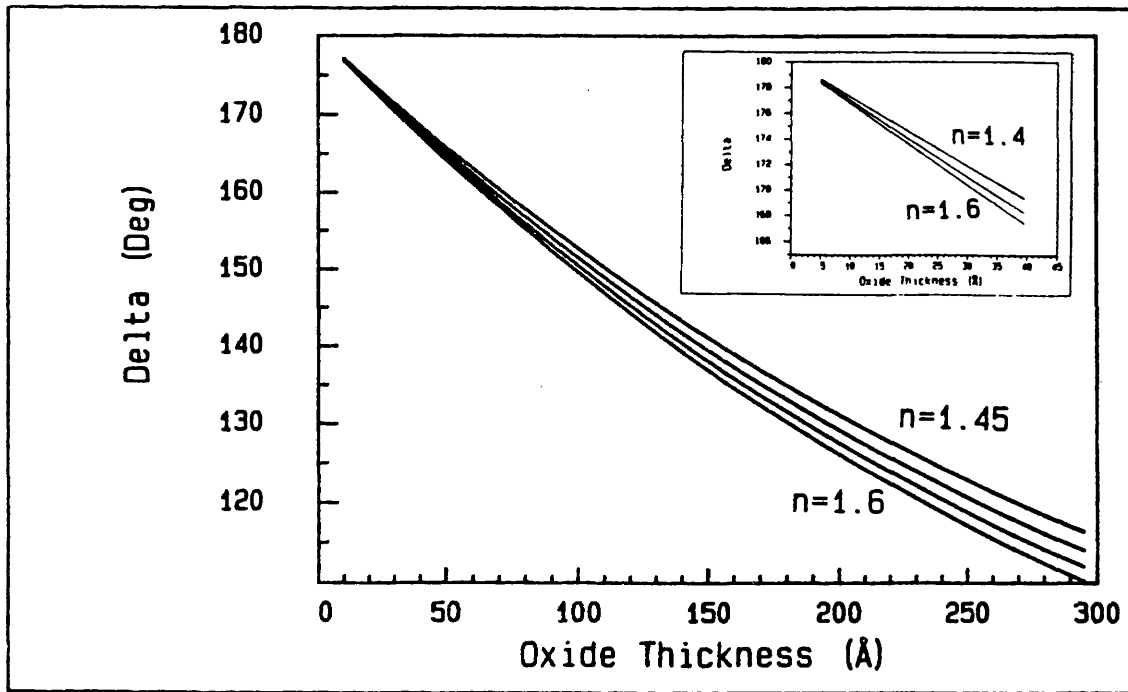

Fig III.19: Oxide thickness dependence of Δ for various values of n_{ox}.

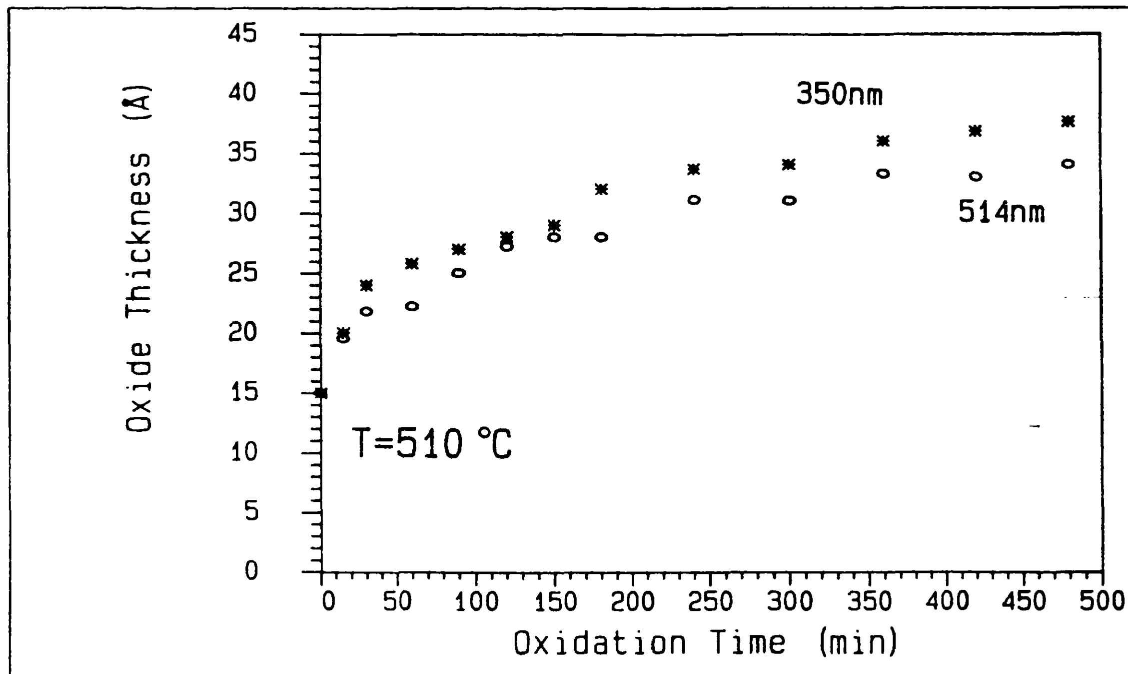

Fig III.20: Oxide thickness as a function of exposure time for <100> Si (low temperature oxidation).

photons appear to have a greater effect on the oxidation rate. Comparing our results with similar low temperature data, our thicknesses are a little higher than those obtained by incoherent light irradiation in the visible and UV at ≈ 400 °C by Nayar and Boyd [NAYAR et al., 1988], but lower than the values reported by Ishikawa et al. [ISHIKAWA et al., 1989] for dry oxidation at 500 °C by a tungsten halogen lamp. In this last example the light power density is likely to have been considerably higher than in our experiment. Interestingly, our data points are fairly close to the thermal oxidation data reported by Taft [TAFT, 1984] at 612 °C and Goodman and Breece [GOODMAN et al., 1970] at 600 °C.

Finally, a brief attempt was also made at examining the effect on the oxidation rate of Si of a pulsed irradiation with visible light.

The mode-locked Argon laser generates 85-90psec wide pulses at a pulse repetition frequency of 76MHz. The optimum average power output is ≈ 1W at 514nm, providing a peak power of 150W per pulse. In this regime, therefore, though the average power (and, consequently, the average temperature) is quite low, the peak power and temperature are increased considerably, thereby providing short bursts of a very large number of photons to interact with the Si surface. In these circumstances, the reflectometer can only measure an average value of the temperature and this was measured to be ≈ 270 °C.

A <111> Si sample, with a native oxide of approximately 16-18Å, was irradiated in dry O_2 for 8 hours. The final thickness was approximately 25Å. An identical sample was oxidized in identical conditions with 1W of CW 514nm light. A final thickness of ≈ 26Å was measured. Though the experiment is undoubtedly very limited, it seems to exclude any major effect on the growth of oxide due to pulsing of the light.

Last, but not least, in this experimental section we will briefly mention an experiment aimed at evaluating the possible influence on the growth rate of the oxide of water vapour absorbed on the internal walls of the stainless steel vessel during the short opening times and in excess of the concentration specified by the O_2 supplier. The DSP Si F/B test was obviously inherently immune from such interference as front and back surfaces were likewise affected.

As we had no means of directly measuring the infinitesimally low

concentrations expected, we followed a recommended procedure [Dr DRAYTON (UCL), priv.comm.] to eliminate all traces of water possibly absorbed on the chamber walls and then repeated a standard oxidation experiment. The procedure consisted of leaving the chamber (loaded with the silicon) under continuous evacuation and heated to ≤ 100 °C for a period of ≈ 12–14 days. The resulting growth curve was then analysed with the computer model and it was found that, up to thicknesses of ≈ 800Å, the global growth rate had decreased only by ≈ 2% with respect to a normal and otherwise identical oxidation. Such small difference is within the usual experimental error and model tolerances and can therefore be neglected.

III.5 SiO_2 films characterization

We entered upon this study of the properties of laser grown silicon dioxide films not only as a purely scientific interest but also with the aim of investigating its use as part of a fully integrated laser processing facility for microelectronics and optoelectronics applications. On that basis, we carried out a small amount of structural and electrical characterization of the films.

III.5.1 Infrared characterization

Infrared spectroscopy has been used for the structural evaluation of crystalline and amorphous bulk silicon dioxide for many decades and, more recently, the same technique has been adapted to grown or deposited oxide films [PLISKIN et al.,1965].

We have examined our laser grown oxides with a Fourier Transform infrared spectrometer (FT-IR). The data were taken at room temperature using a Brucker IFS 45 spectrometer fitted with a microscope attachment resulting in a sampling spot diameter of 80μm, a compromise between ultimate resolution and signal to noise ratio. Each spectrum was recorded as the summation of 800 scans with a resolution of 2cm^{-1}. A smoothing routine was used to remove the remaining noise and interference fringes.

The silicon used in the previously described experiments was mainly

Czochralski-grown, but it is well known that this type of silicon contains a high concentration of interstitial oxygen ($\approx 10^{18} cm^{-3}$), very sensitive to any heat treatment, which could in the end interfere with the required response peaks in the output spectrum. Therefore, all the infrared data were collected from a new set of float zone, p-type, lightly doped Si samples oxidized in the usual way. An identical, unoxidized, sample was used as a reference to eliminate background spectral features from the crystal silicon substrate.

The three main vibrations in the spectral response of SiO_2, associated with the various vibrational modes of atoms in the Si-O-Si group can be found at $450 cm^{-1}$ (rocking mode), $810 cm^{-1}$ (bending mode) and $1075 cm^{-1}$ (stretching mode). We have limited our interest to the strongest absorption feature, the $1075 cm^{-1}$ stretching band, principally for reasons of sensitivity. No SiOH, H_2O or SiH peaks (around 3600, 1640 and $2250 cm^{-1}$ respectively) were observed within the sensitivity of the instrumentation.

The infrared transmission minima near $1075 cm^{-1}$ ($9.2 \mu m$) of thermally grown SiO_2 films have previously been shown [DIAL et al.,1968; BOYD et al.,1982] to obey Lambert-Bouguer's law, within experimental error, for film thicknesses from $3.5 \mu m$ to approximately 28Å. This law states:

$$A = \log I_0/I = 0.434 \quad \alpha_{app}(x-x_0) \qquad (3.3)$$

where A is the absorbance, I_0 and I the incident and transmitted intensities, respectively, α_{app} the apparent absorption coefficient and x_0 the oxide thickness in the reference sample, i.e. the usual native oxide ($\approx$ 20Å) present on the surface of our silicon samples a few days after cleaning . We have verified the law for our Ar laser grown oxides in the range 100 to 1200Å (Fig III.21), finding $\alpha_{app} \approx 3.32 \times 10^4 cm^{-1}$, in good agreement with previous results.

Fig III.22 shows a typical example of the absorbance spectrum of SiO_2 in the range 700 to $1500 cm^{-1}$ and the definition of the parameters commonly used in the characterization.

Fig III.23 to III.25 show, respectively, the thickness dependence of the Si-O stretching mode absorption peak F_{max}, of the full width

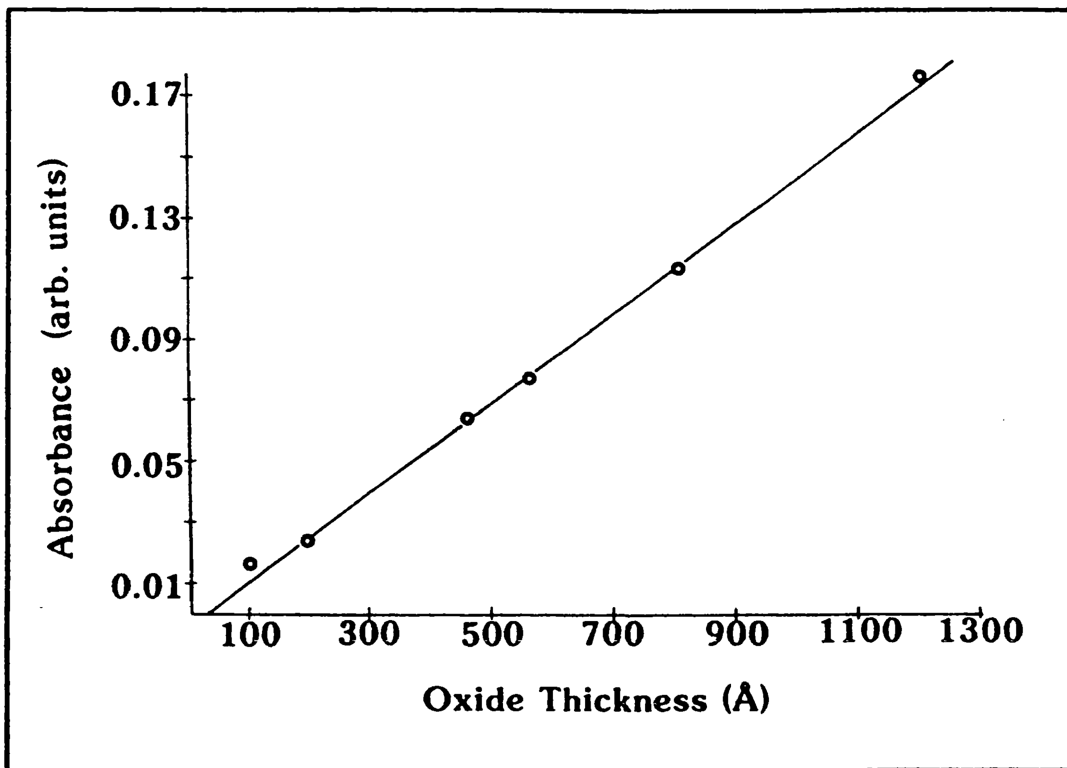

Fig III.21: SiO_2 absorbance at F_{max} as a function of oxide thickness.

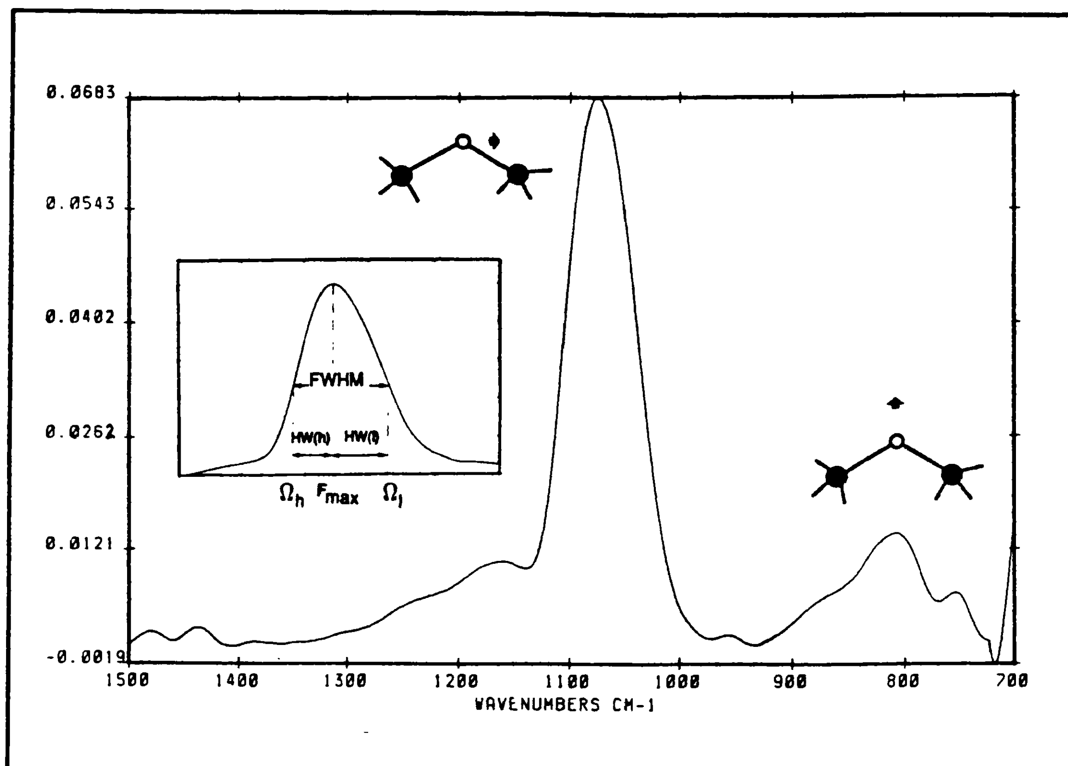

Fig III.22: Example of SiO_2 absorbance spectrum (and definition of parameters).

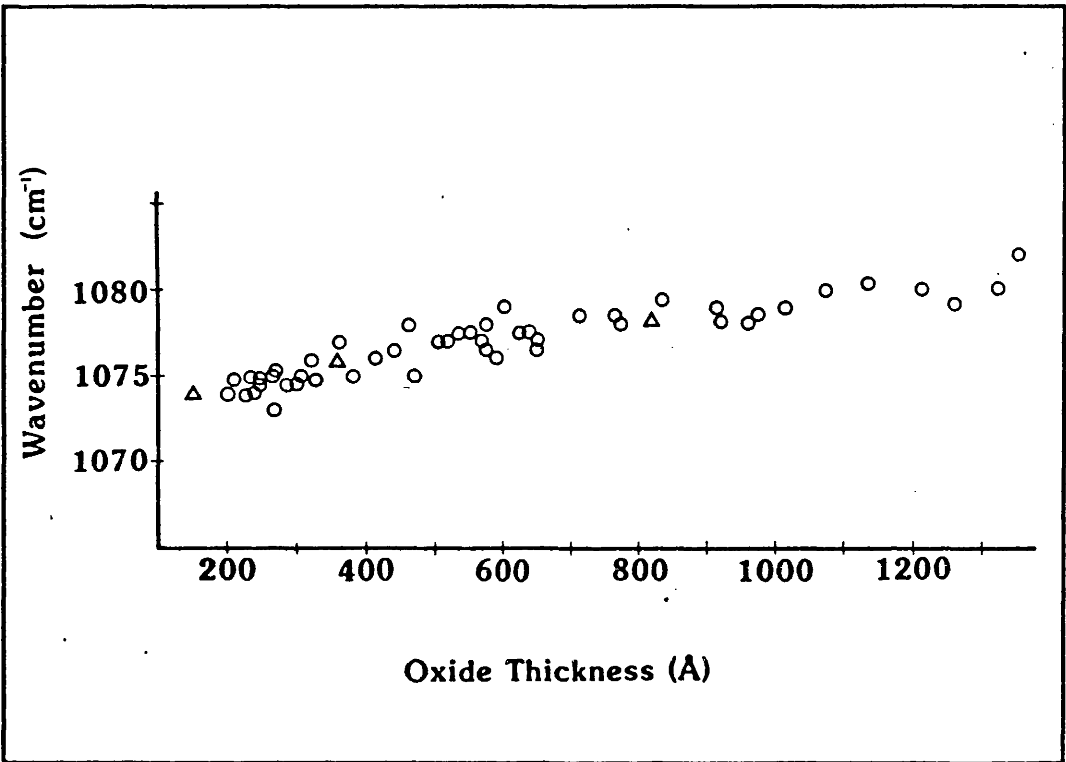

Fig III.23: Oxide thickness dependence of Si-O stretching mode absorption peak F_{max} (△ : examples of annealed furnace oxides).

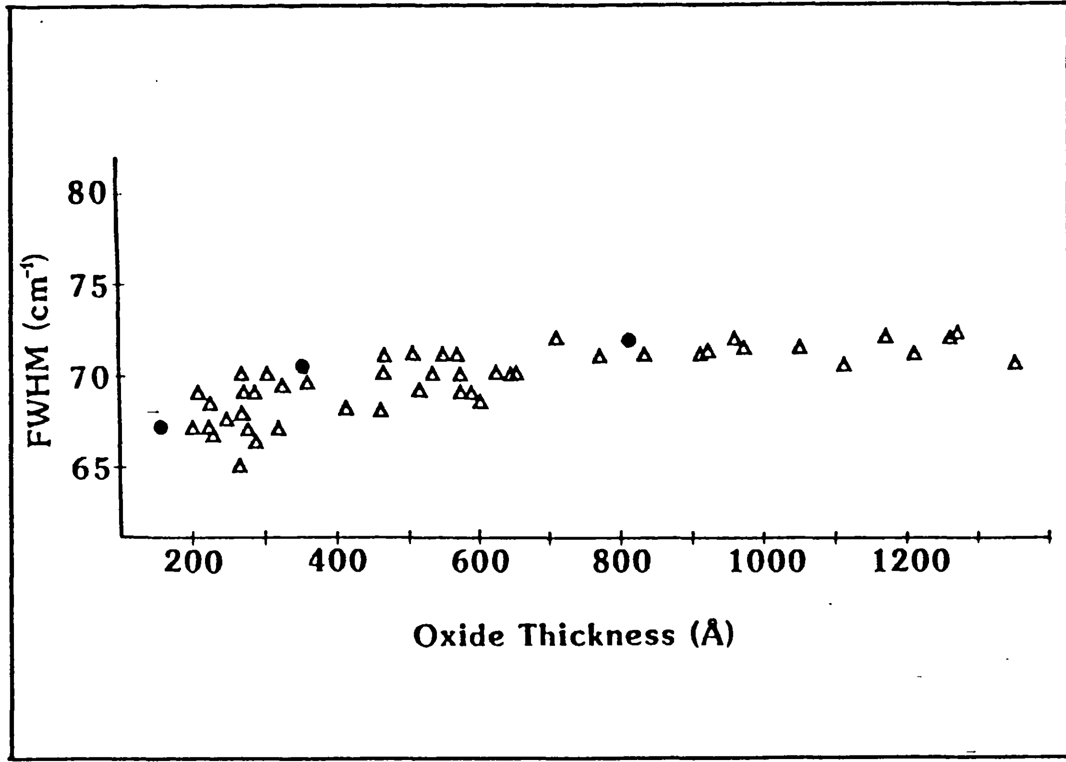

Fig III.24: Oxide thickness dependence of FWHM (● : examples of annealed furnace oxides).

at half maximum (FWHM) and of the two bands (low and high) on the either side of F_{max} whose sum is FWHM. Our measured data show a high degree of similarity with those obtained from CO_2 laser grown oxides [BOYD et al.,1987]. Moreover, a similar degree of asymmetry as was recently reported for furnace and CO_2 laser grown oxides was found and, as with those films, the data for FWHM show only a mild thickness dependence in this thickness range [BOYD et. al.,1987].

Some points obtained from furnace grown and annealed oxides are also plotted on the graphs and show no significant difference. This suggests that our oxides are very similar to conventional thermally grown layers, and not to CVD deposited films, which exhibit rather different IR characteristics (see, for instance, [PAI et al.,1986]).

It has been suggested that the stretching band at 9.2μm is strongly influenced by the chemical bonding character, stoichiometry, porosity, density and level of compressive strain in the film [PLISKIN et al.,1965; BOYD et al.,1982, 1987; OLSEN et al.,1988]. Recently it has also been shown [LUCOVSKI et al.,1987] that, for thermal oxides, the growth temperature can affect the density and produce changes in the Si-O-Si angle and Si-Si distances, which would shift the position of the stretching vibration peak. It should be stressed that our oxides were not grown at a uniform temperature, either temporally or spatially.

Together with the results obtained previously from furnace and CO_2 laser grown oxides [BOYD et al.,1987], this would indicate that temperature is not the only controlling influence on the position and FWHM of this absorption feature. In fact, Fitch and Lucovski [FITCH et al.,1988] have recently found that the position of the band maximum is often uniquely related to its width and proposed a model, for films prepared by a wide variety of methods. Boyd [BOYD,1988] confirmed this observation, but pointed out that it seemed to be valid only for films thicker than approximately 400Å.

Due to practical consideration (i.e. sensitivity of the focused instrument and instrument-time available), we couldn't investigate the range of thicknesses below 150Å where, due to the proximity of the interface, the effects of strain are stronger and possible structural differences might be present [BOYD et al.,1987].

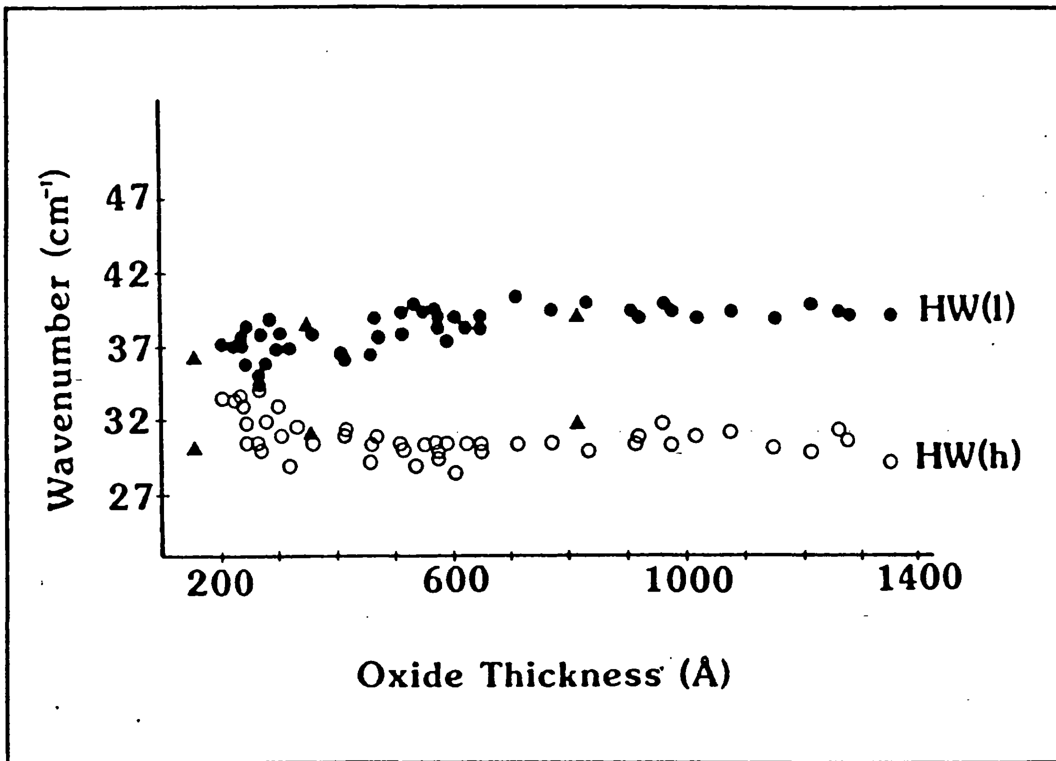

Fig III.25: Oxide thickness dependence of the high [HW(h)] and low [HW(l)] bandwidths (▲ : examples of annealed furnace oxides).

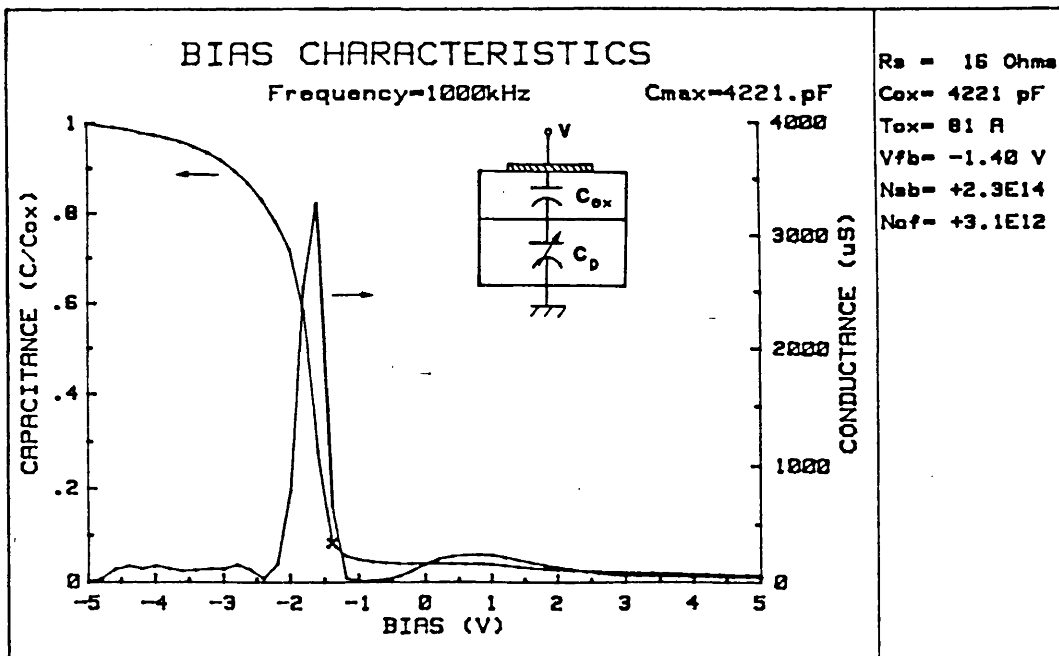

Fig III.26: Example of high frequency C-V curve for laser grown oxides.

III.5.2 Electrical characterization

The electrical properties of interest in oxides to be used in MIS devices are mainly related to the quality of the interface with silicon, but resistivity and breakdown voltage are also very important characteristics. These properties are normally probed with capacitance-voltage (C-V) and current-voltage (I-V) measurements on MIS diodes [SZE, 1981; NICOLLIAN et al., 1982].

We chose to characterize only very thin oxides, firstly because that would guarantee a more uniform thickness over the entire silicon sample (our particular growing conditions made the oxides quite peaky with increasing thickness) and, secondly, because this is the area where laser processing is most likely to be used. This is meant to be only a preliminary investigation of the properties of these oxides and, therefore, only a small number of samples were actually characterized. The main area which will require attention in further laser oxidation studies is a proper in-situ cleaning facility: it is clearly not possible to clean such small samples to the high standard required for best electrical characterization, even when the purest chemicals are used.

Aluminium electrodes were evaporated on both sides of the oxidized samples (≈ 0.5mm square pattern). Fig III.26 shows a typical high frequency MIS C-V curve obtained for a lightly doped p-Si sample. The insert shows a schematic representation of the total capacitance of the system. This is a series combination of the oxide capacitance C_{OX} (fixed) and the semiconductor variable depletion layer capacitance C_D:

$$C = \frac{C_{OX} C_D}{C_{OX} + C_D} \qquad [F/cm^2] \qquad (3.4)$$

For high negative values of the applied bias (left hand side in the picture) the curve should, in theory, be flat and equal to 1 (i.e. $C=C_{OX}$). All our oxides exhibited a more or less pronounced slope (also apparent at high positive values of the bias). This implies the presence of some leakage current. This is a very common problem whenever the highest level of pre-oxidation cleaning (i.e. as in a

production line of gate quality oxides or when in-situ cleaning is used in a laboratory) cannot be achieved.

The conductance curve shown in Fig III.26 was needed to obtain a correct value of C_{ox} (once the value of R_s was measured).

A voltage shift in the C-V curve towards more negative values of gate bias with respect to the ideal C-V curve is caused by the presence of fixed positive charges Q_f in the oxide (see Appendix I). This shift is represented by the flat band voltage V_{fb}. From this value the density of these charges can be obtained:

$$\frac{Q_f}{q} = \frac{C_{ox}}{q}\left[\varphi_w - \varphi_f - V_{fb}\right] \qquad [cm^{-2}] \qquad (3.5)$$

where φ_w and φ_f are the silicon and metal work functions, respectively. The measured value was slightly higher than the corresponding one for as-grown high quality thermal oxides of similar thickness.

With the present test facilities available to us, the interface trap density D_{it} (see Appendix I) is obtained by the capacitance method [SZE, 1981] The expression for D_{it} is given by:

$$D_{it} = \frac{C_{ox}}{q}\left[(d\,\psi_s/dV)^{-1} - 1 \right] - \frac{C_D}{q} \qquad [cm^{-2}\ eV^{-1}] \qquad (3.6)$$

where ψ_s is the silicon surface potential. This requires the measurement of low frequency C-V curves for the capacitors [Sze, 1981]. Unfortunately, the thicknesses of interest were too low for this to be possible at the time when these measurements were taken. An approximate value for D_{it} can be obtained by the slope of the high frequency C-V curves only. Values of the order of $10^{12} cm^{-2}\ eV^{-1}$ were obtained in as-grown oxides, not unreasonable at these thicknesses and temperatures.

Breakdown voltages (defined at 1 A/m^2) were measured through I-V characterization. The best values obtained were around 8MV/cm, again quite acceptable with our experimental conditions.

CHAPTER IV

Computer Modelling and Discussion of Results

IV.1 Computer modelling of growth process

We fitted Massoud's thermal oxidation model (par.I.9) to a large number of thermally grown oxides (up to ≈830Å) for which growth conditions were exactly known and found it to be a remarkably good fit. This model was subsequently modified to simulate our processing conditions by introducing the thermal model described in par.III.2.

In the next sections we will describe the application of the computer model first to the evaluation of the relative effects and, secondly, to the comparison with the purely thermal case.

IV.1.1 514 nm versus 488 nm

The thermal growth rate suggested by Massoud [MASSOUD et al., 1987] (and strictly valid in the temperature range 800 to 1000 °C) is:

$$dx/dt = [B + K_1 \exp(-t/\tau_1) + K_2 \exp(-t/\tau_2)] / [2x+A] \qquad (4.1)$$

where A and B were defined in (1.2) and (1.3); K_1 and K_2 [$Å^2$/min] and τ_1 and τ_2 [min] are temperature and orientation-dependent parameters found from curve fitting of the experimental data.

Keeping Massoud's original values, it was decided to increase the global growth rate for both wavelengths used until the models approximated the experimental curves (obtained by curve fitting), as this would highlight any difference.

For example, consider the case of Fig IV.1: the 514nm experimental growth data are compared with curves obtained from the computer model by progressively increasing the global growth rate. It is apparent that no single curve fits all the experimental data. To obtain, for instance, ≈ 112Å in 15min, the required enhancement is of the order

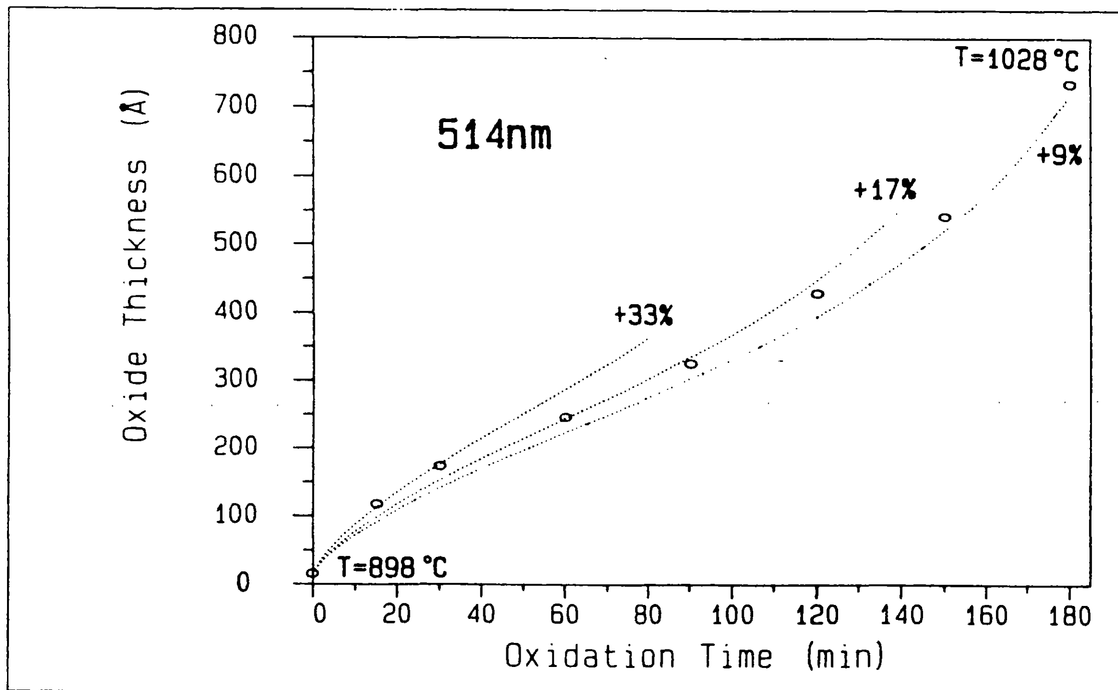

Fig IV.1: Experimental growth data (O) and enhanced thermal growth models (514nm, high oxidation temperature, <100> Si).

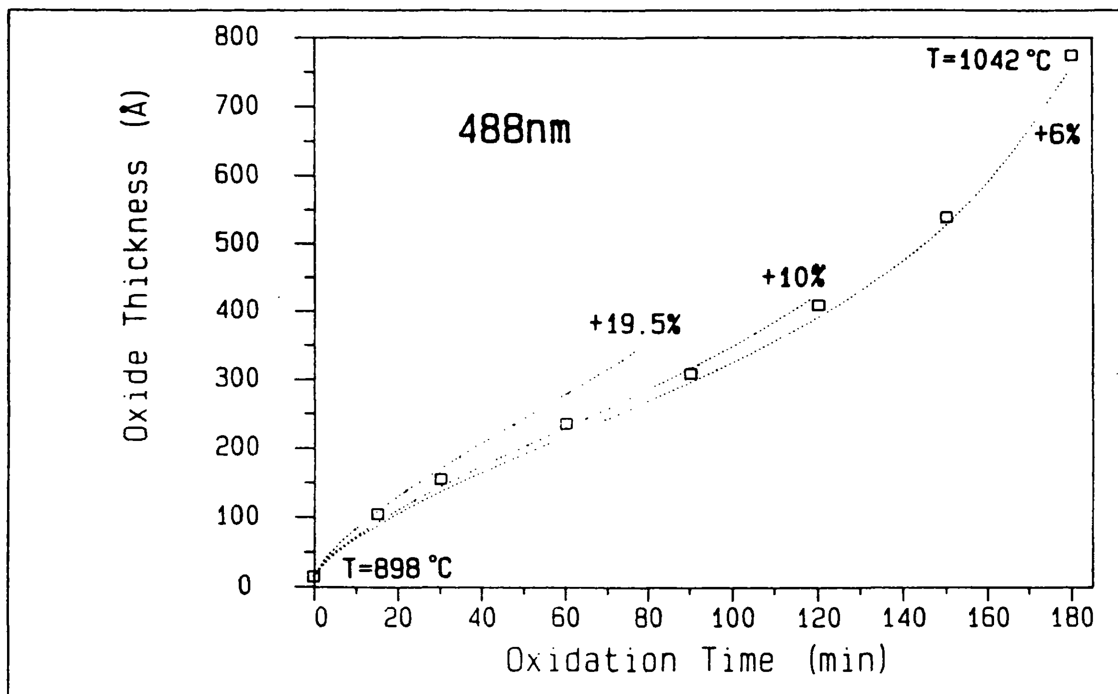

Fig IV.2: Experimental growth data (□) and enhanced thermal growth models (488nm, high oxidation temperature, <100> Si).

of ≈ 33%, decreasing to ≈ 17% to obtain thicknesses of ≈ 300Å in 80min and down to ≈ 9% for a ≈ 700Å oxide in a period of 180min.

Fig IV.2 shows the case of the corresponding 488nm thickness/time data: again, no single curve can be used for the whole range. The three curves drawn have been chosen to show the required enhancement in growth rate needed at approximately the same three thicknesses under consideration in the 514nm case: we can see that there is a noticeable decrease in this enhancement, especially for the thinnest oxides. If we define the differential enhancement as $\delta g514/488$ = percent increase in 514nm thermal rate - percent increase in 488nm thermal rate, from the above plots this quantity is clearly dependent on oxide thickness and temperature. But, as an increase in thickness implies an increase in temperature in our experiments, a single plot doesn't enable discrimination between the two effects.

This comparison has, therefore, been performed on a large number of 514/488 couples for <100> p-Si with a variety of initial temperatures over the 750-950 °C range.

Figs IV.3 to IV.6 show two more examples of 514/488 rate comparison through modelling. The three sets presented cover a fairly large range of initial temperatures. Both thickness and temperature dependence are now distinguishable and the trend can be seen to be quite similar to what was found for the DSP Si case. Table I lists examples of values of $\delta g514/488$ for <100> p-Si (light doping) samples in the range of thicknesses and temperatures of interest.

It should be stressed that the absolute values of required enhancements in the global growth rate at each thickness and wavelength are subject to tolerances. The aim of the exercise, though, is to find an order of magnitude for $\delta g514/488$ and its qualitative dependence on thickness and temperature and this can still be achieved.

We then considered the case of an oxidation starting with a pre-existing thick thermal oxide of ≈ 825Å on a <100> p-Si. Fig IV.7 shows the experimental data for both wavelengths and the corresponding altered thermal models. Confirming what we had anticipated in the previous chapter, there is a remarkable similarity between the model and the actual data for both wavelengths, i.e. $\delta g514/488 \approx 0$. The minor discrepancy could, perhaps, be due to a small effect of water vapour on the growth rate (see par.III.4.6).

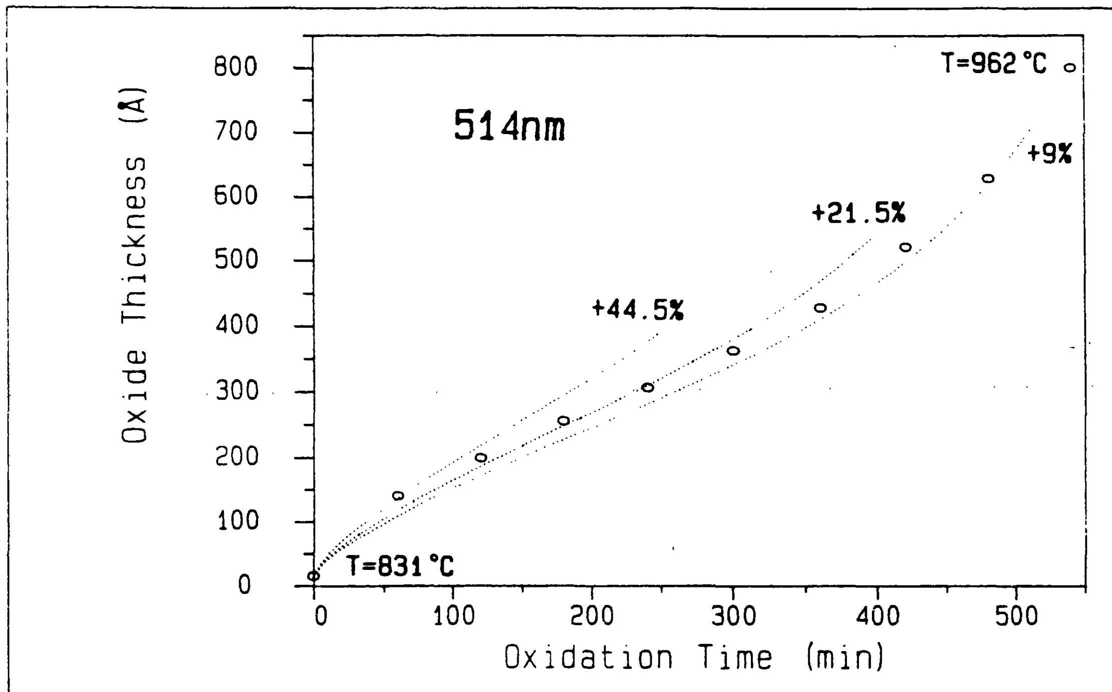

Fig IV.3: Experimental growth data (○) and enhanced thermal growth models (514nm, medium oxidation temperature, <100> Si).

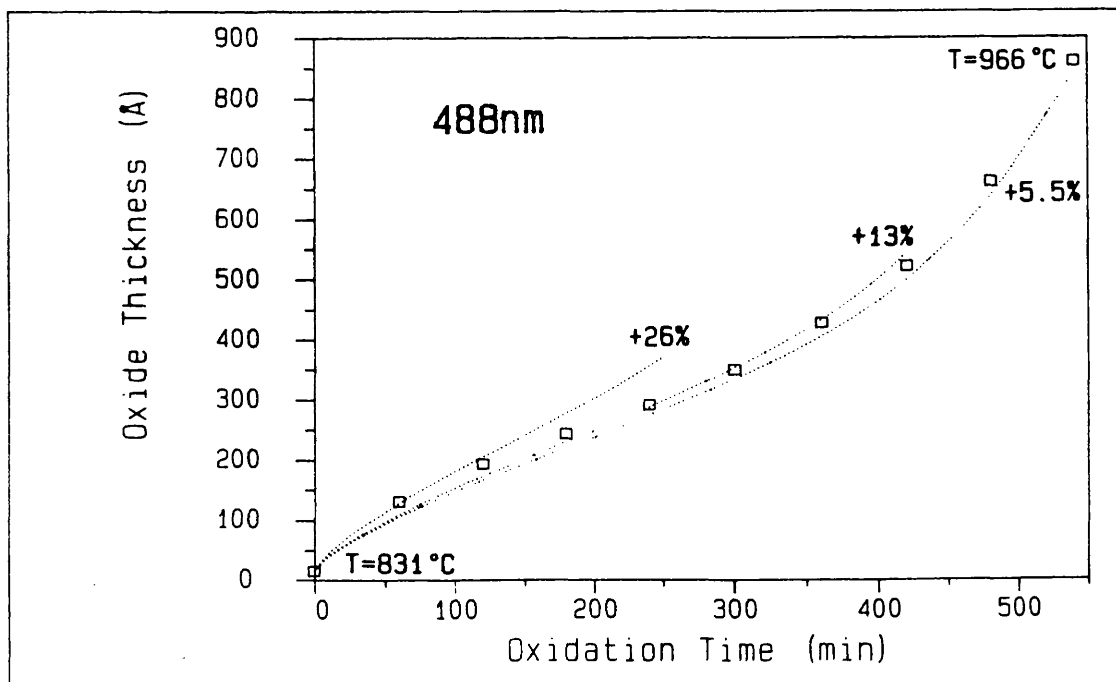

Fig IV.4: Experimental growth data (□) and enhanced thermal growth models (488nm, medium oxidation temperature, <100> Si).

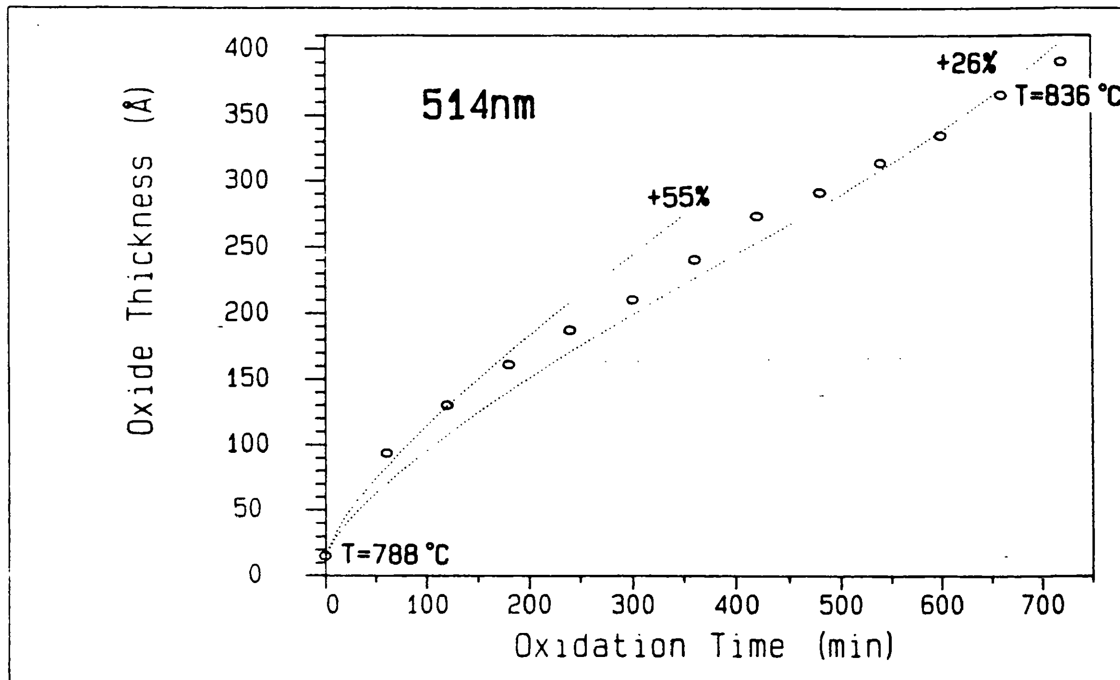

Fig IV.5: Experimental growth data (O) and enhanced thermal growth models (514nm, low oxidation temperature, <100> Si).

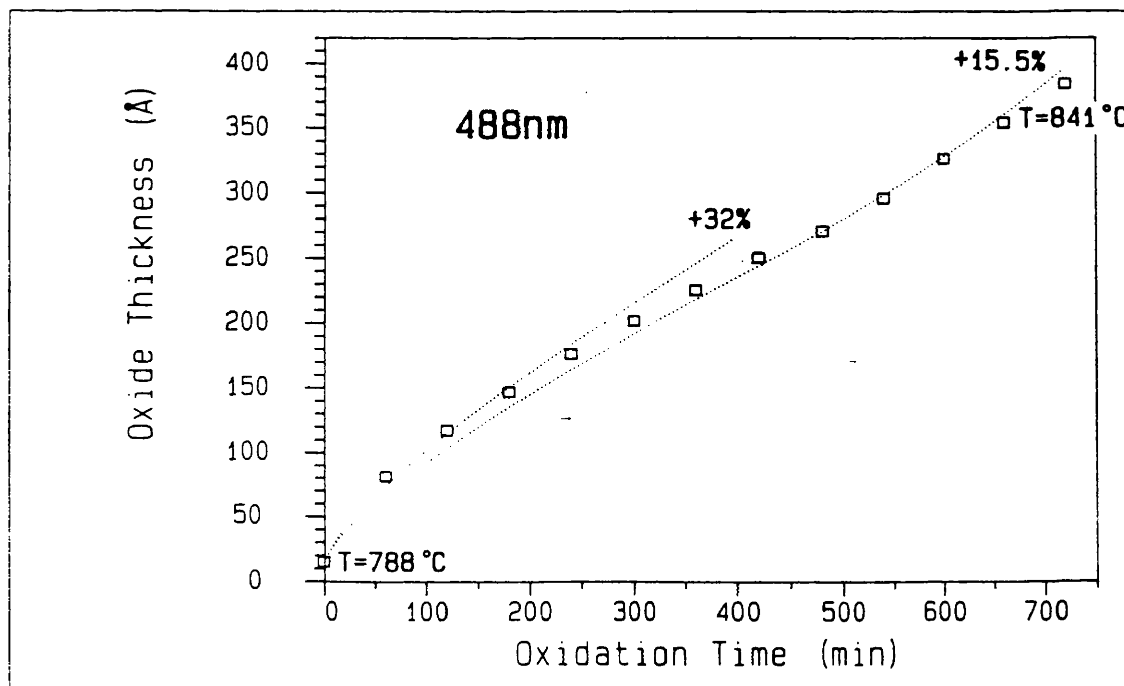

Fig IV.6: Experimental growth data (□) and enhanced thermal growth models (488nm, low oxidation temperature, <100> Si).

50Å	25 (@ 790 °C)	21 (@ 833 °C)	15.5 (@ 900 °C)
112Å	22.5 (@ 795 °C)	18.5 (@ 837 °C)	13.2 (@ 904 °C)
300Å	10.5 (@ 820 °C)	8.5 (@ 863 °C)	6.8 (@ 930 °C)
433Å	6.5 (@ 840 °C)	5.5 (@ 892 °C)	4.2 (@ 960 °C)
700Å	N/A	3.8 (@ 960 °C)	3.0 (@ 1010 °C)

Table I: Examples of $\delta g_{514/488}$ for <100> p-type Si. For each oxide thickness (left hand column) three values of $\delta g_{514/488}$ are reported, corresponding to low, medium and high temperature oxidations in each thickness range.

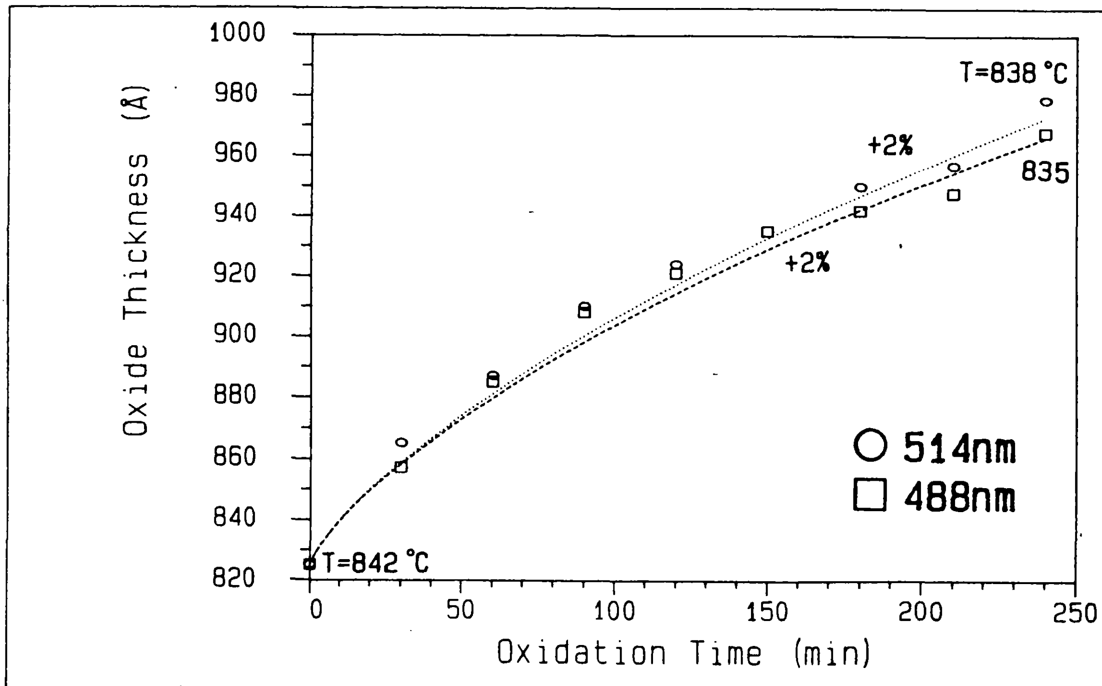

Fig IV.7: Experimental growth data (○,□) and enhanced thermal growth models (pre-oxidized <100> Si).

The present findings show a $\delta g_{514/488}$ rapidly tending towards zero (or, at least, below our capability to detect it) as the oxide thickness reaches a few hundreds of Ångstroms. This appears to be due to the growth rate being less and less affected by the effect of the photons and settling to a (more or less) purely thermal value for both wavelengths.

A similar comparative analysis has been performed on the <111> n-Si samples. Though the <111> thermal growth rate is considerably higher than the <100> one, the 514/488 enhancement appears to be again of a similar magnitude (and with a similar thickness and temperature dependence) as the <100> case. An example is shown in Figs IV.8 and IV.9.

Special attention was paid to the very initial stages of the oxidation process for both crystal orientations (Fig IV.10 is an example).

For the heavily doped samples no ready made thermal model is available and it was decided not to try to artificially fit Massoud's model in order to extract the difference in growth kinetics between the 514 nm and the 488 nm cases.

IV.1.2 Photonic versus thermal growth

In the following paragraph only the oxide growth induced by the 514 nm line will be considered.

As we have mentioned in par.III.4.2, the experiments on DSP Si proved to be very important in the analysis of the photonic enhancement of the growth rate. To make sure that the ratios front-side oxide / back-side oxide (F/B) were not representative of a purely thermal differential between the two silicon faces, we used our computer model to simulate F/B oxidations separated by a variable δT (at the same temperature and up to the same thickness as each experimental data) to verify the 'expected' thickness for the back oxide under these conditions. It was found that, in order to justify our experimental results, a $\delta T \approx 9$ °C would be required at 747Å, while a $\delta T \approx 27$ °C would be needed at 105Å to account for the measured F/B. These values are clearly not realistic with a $\approx 250\mu m$ thick silicon sample in our processing configuration.

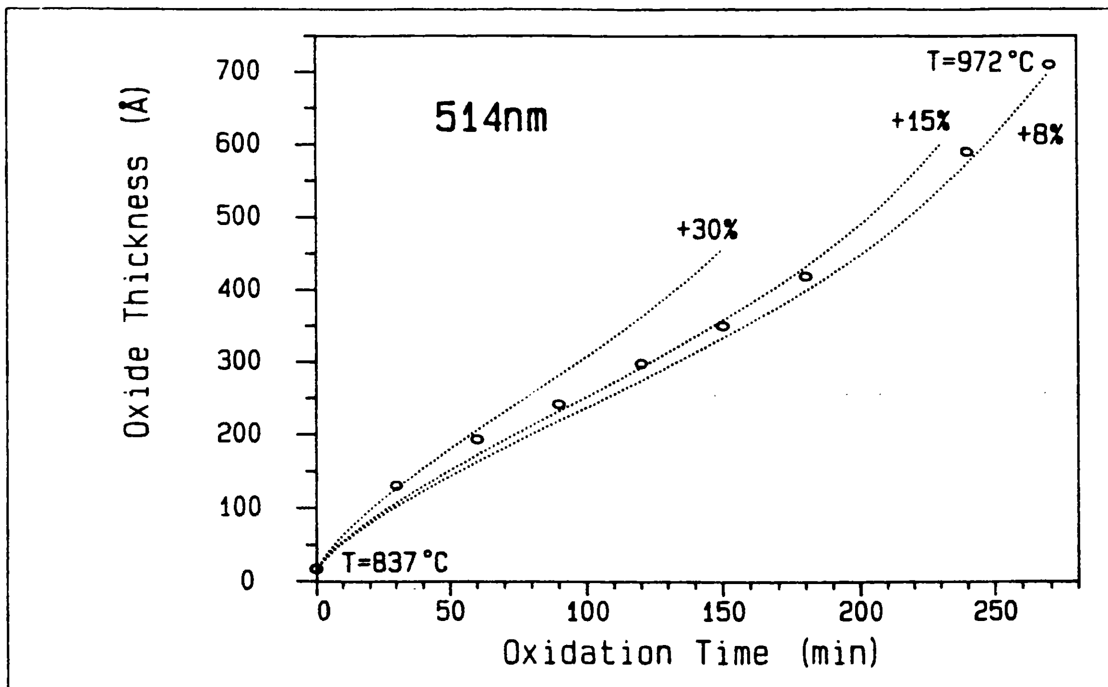

Fig IV.8: Experimental growth data (○) and enhanced thermal growth models (514nm, <111> Si).

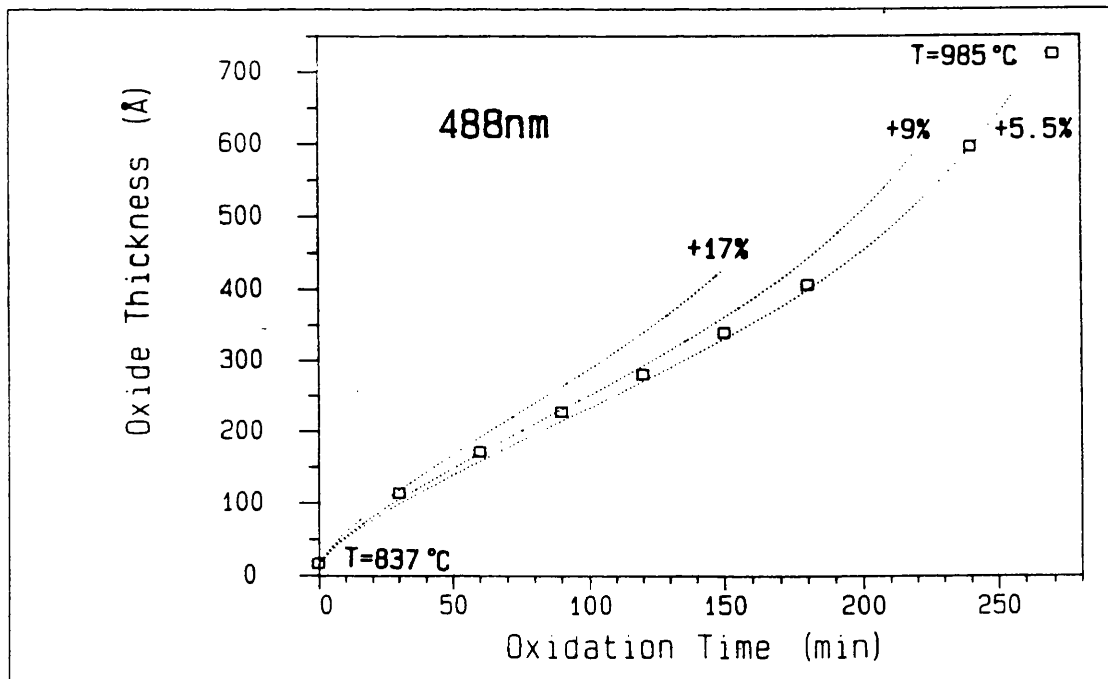

Fig IV.9: Experimental growth data (□) and enhanced thermal growth models (488nm, <111> Si).

Although both the F/B data and the rate enhancement obtained with the computer model are representative of the same phenomenon, that is a photonic enhancement in the early stages of oxide growth, they are not exactly the same quantity. We can express F/B as:

$$\frac{F}{B} = \frac{\int_0^t \{Rate_T[x,T(x)] + f[x,T(x)]\}dt}{\int_0^t \{Rate_T[x,(T(x)-\delta T)]\}\,dt} \qquad (4.2)$$

where $Rate_T(x,T)$ is the thermal rate and $f(x,T)$ an enhancement term due to the laser; the modelling we have performed in par.IV.1.1 finds the solution of the following equation:

$$\int_0^t \{Rate_T\,[x,T(x)]\cdot 1.XX\}\,dt = \int_0^t \{Rate_T\,[x,T(x)] + f[x,T(x)]\}\,dt \qquad (4.3)$$

where 1.XX provides the global enhancement (XX% is the label on each of the previous curves).

The availability of a good thermal model and a large pool of experimental data allowed us to attempt a search for the enhancement term f(x,T). It was decided to use a term of the type:

$$f(x,T) = C\,\exp(-E/kT)\,\exp(-x/L) \qquad [\text{Å/min}] \qquad (4.4)$$

This choice follows directly Massoud's work on thin oxide growth [MASSOUD et al., 1987]. Clearly this expression could be an over simplification: for instance, the characteristic length L (Å) was assumed to be temperature independent and a single activation energy E (eV) for the process over the whole temperature range was used. Eventually, the following expression was chosen for the <100> Si (514 nm):

$$f(x,T) = 2.8\text{x}10^6\,\exp(-1.35/kT)\,\exp(-x/64) \qquad [\text{Å/min}] \qquad (4.5)$$

It is perhaps interesting to notice that the characteristic length

we arrived at is similar to that used by Massoud in his empirical expression for fast initial thermal growth of SiO_2, though the activation energy of our laser enhanced process is considerably smaller.

From Fig IV.8 it is possible to see that the required global rate enhancement for <111> is somewhat smaller than the corresponding one in <100> Si (at each thickness and within the accuracy of our analysis), indicating a slightly higher percentage laser-induced increase in growth rate for the <100> than for the <111>. As modelling the <111> growth rate indicated similar temperature and thickness dependences of the laser enhancement (again within the accuracy of our analysis), all the difference was included in the multiplicative factor C, which was found to be $\approx 3.6 \times 10^6$.

Computer modelling for the 488nm growth data indicated a similar dependence on temperature and thickness as the 514nm. Once again, all the difference could be incorporated in the multiplicative factor C.

In Fig IV.11 and IV.12 the enhancement term for the <100> 514nm Si is expressed as a f(x) and as a f(T), respectively.

We have empirically measured the average growth rate over short periods of time (the length depending on the processing temperature). With the knowledge of the thermal values, we extracted the 'excess rate' and fitted our model to the data (only low temperatures were used). The results were very encouraging, considering the tolerances involved.

We can now visually compare, directly, the thermal and enhanced growth rates for various temperatures. The particular choice of temperature is only dictated by the availability of sufficient data. In Fig IV.13 the dotted curves are from the purely thermal model [MASSOUD et al., 1985, 1987], the dashed lines are from our new model with the enhancement term added to the reaction rate, the circles represent experimental values obtained (at measured points) from curve fitting of measured thickness data and the full circles are a few directly measured values of growth rate.

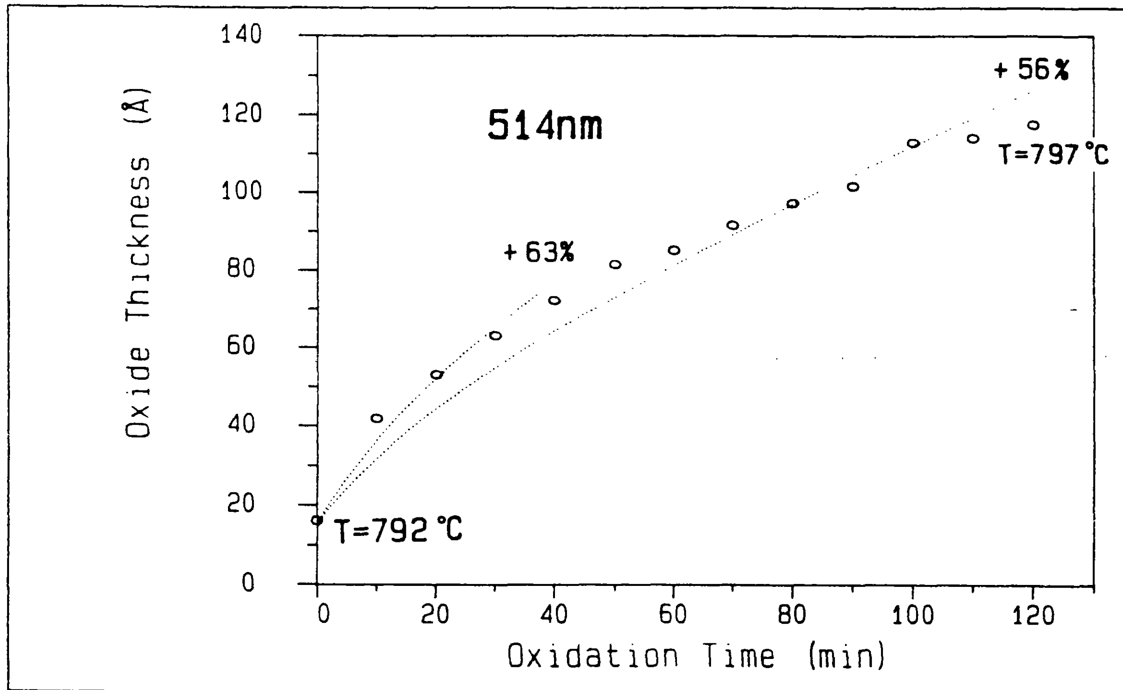

Fig IV.10: Experimental growth data (O) and enhanced thermal growth models (514nm, <100> Si, thin oxide).

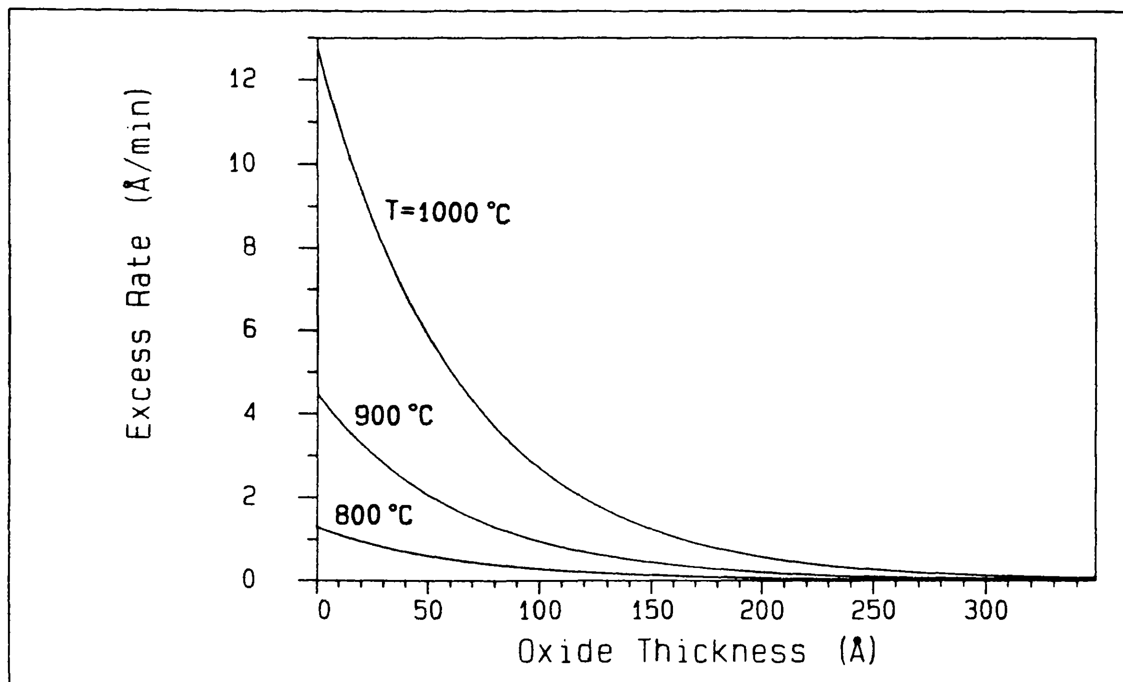

Fig IV.11: f(x,T) as a function of oxide thickness for three values of temperature (514nm, <100> Si).

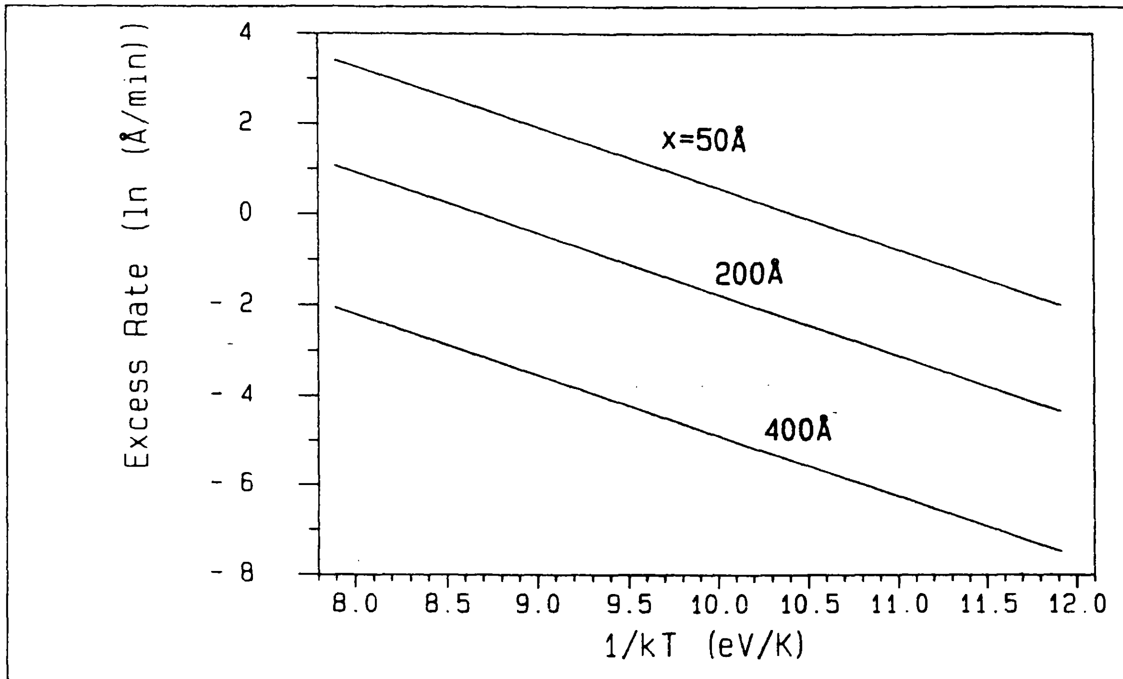

Fig IV.12: f(x,T) as a function of the inverse of the temperature for three values of oxide thickness (514nm, <100> Si).

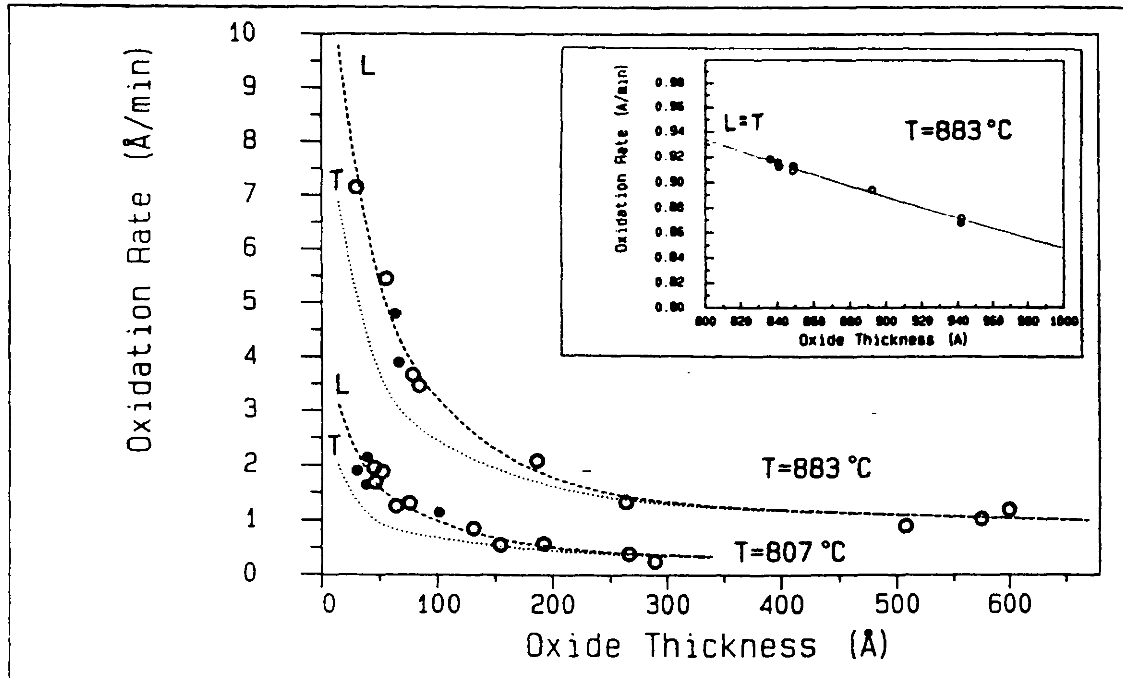

Fig IV.13: Thermal (T) and laser enhanced (L) growth rates as a function of oxide thickness (computer models).

○ : Experimental data from curve fitting;

● : Measured data. All data for 514nm and <100> Si.

The model fits well practically all the experimental data on lightly doped silicon. Fig IV.14 shows examples for <100> p-Si. High temperature discrepancies are to be expected as our largest experimental error is in that range and Massoud's model is quoted as valid only up to 1000 °C.

It must be stressed that the choice of the form of the mathematical expression for the excess growth rate could equally have been a Cabrera-Mott or a power-of-time type of expression (see par.I.7, [REISMAN et al., 1987]). It follows that fitting a model to a particular set of data doesn't automatically prove the correctness of the underlying physical explanation.

IV.1.3 Low temperature oxidation

Modelling of these growth data has been kept separate from the main body of results as the processing conditions and thicknesses involved are quite different from the previous situation.

In Fig IV.15, the lowest continuous curve represents the growth process modelled with an extrapolation of Massoud's high temperature model, though it should be emphasized that it does not claim to be applicable at low temperatures. Following suggestions by Fehlner, Atkinson and Taft [FEHLNER, 1984; ATKINSON, 1985 and 1987; TAFT, 1984] we tried to fit our growth data to a Cabrera-Mott expression (see expression 1.6). For N, Ω and v we used published values appropriate to Si (10^{-10}Å^{-2}, 45Å^3 and 6×10^{13}, respectively. The coefficient of 1/x inside the argument of the hyperbolic sine has the dimension of length and a value of 100Å was chosen at our processing temperature [FEHLNER, 1984]. With these assumptions, the only variable left in the model was W, the activation energy for the ionic defect diffusion (whatever the nature of this diffusing ionic defect). Fehlner and Atkinson reported a value of $\approx$ 1.5eV at these temperatures.

The Cabrera-Mott growth model so constructed fits our experimental data quite well <u>if</u> we choose a somewhat reduced value of W $\approx$ 1.3eV at 514nm and W $\approx$ 1.26eV at 350nm, as shown by the two continuous dotted

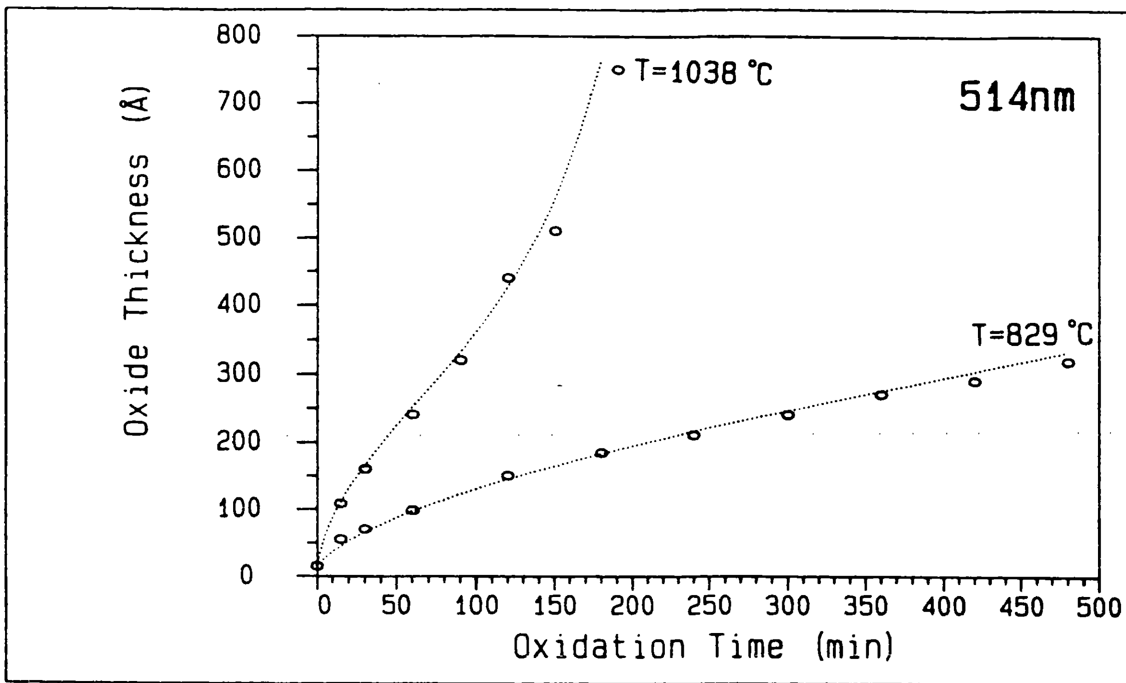

Fig IV.14: Experimental growth data (○) and computer models of laser enhanced oxidation (514nm, <100> Si).

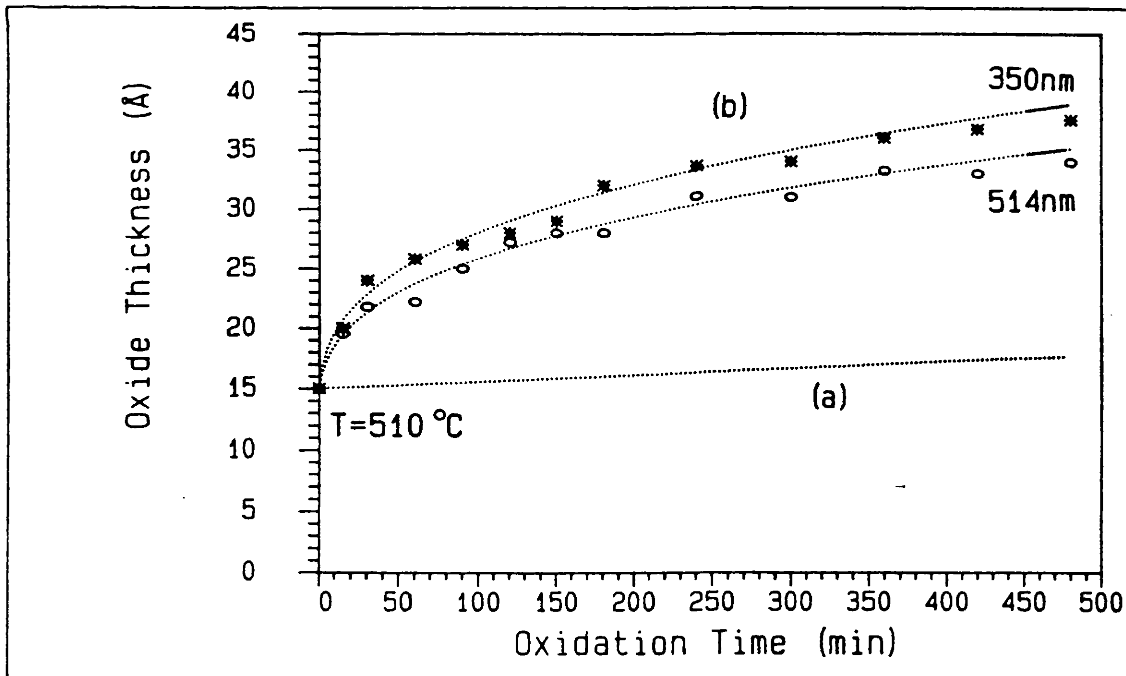

Fig IV.15: Experimental results for visible and UV laser oxidation of Si at 510 °C (data points). The dotted curves represent: (a) extrapolation of the laser oxidation model to 510 °C (514nm); (b) curve fitting of experimental data with the Cabrera-Mott model.

curves in Fig IV.15.

Our limited results seem to confirm the opinion that low temperature oxidation of Si can be modelled by a Cabrera-Mott growth expression.

IV.2 Comparative evaluation of experimental results in the light of previous laser oxidation experiments

As mentioned in the Introduction, the first suggestion that photons could somehow enhance the silicon oxidation rate came from the early work with UV incoherent light by Oren and Ghandhi [OREN et al., 1971] They concluded that, because the energy of their UV source (4.63 eV) was above that required to promote electrons from the Si valence band into the SiO_2 conduction band, this increase in electron population in the oxide was the reason behind the increase in the reaction rate, though no further physical explanation for this enhanced rate was attempted.

A large number of photo-enhanced reactions can be found in the literature; in many instances the photo-generated carriers are considered to be responsible for the enhancement and a brief synopsis of the most relevant examples is presented in Appendix II.

In Fig IV.16 is shown the band structure of Si while Fig IV.17 shows a schematic diagram of the room temperature Si/SiO_2 interface band structure, first studied by Williams [WILLIAMS, 1965]. This is a simplified version of the far more complex, not yet fully characterized, situation which might also depend on type of c-Si and processing conditions. Finally, Fig IV.18 gives the (intrinsic) Si band gap narrowing as a function of temperature (from the approximated expression suggested in [SZE, 1981]).

The range of photon energies available from an Argon laser in the visible range is $\approx$ 2.4 to 2.6eV , clearly not enough to allow any Si/SiO_2 band gap transition via photon absorption (Fig IV.17).

This was also the laser used by Schafer and Lyon [SCHAFER et al., 1981] as an accessory tool in their furnace oxidations.

Our photon-induced enhancement in the green-blue range of the spectrum (and similar range of temperatures) is somewhat smaller

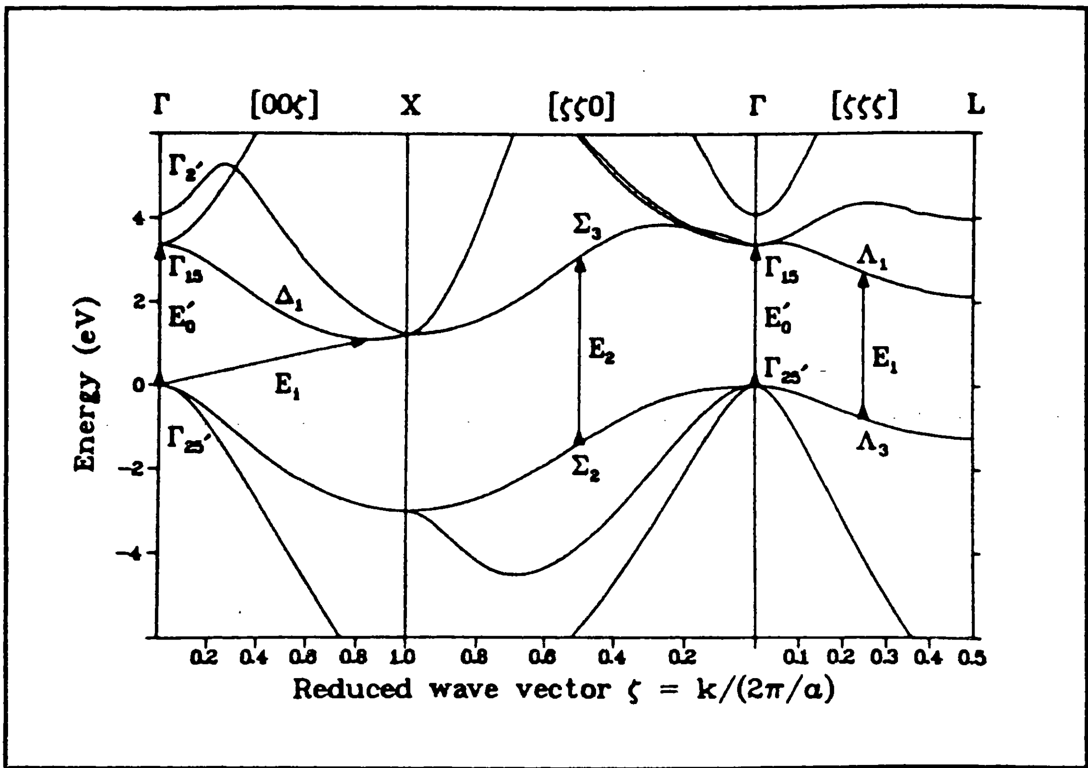

Fig IV.16: Band structure of silicon [JELLISON, 1984].

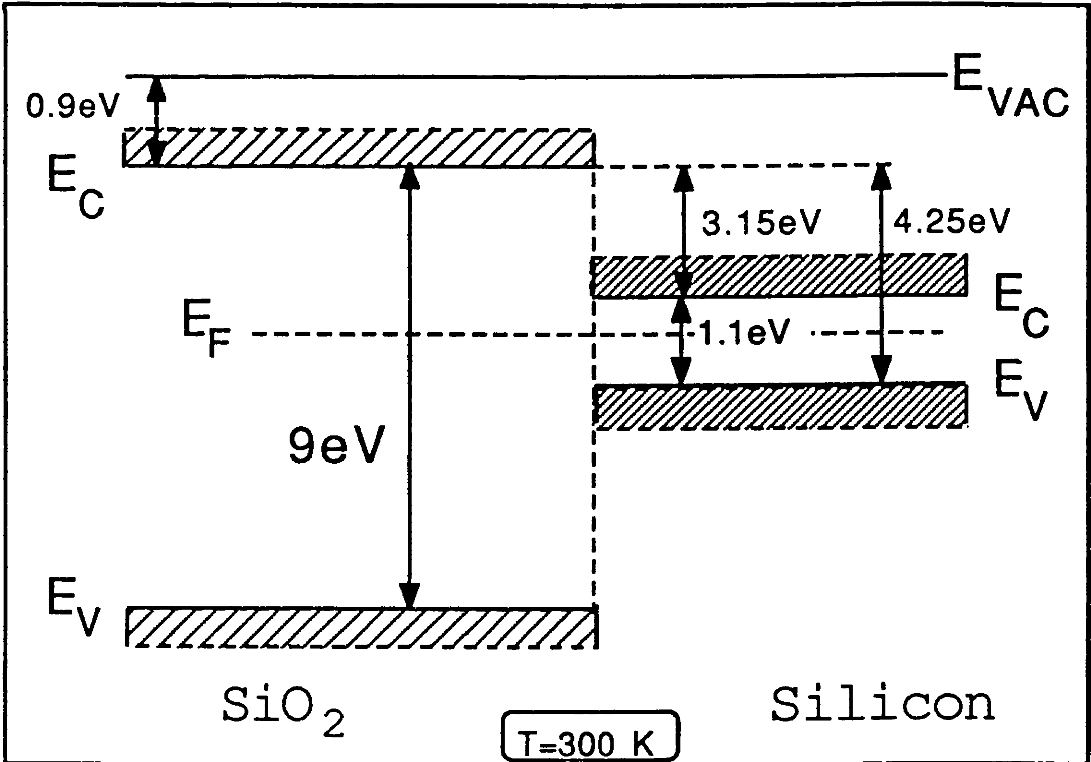

Fig IV.17: Schematic diagram of band structure at Si/SiO_2 interface.

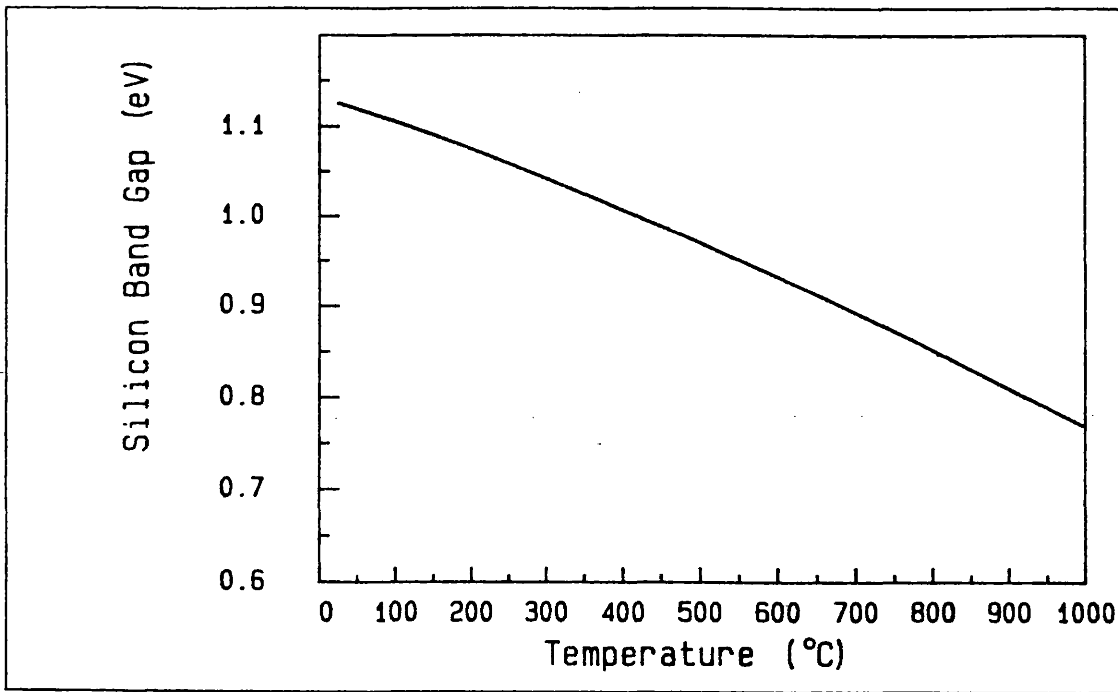

Fig IV.18: Silicon band gap as a function of temperature.

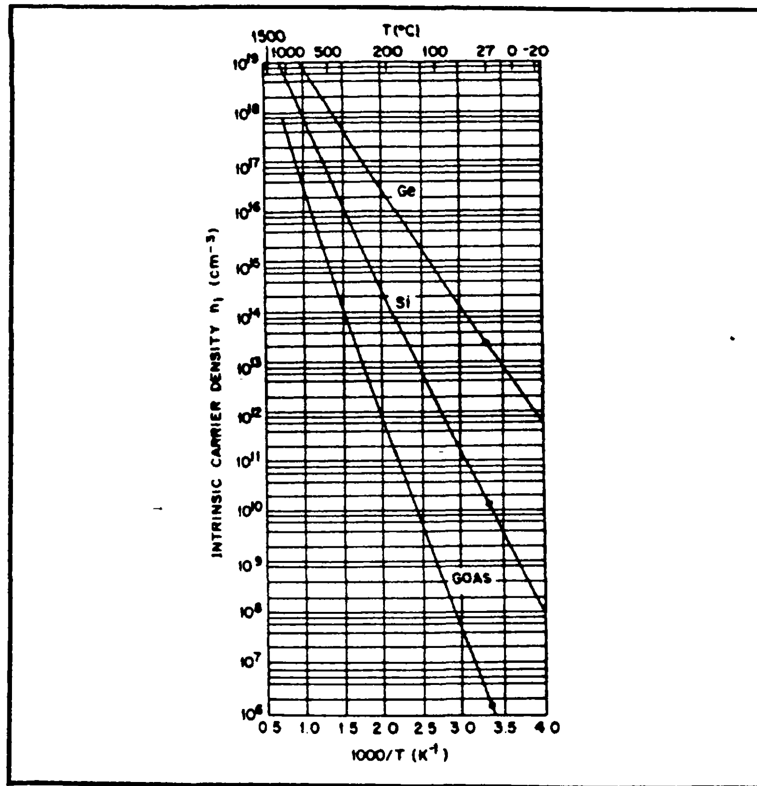

Fig IV.19: Intrinsic carrier densities of Ge, Si and GaAs as a function of reciprocal temperature [SZE, 1981].

than the value found by Schafer and Lyon for similar thicknesses and processing temperatures (≈ 40% at ≈ 300Å), though our photon flux was generally much higher (450 to 650W/cm^2 against their 60W/cm^2 or 150W/cm^2).

A possible explanation for the optical effect on the silicon oxidation was proposed by Schafer and Lyon in the form of a generation of electron-hole pairs beyond the equilibrium intrinsic carrier concentration (see Fig IV.19) and the consequent breaking of Si-Si bonds at the Si-SiO_2 interface.

This view was reinforced by their oxidation experiments on InP and GaAs, where global enhancements of 70% and 500%, respectively, were measured; the large difference between the rate increases in Si and GaAs was attributed to the difference in equilibrium intrinsic carrier concentration (≈$2x10^{18}cm^{-3}$ for Si at 820 °C and $4x10^{14}cm^{-3}$ for GaAs at 480 °C).

Quenon et al. [QUENON et al., 1987] proposed an oxidation model to explain Schafer and Lyon's results in the visible range of the spectrum. They suggested that oxidation is limited by the dangling bond formation rate and that this formation is enhanced by localized interface electronic excited states created by absorbed photons. These states would induce lattice distortion through electron-phonon couplings, from which easier bond breaking could result.

In a successive paper, Schafer and Lyon also noticed [SCHAFER et al., 1982] a minor difference in this rate enhancement between red and violet light (≈ 8% at ≈ 300Å), qualitatively in the same direction as our 514/488 ratio, while a considerable increase with respect to the blue-green light (≈ 20%) was measured when the silicon was irradiated with UV light (350nm, ≈ 3.5eV).

Our limited experiments with the 350nm Argon line confirm this last finding. This indicates the presence, or increased relevance, of a mechanism somewhat different from the visible enhancement of the 514nm with respect to the 488nm line, as the 350nm and 488nm radiations contain less photons/cm^2 for the same power density than the 514nm light. As no effect on the oxide or the oxygen is expected at this UV wavelength, the much higher value of the photonic energy (≈ 3.5eV against the ≈ 2.5eV of the 488nm) must be responsible for the difference (see Fig IV.17), possibly by exciting electrons from the Si conduction band to the SiO_2 conduction band [SCHAFER et al., 1982]. It should be noted that ≈ 3.4eV is the energy for the first

direct transition in Si (Fig IV.16) and consequent increase in absorption coefficient (Fig III.16) (see also [NAYAR & BOYD, 1989]). However, this apparent threshold energy of ≈ 3 to 3.5eV was not present in the wet oxidation of Si, implying that the UV light must affect some component of the dry oxygen reaction that is not present, or not important, in wet thermal oxidation [SCHAFER et al., 1982].

Approximately $2.2\times10^{22}cm^{-3}$-3 O_2 molecules are incorporated in the oxide layer. This means that at the fastest rate measured by Schafer and Lyon ≤ 2×10^{14} molecules/cm^2 sec were consumed. They calculated an available photon flux of ≈ 10^{20} photons/cm^2sec at their power density thus, even assuming a very low electron injection efficiency, it would still be possible for the laser to promote a large amount of electrons into the SiO_2 conduction band. Once there, the electrons could combine with oxygen to form negatively charged species which, as was previously suggested by other researchers (see par.II.6) could play an important role in the oxidation of Si.

To evaluate this suggestion, we examined values reported in the literature for this injection efficiency. A quantum yield of the order of 10^{-7} [WILLIAMS, 1965] and ≤ 10^{-8} [DRESSENDORFER et al., 1980] for photon energies ≈ 3.5eV was extrapolated from work on photo-emission measurements at the Si/SiO_2 interface (at room temperature, low or unspecified doping levels). A value of ≈ 10^{-6} for the percentage of free carrier absorption for carrier concentrations > 10^{18} (n_i at Schafer and Lyon's processing temperatures) was obtained from recently published data [SERNELIUS, 1989]. Viña and Cardona [VIÑA et al., 1984] suggested that the contribution of free carriers to the optical properties of very heavily doped Si starts becoming relevant at energies lower than ≈ 2.5eV.

Clearly, the considerable differences between our experimental arrangement and approach and Schafer and Lyon's could be partly responsible for some of the discrepancies in the results, as the quantitative evaluation of the enhancements or the fact that their rate enhancements, at all wavelengths, were found to be independent of processing temperature (contrary to our findings). The thermal model Schafer and Lyon claim to have used for the calculation of the excess surface temperature due to the laser didn't include the strong temperature dependence of the Si thermal conductivity (while this is a very important consideration when using a sample positioned on a

semi-infinite heat sink, as was in their experiment). Moreover, they ignored the effect of a wavelength dependent reflectivity (though in the comments they mentioned this aspect) and of the oxide-thickness dependence of the sample reflectivity at each wavelength under examination. Finally, they used, in their evaluations, a time-average growth rate, i.e. $R=\delta x/\delta t$. It is generally accepted (and they recognized this point) that the growth rate is a rapidly varying function of time (i.e. thickness) during the first ≈ 300Å of oxide. By taking the average, any possible thickness dependence of the enhancement was cancelled out, therefore removing a factor which could shed some light onto the physical mechanisms involved, especially in the thin oxide regime which is most of interest for laser processing purposes.

Boyd's experiments in the blue-green region of the spectrum [BOYD, 1983] resulted in a laser induced rate enhancement considerably higher than the value reported in this work for temperatures around 800–850 °C. But his experiment was so different from the present one, with its very high power densities, scanning laser beam and very thin oxide films grown, that quantitative differences were expected.

The photo-enhanced growth was again related to the Si-Si broken bond density and found to be strongly dependent on temperature (i.e., the enhancement decreased with the increase of equilibrium intrinsic carrier concentration).

Fig IV.20 shows the thermal and laser enhanced growth rates, as obtained from our experiments, as a function of temperature for two values of oxide thickness. While the absolute value of the excess rate increases with temperature, though, the percent rate enhancement decreases, at every thickness, in agreement with Boyd [BOYD, 1983] and Young and Tiller [YOUNG et al., 1987] (see an example in Fig IV.21).

The oxidation experiments of Young and Tiller [YOUNG, 1988 and references therein] were quite similar to those performed by Schafer and Lyon, inasmuch as they involved a standard furnace and an auxiliary laser (Argon laser for the visible part of the spectrum), but in this case the silicon was held in thermal isolation (as in our experiments). An example of the measured <u>global</u> (thermal + photonic) percent growth enhancement (%E) as a function of control oxide

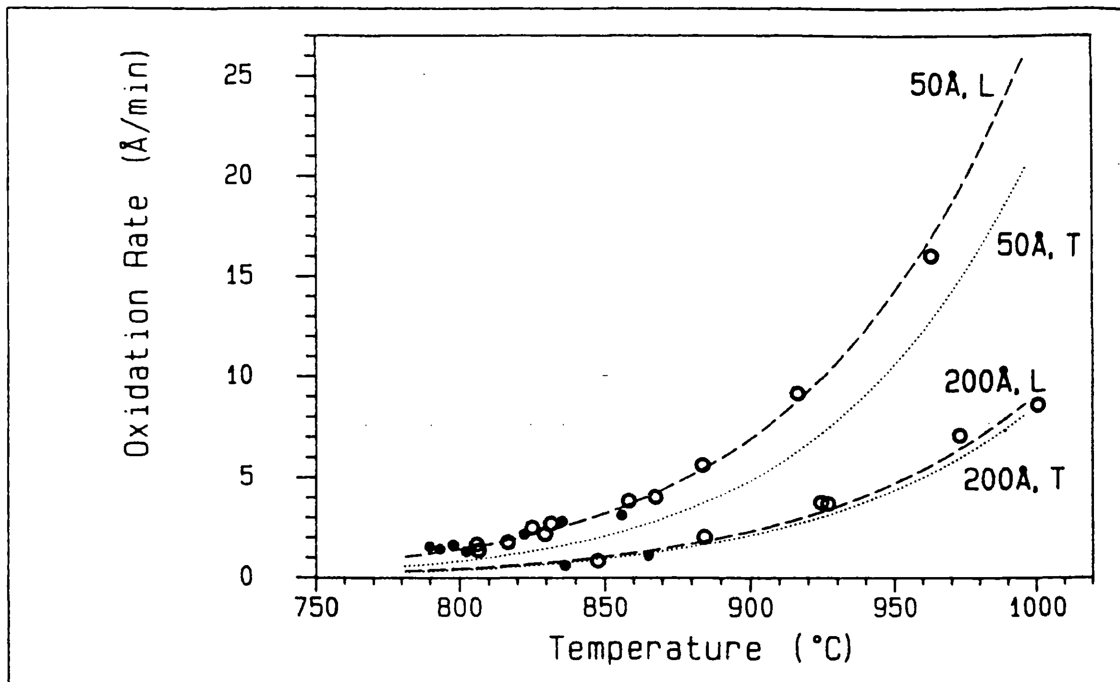

Fig. IV.20: Thermal (T) and laser enhanced (L) oxidation rates for two oxide thicknesses (computer models).
o : Experimental data from curve fitting;
• : Measured data. All data for 514nm and <100> Si.

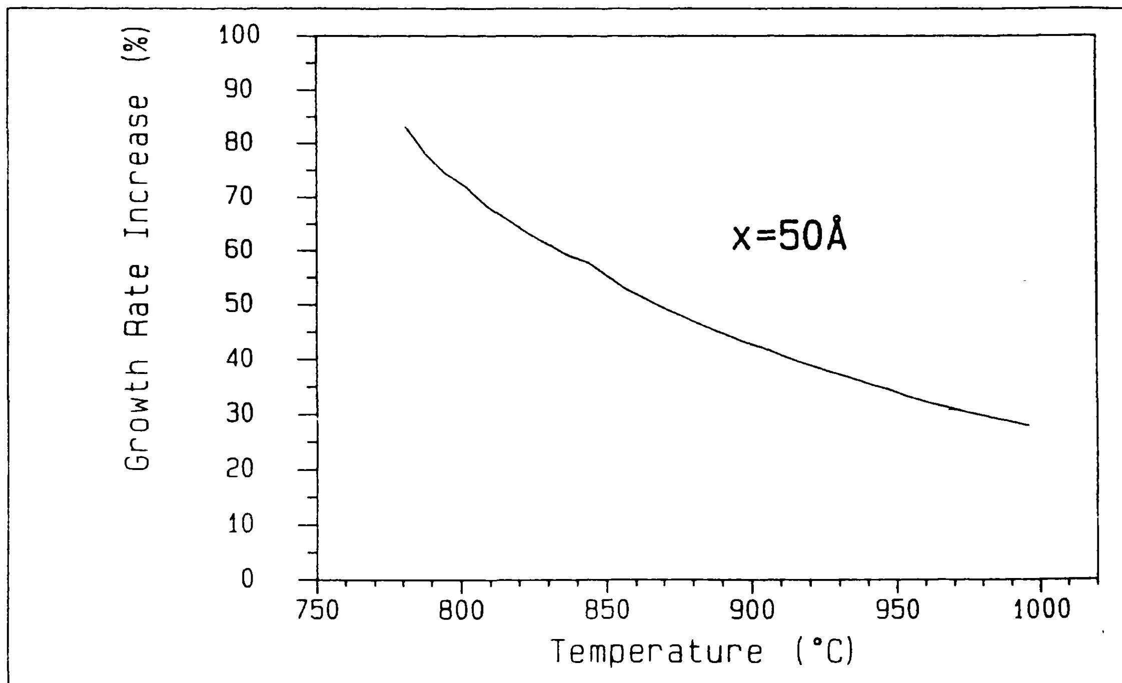

For IV.21: Percent rate enhancement due to 514nm radiation (with respect to thermal) as a function of oxidation temperature at x=50Å.

thickness for various background temperatures is shown in Fig IV.22 (a) and (b). Little or no difference in %E was found between wet and dry oxidation, as previously reported by Schafer and Lyon. Contrary to these authors, though, the enhancement was dependent on processing temperature. The optical part of the enhancement was extracted through complex calculations on the thermal model of their oxidizing sample.

The %E (optical) found by Young and Tiller was of the same order of magnitude as ours in the same range of thicknesses and temperatures, even though their power density was about one order of magnitude smaller than ours (between 17 and 85W/cm^2). The similarity in the value of enhancement is even more conspicuous if one re-calculates the thermal component of the growth with Massoud's latest thermal model (see par.IV.1.1), not available at the time of their work. However, despite this similarity, our enhancement was shown to be a rapidly decreasing function of film thickness, contrary to Young's findings (Fig IV.22).

They also reported evidence for a wavelength dependence of this %E, which we qualitatively confirmed (though they considered negligible the effect of the oxide thickness dependence of the Si reflectivity).

From all the data points with thicknesses ≥ 350Å they extracted the B/A and B rate constants of the Deal and Grove model (see par.I.2) and showed that the major photonic effect occurred in B rather than B/A, i.e. the oxidant diffusion appeared to be most affected by the photonic intervention (they recognized, however, that the linear-parabolic formalism for a single oxidant species, O_2, might not be the appropriate one if more than one oxidant is present and this could affect the previously discussed allocation of enhancements). Considerable differences were noticed in the behaviour of the <100> and <111> rate constant B with 1/T. Our results confirmed the existence of a small orientation dependence in the laser enhancement, as embodied in the different pre-exponential constants (par.IV.1.2). Unfortunately, the omission of thinner oxides from the analysis, though unavoidable for them at the time of their research as no generally accepted model was available covering this range, makes a large percentage of their results difficult to compare with our work.

One of the most conclusive results from our experiments came from

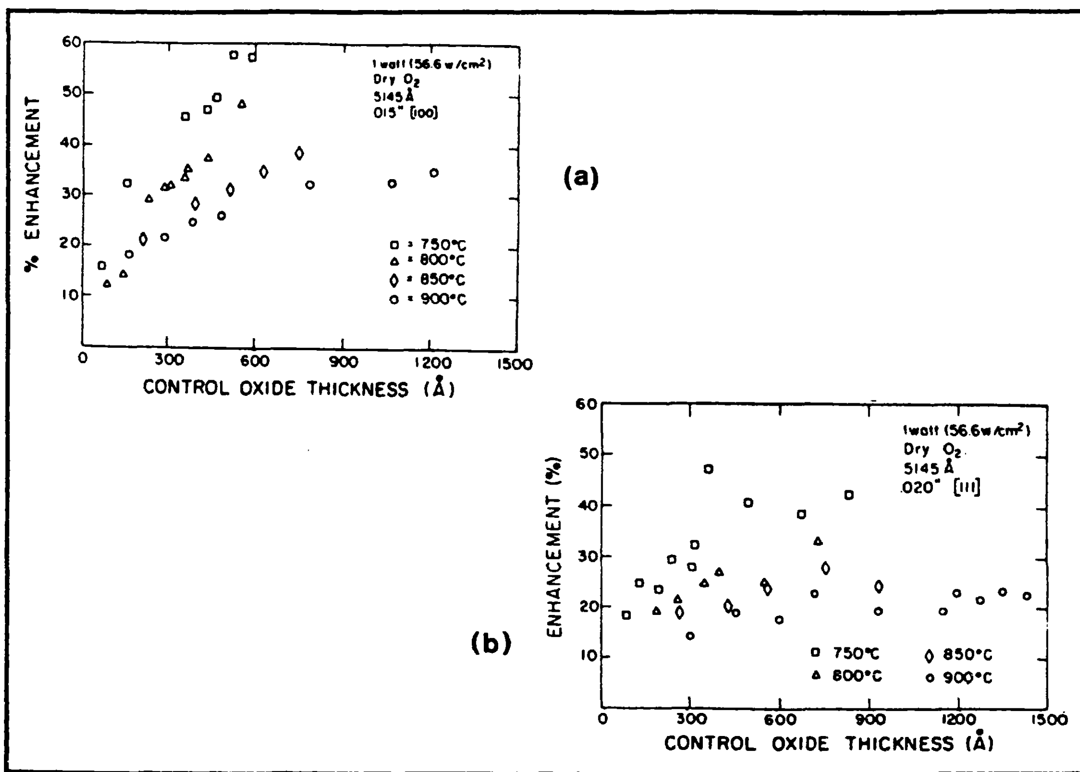

Fig IV.22: Percent enhancement (%E) as a function of control oxide thickness for (a) <100> Si and (b) <111> Si [YOUNG et al., 1987].

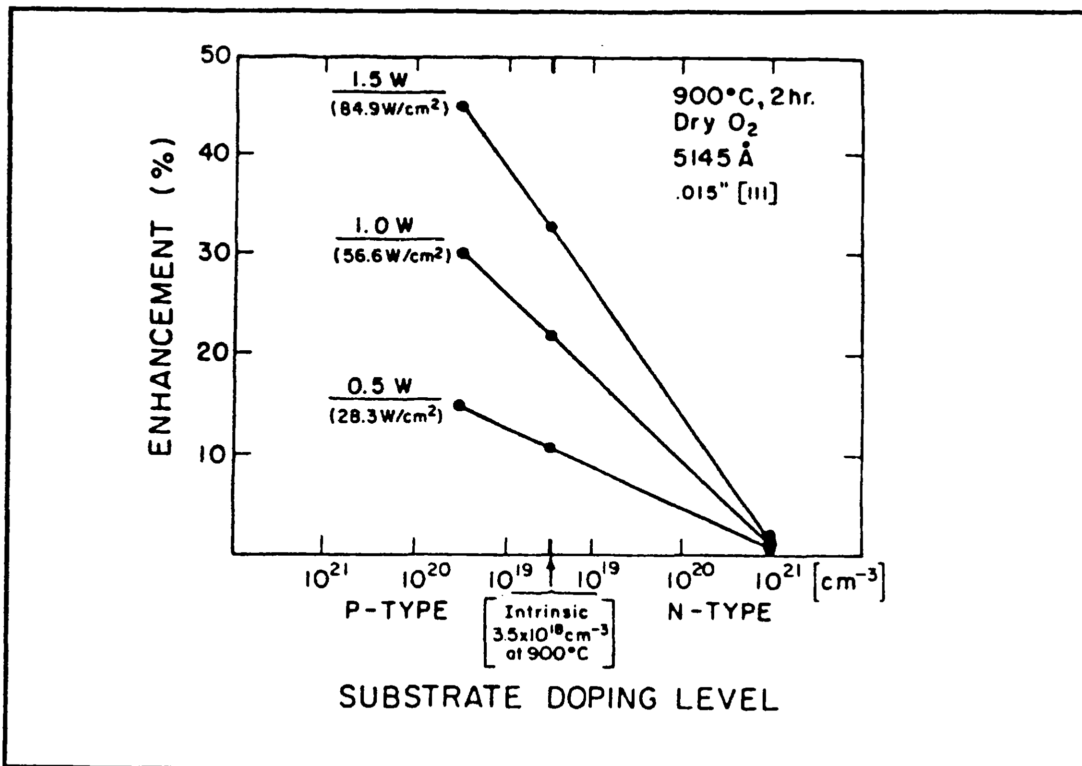

Fig IV.23: Variation of %E with Si sample extrinsic doping level [YOUNG et al., 1987].

the oxidation of heavily doped samples (see par.III.4.5). To draw any conclusion from these experiments, in the absence of an appropriate model, we must assume that the oxidation for heavily doped Si is governed by the same mechanism that applies to lightly doped or intrinsic Si.

The clear differences in our 514/488 experiments on p^+ and n^+ samples clearly confirm Young and Tiller's very important conclusion that the enhanced growth rate is primarily due to the photo-generated increase in the equilibrium electron population at the Si/SiO_2 interface. They reached this conclusion [YOUNG et al., 1987] by carrying out an interesting experiment with Si samples of widely different doping levels, whose results are shown in Fig IV.23. Clearly the light produced less enhancement when the initial component of the conduction band electrons was greater, justifying the conclusion that it was the excess electron generation which played the active role in the enhancement. Though this might not alter the validity of their physical explanation, it is worth noting that the values of enhancement shown in Fig IV.23 are misleading: the ordinate axis represents the total enhancement (as can be easily worked out from published data [YOUNG et al., 1987]; rather surprisingly, then, the heavily doped n^+ substrates in Fig IV.23 not only do not show any photonic enhancement, but they do not seem to exhibit any thermal enhancement either!

This result cannot support the suggestions of Schafer and Lyon and Boyd that the photo-induced increase in Si-Si broken bond density is the main cause of the photo-enhancement.

If the hypothesis of the effect of photo-generated extra electrons is correct, a tentative explanation could be suggested for the relative experiments 514/488 [YOUNG et al., 1983]. The number of photons absorbed at every wavelength by the silicon per unit area and time is given by:

$$\frac{P\,(1-R)\,\lambda}{h\,c\,A} \qquad [\text{abs.photons/cm}^2\ \text{sec}] \qquad (4.6)$$

where P is the incident laser power, R the silicon reflectivity, h Planck's constant, c the velocity of light and A the laser beam area.

For equal absorbed powers (as in our 514/488 experiments), the longer wavelength will provide ≈ 5.1% more photons than the shorter one (as the ratio $\lambda_{514}/\lambda_{488}$).

From DSP Si experiments (par.III.4.2), the relative enhancement is of the same order of magnitude, though the reason for its thickness and temperature dependence is not obvious, using this argument.

When light is applied, even for photon energies below the Si/SiO_2 band edge transitions, there would be enough energetic free electrons in the Si conduction band able to enter the SiO_2 conduction band, thereby increasing an already present thermal population [YOUNG, 1988] Once there, they could play a critical role in the dissociation of oxygen, thereby facilitating the diffusion through the constrained oxide network close to the interface. The effect was shown to be much more significant when Si is irradiated with UV light (i.e. higher energy photons) and particularly when the energy is above the O_2 dissociation level of ≈ 5.1eV [YOUNG et al., 1987].

IV.3 Oxygen interaction with electrons

It is necessary at this stage to discuss briefly some possible interaction of light and electrons with the incoming oxygen molecule.

The photo-dissociation energy of O_2 is ≈ 5.1eV (≈ 240nm), well above our range. There are electronically excited states for O_2 at ≈ 0.98eV and ≈ 1.63eV, but the direct transition from the ground state to the first by light absorption is forbidden by the selection rules [OKABE, 1978] and the probability of a transaction to the second is negligible [OKABE, 1978]. Nevertheless, these rules are valid only for free molecules and it has recently been suggested [MESARWI et al., 1989] that light induced excitation (at $E \geq 1.63$ eV) of adsorbed O_2 on Ni might be a possible pathway to enhanced dissociation and atomic oxygen production, with resulting increase in oxidation rate.

As no specific treatment is available, to our knowledge, for the case of adsorbed or interstitially dissolved oxygen, we are constrained to assume a similar behaviour to the well documented gas case (to which the following notes apply), even at the low concentrations of dissolved oxygen found in SiO_2 (of the order of $5\text{–}6\times10^{16}cm^{-3}$ at 1atm [SZE, 1988]).

Fig IV.24 shows the potential curves for ground and excited state of O_2 and O_2^-. From the graph, a positive electron affinity (i.e. stable configuration) of ≈ 0.44 eV and a dissociation energy of ≈ 4.1eV can be deduced for O_2^- [MCDANIEL, 1964].

The dissociative attachment reaction by capture of an electron by the ground state O_2, probably proceeding through an unstable excited state of O_2^-, as

$$O_2 + e \longrightarrow O_2^{-*} \longrightarrow O + O^- + KE \qquad (4.7)$$

requires energies above those which our process might be able to generate, even at the highest oxidation temperatures (see Fig IV.25 for room temperature and high temperature attachment cross-sections as a function of electron energy [MASSEY, 1976]).

But the experiments by Chanin, Phelps and Biondi [CHANIN et al., 1962] on attachment coefficients of low energy electrons (at room temperature) demonstrated the possibility of some dissociative attachment even at electron energies of the order of ≈ 2eV and a different mechanism for negative ion formation at electron energies below ≈ 1eV (these experiments have been invoked by Young and Tiller in their suggested explanation of laser enhanced silicon oxidation [YOUNG et al., 1987].

Fig IV.26 [MASSEY, 1976] shows the variation of α/p with average electron energy (where α is the attachment coefficient per unit drift distance of an electron drifting through the gas under the influence of an electric field E and p is the gas pressure). For values of energies higher than ≈ 1eV the quantity α/p is independent of pressure, indicating a two-body dissociative attachment while at energies below ≈ 1eV the quantity α/p is proportional to pressure, indicating that a three body attachment process predominates. The mechanism proposed (see [MASSEY, 1976]) is that an electron undergoes resonant capture into a vibrational state of O_2^- which lies above the ground state of O_2. Left to itself, the O_2^- state would revert through autodetachment to the initial O_2 state loosing an electron. However, if a third body is present, stabilization can occur through collision:

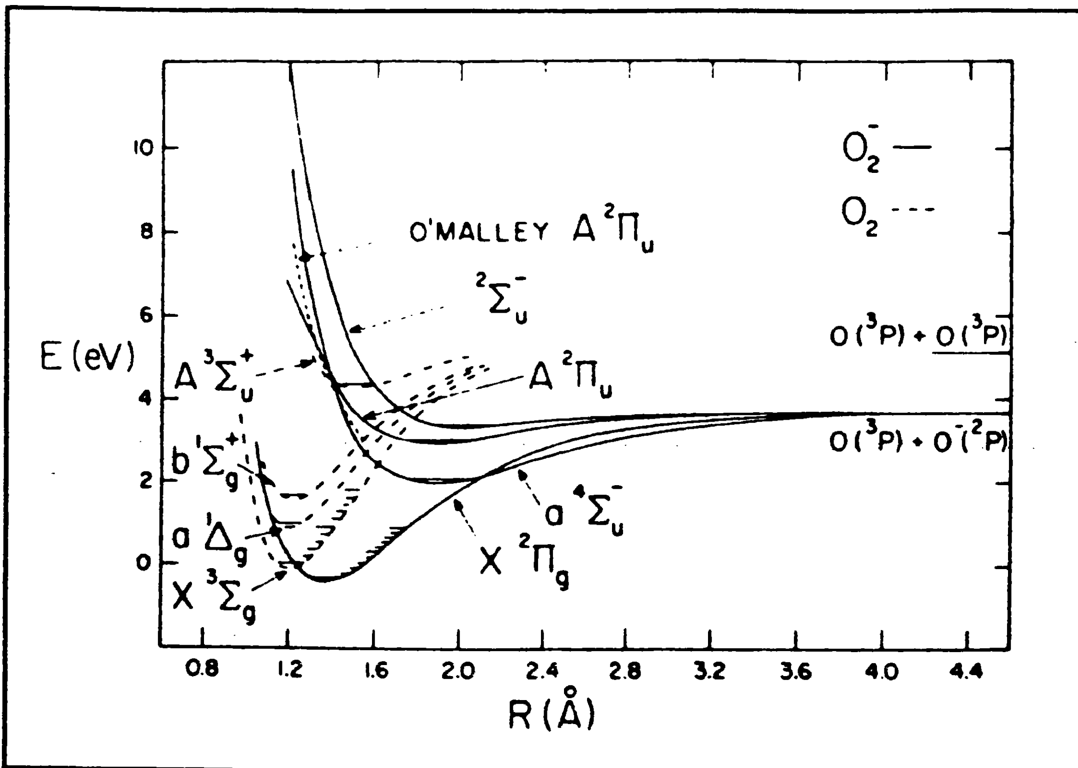

Fig IV.24: Potential energy curves for ground and excited states of O_2 and O_2^- [DAS et al., 1978].

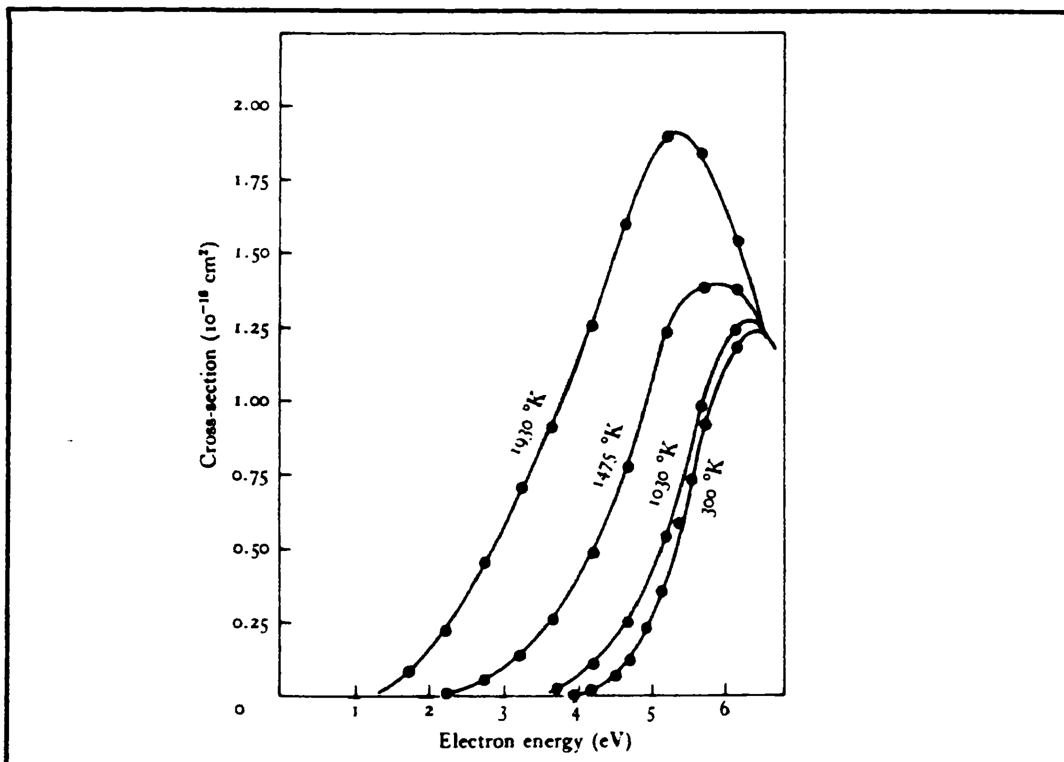

Fig IV.25: Total cross section for dissociative attachment of electrons to O_2 as function of electron energy for different gas temperatures [MASSEY, 1976].

$$O_2 + e \longrightarrow O_2^{-*} \qquad (4.8)$$

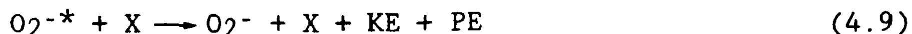

$$O_2^{-*} + X \longrightarrow O_2^{-} + X + KE + PE \qquad (4.9)$$

Fig IV.27 shows the measured three-body attachment coefficient for oxygen versus average electron energy [McDANIEL, 1964].

In our processing situation, the third body X could be another oxygen molecule. But this option doesn't seem very likely as, given the low concentration of occupied solubility sites for oxygen in silica, the average distance between two oxygen molecules is ≈ 270Å; more probably, the silica network itself or water molecules act as third body. Indeed, it has been shown that H_2O, even in very small concentrations, is particularly effective as a third body in O_2^- formation [MASSEY, 1976] via a three-body attachment mechanism. It is interesting to compare these results with the recently confirmed fact that the silicon native oxide growth in air and ultra-pure water at room temperature requires coexistence of water and oxygen in each ambient [MORITA et al., 1989]. In wet oxygen oxidations this mechanism could become most efficient. We have seen (par.IV.2) that Schafer and Lyon did not find any wavelength dependence during wet Si oxidation under visible and UV illumination, contrary to the dry O_2 case. It is possible that this mechanism could be somehow responsible for these findings. However, water molecules are known to exchange with the oxide network and are therefore able to introduce a completely different transport mechanism which could explain the observed results.

Fig IV.28 shows experimental photo-detachment cross-sections for O_2^- and O^- (within the energy range of our experiments) and Fig IV.29 the energy spectrum of the photo-electrons arising through photo-detachment from O_2^- by argon laser light. Whether this mechanism would be able to generate a non-negligible percentage of electrons with energy higher than those emitted from the silicon and capable of participating in a two-body dissociative attachment with oxygen (see above) remains to be proven and, at present, can only be a tentative speculation.

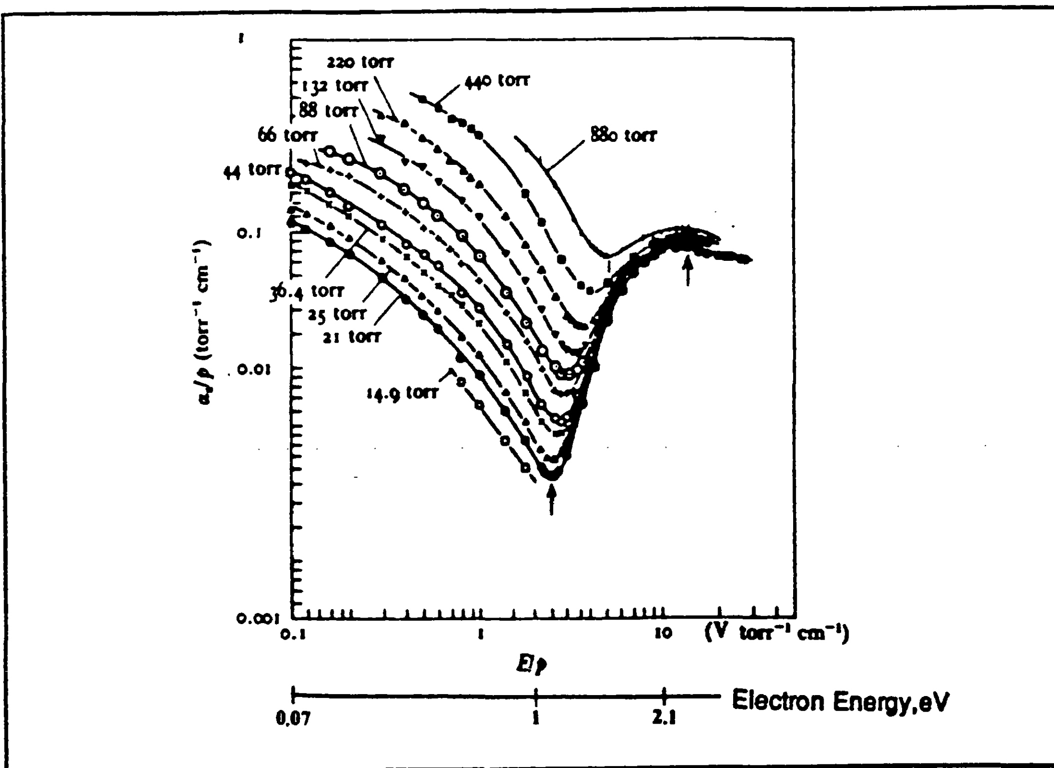

Fig IV.26: Variation of α/p with E/p (and electron energy) for electrons in O_2 [MASSEY, 1976].

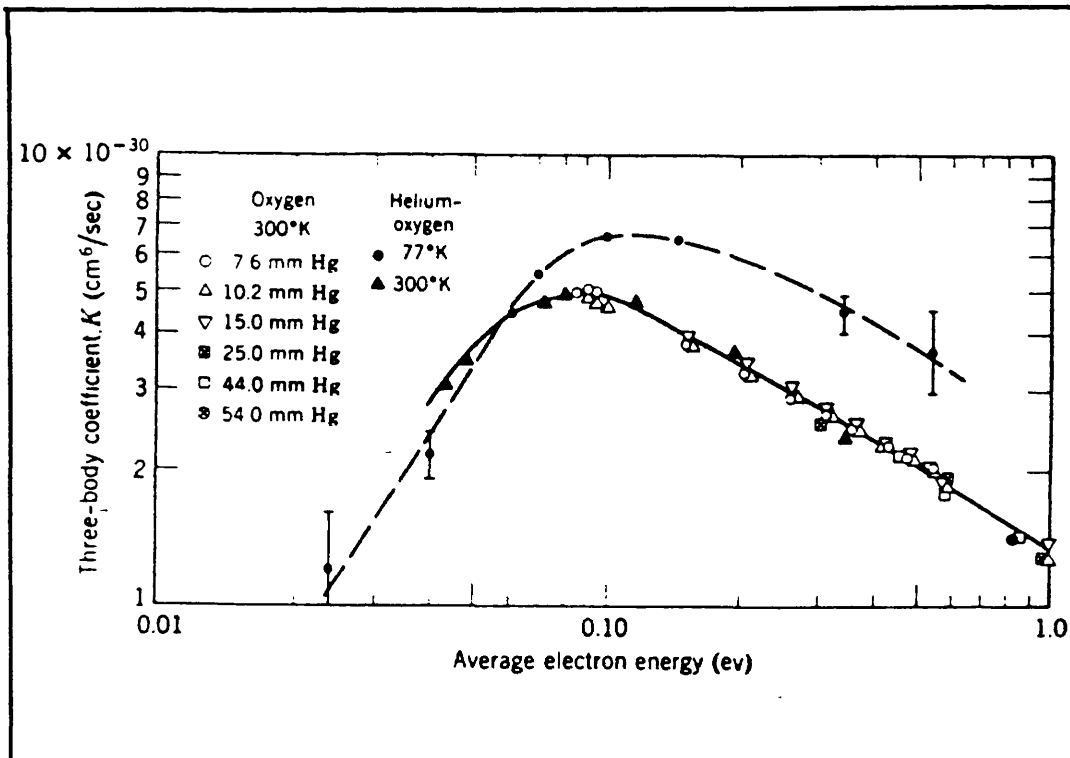

Fig IV.27: Three-body attachment coefficient for oxygen as a function of average electron energy for gas temperatures of 77 and 300 K [McDANIEL, 1964].

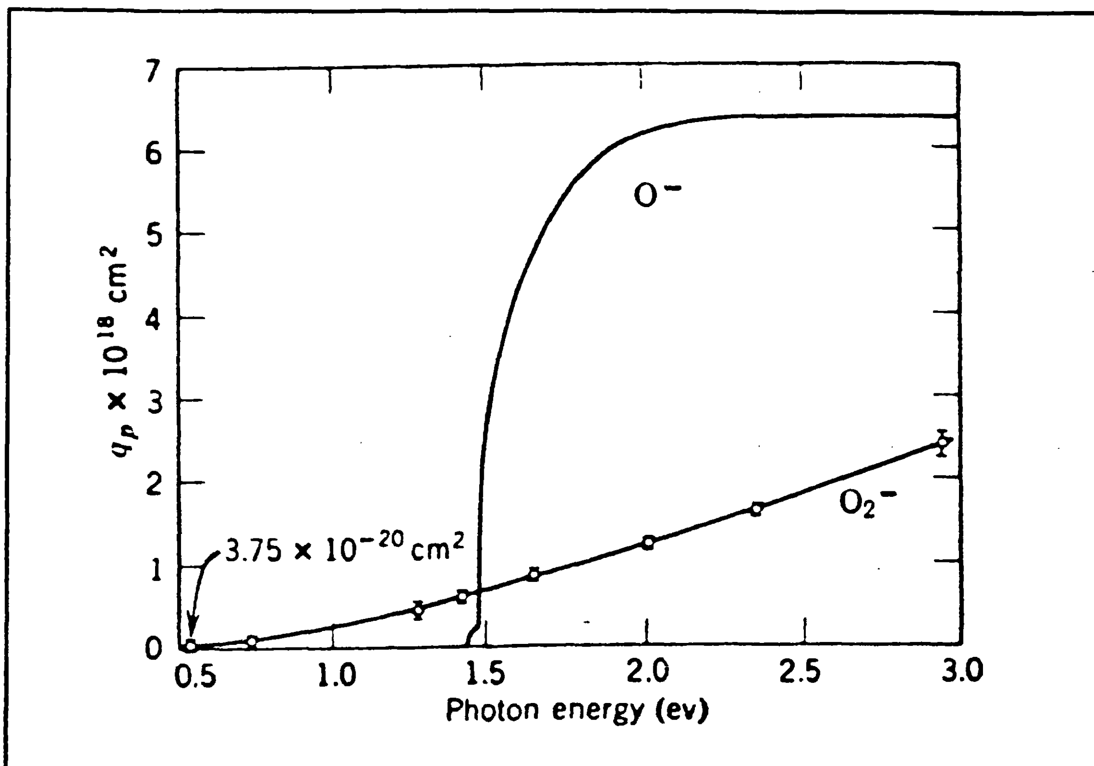

Fig IV.28: Experimental photo-detachment cross sections for O_2^- and O^- ions [McDANIEL, 1964].

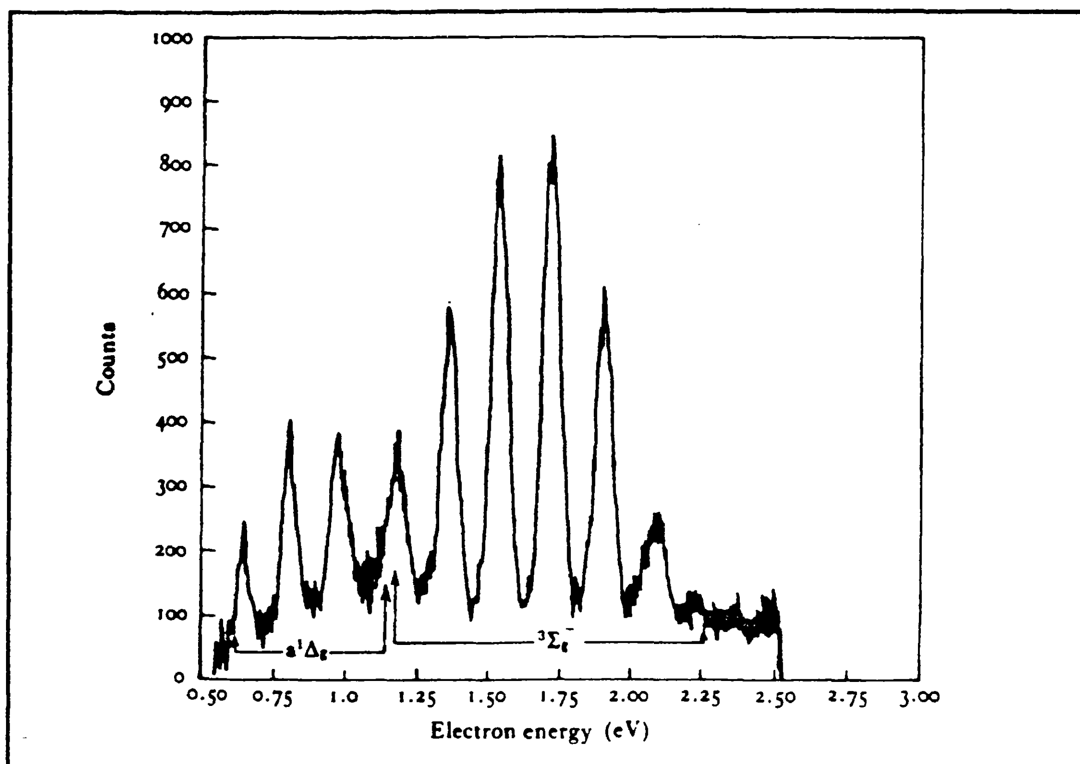

Fig IV.29: Energy spectrum of the photo-electrons arising through photo-detachment from O_2^- by Argon laser irradiation [MASSEY, 1976].

IV.4 Discussion of laser enhancement mechanisms

To summarize briefly our main results, the growth kinetics with visible radiation indicated the presence of a photo-enhanced process, either acting in parallel with the usual thermal mechanism(s) (but orientation dependent) or influencing it (them) directly. Excess electrons appear to be responsible for this process. The effect decays exponentially with oxide thickness with a characteristic length of the order of 60 Å. Extra enhancement was noticed with near-UV light in temperature conditions where the high temperature mechanisms might not apply.

We will now examine some qualitative aspects of the generation of electrons at the Si/SiO_2 interface (with or without the laser influence), the mechanics of their injection into the growing oxide and the region of space charge near the interface. In the light of the many models we have presented in Chapter I, the degree to which this mechanism participates in the overall reaction is still unresolved, but some tentative suggestions will be made.

IV.4.1 Electron tunnelling and thermoionic emission

Even <u>in the absence</u> of any external conditioning or internal electric field, a considerable percentage of Si electrons would be able, by quantum mechanical tunnelling, to penetrate some distance into the sub-oxide or strained oxide layer (we will neglect any scattering phenomenon or reflection effect as the discussion is purely qualitative) where they would be either turned back or trapped. It is immediately clear how important the issue of interface and oxide trap states is by envisaging the possibility of a two-way exchange of carriers between these states and the Si and SiO_2 bands. The poor understanding of the subject (see Appendix I for a more comprehensive review) therefore imposes severe limitations to any discussion, on a more atomistic level, on the initial stages of Si oxidation.

The quantum mechanical tunnelling probability T for a one dimensional square energy barrier with barrier height E_0 and thickness W is given by [SZE, 1981; COHEN-TANNOUDJII et al., 1977]:

$$T \approx \frac{16\ E\ (E_0-E)}{E_0^2} \exp\ (\ -2kW) \qquad (4.10)$$

for $W >> 1/k$, where :

$$1/k = \sqrt{(\hbar^2\ /\ 2\ m_{ox}\ (E_0-E))} \qquad (4.11)$$

where $\hbar$ is the reduced Planck's constant, m_{ox} the electron effective mass in the oxide ($m_{ox} \approx 0.5m_0$ [WEINBERG, 1977]), E the electron energy. Assuming that the Si CB/SiO_2 CB energy gap is 3.15eV, independent of temperature and oxide thickness, Fig IV.30 shows Log(T) as a function of barrier thickness.

At the high temperatures characteristic of silicon oxidation considerable electron injection by thermionic emission from the substrate into the oxide conduction band is also possible. It is assumed that the Si CB electrons have a Maxwellian distribution of energies and velocities (at temperatures around 900 °C the mean electron energy is $kT \approx 0.1$ eV). Once in the oxide, the mobility of electrons should be fairly high and they could travel some distance before a trapping event. The lifetime of electrons in the oxide under processing conditions is, to our knowledge, not known. Fromhold [FROMHOLD, 1976] assumes the mean free path in the oxide to be certainly < 300Å. DiMaria and Fischetti [DI MARIA et al., 1988 and references therein] quote an energy relaxation distance of ≈ 30 Å for a hot electron injected at the interface under an electric field (at room temperature). Young and Tiller [YOUNG et al., 1987] suggest a travel distance into the oxide of ≈ 50 to 60Å in the case of visible excitation from the Si. Doubts therefore remain on how to choose a reasonable value for the distance into the oxide travelled by the injected electrons (even if it was possible to determine their initial energy). It is likely, though, that the electrons would be trapped within tens of Ångstroms from the interface.

The Richardson-Dushman equation for thermionic emission from a uniform surface of a metal (or semiconductor) is given by [SZE, 1981]:

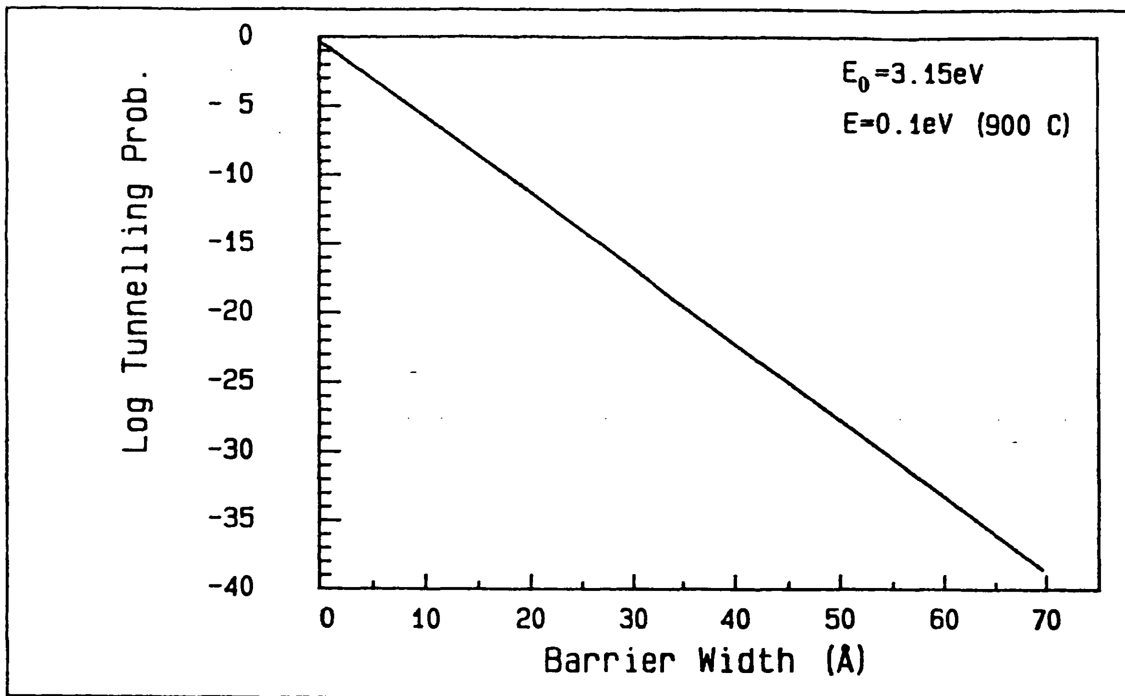

Fig IV.30: Tunnelling probability for a square energy barrier as a function of barrier width.

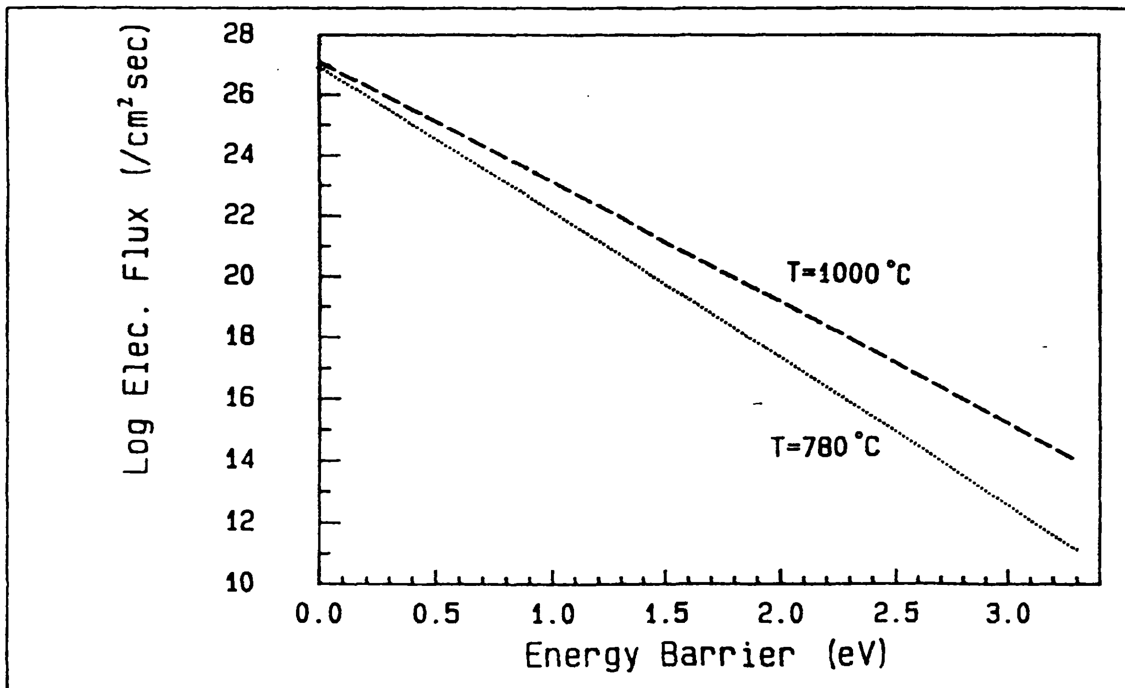

Fig IV.31: Thermionic electron flux as a function of barrier height at two temperatures.

$$J = A^* T^2 \exp(-q\varphi/kT) \quad [A\ cm^{-2}] \qquad (4.12)$$

where

$$A^* = 4\pi mk^2q/h^3 = 120\ Acm^{-2}K^{-2}$$

(where the value is correct for free electrons); $q\varphi$ is the effective energy barrier, k Boltzmann's constant and T the temperature. For silicon Sze [SZE, 1981] suggests a value of $110Acm^{-2}K^{-2}$. Fig IV.31 shows the variation of J as a function of $q\varphi$ for two values of temperature.

IV.4.2 Photogenerated electrons

Let's now superimpose to this picture the effect of CW laser irradiation with 2.41eV photons. The flux of electron/hole pairs (e/h) generated by the absorbed photons (assuming a generation efficiency of 1) can be expressed as:

$$\frac{P(1-R)\lambda}{hc\pi w^2} \exp\left(\frac{-r^2}{w^2}\right) \left[\frac{e/h\ pairs}{cm^2\ sec}\right] \qquad (4.13)$$

where w is the 1/e radius of the laser beam, P the incident power, R the Si reflectivity at a given wavelength λ and temperature, h Planck's constant and c the speed of light.

The generation rate G_L of photo-electrons is given by:

$$G_L = \frac{P(1-R)\alpha\lambda}{hc\pi w^2} \exp\frac{-r^2}{w^2} \exp(-\alpha z) \left[\frac{e/h\ pairs}{cm^3\ sec}\right] \qquad (4.14)$$

At equilibrium these photo-generated carriers will diffuse away from the surface and recombine giving all their energy to the lattice through phonon scattering. At high carrier densities (or doping concentrations) the recombination mechanism in silicon is thought to be dominated by an Auger process (a three-particle process) with the recombination rate R_A expressed by:

$$R_A = C_A N^3 \qquad (4.15)$$

where N is the carrier concentration and C_A a constant. In this case the minority carrier lifetimes are given by:

$$\tau_n = 1/C_{An}\, n^2 \quad \text{or} \quad \tau_p = 1/C_{Ap}\, p^2 \qquad (4.16)$$

where n and p are carrier concentrations. In the literature there is considerable variation in the values of C_A and τ [PASSARI et al., 1983; DZIEWIOR et al., 1977; HULDT et al., 1979; FOSSUM et al., 1983]. Assuming for C_A an average value of $5 \times 10^{-31} cm^6 sec^{-1}$, the corresponding lifetime is of the order of 10^{-7} sec.

To find the steady state electron density at the surface the continuity equation should be solved. The differential equation would require a numerical solution [SCHAFER et al., 1981; MOGYOROSI et al., 1988], but as we are only interested in orders of magnitude, we have followed a simplified approach [BOYD, 1983] by imposing, at equilibrium (and at r=0 and z=0):

$$G_L = R_A; \qquad (4.17)$$

then:

$$N = \{ P(1-R)\alpha\,\lambda \,/\, C_A hc\pi w^2 \}^{1/3} + n_i \quad [cm^{-3}] \qquad (4.18)$$

For $\lambda =$ 514nm, $\alpha = 10^5$, $R \approx 0.425$ and $\pi w^2 = 14.18 \times 10^{-3} cm^2$ the steady state carrier concentration is of the order of $2 \div 6 \times 10^{18} cm^{-3}$ at the laser powers used in our experiments.

The photons are absorbed in $\approx 0.1\mu m$ $(1/\alpha)$ of silicon and the photo-generated carriers (electrons) will diffuse away from the surface with a diffusion length ($L = \sqrt{(\mu k T \tau / q)}$) of the order 5-20$\mu m$ (uncertainty in the lifetime is now compounded by uncertainty in the carrier mobility [WILLANDER et al.,1988]).

With respect to the purely thermal excitation, the CB electrons average energy is now considerably higher: with a photon energy of $\approx$ 2.41eV, a Si band-gap at 900 °C of $\approx$ 0.81eV, the initial excess energy of the photo-generated electron is $\approx$ 1.6eV.

Uncertainty exists over the value of the mean free path for electrons in our oxidizing sample: Pankove [PANKOVE, 1969] reports a value of 60Å for the mean free path in Silicon and a value of 0.06eV for the loss of energy per collision. It would take $\approx$ 26 random collision to lose the excess 1.6eV (and fall to the bottom of the

conduction band prior to recombination) and a total travel of ≈ 1500Å. <u>In the absence of any surface potential</u>, the electrons will diffuse <u>away</u> from the interface into the Si (opposite to our requirement). We estimate that only those generated within ≈ 100Å from the interface (a very rough guess from Pankove data) would have any real chance of 1) approaching the interface and 2) possessing an excess energy high enough to substantially increase their chances of entering the SiO_2. In these conditions, at most ≈ 10% of the electrons photo-generated per cm^2 per sec would be likely to contribute to any electron flux over the Si/SiO_2 barrier (a small percentage, even compared to the small enhancement we have measured, indicating the presence of some other contributing factor).

Given the high Si CB electron density, it is also possible that a very small amount of free carrier absorption could take place in Si (though, from the literature, the probability for such an event at our wavelength seems to range between 10^{-5} and 10^{-9}, see par.IV.2). The photon energy would still not be high enough to allow direct photo-emission into the oxide conduction band, but the average energy of the electrons would increase even further so that there would now be a significant percentage of electrons seeing a very small barrier for thermionic emission or tunnelling.

A considerable enhancement in the injection process would be obtained by using UV light, as confirmed by Young and Tiller [YOUNG et al., 1987] who found a ten-fold enhancement in the oxidation rate for photon energy ≈ 4eV, which happens to be, approximately, the Si VB /SiO_2 CB barrier at their processing temperature.

It is also conceivable that our 2.4-2.5eV light might excite electrons from trap sites not too deep into the <u>oxide</u> gap, thereby increasing the flux. Trap levels of ≈ 2eV [WILLIAMS, 1965] and ≈ 2.4eV [NG et al., 1980] below the SiO_2 CB have been reported in the literature.

The probability of transitions from, or into, trap states at the interface (and energetically in the Si gap) is likewise enhanced.

IV.4.3 Experimental verification

It is very tempting at this stage to show that there is some correlation between the flux of electrons and the amount of consumed oxygen. Various researchers have performed similar calculations [SCHAFER et al., 1982; YOUNG et al., 1987; WOLTERS et al., 1989; IRENE et al., 1987]. From the experimental growth rate at various temperatures and thicknesses, one obtains the number of oxygen molecules (or atoms) consumed per unit area and time ($\approx 2.2 \times 10^{22}$ oxygen molecules, or $\approx 4.4 \times 10^{22}$ oxygen atoms, are incorporated in a cm^3 of oxide). This value is then equated to the flux of thermionically emitted electrons and an 'equivalent' Si/SiO_2 energy barrier is calculated and compared with the actual value of 3.15eV.

Table II shows some results from our kinetic data (we have arbitrarily used the flux of oxygen atoms, not molecular oxygen, although the trend is identical in both cases and, even numerically, the difference in barrier height is quite small). It can be seen that, at the same oxide thickness, the barrier 'seen' by the electrons is very close to the actual one at the higher temperatures, but somewhat smaller at the lower temperatures. Notwithstanding the fact that any error in our system is highest at higher temperatures, the percent increase in oxidation rate due to the laser is higher for lower temperatures (Fig IV.21), in agreement with the present results. Furthermore, at the same (low) temperature, the apparent barrier tends to the actual value with increasing thickness (Table II). Similarly, the excess growth rate tends to zero with increasing thickness (Fig IV.11). An apparent lower barrier could, for instance, imply the relevance of the tunnelling electrons, but also a higher average energy in the Si CB electrons due to laser excitation.

Clearly this doesn't constitute a proof for the suppositions made (note that a difference in energy of only ≈ 0.2eV produces a variation of approximately one order of magnitude in the electron flux), but the trends are, nevertheless, encouraging. It must be pointed out that such a thickness dependent thermionic emission flux (laser enhanced or not) is unusual and the process is much more complex than these simplified calculations imply.

Temperature °C	Thickness Å	Oxid. Rate Å/min	Si/SiO_2 Energy Gap eV
795	30	1.84	2.9
	50	1.29	2.93
837	30	3.68	2.95
	50	2.6	2.98
	128	1.28	3.07
	413	0.53	3.158
868	50	4.24	3.05
	80	3.02	3.09
912	50	8.23	3.11
961	50	16.41	3.16

Table II: Si/SiO_2 energy gap as obtained from experimental growth rate and thermionic emission data.

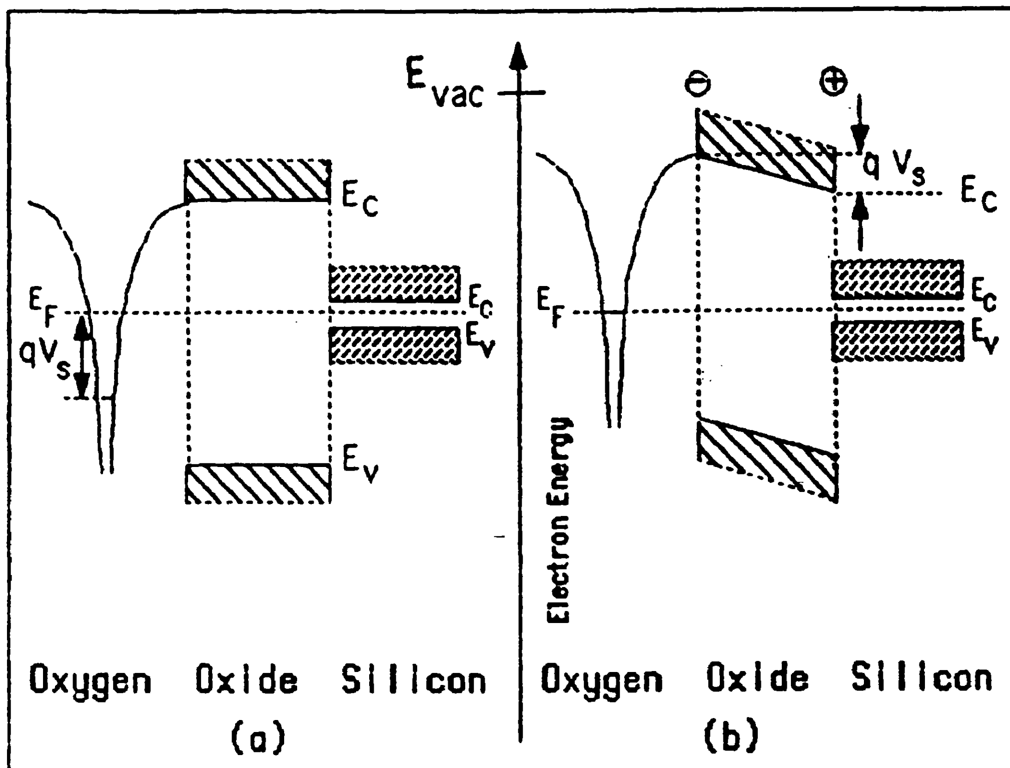

Fig IV.32: Electronic levels in Si, SiO_2 and adsorbed oxygen (a) before electrons have passed through the oxide and (b) once equilibrium is reached [CABRERA et al., 19848].

IV.4.4 Photonic enhancement and oxidation models

We will now try to correlate the presence of photo-generated electrons with some available oxidation model (see par.I.6).

The exponential decay in the laser induced enhancement could be explained in the light of Murali and Murarka's rather unusual theory of the existence of an oxygen-diffused zone in the silicon substrate, a few tens of Ångstroms wide (see par.I.8 [MURALI et al., 1986]). The presence of excess CB electrons could somehow facilitate the bonding between Si and the interstitially dissolved oxygen within this region. By its own nature, this effect diminishes with increasing oxide thickness. An estimate of the time required for oxygen to diffuse to a profile with a diffusion length of ≈ 30Å (which corresponds to an average value of 60-70Å measured for the characteristic length in the data analysis) at 900 °C gives 40ms [WATKINS et al., 1982]. However, it should be remembered that our oxidations start with Si already covered by a few monolayers of SiO_2 and this could affect the initial oxygen diffusion into the substrate.

In par.IV.1.3 we have shown that Cabrera-Mott model (described in par.I.6) fits quite reasonably our <u>low temperature</u> oxidation data, provided we use a somewhat reduced value for the activation energy for the ionic defect diffusion. This value (≈1.3eV at 514nm) is also remarkably close to the activation energy for our high temperature enhancement mechanism (see expression (4.5)). It is therefore worthwhile to examine whether this model could also be invoked for the initial stages of high temperature, laser-driven, oxidation. Fig IV.32 is a schematic representation of the setting up of the uniform field by tunnelling electrons. According to the model, this field then opposes electron motion and drives oxygen ions to the interface. Because of its high electron affinity, the energy levels of chemisorbed oxygen states are mainly below the Si midgap, they may extend well below the Si valence band, but are certainly above the SiO_2 valence band [HU, 1984; ATKINSON, 1987; ROBERTSON, 1987]. It can be shown [HAYES et al., 1985; HU, 1984] that even a low density of surface ions O^- (assuming a dissociative chemisorption) gives large electric fields; a value of 1V for the chemical potential present generates a field of 1MV/cm for a 100Å thick layer and can be

achieved by about 10^{-4} of a monolayer of surface O^-. In the literature, values ranging between 1 and 2V have been reported for the emf (V) of the electrolytic cell $O_2/SiO_2/Si$, which provides the driving force for electronic transport (at 1atm of O_2 and in the temperature range of interest).

Stoneham et al. [STONEHAM et al., 1987] have highlighted the importance of accounting for image charges when evaluating the fixed potential difference V_s in C-M model. In this case, V_s would become dependent on thickness and also the energetics of charged-ion injection at an interface would depend on the proximity of the other surface, introducing another dependence on oxide thickness. Though this effect doesn't change much to our qualitative picture, it stresses the potential complexity of the process.

At high temperatures and ≈ 1atm of oxygen, there is some diffusion of interstitial neutral O_2 through the network (see Chapt.I). If O_2 is interstitially dissolved in the oxide the electrons do not have to travel to the surface to form oxygen ions (as in the Cabrera-Mott model), but they could interact within, or at, the boundary of the 'reaction layer' or 'blocking layer' (the altered, perhaps strained, layer extending as far as 60Å from the interface, according to many authors (see par.I.8 and Appendix I). However, under the assumption [HERMAN, 1981; ATKINSON, 1985] that the electronic levels in dissolved ionized oxygen are the same as in adsorbed ionized oxygen on the surface and that the equilibrium oxygen solubility in bulk SiO_2 ($C^* \approx 5.5 \times 10^{16} cm^{-3}$ at 1atm of O_2 [MOTT, 1981]) is valid also for thin films [Massoud et al., 1985], it can be shown [ATKINSON, 1985] that the voltage drop across the oxide layer containing a uniform charge density qC^* would be ≈ 30mV for film thicknesses ≈ 60Å, well below the potential difference $V_s \approx 1V$ (see par.I.6 and Fig IV.32). The low concentration of O_2 is therefore not sufficient to enable equilibration of electronic levels within the alleged dimensions of the 'strained' layer; the space charge in the film is therefore quite small, as required by C-M model, and voltage must be still developed by charges at the interfaces.

Therefore, as long as the oxide is thin, a Cabrera-Mott type of mechanism might be envisaged, perhaps acting in parallel with Deal and Grove suggested mechanism (see Chapter I). Our experiments do not enable identification of the particular ionic species involved

(oxygen anion or network defect). We cannot exclude the possibility of interaction of electrons with oxide/interface defects, or even the possibility of generation of such defects by photo-injected electrons [ROBERTSON, 1987], especially in a situation where the electron injection into the oxide is somehow enhanced.

IV.4.5 Fixed positive charge and its effects on electronic and ionic fluxes

So far we have not addressed the effect, near the Si/SiO_2 interface, of the fixed positive charge Q_f (see Appendix I). The main reason was the desire to present the various issues progressively, starting from the more obvious and less controversial ones and finish with the more doubtful and speculative. Cabrera-Mott original model did not consider the presence of these charges and, though no physical impediment exists to their integration into the model, it will be clear that their presence complicates the picture considerably (see par.I.6).

It is known that fixed positive charges exist in all as-grown oxides and it seems reasonable to expect that the charges exist in the oxide layer near the interface also <u>during</u> oxidation. It is not known for certain what the effect of the high temperature would be, but Wolters and Zegers-van Duynhoven [WOLTERS et al., 1989] have suggested that, as the charge is induced by the growth, stopping the growth would reduce Q_f and, therefore, Q_f at the high processing temperatures is likely to be much higher, perhaps as much as an order of magnitude.

Other studies, however, have shown that fixed oxide charges (measured <u>after</u> oxidation) decrease with increasing processing temperature or following a high temperature anneal (see, for instance, [AKINWANDE et al., 1987]). Various experiments [HAMASAKI, 1982; LANDSBERGER et al., 1987; McGRUER et al., 1987; SINGH et al., 1988] have shown considerable enhancements in growth rate when intermediate anneals were performed on the oxides (clearly any stress present would have been relaxed at the same time).

To be able to correlate the presence of the charge density with

the oxide growth, a detailed spatial and temporal distribution of their entity with varying oxide thickness, oxidation conditions, silicon orientation and doping levels (and all possible combination of them) would be required. To the best of our knowledge, this information is not available yet. Vyas et al. [VYAS et al., 1982] found an increase in fixed charged density with decreasing oxide thickness, but their data don't include oxides thinner than ≈ 300Å.

Moreover, a description of the actual dynamic field in the near-interface area would require the solution of Poisson's equation with the charge term including not only the fixed oxide charge, but also interface trapped charge, ionized oxygen ions or other point defects, image charges, electrons and holes.

In oxidation models using fixed positive charges (see par.I.6) an exponential spatial distribution has been used of the type:

$$Q = Q_S \exp(-x/L_S) \qquad (4.19)$$

but with widely varying values for L_S, with reported values ranging from less than approximately 15Å [HAMASAKI, 1982], to ≈ 150Å [LU et al., 1984] or between 90 and 200Å [SCHAFER et al., 1985].

In a recent study [WOLTERS et al., 1989] a 2D δ-function of charges at, approximately, 30Å from the interface has instead been adopted. They modelled the time evolution of this space charge taking into account the strong Coulomb repulsive forces which affect trapping probabilities when traps are closer than ≈ 100Å to each other (i.e. a density of ≈ 10^{12}cm^{-2}).

Assuming $Q_f \approx 10^{13}$cm^{-2} (at high temperature) and $\epsilon_{ox} = 3.9$, the electric field generated by these charges (near the interface) would be of the order of :

$$\frac{qQ_f}{\epsilon_{ox}\epsilon_o} \approx 4.5 \text{ MV/cm} \qquad (4.20)$$

Clearly, choosing instead the room temperature value of Q_f (≈ 10^{12} cm^{-2}) would give a field of < 0.5MV/cm.

The associated surface potentials reported in the literature vary between 0.1V for oxides less than 100Å thick [HATTORI et al., 1988],

0.2V (fixed value) for the first few hundreds of Ångstroms of oxide [NAITO et al., 1986] and ≈ 0.4V for oxides approximately below 100Å [HAMASAKI, 1982]. Clearly, all these value should only be taken as an indication of orders of magnitude.

The internal electric field (and image charge) so generated is bound to have a dramatic effect on any ionic and electronic fluxes present in the near-interface region.

In the presence of fixed positive charges in the oxide the bands at the interface will look as in the schematic diagram of Fig IV.33 (arbitrary band bending). Hattori (see above) measured an oxide charge induced band bending of ≈ 0.3eV for oxides thinner than 100Å. The electron concentration at the interface would, in this case, increase by approximately 20 times at 900 °C, according to [SZE, 1981]:

$$n = n_i \exp(q\varphi/kT) \qquad (4.21)$$

where n_i is the intrinsic carrier concentration and φ the surface potential. The electric field thus <u>enhances</u> electron emission into the oxide. Photo-generated electrons can then drift towards the interface under the effect of the field from deeper into the Si substrate (see par.IV.4.2).

The expression for a tunnelling current over a barrier φ_B in the presence of a field E is given by [SZE, 1981; WOLTERS, 1987]:

$$J = \frac{q^3 m_0 E^2}{16\pi^2 \hbar m_{ox} \varphi_B} \exp\left(- \frac{4\sqrt{(2m_{ox})}\ \varphi_B^{3/2}}{3q\hbar E}\right) \ [A/cm^2] \qquad (4.22)$$

where all symbols have the usual meaning (Fig IV.34).

Furthermore, if we assume the existence of trap states at a distance d from the interface and at energy $q\varphi(d)$ from the SiO_2 CB (Fig IV.33):

$$q\varphi(d) = q\varphi_B - qEd \qquad (4.23)$$

the probability of electrons escaping through a trapezoidal potential barrier by tunnelling from the Si CB to these states is given by:

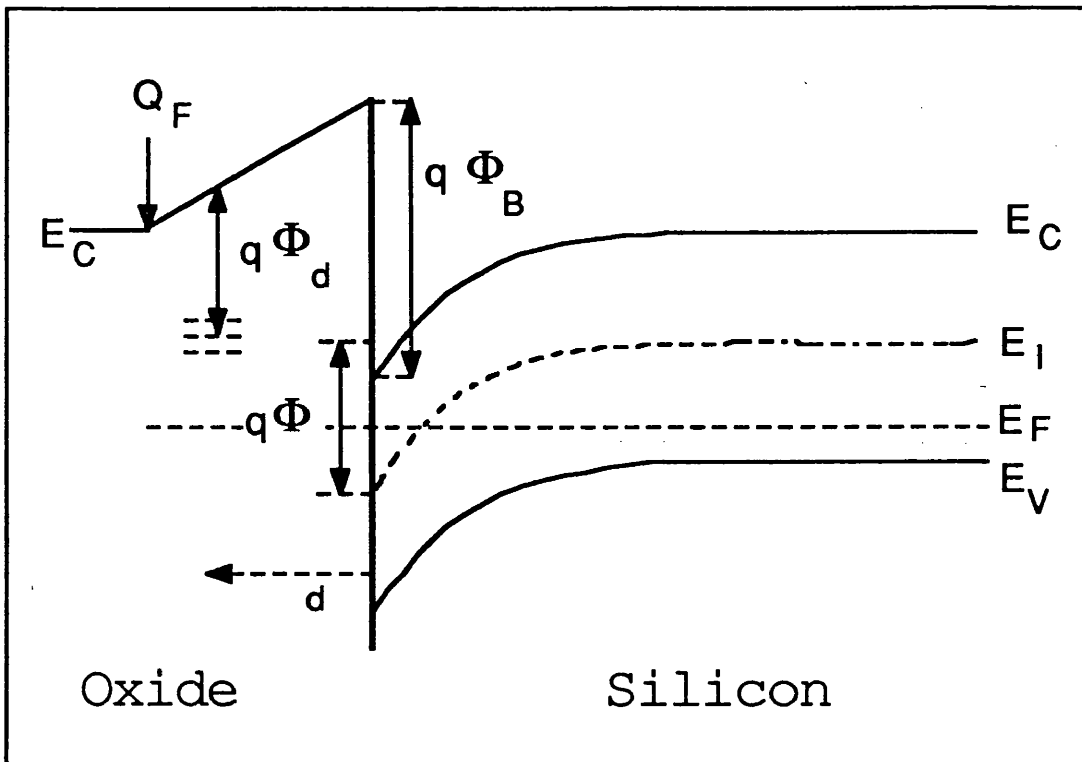

Fig IV.33: Si/SiO2 interface band diagram in the presence of positive charges (Q_f). Trap states at distance d from the interface are also shown.

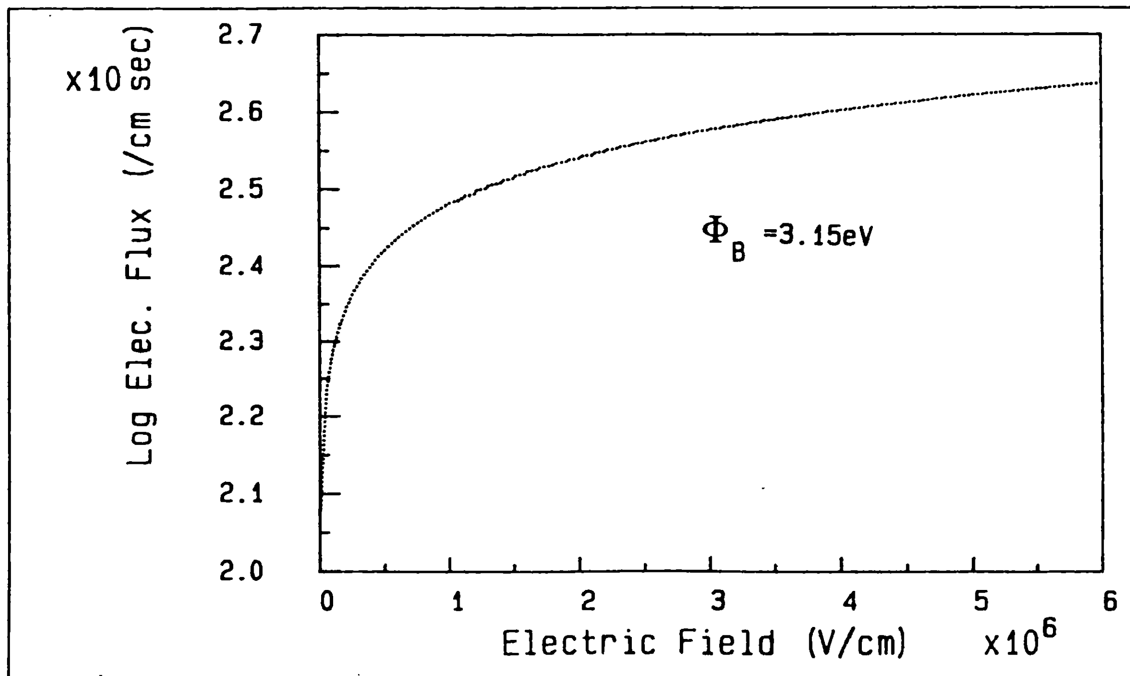

Fig IV.34: Tunnelling electron flux as a function of electric field.

$$\alpha \exp\left(-\frac{4\sqrt{(2m_{ox})}\,(\varphi_B^{3/2} - \varphi(d)^{3/2})}{3\hbar qE}\right) \qquad (4.24)$$

[LAKHDARI et al., 1988], where α depends on the particular defect.

At high oxidation temperatures, an increase in thermionic emission is introduced by the field and we have [SZE, 1981]:

$$J = A^{*}T^{2} \exp\left(-\frac{q[\varphi_B - \sqrt{(qE/4\pi\epsilon_{ox}\epsilon_o)}]}{kT}\right) \quad [A/cm^2] \qquad (4.25)$$

Table II showed (from oxidation kinetic data) that the effective Si/SiO_2 barrier appeared to be reduced for very thin oxides. From the above expression we can extract the value of electric field which would produce such a reduction in the total barrier and, subsequently, the density of fixed oxide positive charge necessary to establish such a field. A value of $\approx 3.65\times10^{12} cm^{-2}$ is found, in very good agreement with the experimental value shown in Fig III.26 and typical of our oxides.

The electrons injected into the oxide (and accelerated by the field there) could reach the SiO_2 surface (as required by Cabrera-Mott model) or could be trapped and contribute to a negative charge (always close to the interface) which might result in an apparent decrease in net fixed positive charge. Alternatively, the positive charges could themselves capture electrons (though this annihilation process doesn't seem to happen during electrical testing, at least at room temperature). Any increase in the negative trapped charge would distort the field at the interface and decrease the electron flux into the oxide. The trapping process of electrons near the interface might again be regulated by Coulomb repulsive forces [WOLTERS et al.,1987, 1989].

Oren and Ghandhi [OREN et al., 1971] found a considerable decrease in Q_f when the silicon was irradiated with UV light during oxidation, while Kassabov et al. [KASSABOV et al., 1988] measured a small increase when UV light was applied at room temperature on a as-grown oxide.

The same fixed positive charges which, on one hand, enhance the electron emission, on the other must retard any negative ions present in the region close to the interface and travelling towards it, as discussed in a few oxidation models in par.I.6. In these models, the build-up of charge was deemed to be responsible for the decrease in growth rate which appears within the first 200-300Å of oxide (just outside the range where the photonic enhancement appears to be active).

As mentioned at the beginning of this section, even if we assume, qualitatively, that a Cabrera-Mott type of mechanism is behind the photonic enhancement, it is not possible, at the present stage of understanding, to formulate a more quantitative picture of the growth process.

IV.4.6 Summary and comments on orientation dependence

A picture of the main mechanisms which, in our view, regulate the oxide growth has been presented. The emphasis was on space-charge effects as our experiments indicate that the increased pool of electrons available for reaction have a role to play in the initial stages of the Si oxidation (at least). A role for stress-related effects or the presence of micropores or other structural characteristics cannot be excluded a priori, but we do not find any direct correlation with our experimental evidence, although there is some evidence that the density of fixed positive charge might be related to stress in the oxide (see [IRENE, 1987; WOLTERS et al., 1989] for references).

As with thermal oxidation, it is not possible to determine the precise role of electrons in the photonic oxidation. Even in the case of low temperature oxidation, the fact that the data could be fitted by a Cabrera-Mott type of growth rate doesn't in itself justify the existence of a particular mechanism. Furthermore, the kinetic data do not give enough information to uniquely pin-point a reason for the apparent reduction in the activation energy for the ionic movement into (and within) the oxide network.

It is reasonable to suppose that the extra flux of electrons

enhances the adsorption (with creation of negative ions) and/or the dissociation of oxygen at the oxide surface in the initial stages. O, O_2^- or O^- could generate a flux of oxidant (migrating to the interface either interstitially or by some exchange mechanism, with or without the assumption of an electric field) in parallel with the main interstitial O_2 (in the assumption that oxygen moves mainly interstitially in our experimental conditions, which is by no means certain for thin oxides). This possibility would diminish with increasing oxide thickness as less electrons would be able to reach the oxide surface. If, instead, we assume that electrons interact with oxygen mainly at the boundary of the 'blocking' or 'reactive' layer, it is more difficult to explain why the enhancement should decrease exponentially with oxide thickness, as such a layer is likely to be always present during all stages of oxidation. However, it has been recently suggested [MOTT et al., 1989] that this reactive layer might increase in thickness with time (and total oxide thickness) until a dynamic equilibrium is reached, at each temperature.

On the other hand, the extra flux of electrons likely to be trapped into the oxide could, initially, compensate for the high density of fixed positive charge, thereby allowing a greater flux of ionic oxidant to reach the Si/SiO_2 interface. Accounting for Coulomb repulsion, the trapping rate is proportional to $\exp(-N/N_0)$ [WOLTERS et al., 1989 and references therein], where N is the number of trapped charges and N_0 the maximum number of places where charges can be accommodated (generation of traps with visible light is not very likely as the photon energy is too low for breaking Si-O bonds). This neutralizing effect could therefore diminish down to an equilibrium situation as the oxidation progresses. The ionic current would decrease accordingly [and so would the compensating electronic current, as required by Wagner's theory (see Wolters et al. model in par.I.6)].

In this last section IV.4, all the comments applied equally to both <100> and <111> orientations. We have seen (IV.1.1) that <100> Si exhibits a slightly higher percent rate enhancement than <111> Si, with a similar thickness and temperature dependence. This confirms that the oxidation rate enhancement is not uniquely determined by the

number of photo-generated carriers, but is also moderated by the interfacial chemical/physical structure and/or charge and trap distribution at, or near, the interface (which are all orientation dependent, as briefly discussed in Appendix I). It must be remarked that in the Cabrera-Mott model no great sensitivity to crystal orientation is expected [MOTT, 1981, 1982].

Young [YOUNG, 1988] tentatively explained the difference between <100> and <111> enhancements by referring to recent studies on dipole moments at the Si/SiO_2 interface [MASSOUD, 1988] according to which the <111> orientation has the largest electron retarding potential by ≈ 0.47eV. Therefore, under equivalent irradiation conditions, the <111> Si would emit a somewhat smaller flux of electrons than the <100> Si. A confirmation of this suggestion comes also from an older article by Weinberg and Hartstein [WEINBERG et al., 1983] on tunnelling from Si to SiO_2. The reduced tunnelling found for <111> was explained by a higher barrier (≈ 0.5eV) . It was suggested that the barrier increase could be due to a bonding arrangement at the <111> Si/SiO_2 interface which resulted in a dipole layer of higher density.

Though it is a quite convincing explanation, it opens up some doubts on how to explain the greater thermal rate for <111> than for <100> if one assumes that the hot electron flux "moderating" role in O_2 dissociation is <u>the</u> rate limiting step. Besides, if the densities of bonds in sub-oxides at the interface are assumed to be those reported by Grunthaner et al. [GRUNTHANER et al., 1987] for <100> and <111> Si, then this difference in dipole moments could decrease to ≈ 0.05V [MASSOUD, 1988].

CONCLUSIONS

The main results of this study on oxidation of silicon with visible radiation from an Argon laser as the sole source of energy will be briefly summarized and a few suggestions for future work introduced.

A preliminary experiment carried out at the beginning of this research with laser light at 514nm and 488nm confirmed the existence of a photonic component to the mainly thermal oxidation reaction, the first time this result was reported outside the framework of a classical furnace oxidation.

The experimental technique capitalized on optical interference effects due to the presence of the growing film thereby not requiring knowledge of the absolute value of the temperature (a recurrent problem in all types of laser processing). Although the preliminary experiment was qualitatively successful, its nature did not enable us to obtain a reliable quantitative evaluation of the process.

To this end, an in-situ thickness and temperature monitor was designed and implemented, as no such instrument was commercially available at the time. This reflectometer (built within the constraint of a small budget) was then used in a large number of oxidation experiments, similar to the original one, with a range of laser powers, different Si orientations and doping levels and types.

A considerably more accurate evaluation of the photonic enhancement to the thermal growth rate and of its possible causes was thus possible. The monitor also enabled us to notice a wavelength dependence at wavelength differences as small as ≈ 5% (as the 514nm and 488nm).

The experiments with double-side polished (DSP) silicon samples and heavily doped wafers proved to be especially revealing. The DSP samples acted as a sort of 'filter' for the photonic enhancement to the oxidation rate. This was due to the front-side oxide being subjected to both thermal and photonic effect while the back-side oxide was purely thermally controlled. Therefore, not only was it possible to extract a 514nm/488nm relative effect, but we could also determine an upper limit for the absolute enhancement with respect to the purely thermal case, this being not achievable with the

standard single-side polished samples. The resulting value proved to be both temperature and thickness dependent.

The heavily doped samples provided direct information on the cause of the laser induced enhancement. We confirmed that the effect appears to be related to the photo-generated excess electron population at the Si/SiO_2 interface. The photonic contribution to the SiO_2 growth rate was found to be exponentially decaying with oxide thickness, with a characteristic length of ≈ 60 to 65Å (within the framework of our extensive computer modelling based on a widely accepted published thermal model adapted to our processing conditions).

A rate enhancement of the order of 55 % with respect to the purely thermal case was measured for 50Å thick oxides grown by 514nm light at temperatures around 835 °C. This enhancement decays rapidly to only ≈ 10 % for 200Å thick oxides grown at a similar temperature.

Our results give qualitative support to the body of oxide growth models based on space charge effects.

A small numberof experiments were carried out with near-UV light from the argon laser (350nm). A comparison of these low temperature oxidation data with those obtained by 514nm irradiation at identical temperature showed a definite enhancement for the 350nm line. The growth curves were shown to fit a Cabrera-Mott type of model with a reduced activation energy for the ionic diffusing species.

The laser generated excess electron population is likely to give relevance to (parallel) oxidation mechanisms normally masked by a predominant Deal and Grove type of kinetics. The presence and evolution (with time, temperature, oxide thickness or stress) of fixed positive charges at the interface constitute, in our opinion, an important milestone in the localized photonic effects brought about by the laser light.

Further investigation into some aspects of visible laser oxidation of Si can be suggested. For instance, other Si orientations could be examined, in single and double-side polished samples or the oxidant pressure dependence of the photonic enhancement measured. Laser

oxidation under steam conditions has only had preliminary attention so far.

Of considerable importance, both from an application and a scientific point of view, is the further electrical and chemical/physical characterization of the laser grown oxides, especially very thin oxides. A knowledge of the kinetics of formation/destruction of fixed oxide charges and interface states with oxide thickness and processing conditions would not only improve device reliability, but could also shed some light into the critical Si/SiO_2 interface region. In order to build up a complete picture, it would be very interesting to combine the results of such studies with those from other analytical techniques, such as X-ray photoelectron or infrared spectroscopy, spectroscopic ellipsometry and transmission electron microscopy.

From a technological point of view, we confirmed the feasibility of growing silicon dioxide films a few hundreds of Ångstroms thick with a visible laser as the sole source of energy. Our study successfully confirmed the presence of a photonic enhancement, albeit relatively small and limited to thin oxides. The process could, therefore, be successfully integrated in a complete laser processing system for microelectronics or optoelectronics applications, especially considering that the future trend is for oxides of thicknesses comparable to those for which an enhancement was measured. The growth model generated during this study is the only one available at present for Ar laser grown oxides.

Comparing our growth technique to the classical furnace oxidation we find that, for similar oxide characteristics and processing time, the reduction in processing temperature that the photonic enhancement would allow is quite small. Therefore, silicon oxidation with coherent <u>visible</u> radiation does not offer any particular advantage, unless high resolution oxide patterns are required. Our results, though, strengthen the interest in the very promising field of UV light (be it pulsed or CW, coherent or incoherent) oxidation of Si, where the high energy of the photons and the very high fluences obtainable (from excimer lasers) might open up new photochemical mechanisms. Work is currently being carried out at UCL on this subject [NAYAR et al., 1989, 1990].

APPENDIX I

SiO_2 bulk and interface properties

A brief overview of the oxide properties is necessary to understand the difficulties encountered when trying to model the oxidation process in the first few hundreds of Ångstroms. Particular emphasis will be towards the region near the interface with Si. This is indeed the most crucial area as far as silicon oxidation is concerned, as the oxide forms there. Clearly, the thinner the oxide the greater the relative significance of this transition region between c-Si and a-SiO_2.

The essential building block of all silica structures is the SiO_4 tetrahedron with a central Si atom and four O atoms at the corners. In SiO_2 these tetrahedra are linked by shared corners, i.e. each oxygen atom forms a bridge between two silicon atoms. Probably the most significant models proposed for vitreous silica are the continuous random network (CRN) first proposed by Zachariasen [ZACHARIASEN, 1932] and the microcrystalline model [RANDALL, 1930]. In the CRN model the Si-O-Si angle will vary from one tetrahedron corner to another within the range 120-180° (with a mean value of $\approx$ 144°). In the microcrystalline model, the SiO_2 is viewed as constructed from microcrystallites of the various forms of crystalline SiO_2. More recently Phillips [PHILLIPS, 1982] has suggested a structure made up of ß-cristobalite paracrystals of $\approx$ 66 Å in diameter, but this model has encountered considerable opposition [GALEENER, 1986].

A modified version of the CRN model assumes that the tetrahedra form interconnecting rings, thereby introducing some level of order. The rings consist of 8 to 3 tetrahedral units.

The structural, physical and chemical properties of the Si/SiO_2 interface region appear to be rather different from those of the bulk and have attracted a great deal of attention due to its enormous importance in the fabrication of MOS devices (for a comprehensive review see, for instance, [PANTELIDES et al., 1988]).

A considerable insight has been obtained in recent years due to the widespread availability of sophisticated analytical techniques; a rapid scan through the relevant literature confirms this point : high-resolution transmission (and reflection) electron microscopy (HRTEM and REM), scanning tunnelling microscopy (STM), low energy electron diffraction (LEED), high resolution energy loss spectroscopy (HREELS), positron annihilation, ellipsometry (single wavelength or spectroscopic), vibrational spectroscopy, Rutherford backscattering (RBS), X-ray scattering, field-ion microprobe, Auger spectroscopy, X-ray and UV photoelectron spectroscopy (XPS and UPS), core-level spectroscopy, tunnel deep level transient spectroscopy (TDLTS), ^{29}Si nuclear magnetic resonance (NMR), surface-extended X-ray absorption fine structure (SEXAFS), plus a variety of electrical techniques have all been used to probe different aspects of the very first few Å of oxide (one monolayer of oxide is ≈ 2.5 Å thick). The same literature scan would show that there is still considerable uncertainty in the knowledge of the details of this interfacial region and disagreement in the interpretation of often similar results.

The transition between c-Si and a-SiO_2 proceeds via a 'layer' of sub-stoichiometric oxide SiO_x ($x < 2$). Suggestions about the thickness of this interlayer have ranged between sub-monolayer to tens of Ångstroms over the years, made all the more difficult by the fact that the interface is possibly not flat due to the presence of steps and kinks and Si protrusions. Limiting our interest to recent estimates, most researchers seem to agree on thicknesses between 3÷5 Å and a maximum of 7±2 Å [ASPNES et al., 1980; TAFT et al., 1979; GRUNTHANER et al., 1986; BRAUN et al. ,1987; HELMS, 1988; HIMPSEL et al., 1988; AOTO et al., 1988; CEREZO et al., 1986], though Halbritter [HALBRITTER, 1988] has suggested that at most one monolayer of sub-stoichiometric oxide is present and Yu et al. [YU et al., 1986] found an interlayer varying inversely with oxide overlayer thickness, with values ≈ 17 Å for 163 Å oxides; a widening of the interface (to ≤ 10 Å) could be introduced depending on cleaning procedures [NAKAZAWA et al., 1989].

Si^{3+}, Si^{2+}, Si^{1+} (Si bonded to 3, 2 or 1 oxygen atoms) have all been found in this region, in varying absolute and relative quantities, spatial distributions through the area and their dependence on oxide thickness and silicon orientation. Considerable

disagreement still exists on this subject.

Microroughness has been seen at the interface, possibly due to growth of protrusions caused by localized stress. Carim and Sinclair [CARIM et al., 1987] measured a maximum roughness of ≈ 14Å, decreasing subsequently with increasing oxide thickness, while Ravindra et al. [RAVINDRA et al., 1987] couldn't confirm any thickness variation but measured ≈ 10Å of crystalline silicon protruding into the SiO_2. Recent STM studies of oxidized silicon surfaces confirmed the existence of fine rippled corrugations with ≤ 10Å height [NIWA et al., 1989] or random pitting of the Si surface [KAISER et al., 1988]. The oxidation conditions should have a considerable influence over this phenomenon.

To complicate matters further, experimental evidence of a crystalline oxide at the Si/SiO_2 has been reported. Ourmazd et al. [OURMAZD et al., 1987] found ≈ 5 Å of trydimite (a crystalline version of SiO_2) at the interface with molecular beam epitaxy-deposited silicon. Fuoss et al. [FUOSS et al., 1988] observed microcrystalline phases at the SiO_2-Si<001> interface and the most likely assignment was thought to be α-crystobalite structures (another form of crystalline SiO_2). Rochet et al. [ROCHET et al., 1989] have reported the growth of microcrystals of a non standard phase in the initial stages of Si oxidation under very dry conditions.

After the sub-stoichiometric oxide, a layer of strained, denser, and somewhat 'altered' oxide exists, extending to ≈ 15-40Å at least, as suggested in various studies [HELMS et al., 1988; THIRY et al., 1985; GRUNTHANER et al., 1986; BRAUN et al., 1987; HALBRITTER et al., 1988; BOYD et al., 1987]; a region of up to ≈ 100Å of stressed oxide was found at the interface [FITCH et al., 1989]. From a growth kinetics point of view, this findings are in good agreement with the often mentioned 'blocking layer' [FARGEIX et al., 1983; TILLER, 1980] or 'reaction layer' [STONEHAM et al., 1987; MOTT et al., 1989]. A change in ring statistics near the interface was postulated [GRUNTHANER et al., 1986], favouring smaller rings (3 or 4 members). They also measured ≈ 0.8 eV reduction in the band gap of this strained layer (≈ 0.35 eV between SiO_2 conduction band and Fermi level). Recent studies showed that, for oxide films ≈ 50-200Å thick, the optical absorption below the absorption edge of fused quartz

depends on thickness and processing temperature [MIYATA et al., 1989].

The issue of energy barrier for tunnelling electrons and its variations with oxide thickness was examined by Dressendorfer and Barker [DRESSENDORFER et al., 1980]. In Fig AI.1 values reported in the literature (at the time of their study) are presented. Their results suggested that oxides down to ≈ 43Å can be characterized by the same barrier height as much thicker oxides, all grown in the same conditions. Later studies [HORIGUKI et al., 1985] found a significant decrease from thicknesses ≈ 31Å (a barrier drop of ≈ 1.5eV was measured for ≈ 15Å oxides).

Whether there is an effective drop in barrier height in the first few tens of Ångstroms of oxide or whether it is an effect due to the measuring technique or particular type of processing, it is not completely clear. Very close to the interface though (1 or 2 monolayers), the presence of the SiO_x layer is certainly going to alter somewhat the picture of the band structure, though exactly how much is not known (Fig AI.2 shows SiO_x absorption coefficient as a function of x).

Hydrogen and carbon contamination are quite difficult to avoid completely (sodium and aluminium contamination can probably be neglected if highest quality cleaning chemicals are used) and have been often observed in thermal oxides [REVESZ et al., 1979; THIRY et al., 1985; NIELSEN et al., 1989; OLSEN et al.,1989]. SiH levels of the order of $10^{14}cm^{-2}$ have been reported at the interface, where the majority of SiH is found [GRUNTHANER et al., 1986]. The presence of Si^{3+} at the interface has been correlated with SiH bonds [HATTORI et al., 1989]. This can alter the chemical reactivity of the interface as well as its electrical activity. According to Robertson [ROBERTSON, 1987], the SiH group produces a filled state just below the valence band edge and an empty one just below the conduction band edge and is probably both an electron and hole trap. A shift in the bands line-up between Si and SiO_2 due to changes in the net dipole moments at the oxide-silicon boundary was attributed to the presence of SiH bonds [GRUNTHANER et al., 1986]. Considerable uncertainty exists over the value of the net dipole at the interface as it is dependent on a variety on unknown quantities [MASSOUD, 1988; HATTORI et al., 1989].

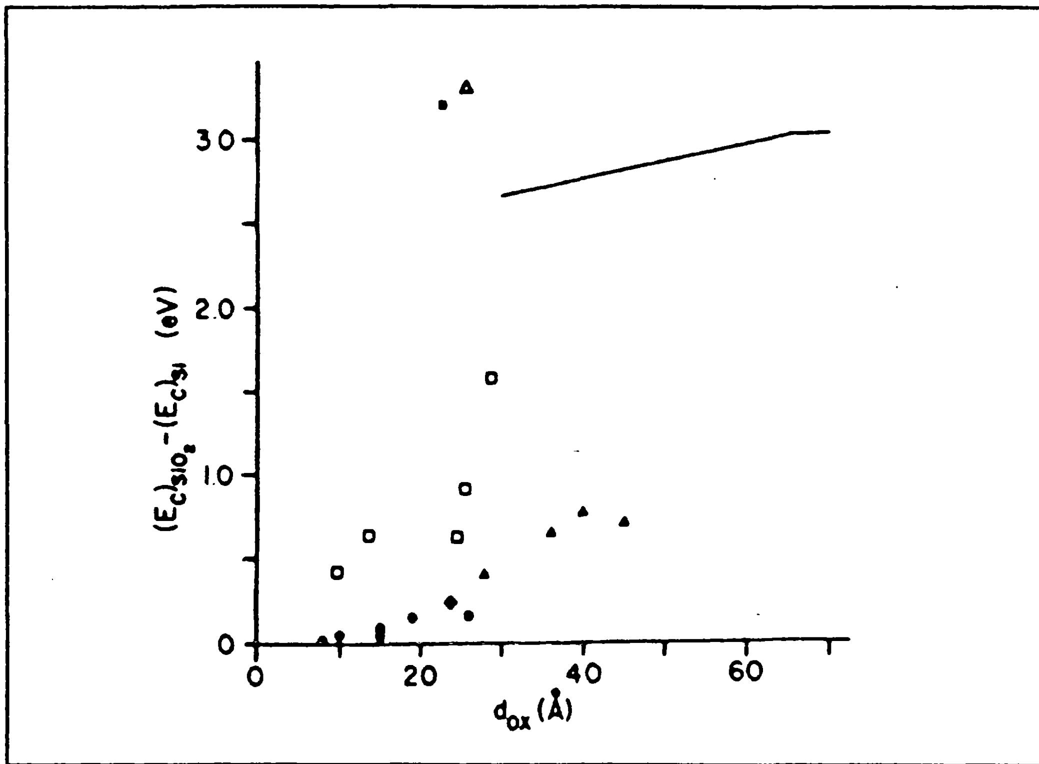

Fig AI.1: Plot of tunnelling barrier height as a function of oxide thickness [DRESSENDORFER et al., 1980].

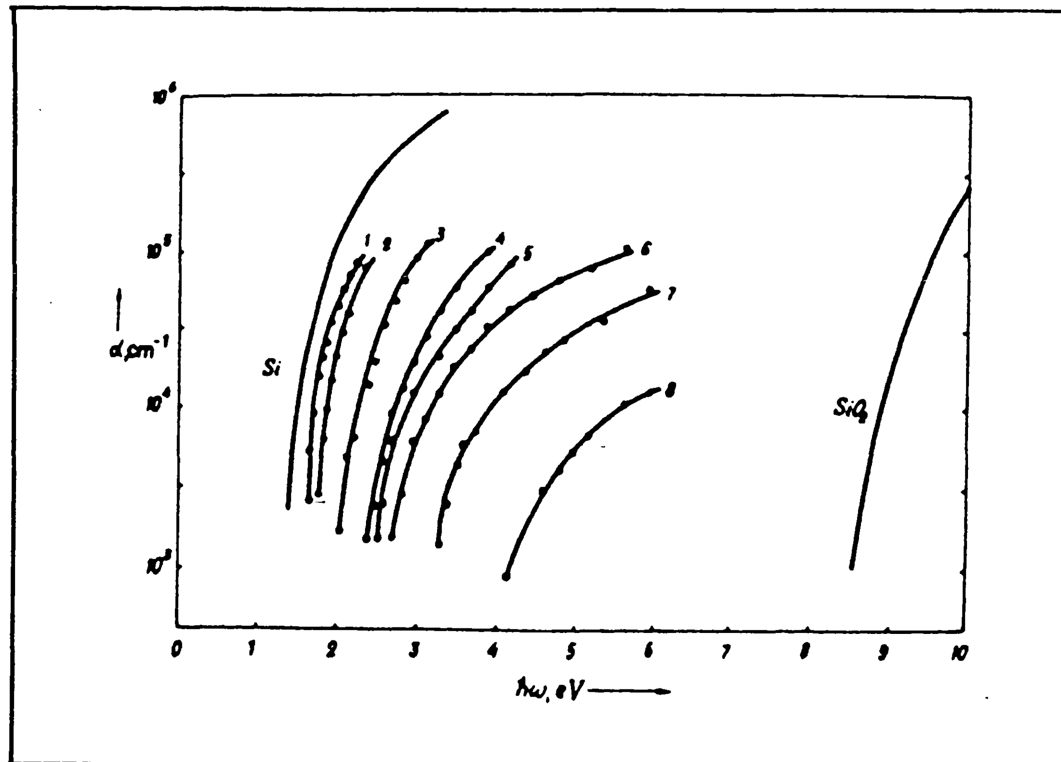

Fig AI.2: Spectral dependence of the absorption coefficient of SiO_x films for: (1) x=0.2; (2) x=0.5; (3) x=0.95; (4) x=1.2; (5) x=1.3; (6) x=1.37; (7) x=1.52; (8) x=1.7 [SHABALOV et al., 1987].

Apart from impurities, a-SiO_2 can have a variety of intrinsic defects, defined as sites of different co-ordination or like-atom bonds. Generally, such defects introduce states into the band gap. Electron spin resonance has suggested the presence of such defects as the nonbridging oxygen, oxygen vacancies and the peroxy bridge ≡Si-O-O-Si≡. Another important class of co-ordination defects, the valence alternation pairs (VAP), has not been directly observed yet, but theoretically inferred. The pair consists of a O_3^+ and a O_1^-, where the subscript is the co-ordination and the superscript the charge (O_3^+ can be seen as a derivative of a Si dangling bond and, hence, of an oxygen vacancy). From an experimental point of view, anomalous bonding configurations have been found at the SiO_2/Si interface [HOLLINGER et al., 1987]; excluding the possibility of a strained SiO_2 layer with smaller ring-statistics, the authors favoured the existence of threefold co-ordinated oxygen centres O_3^+, probably associated with another defect as in the VAP model. A recent experimental study [LAKHDARI et al., 1988] has shown the presence of electron trap states 3.1÷3.2eV below the SiO_2 CB at a depth of 17÷19Å from the Si/SiO_2 interface, with a density of ≈ $4x10^{16}cm^{-3}$ for device quality oxides. As a possible origin of these trap states, previous suggestions as Si-O-Si angle variations and O_3^+ were mentioned.

While referring to recent work [ROBERTSON, 1987; GRISCOM, 1987; POINDEXTER et al., 1988] for a detailed description of such a complex and still hotly debated issue, we show in Fig AI.3 suggested assignments for some of these defects' gap states.

The importance of these defects in the oxidant transport during silicon oxidation, especially in the thin regime, has been recently stressed [COLLOT et al., 1985; ROBERTSON, 1987; MOTT et al., 1989 and references therein] and though no clear definitive picture is yet available, it is now accepted that their presence cannot be ignored in any discussion on the mechanisms of silicon oxidation. Similarly, the presence of structural defects as 'micropores' in the oxide has been postulated as an alternative oxidant path in kinetical analyses and also experimentally verified (see par.I.4).

From an electrical point of view, the characteristics of MOS devices will be affected by charges and traps in the oxide and considerable experimental and theoretical effort has been spent in the understanding of their nature, origin and how to diminish them.

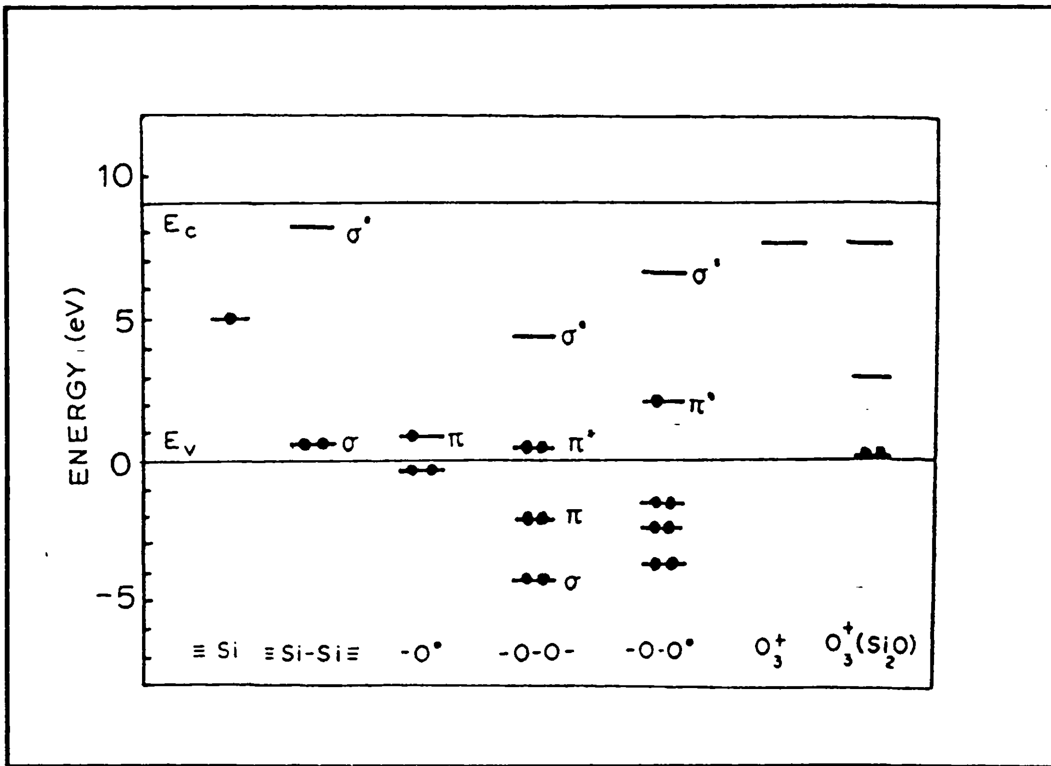

Fig AI.3: Gap states associated with various intrinsic centres [ROBERTSON, 1987].

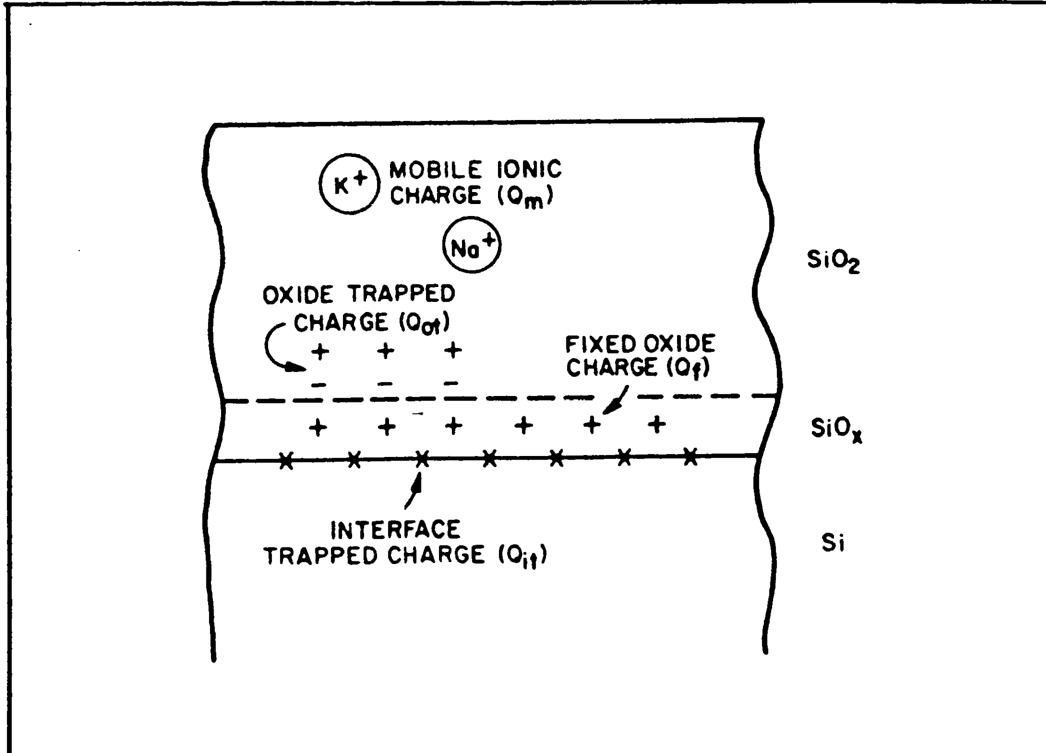

Fig AI.4: Charges in thermally oxidized silicon [SZE, 1988].

Various charges are known to be associated with thermally oxidized silicon and some of them are particularly concentrated in the region closest to the interface or at the interface itself. Fig AI.4 shows general types of charges usually found in the oxide [DEAL, 1980].

Interface trapped charges are localized spatially at the SiO_2/Si chemical interface and energetically within the Si band gap. The typical distribution of interface-trap density in the gap is U-shaped, with a bottom level (at mid-band gap) of the order of 10^{10}-10^{12} $cm^{-2}eV^{-1}$ (dependent on processing conditions and post-oxidation treatment), increasing towards the conduction and valence-band edges. Substantial differences exist between <100> and <111> Si [SZE, 1988] and thickness and doping dependence in the thin oxide regime has been recently demonstrated [KAR et al., 1987]. In particular, interface trap density increases considerably for oxide thicknesses below ≈ 300Å. These traps can exchange charges with the neighbouring valence and conduction band (the process being enhanced under illumination [KAR et al., 1987]).

The most widely accepted model for interface traps is probably a trivalently bonded Si atom at the Si/SiO_2 interface, denoted as $Si_3{\equiv}Si^*$ (where the * represents the fourth unpaired valence electron, or dangling bond). But a variety of other defect species have been suggested (see Reed and Plummer [REED et al., 1988] for an extensive study on the subject).

The fixed oxide charge Q_f (usually positive) is located within a few tens of Ångstroms of the Si/SiO_2 interface. It cannot be charged or discharged, its density does not seem to be greatly affected by oxide thickness or the type or concentration of impurities in Si, it depends on oxidation and annealing condition and ranges between $< 10^{10}$ and $> 10^{12} cm^{-2}$ [SZE, 1988]. It is always higher in <111> than in <100> Si.

Several qualitative models have been proposed to explain the origin of this fixed positive charge [for a comprehensive study and references see,for instance, [AKINWANDE et al., 1987]).

One group of models is based upon the idea of (incompletely oxidized) excess Si or Si interstitials (excess Si could also mean oxygen vacancy). It is known that silicon interstitials are generated at the interface during oxidation and recent studies have concluded that most of them flow back into the oxide where they react with the

incoming oxidant, thus completing the oxidation reaction [DUNHAM, 1989; TANIGUCHI et al., 1989]. Theoretical studies [HERMAN, 1981] suggested that they produce a level roughly midway in SiO_2 band gap, while Deal et al. [DEAL et al., 1967] considered a likely position (energetically speaking) somewhere between the Si CB and the SiO_2 CB.

Others have assumed the source of the charges to be in sub-oxides formed by SiO evaporation from the interface and diffusion within the first few tens of Ångstroms of oxide [RAIDER et al., 1978].

Another group of models is based upon the idea of lattice mismatch and strained bonds in the thin layer adjacent to the interface.

A third group associates the charges with the presence of surface roughness, ledges and kinks.

Akinwande and Plummer (see above) suggest a model based on a balance between a generation mechanism (kink generation) and an annihilation process (silicon-interstitial/kink recombination), similar in concept to the surface re-growth mechanism suggested by Hu [HU, 1974].

The bulk oxide trapped charge Q_{ot} can be positive or (more often) negative, due to holes or electrons trapped at defect sites or impurities. Densities vary between 10^9 and $10^{13} cm^{-2}$ [SZE, 1988].

APPENDIX II

Photo-enhancement and electronic effects

We will briefly review a few examples of photo-enhanced or photo-induced reactions where the photogenerated carriers have been considered to play an important role in the enhancement of the reaction rate.

Petro et al. [PETRO et al., 1982] studied the very initial stages of GaAs oxidation under 514nm Argon light and found an increase by a factor of 10^3 in the oxygen sticking probability. They suggested that the molecular oxygen dissociation might be enhanced with the increase in the number of electrons at, or near, the surface. Bartels and Mönch [BARTELS et al., 1984] added that the photo-stimulated uptake only occurs if the photon energy exceeds the GaAs band gap energy. Under the commonly accepted assumption that oxygen uptake on cleaved <110> GaAs at room temperature proceeds by two successive mechanisms, Mönch [MÖNCH, 1986] explained the photostimulation by:

a) the formation of O_2^- (due to the increased availability of electrons) with a lower dissociation energy than O_2;

b) a Cabrera-Mott type of field aided growth [see par.I.6].

The wavelength dependence of optically induced room temperature oxidation of <100> GaAs in the range 248-514nm was reported [YU et al., 1987]. The oxidation rates followed the order:

deep UV >> near UV > visible

and they attributed the effect to the generation of hot carriers (tentatively holes) at the semiconductor surface under UV light. These could play a role in weakening the substrate atoms at the surface, thereby stimulating the oxygen uptake. In a later paper, though, the same authors [YU et al., 1988] reviewed their suggestions in light of further experimental results. The wavelength dependent enhancement was confirmed, but found to be dependent on oxygen coverage. For a coverage above 0.5 to 1 monolayer the very marked deep UV enhancement ($\approx$ 4 eV), rapidly increasing with coverage, was attributed to the dissociation of O_2^- ($\approx$4.1 eV) with production of the very reactive atomic oxygen (in agreement with Mönch's suggestion). Below $\approx$ 0.5 monolayer of oxygen a different

photo-enhancement mechanism could prevail. Possibilities were presented, as the instantaneous dissociative chemisorption of physisorbed O_2 due to a) attachment of photogenerated electrons or b) energy released from surface recombination of photogenerated carriers, possibly in the form of non thermal phonons (in accordance with [BARTNESS et al., 1988 and references therein].

Most relevant to our study is the reaction of Si with halogenated gases under laser illumination.

Experiments have been carried out on Si-Cl_2 systems with pulsed and CW light, both in the visible and UV range [CHUANG, 1983; HORIIKE et al., 1987; KULLMER et al., 1988; and references therein]. The experiments demonstrated that etching at low laser powers requires both photogenerated carriers and chlorine radicals. The proposed etching model is a Cabrera-Mott type of field assisted mechanism. In this case, capture of a photogenerated electron by adsorbed Cl to form Cl^- assists field-driven diffusion into undoped and p-Si, thereby increasing the reaction rate (followed by desorption of volatile products). The high surface electric field is produced by the separation of photoelectrons and hole pairs which have different carrier mobilities. n-Si is not so strongly influenced by the photogenerated carrier density having a high Fermi level to start with.

Adsorbed fluorine atoms (from photo-dissociation of NF_3), having the largest electronegativity, can take valence electrons from Si surface atoms to become F^- and, as a results, they react spontaneously with Si atoms [HORIIKE et al., 1987].

Similar findings have also been reported for poly-Si etching [BALDI et al., 1986; HORIIKE et al., 1987]. Spontaneous etching by chlorine radicals of n^+-Si was noticed, in contrast to the p-type or undoped Si case which required photo-irradiation. This confirmed the requirement of a sufficient population of conduction band electrons.

But the photo-enhancement mechanism will not necessarily be the same for all silicon-halogen etching systems.

Photo-enhancement effects have been reported for the reaction between Si and XeF_2 under low intensity visible light irradiation [HOULE, 1983]. Two major light induced processes have been

identified: photogenerated charge carriers induce faster fluorine insertion rates into Si-Si bonds and enhance diffusion below surface. In a subsequent paper [HOULE, 1989] the role of photogenerated carriers has been clarified further: they appear to enhance the etch rate by inducing a surface process leading to stimulated desorption of surface SiF_3 groups. The nature of this surface process has been proposed to be a highly selective charge carrier-mediated chemical reaction. No evidence is instead found for a field-enhanced etch rate.

Experimental results on 350-647nm laser enhanced plasma etching of silicon [REKSTEN et al., 1986] were consistent with an etch rate controlled by the flux of photogenerated carriers at the semiconductor surface. At each laser intensity the photo-enhancement scaled with the magnitude of the dark etch rate, indicating that the light directly affects the reactions responsible for Si etching in the dark.

Following the early work of Kuhn-Kuhnenfeld [KUHN-KUHNENFELD, 1972], there have been a number of reports of electrochemical etching of binary and ternary III-V compound semiconductors (bulk and layered) where the etching process was assisted by the production of photogenerated minority carriers [HOFFMANN et al., 1981; OSTERMAYER et al., 1981; OSGOOD et al., 1982; TISONE et al., 1983; MOUTONNET, 1987; RUBERTO et al., 1989]. Field-assisted etching was used for p-GaAs etching [OSTERMAYER et al., 1981]. A wavelength dependence of the etching rate of GaAs which correlates strongly with the optical absorption coefficient was reported [TISONE et al. 1983].

Ashby [ASHBY, 1986 and references therein] found that also the dry etching of these semiconductors in chlorine environments, under appropriate conditions, can be greatly enhanced by laser irradiation. At low fluences, the process is dominated by the photo-generation of minority carriers. A high level of etching selectivity is then obtained by acting on the surface electronic properties of the material.

The interaction of CW laser radiation with NO adsorbed on GaAs <110> at low temperature has been studied over a wide range of wavelengths from 457 to 900nm [SO et al., 1988]. The observed

desorption and dissolution of NO have been attributed to interactions of the adsorbed NO with hot photogenerated carriers (holes, in this case) which succeed in migrating to the surface. A similar model was used to explain the photon induced desorption of NO from Si, where a peak enhancement occurred at a photon energy ≈ 3.37eV (Si first direct band gap) [YING et al., 1988].

Photogenerated carriers have been shown to initiate deposition of Cu and Ni films on oxidized Si wafers [KRAWCZYK et al., 1987]. Internal electron photo-emission at the Si-SiO_2 interface in the semiconductor-insulator-electrolyte system was used to initiate the chemical reaction at the insulator-electrolyte interface. There was a definite threshold for the reaction at 4.3eV, the Si/SiO_2 barrier height, indicating the direct involvement of Si valence band electrons.

Directly in our field of silicon oxidation, there are other examples of photonic interactions where the generations of carriers might have played a role. This is the case, for instance, of fluorine enhanced silicon oxidation under UV light [MORITA et al., 1986] or the evidence for Si-O bonds re-arrangement with 4.99 eV photons [FIORI, 1984; FIORI et al., 1984]. The use of very energetic photons, though, can introduce other photo-chemical processes which can overwhelm (or mask) any carrier effect and will be ignored in our study (as our energies are far below those used in these experiments).

In contrast to this body of experimental evidence, studies on IR, visible and near UV laser enhanced metal oxidation in the initial stages don't seem to indicate the presence of a photogenerated-carriers effect, consistently with the metal intrinsic high population of free electrons [URSU et al., 1986; ANDREW, 1986; MESARWI et al., 1989].

A study of other, less conventional, forms of silicon oxidation introduces further evidence of the important role that electrons (and their interaction with oxidant species) might play in the oxidation

process. Clearly, the mechanisms involved can be substantially different from each other (and our own) and it is certainly not possible to draw any direct conclusion.

The most obvious process under these circumstances is the electron beam oxidation of Si. Very low oxygen pressures and background temperatures in the range 25 to 700 °C have been generally used, together with a wide range of electron energies. The ionization of chemisorbed oxygen (O^+) and the surface trapping of the incoming electrons at oxygen chemisorption sites were proposed as the main effects of the electron beam [MUÑOZ et al., 1981]. The net positive surface charge would provide the field necessary for ionic motion; along with this, there is an electron tunnelling current in the same direction, according to a modified approach to Cabrera-Mott theory.

Collot et al. [COLLOT et al., 1985], using low energy beams, found a strong increase in the initial oxide growth rate when the electron energy decreased to 10eV. They proposed a mechanism of dissociative attachment of oxygen on the oxide surface (known to have a maximum cross section at electron energies ≈ 6.7eV), leading to the creation of adsorbed oxygen anions which induce a strong electric field in the oxide. Growth follows as a step-by-step motion of charged silica defects under constant electric field.

The dissociative attachment of oxygen as the principal effect of the electron beam was also favoured by Carrière et al. [CARRIERE et al., 1986], while a further indirect proof came from experiments [KUNZ et al., 1987] which proved that the highest oxide growth rate was achieved for impinging electrons beam of energy close to the secondary electron yield maximum. The energy distribution maximum of secondary electrons is around 3-5eV, sufficiently close to the dissociative electron attachment cross-section maximum, as previously seen. Independent experiments with similar initial electron energies supported this view [SUN et al., 1989].

Vinckier et al. [VINCKIER et al., 1987] studied the kinetics of SiO_2 growth in afterglows of microwaves induced plasmas (MIP). They proved the very important role of charged species in the overall plasma oxidation process. These species seem to be orders of magnitude more efficient than the ground state oxygen atoms present

in their MIP afterglows. Especially the role of negative ions, most probably O^-, has been stressed in a number of studies on plasma oxidation mechanisms [KIMURA et al., 1986; PERRIERE et al., 1984; HO et al., 1980; and references therein]. It has been suggested that the negative ions are formed at the plasma/SiO_2 interface through an electron capture process by adsorbed neutral radicals, while the formation of negative ions in the plasma itself seems to be unimportant [SIEJKA et al., 1985; KIMURA et al., 1988]. A study on ionic species responsible for the plasma anodization of Si confirmed again the major role of O^-, with a possible minor role for O_2^- [BARLOW et al., 1988]. The reaction of neutral oxygen with electrons at the surface was not discounted even in the presence of a bias.

A low energy O^- beam has also been used to oxidise silicon at room temperature [HECHT et al., 1989]. The initial reaction efficiency was found to be near unity and the process rapidly becomes self-limited by diffusion through the film. A similar experiment with a neutral atom beam would greatly help the understanding of the role of the electron population in oxidation kinetics.

In a recent extensive study of oxygen absorption on <111> Si [HÖFER et al., 1989], a metastable molecular state was found to precede dissociation and insertion of oxygen atoms in the Si network. This precursor has been characterized as a negatively charged molecular species, chemisorbed in a bridge configuration at the surface, possibly followed by a decay and conversion to a stable state by a thermally or electronically activated process.

A few examples of the room temperature interaction of oxygen with silicon surfaces covered by a non-annealed monolayer of a noble metal show that oxygen reacts with Si rather than metal and that the oxidation rate is strongly increased by the presence of this metal overlayer [CROS et al.,1981; ABBATI et al., 1982; MOLLER et al., 1987]. Cros relates this effect to the increased metallic character of the surface [CROS, 1983]: therefore the increased presence of electron states at the Fermi level (due to the presence of the disordered metal monolayer) may ease the breaking of the oxygen

molecule and/or the creation of atomic oxygen excited species.

'Metallization' of the Si surface by chemisorption of monolayers of alkali metals (Cs and Na) and establishment of a surface dipole capable of enhancing charge transfer and dissociation of molecular adsorbed oxygen, has been suggested as the explanation for the observed enhanced oxidation of Si with monolayer coverages of Cs or Na [FRANCIOSI et al., 1987 and references therein].

The role of electrons on the Si surface has been further substantiated by recent studies on the oxidation behaviour of a variety of metal silicides. The conclusions of an extensive comparative examination [IRENE et al., 1987 and references therein] show that the free carrier concentrations and the optical absorption index (related to this concentration) all display the same order as the oxidation rate.

REFERENCES

ABBATI, I., ROSSI, G., CALLIARI, L., BRAICOVICH, L., LINDAU, I., SPICER, W.E. : J. Vac. Sci. Technol. 21, 409 (1982).

The AIP Handbook, 3rd ed. (McGraw-Hill,NY,1973).

AKINWANDE,A.I., PLUMMER,J.D.: J.Electrochemical.Soc. 134,2565 (1987).

ALEXANDRESCU,R., MORJAN.J., GRIGORIU,C., MIHAILESCU,I., BASTL,Z., TLASKAL,J., MAYER,R., POLA,J. : Appl. Phys. A 46, 275 (1988).

ANDERS, H.: 'Thin Films in Optics', The Focal Press,London 1967.

ANDREW,R.: Proceedings of 1986 E-MRS Conference, ed., Les Editions de Physique, Les Ulis; Appl. Phys. B 41, 205 (1986).

AOTO, N., IKAWA, E., ENDO.N., KUROGI,Y. : Extended Abstracts of the 20th (1988 International) Conference on Solid State Devices and Materials, Tokyo, 487 (1988).

ASHBY,C.I.H. : J. Vac. Sci. Technol. A 4, 666 (1986).

ASPNES,D.E.,STUDNA,A.A.: Phys.Rev. B 27, 985 (1983).

ASPNES,D.E., THEETEN,J.B. : J. Electrochem. Soc. 127, 1359 (1980).

ATALLA,M.M.: 'Properties of Elemental and Compound Semiconductors', ed. H. Gatos,vol. V,Interscience,New York,(1960).

ATALLA,M.M., TANNENBAUM,E., SCHEIBNER,J. : Bell Sys. Tech. J. 38, 749 (1959).

ATKINSON,A.: Rev.Mod.Phys. 57,437 (1985);Phil.Mag.B 55,637 (1987).

BALDI,L., BEARDO,D., LANDI,E.: J. Electrochem. Soc. 133, 2202 (1986).

BARLOW, K.J., KIERMASZ, A., ECCLESTON, W., MORUZZI,J.L. : Appl. Phys. Lett. 53, 57 (1988).

BARTELS,F., MÖNCH,W. : Surf. Sci. 143, 315 (1984).

BÄUERLE,D.: Appl. Phys. B 46, 261 (1988); ibidem A 48, 527 (1989).

H.E.BENNETT, J.O.PORTEUS: J. Opt. Soc. Am. 51, 123 (1961).

BERTNESS,K.A., MAHOWALD,P.H., McCANTS,C.E., WAHI,A.K., KENDELELEWICZ, T., LINDAU,I., SPICER,W.E. : Appl. Phys. A. 47, 219 (1988).

BLANC,J. : Appl. Phys. Lett. 33, 424 (1978).

BOYD,I.W. : 'Laser Processing of Thin Films and Microstructures', Springer Verlag, Berlin (1987); Appl. Phys. Lett. 42, 728 (1983); Electronics Letters 24, 1062 (1988).

BOYD,I.W., MICHELI,F. : Elec. Letters 23, 298 (1987).

BOYD,I.W.,WILSON,J.I.B: J. Appl. Phys. 53, 4166 (1982); J. Appl. Phys. 62, 3195 (1987); Appl. Phys. Lett. 50, 320 (1987).

BRAREN,B., SRINIVASAN,R. : J. Vac. Sci. Technol. B 6, 537 (1988).

BRAUN,W., KUHLENBECK,H. : Surf. Sci. 180, 279 (1987).

CABRERA,N., MOTT,N.F.: Rept. Progress Phys. 12, 163 (1948).

CAMERA RODA,G., SANTARELLI,F., SARTI,G.C. : J. Electrochem. Soc. 132,1909 (1985).

CARIM,A.H., SINCLAIR,R. : J. Electrochem. Soc. 134, 741 (1986).

CARRIERE,B., DEVILLE,J.P., SEFSAF,B. : Proceedings E-MRS Meeting, Strasbourg (1986).

CARSLAW,H.S.,JAEGER,J.C.: "Conduction of Heat in Solids",(Oxford Clarendon Press), 1959.

CASEY,J.D., HAGGERTY,J.S. : J. Mat. Sci 22, 4307 (1987).

CAWLEY,J.D.,HALLORAN,J.W.,COOPER,A.R.: Oxid.of Metals 28,1 (1987).

CEREZO,A., GROVENOR,C.R.M., SMITH,G.D.W. : J. Appl. Micros. (Oxford) 141, 155 (1986).

CHANIN,L.M., PHELPS,A.V., BIONDI,M.A. : Phys. Rev. 128, 219 (1962).

CHUANG,T.J. : Surf. Sci. Rep. 3, 1 (1983).

CHOU,S.Y., CHANG,Y., WEINER,K.H., SIGMON,T.W., PARSONS,J.D. : Appl. Phys. Lett. 56, 530 (1990).

COHEN-TANNOUDJI,C., DIU,B., LALOE,F. : 'Quantum Mechanics' Vol.I, John Wiley & Sons, New York, 1977.

COLLOT,P., GAUTHERIN,G., AGIUS,B., RIGO,S., ROCHET,F. : Philos. Mag. B. 52, 1051 (1985).

COSTELLO,J.A., TRESSLER,R.E.: J.Electrochem.Soc. 131, 1944 (1984).

CRISTY,S.S., CONDON,J.B. : J. Electrochem. Soc. 128, 2170 (1981).

CROS,A. : J. Phisique. 44, 707 (1983).

DAS,G., WAHL,A.C., ZEMKE,W.T., STWALLEY,W.C.: J. Chem. Phys. 68, 4252 (1978).

DASH,W.C., NEWMANN,R.: Phys. Rev. 99, 1151 (1955).

DASGUPTA,S., JACKSON,H.E., BOYD,J.T.: J. Appl. Phys. 64, 2069 (1988).

DEAL,B.E.:J.Electrochem.Soc. 110,527 (1963);ibidem 125,576 (1978); IEEE Transactions ED-27, 606 (1980).

DEAL,B.E., GROVE,A.S. : J. Appl. Phys. 36, 3770 (1965).

DEAL,B.E., SKLAR,M., GROVE,A.S., SNOW,E.H. : J. Electrochem. Soc. 114, 226 (1967).

DE LARIOS,J.M., KAO,D.B., HELMS,C.R., DEAL,B.E.: Appl. Phys. Lett. 54, 715 (1989).

DIAL,J.E.,WONG,R.E.,FORDEMWALT,J.N.: J. Electrochem. Soc. 115, 327 (1968).

DILHAC,J.M.,GANIBAL,C.,CASTAN,T. : Appl.Phys.Lett. 55,2225 (1989).

DI_MARIA,D.J., FISCHETTI,M.V. : J. Appl. Phys. 64, 4683 (1988).

DOREMUS,R.H. : J. Phys. Chem. 80, 1773 (1976); Thin Solid Films 122, 191 (1984); J. Electrochem. Soc. 134, 2001 (1987); J. Appl. Phys. 66, 4441 (1989).

DOREMUS,R.H., SZEWCZYK A. : J. Mat. Sci. 22, 2887 (1987).

DRESSENDORFER,P.V., BARKER,R.C. : Appl. Phys. Lett. 36, 933 (1980).

DUNHAM,S.T. : J. Electrochem. Soc. 136, 250 (1989).

DZIEWIOR,J., SCHMID,W. : Appl. Phys. Lett. 31, 346 (1977).

EDWARDS,M.W.: in "Handbook of Optical Constants of Solids", Ed. E.D.PALIK (Academic Press,NY,1985).

EERNISSE,E.P. : Appl. Phys. Lett. 30, 290 (1977); Appl. Phys. Lett. 35, 8 (1979).

ELIZALDE,E., FRIGERIO,J.M., RIVORY,J.: Appl. Opt. 25, 4557 (1986).

EYETT,M., BÄUERLE,D., WERSING,W., LUBITZ,K., THOMANN,H. : Appl. Phys. A 40, 235 (1986).

FARGEIX,A.,GHIBAUDO,G.,KAMARINOS,G.: J.Appl.Phys. 54, 2878 (1983).

FARGEIX,A., GHIBAUDO,G. : J. Appl. Phys. 56, 589 (1984).

FEHLNER,F.P.: J. Electrochem. Soc. 119, 1723 (1970); ibidem 131, 1646 (1984).

FIORI,C. : Phys. Rev. Lett. 52, 2077 (1984).

FIORI,C., DEVINE,R.A.B. : Phys. Rev. B. 33, 2972 (1986).

FITCH,J.T.,LUCOVSKI,G.: in Proc. MRS Spring Meeting, eds. S.Wilson, E.Davies, MRS, Pittsburgh, 1988.

FITCH,J.T., LUCOVSKY,G., KOBEDA,E., IRENE,E.A.: J. Vac. Sci. Technol. B 7, 153 (1989).

FITCH,J.T., BJORKMAN,C.H., LUCOVSKY,G., POLLAK,F.H., YIN,X. : J. Vac. Sci. Technol. B 7, 775 (1989).

FOSSUM,J.G., MERTENS,R.P., LEE,D.S., NIJS,J.F.: Solid-State Electron. 26, 569 (1983).

FOULON,F., FOGARASSY,E., SLAOUI,A., FUCHS,C., UNAMUNO,S., SIFFERT,P.: Appl. Phys. A 45, 361 (1988).

FRANCIOSI,A., SOUKIASSIAN,P., PHILIP,P., CHANG,S., WALL,A., RAISANEN, A., TROULLIER,N. : Phys. Rev. B. 35, 910 (1987).

FROMHOLD,A.T.:'Theory of Metal Oxidation-Volume 1, Fundamentals', Defects in Crystall. Solids (North Holland,Amsterdam,1976), vol.9.

FROSCH,C.J., DERICK,L., J. Electrochem. Soc. 104, 547 (1957).

FUOSS,P.H., NORTON,L.J., BRENNAN,S., FISCHER-COLBRIE,A. : Phys. Rev. Lett. 60, 600 (1988).

GALE,M., LEHMANN,H., BRUNNER,H., FRICK,K. : Proc. SPIE, Hamburg 1988.

GALEENER,F.L., WRIGHT,A.C. : Solid State Commun. 57, 677 (1986).

GEYSELAERS, M.L., HAISMA, J., WIDDERSHOVEN, F.P., MICHIELSEN, T.M., READER, A.H. : Appl. Phys. Lett. 54, 1311 (1989).

GHEZ,R.J : J. Chem. Phys. 58, 1838 (1973).

GHEZ,R.J, van der MEULEN,Y.J.: J.Electrochem.Soc. 119,1100 (1972).

GHIBAUDO,G. : Phil. Mag. B 55, 147 (1987).

GIBSON,J.M., DONG,D.W. : J. Electrochem. Soc. 127, 2722 (1980).

GLUCK,N.S., SANKUR,H., GUNNING,W.J. : J. Vac. Sci. Technol. A 7, 2983 (1989).

GOODMAN,A.M, BREECE,J.M. : J. Electrochem. Soc. 117, 982 (1970).

GRISCOM,D.L. : 'The Physics and Technology of Amorphous SiO_2', ed. R.A.Devine, Plenum (New York, 1988).

GROS,A., DERRIEN,J., SALVAN,F. : Surf. Sci. 10, 471 (1981).

GROVE,A.S.: 'Physics and Technology of Semiconductor Devices', John Wiley & Sons, New York,1967, p.102.

GRUNTHANER,F.J., GRUNTHANER,P.J.: Material Sci. Reports. 1,69 (1986).

GRUNTHANER,P.J., HECHT,M.H., GRUNTHANER,F.J., JOHNSON,N.M. : J. Appl. Phys. 61, 629 (1987).

HAIGH,J., AYLETT,M.R. : Prog. Quant. Electr. 12, 1 (1988).

HALBITTER,J. : J. Mater. Res. 3, 506 (1988).

HAMASAKI,M. : Solid State Electronics. 25, 479 (1982).

HAN,C.J., HELMS,C.R. : J. Electrochem. Soc. 132, 516 (1985); ibidem 134, 1297 (1987); ibidem 135, 1824 (1988).

HANSEN,S.G., ROBITAILLE,T.E. : Appl. Phys. Lett. 52, 81 (1988).

HATTORI,T. : Extended Abstracts of the 20th Conf. on Solid State Devices and Materials, Tokyo, 479 (1988).

HATTORI,T., IGARASHI,T., OHI,M., YAMAGISHI,H. : Japan. J. Appl. Phys. 28, L1436 (1989).

HATTORI,T., TAKASE,K., YAMAGISHI,H., SUGINO,R., NARA,Y., ITO,T. :

Japan. Journal. Appl. Phys. 28, 296 (1989).

HAYES,W., STONEHAM,A.M.: 'Defects and Defect Processes in Nonmetallic Solids', J. Wiley & Sons, New York, 1985.

HECHT,M.H., ORIENT,O.J., CHUTJIAN,A., VASQUEZ,R.P.: Appl. Phys. Lett. 54, 421 (1989).

HELMS,C.R. : 'The Physics and Chemistry of SiO_2 and the Si-SiO_2 Interface', eds. C.R.Helms & B.E.Deal, Plenum Press, New York, 1988.

HELMS,C.R., de LARIOS,J. : Proceedings of the Electrochemical Society Meeting on SiO_2, Florida 1988.

HERAK,T.V., CHAU,T.T., THOMPSON,D.J., MEJIA,S.R., BUCHANAN,D.A., KAO,K.C. : J. Appl. Phys. 65, 2457 (1989) and references therein.

HERMAN,F. : 'Insulating Films on Semiconductors', eds. M.Schulz and G.Pensl, Springer-Verlag (New York, 1981).

HIMPSEL, F.J., McFEELY, F.R., TALEB-IBRAHIMI, A., YARMOFF, J.A., HOLLINGER, G. : Phys. Rev. B. 38, 6084 (1988).

HIROSE,M. : 'Photon, Beam & Plasma Assisted Processing', eds. I.W.Boyd, E.F.Krimmel, North Holland, Amsterdam 1988.

HO,C.P.,PLUMMER,J.D.: J. Electrochem. Soc. 126, 1516 & 1523 (1979).

HO,C.Y.,POWELL,R.W.,LILEY,P.E.: J. Phys. Chem. Ref. Data 3, Suppl.1, 587 (1974).

HO,V.Q., SUGANO,T. : IEEE Transactions ED-27, 1436 (1980).

HODGE,A., PICKERING,C., PIDDUCK,A., HARDEMAN,R. : Proc. E-MRS Symp.on RTP 52, 313 (1986).

HOFER,U., MORGEN,P., WURTH,W., UMBACH,E. : Phys. Rev. B. 40, 1130 (1989).

HOFFMANN,H.J., WOODALL,J.N., CHAPPELL,T.I. : Appl. Phys. Lett. 38,

564 (1981).

HOLLINGER,G., BERGIGNAT,E., CHERMETTE,H. : Philos. Mag. B. 55, 735 (1987).

HOPPER,M.A., CLARKE,R.A, YOUNG,L.: J. Electrochem. Soc. 122, 1216 (1975).

HORIGUCHI,S., YOSHINO,H. : J. Appl. Phys. 58, 1597 (1985).

HORIIKE,Y., HAYASAKA,N., SEKINE,M., ARIKADO,T., NAKASE,M., OKANO,H.: Appl. Phys. A 44, 313 (1987).

HOULE,F.A. : J. Phys. Chem. 79, 4237 (1983); Phys. Rev. B. 39, 10120 (1989).

HU,S.M. : J. Appl. Phys. 45, 1567 (1974); Appl. Phys. Lett. 42, 872 (1983); J. Appl. Phys. 55, 4095 (1984).

HULDT,L., NILSSON,N.G., SVANTESSON, K.G. : Appl. Phys. Lett. 35, 776 (1979).

IBRAHIM,M.M., BASHARA,N.M: J. Vac. Sci.& Technol. 9, 1259 (1972).

IRENE,E.A. : J.Electrochem.Soc. 125,1708 (1978); ibidem 129, 413 (1982); J.Appl.Phys. 54,5416 (1983); Phil.Mag. 55,131 (1987).

IRENE,E.A., DONG,D.W. : J. Electrochem. Soc. 125, 1146 (1978).

IRENE,E.A., GHEZ,R. : Appl. Surf. Sci. 30, 1 (1987).

IRENE,E.A., LEWIS,E.A. : Appl. Phys. Lett. 51, 767 (1987).

IRENE,E.A., MASSOUD,H.Z., TIERNEY,E. : J. Electrochem. Soc. 133, 1253 (1986).

IRENE,E.A., TIERNEY,E., ANGILELLO,J. : J. Electrochem. Soc. 129, 2594 (1982).

IRVINE,S.J., MULLIN,J.C. : J. Vac. Sci. Technol. A 5, 2100 (1987).

ISHIKAWA,Y., TAKAGI,Y., NAKAMICHI,I. : Japan. J. Appl. Phys. 28, L1453 (1989).

JELLISON,G.E.: in "Pulsed Laser Processing of Semiconductors", vol 23 of Semiconductors and Semimetals, Eds. R.F.WOOD, C.W.WHITE, R.T.YOUNG (Academic Press, NY, 1984), p.95.

JELLISON,G.E., MODINE,F.A.: Phys. Rev. B 27, 7466 (1983).

JORGENSEN,P.J.: J.Chem.Phys. 37,874 (1962); ibidem 49,1594 (1968).

KAISER,W.J., BELL,L.D., HECHT,M.H., GRUNTHANER,F.J. : J. Vac. Sci. Technol. 6, 519 (1988).

KAMIGAKI,Y., ITOH,Y. : J. Appl. Phys. 48, 2891 (1977).

KAR,S., TEWARI,M. : IEEE Transactions ED-34, 420 (1987).

KAR,S., NARASIMHAN,R.L. : J. Appl. Phys. 61, 5353 (1987).

KARAM,N., LIU,H., YOSHIDA,I., BEDAIR,S.M.: Appl. Phys. Lett. 53, 767 (1988).

KASSABOV,J., DIMITROV,D., GRUEVA,A. : Solid State Electron. 31, 49 (1988).

KIMURA,S., MURAKAMI,E., WARABISAKO,T., SUNAMI,H. : J. Electrochem. Soc. 135, 2009 (1988) and references therein.

KIMURA, S., MURAKAMI, E., MIYAKE, K., WARABISAKO, T., SUNAMI, H., TOKUYOMA, T. : J. Electrochem. Soc. 132, 1460 (1985).

KOBEDA,E., IRENE,E.A. : J. Vac. Sci. Technol. B 4, 720 (1986); ibidem B 5,15 (1987);ibidem B 6,574 (1988);ibidem B 7,153 (1989).

KRAWCZYK,S.K., KUMAR,S.N. : Appl. Phys. Lett. 50, 215 (1987).

KUHN-KUHNENFELD,F. : J. Electrochem. Soc. 119, 1063 (1972).

KULLMER,R., BÄUERLE,D.: Appl. Phys. A 43, 227 (1987).

KUNZ,R.R., MAYER,T.M. : J. Vac. Sci. Technol. B. 5, 427 (1987).

KUNZ,R.R., ROTHSCHILD,M., EHRLICH,D.J.: Appl. Phys. Lett. 54, 1631 (1989).

LAKHDARI,H., VUILLAUME,D., BOURGOIN,J.C. : Phys. Rev. B. 38, 13124 (1988).

LANDSBERGER,L.M., TILLER,W.A., : Proc. of Symp. on Si_3N_4 nd SiO_2 the Electrochem. Soc., eds. V.Kapoor and K.T.Hankins, vol. 87-10 (San Diego, 1987); Appl. Phys. Lett. 49, 143 (1986); Appl. Phys. Lett. 51, 1416 (1987).

LEROY,B. : Phil. Mag. B 55, 159 (1987).

LEWIS,E.A.,IRENE,E.A.: J. Electrochem. Soc. 134, 2332 (1987).

LIE,L.N.,RAZOUK,R.R.,DEAL,B.E.:J.Electrochem.Soc. 129,2898 (1982).

LIGENZA,J.R., SPITZER,W.G. : J. Phys. Chem. Solids 14, 131 (1960).

LORA—TAMAYO,A., DOMINGUEZ,E., LORA —TAMAYO,E., LLABRES,J. : Appl. Phys. 17, 79 (1978).

LOWNDES,D.H., GEOHEGAN,D.B., ERES,D., PENNYCOOK,S.J., MASHBURN, D.N., JELLISON,G.E. : Appl. Phys. Lett. 52, 1868 (1988).

LU,Y.Z., CHENG,Y.C. : J. Appl. Phys. 56, 1608 (1984).

LU,Y., TAKAI,M., NAGATOMO,S., NAMBA,S.: Appl.Phys. A 47,319 (1988).

LUCOVSKY,G., KIM,S.S., TSU,D.V., FOUNTAIN,G.G., MARKUNAS,R.J.: J. Vac. Sci. Technol. B 7, 861 (1989) and references therein.

LUCOVSKI,G.,MANITINI,M.,SRIVASTAVA,J.K.,IRENE,E.A.: J. Vac. Sci.& Technol. B5, 539 (1987).

LUKES,F.: J. Phys. Chem. Solids 11, 342 (1959).

MACK,L.M., REISMAN,A., BHATTACHARYA,P.K. : J. Electrochem. Soc. 136,

3433 (1989).

MAKI,P.A., EHRLICH,D.J. : Appl. Phys. Lett. 55, 91 (1989).

MASSEY,H. : 'Negative ions', Cambridge University Press, Cambridge, 1976.

MASSOUD,H.Z. : J. Appl. Phys. 63, 2000 (1988).

MASSOUD,H.Z., PLUMMER,J.D. : J. Appl. Phys. 62, 3416 (1987).

MASSOUD,H.Z., PLUMMER,J.D., IRENE,E.A. : J. Electrochem. Soc. 132, 1745 (1985); ibidem 132, 2685 (1985); ibidem 132, 2693 (1985).

McCRACKIN,F.L., PASSAGLIA,E., STROMBERG,R.R., STEINBERG,H.L.: J. of Res. of the Nat. Bur. of Standards 67A, 363 (1963).

McDANIEL,E.W. : 'Collision Phenomena in ionized gases', John Wiley & Sons, New York, 1964.

McGRUER,N.E., SINGH,R., WEISS,J.A., RAJKANAN,K. : J. Appl. Phys. 62, 3405 (1987).

MESARWI,A., IGNATIEV,A. : J. Vac. Sci. Technol. A7, 1754 (1989).

MICHELI,F., BOYD,I.W.: Opt.& Laser Technol. 18, 313 (1986);ibidem 19, 19 (1987); ibidem 19, 75 (1987); Appl. Phys. Lett. 51, 1149 (1987); Appl. Phys. A 47, 249 (1988).

MIKKELSEN,J.C., GALEENER,F.L., MOSBY,W.J. : Appl. Phys. Lett. 37, 712 (1980); ibidem 39, 402 (1981).

MILLER,L.S., A.J.WALDER, P.LINSELL, A.BLUNDELL: Thin Solid Films 156, 11 (1988).

MILLS,T.G., KROGER,F.A. : J. Electrochem. Soc. 120, 1582 (1972).

MIYATA,N., MORIKI,K., FUJISAWA,M., HIRAYAMA,M., MATSUKAWA,T.,HATTORI, T. : Japan. J. Appl. Phys. 28, 2072 (1989).

MODLIN,D.N., TILLER,W.A. : J. Electrochem. Soc. 132, 1659 (1985).

MOGYOROSI,P., PIGLMAYER,K., KULLMER,R., BÄUERLE,D.: Appl. Phys. A45,,293 (1988).

MOHARIR,S.S.,CHANDORKAR,A.N.,VASI,J.: J.Appl.Phys. 65,2172 (1989).

MOLLER,P.J., HE,J.W. : J. Vac. Sci. Technol. A. 5, 996 (1987).

MÖNCH,W. : Surf. Sci. 168, 577 (1986).

MORITA,M., ARITOME,S., TANAKA,T., HIROSE,M. : Appl. Phys. Lett. 49, 699 (1986).

MORITA,Y., NOGUCHI,T. : Japan. J. Appl. Phys. 28, 309 (1989).

MORITA,M, OHMI,T., HASEGAWA,M., KAWAKAMI,M., SUMA,K. : Appl. Phys. Lett. 55, 562 (1989).

MOSLEHI,M. : Appl. Phys. A 46, 255 (1988).

MOSLEHI,M., SHATAS,S., SARASWAT,K. : Appl.Phys.Lett. 47, 1353 (1985).

MOTT,N.F. : Proc. Royal Soc. Lond. A 376, 207 (1981); Phil. Mag. A 45, 323 (1982); Phil.Mag. B 55, 117 (1987); ibidem 56, 257 (1987).

MOTT,N.F., RIGO,S., ROCHET,F., STONEHAM,A.M. : Phil. Mag. B 60, 189 (1989).

MOUTONNET,D. : Appl. Phys. B 42, 221 (1987).

MUKAI,R., SASAKI,N., NAKANO,M. : IEEE EDL-8, 76 (1987).

MUÑOZ,M.C., SACEDóN,J.L. : J. Chem. Soc. 74, 4693 (1981).

MURALI,V., MURARKA,S.P. : J. Appl. Phys. 60, 2106 (1986).

MURRAY,P., CAREY,G.F. : J. Appl. Phys. 65, 3667 (1989).

NAITO,M., HOMMA,H., MOMMA,N.: Solid-State Electronics 29, 885 (1986).

NAKAZAWA,M., KAWASE,S., SEKIYAMA,H. : J. Appl. Phys. 65, 4014 (1989).

NAKAZAWA,M., NISHIOKA,Y., SEKIYAMA,H., KAWASE,S. : J. Appl. Phys. 65, 4019 (1989).

NAYAR,V., BOYD,I.W. : Chemtronics 4, 101 (1989).

NAYAR,V., BOYD,I.W., GOODALL,F.N., ARTHUR,G. : Appl. Surf. Sci. 36, 134 (1989).

NAYAR,V., PATEL,P., BOYD,I.W. : Elec. Lett. 26, 206 (1990).

NICOLLIAN,E.H., BREWS,J.R. : 'MOS (Metal Oxide Semiconductor) Physics and Technology', J.Wiley & Sons, New York, 1982.

NICOLLIAN,E.H., REISMAN,A. : J. Electron. Materials 17, 263 (1988).

NIELSEN,B., LYNN,K.G., WELCH,D.O., LEUNG,T.C., RUBLOFF,G.W. : Phys. Rev. B 40, 1434 (1989).

NIWA,M., IWASAKI,H. : Japan. J. Appl. Phys. 28, L2320 (1989).

NORTON,F.J. : Nature 191, 701 (1961).

OELLIG,E.M., MICHEL,E.G., ASENSIO,M.C., MIRANDA,R.: Appl. Phys. Lett. 50, 1660 (1987) and references therein.

OGALE,S.B., NAWATHEY,R. : J. Appl. Phys. 65, 1367 (1989).

OGALE,S.B., KOINCAR,V.N., JOSHI,S., GODBOLE,V.P., DATE,S.K., MITRA, A., VENKATESAN,T., WU,X.D. : Appl. Phys. Lett. 53, 1320 (1988).

OHLIDAL,I., NAVRATIL,K.: Thin Solid Films 156, 181 (1988).

OKABE,H. : 'Photochemistry of Small Molecules', John Wiley & Sons, New York, 1978.

OLSEN,J.E.,SHIMURA,F.S.: Appl. Phys. Lett. 53, 1934 (1988); J. Vac. Sci. Technol. A 7, 3275 (1989).

OPSAL,J., TAYLOR,M.W., SMITH,W.L., ROSENCWAIG,A. : J. Appl. Phys. 61, 240 (1987).

OREN,R., GHANDHI,S. : J. Appl. Phys. 42, 752 (1971).

ORLOWSKI,M., PLESS,V. : Appl. Phys. A 46, 67 (1988).

ORLOWSKI,T.E., RICHTER,H. : Appl. Phys. Lett. 45, 241 (1984).

OSGOOD,R.M., SANCHEZ-RUBIO,A., EHRLICH,D.J., DANEU,V. : Appl. Phys. Lett. 40, 391 (1982).

OSTERMAYER,F.W., KOHL,P.A. : Appl. Phys. Lett. 39, 76 (1981).

OURMAZD,A., TAYLOR,D.W., RENTSCHLER,J.A. : Phys. Rev. Lett. 59, 213 (1987).

PAI,P.G.,CHAO,S.S.,TAKAGI,Y.,LUCOVSKI,G.: J. Vac. Sci. & Technol. A4, 689 (1986).

PANKOVE,J.I. : 'Optical Processes in Semiconductor', Dover Publications, New York, 1971.

PANTELIDES,S.T., LUCOVSKY,G. (editors) : 'SiO_2 and its interfaces', MRS Symp. Proceedings vol.105 , Boston, 1988.

PASSARI,L., SUSI,E. : J. Appl. Phys. 54, 3935 (1983).

PAZ DE ARAUJO,C.A., GALLEGOS,R.W., HUANG,Y.P. : J. Electrochem. Soc. 136, 2673 (1989).

PERRIERE,J., SIEGKA,J., CHANG,R.P.H.: J. Appl. Phys. 56, 2716 (1984).

PETRO,W.G., HINO,I., EGLASH,S., LINDAU,I., SU,C.Y., SPICER,W.E.: J. Vac. Sci. Technol. 21, 405 (1982).

PFEFFER,R., OHRING,M. : J. Appl. Phys. 52, 777 (1981).

PHILIPP,H.R.: J. Appl. Phys. 43, 2835 (1972).

PHILLIPS,J.C. : J. Non-Crystal. Solids 63, 347 (1984).

PITZER,K.S. : J. Am. Chem. Soc. 70, 2140 (1948).

PLISKIN,W.A., GNALL,R.P. : J. Electrochem. Soc. 111, 872 (1964).

PLISKIN,W.A.,LEHMAN,H.S.: J. Electrochem. Soc. 112, 1013 (1965).

POINDEXTER,E., CAPLAN,P.J.: J. Vac. Sci. Technol. A 6, 1352 (1988).

PONPON,J., GROB.,J., GROB,A., STUCK,R.: J.Appl.Phys. 59, 3921 (1986).

QUENON,P., WAUTELET,M., DUMONT,M. : J. Appl. Phys. 61, 3112 (1987).

RAIDER,S.J., BERMAN,A. : J. Electrochem. Soc. 125, 629 (1978).

RALEIGH,O.D. : J. Electrochem. Soc. 113, 782 (1966).

RANDALL,J.T., ROOHSBY,H.P., COOPER,B.: Z. Kristallogr. 75,196 (1930).

RAVINDRA,N.M., NARYAN,J., FATHY,D., SRIVASTRAVA,J.K., IRENE,E.A. : J. Mater. Res. 2, 216 (1987).

RAZOUK,R.R., LIE,L.N., DEAL,B.E.: J.Electrochem.Soc. 128,2214 (1981).

REED,M.L., PLUMMER,J.D. : J.Appl. Phys. 63, 5776 (1988).

REISMAN,A., NICOLLIAN,E.H., WILLIAMS,C.K., MERZ,C.J. : J. Electron. Materials 16, 45 (1987).

REKSTEN,G.M., HOLBER,W., OSGOOD,R.M.: Appl.Phys.Lett. 48, 551 (1986).

REVESZ,A.G. : J. Electrochem. Soc. 126, 122 (1979).

REVESZ,A.G., EVANS,R.J. : J. Phys. Chem. Solids 30, 551 (1969).

REVESZ,A.G., MRSTIK,B.J., HUGHES,H.L., McCARTHY,D. : J. Electrochem. Soc. 133, 586 (1986).

REVESZ,A.G., MRSTIK,B.J., HUGHES,H.L. : J. Electrochem. Soc. 134,

2911 (1987).

ROBERTSON,J. : 'The Physics and Technology of Amorphous SiO_2', ed. R.A.Devine, Plenum (New York, 1988); Phil. Mag. B 55, 673 (1987).

ROCHET,F., AGIUS,B., RIGO,S. : J.Electrochem.Soc. 131, 914 (1984).

ROCHET,F., FROMENT,M., D'ANTERROCHES,C., ROULET,H., DUFOUR.G. : Philos. Mag. B. 59, 339 (1989).

ROCHET,F., RIGO,S. : Phil. Mag. B 55, 747 (1987).

ROCHET,F., RIGO,S., FROMENT,M., D'ANTERROCHES,C., MAILLOT,C., ROULET, H., DUFOUR,G. : Adv. Phys. 35, 237 (1986).

ROSENCHER,E., STRABONI,A., RIGO,S., AMSEL,G. : Appl. Phys. Lett. 34, 254 (1979).

RUBERTO,M.N., WILLNER,A.E., PODLESNIK,D.V., OSGOOD,R.M. :Appl. Phys. Lett. 55, 984 (1989).

RUZYLLO,J., DURANKO,G.T., HOFF,A.M.: J. Electrochem. Soc. 134, 2052 (1987).

SAMALAM,V. : Appl. Phys. Lett. 47, 736 (1985).

SAMESHIMA,T., TOMITA,H., USUI,S.: Japan. J. Appl. Phys.27, L1935 (1988).

SANKUR,H., CHEUNG,J.T. : Appl. Phys. A 47, 271 (1988).

SANKUR,H., GUNNINGW.J., DE NATALE,J., FLINTOFF,J.F. : J. Appl. Phys. 65, 2475 (1989).

SATO,T.: Japan. J. Appl. Phys. 6, 339 (1967).

SCHAFER,S.A., LYON,S.A. : J. Vac. Sci. Technol. 19, 494 (1981); ibidem 21, 422 (1982); Appl. Phys. Lett. 47, 154 (1985).

SCHIROKY,G.H.: J. Materials Science 22, 3595 (1987).

SERNELIUS,B.E. : Phys. Rev. B. 39, 10825 (1989).

SHABALOV,A.L., FELDMAN,M.S. : Thin Solid Films 151, 317 (1987).

SHIRAFUJI,J., MIYOSHI,S., AOKI,H.: Thin Solid Films 157, 105 (1988) and references therein.

SIEGKA,J., PERRIERE,J. : MRS (Boston) Symposium Proc. 38, 427 (1985).

SINGH,R. : J. Appl. Phys. 63, R59 (1988).

SINGH,R., McGRUER,N.E., RAJKANAN,K., WEISS,J.A.: J. Vac. Sci.Technol. A 6, 1480 (1988).

SIQUEIROS,J., REGALADO,L., MACHORRO,R.: Appl. Optics 27, 4260 (1988).

SO,S.K., HO,W. : Appl. Phys. A. 47, 213, (1988).

SPIESS,W., STRACK,H. : J. Vac. Sci. Technol. B7, 127 (1989).

SRIVASTAVA,J.K., PRASAD,M., WAGNER,J.B. : J. Electrochem. Soc. 132, 955 (1985).

SRIVASTAVA,J.K., IRENE,E.A. : J.Electrochem.Soc. 132, 2815 (1985).

SRIVASTAVA,J.K., WAGNER,J.B.: J.Electrochem.Soc. 131, 196C (1984).

STONEHAM,A.M., GROVENOR,C.R.M., CEREZO,A.: Phil.Mag. B 55,201 (1987).

STONEHAM,A.M., TASKER,P.W. : Phil. Mag. B 55, 237 (1987).

SU,J.C., MENG,Q.K., ALLEN,S.D.: J. Vac.Sci.&Technol. A 5,1480 (1987).

SUDARSAN,U., CODY,N., DOSLUOGLU,T., SOLANKI,R.: Appl. Phys. Lett. 55, 738 (1989).

SUN,D., YU,Z., LI,F., DU,Y., WANG,H. : Appl. Phys. A. 48, 567 (1989).

SUYAMA,S., OKAMOTO,A., SERIKAWA,T., TANIGAWA,H. : J. Appl. Phys. 62, 2360 (1987) and references therein.

SZE,S.M. : 'Physics of Semiconductor Devices', John Wiley & Sons, New York, 1981; (editor) : 'VLSI Technology', McGraw-Hill International (New York, 1988).

TAFT,E.A. : J. Electrochem. Soc. 125, 968 (1978); ibidem 127, 993 (1980); ibidem 131, 2460 (1984); ibidem 132, 2486 (1985); ibidem 134, 474 (1987).

TAFT,E., CORDES,L. : J. Electrochem. Soc. 126, 131 (1979).

TANIGUCHI,K., SHIBATA,Y., HAMAGUCHI,C.: J.Appl.Phys. 65, 2723 (1989).

TAYLOR,S., ECCLESTON,W., BARLOW,K.J.: J. Appl. Phys. 64, 6515 (1988) and references therein.

THIRY,P.A., LIEHR,M. PIREAUX,J.J., SPORKEN,R. CAUDANO,R., VIGNERON, J.P., LUCAS,A.A. : J. Vac. Sci. Technol. B3, 1118 (1985).

TILLER,W.A. : J. Electrochem. Soc. 127, 619 (1980); ibidem 127, 625 (1980); ibidem 128, 689 (1981); ibidem 130, 501 (1983).

TIMANS,P.J.,McMAHON,R.A.,AHMED,H.: Appl.Phys.Lett 53, 1844 (1988).

TISONE,G.C., JOHNSON,A.W. : Appl. Phys. Lett. 42, 530 (1983).

TODOROV,S.S., FOSSUM,E.R. : Appl. Phys. Lett. 52, 48 (1988).

TRIMAILLE,I., RIGO,S. : Proceedings INFOS 89, vol.8.

TUNG,N.C., CARATINI,Y. : Electron. Lett. 22, 694 (1986).

URSU,I., NANU,L., MIHAILESCU,I.N. : Appl. Phys. Lett. 49, 109 (1986) and references therein.

VAN DER MEULEN,Y.J. : J. Electrochem. Soc. 119, 530 (1972).

VAN DER MEULEN,Y.J., HIEN,N.C.: J. Opt. Soc. Am. 64, 804 (1974).

VIÑA,L., CARDONA,M. : Phys. Rev. B. 29, 6739 (1984).

VINCKIER,C., COECKELBERGHS,P., STEVENS,G., HEYNS,M., DE JAEGERE,S. : J. Appl. Phys. 62, 1450 (1987) and references therein.

VYAS,H.P., KIRCHNER,G.D., LEE,S.J. : J. Electrochem. Soc. 129, 1757 (1982).

WAGNER,C. : Z. Phys. Chem. B 21, 25 (1933).

WAGNER,J. : Solid-State Electronics 30, 1117 (1987).

WATKINS,G.D., CORBETT,J.W., McDONALD,R.S. : J. Appl. Phys. 53, 7097 (1982).

WEINBERG,Z.A. : Solid State Electronics 20, 11 (1977).

WEINBERG,Z.A., HARTSTEIN,A. :J. Appl. Phys. 54, 2517 (1983).

WILLANDER,M., GRIVICKAS,V. : in 'Properties of Silicon', emis Data Reviews series no. 4, INSPEC, IEE, London 1988 .

WILLIAMS,R. : Phys. Rev. 140, 569 (1985).

WOLTERS,D.R. : 'The Physics and Technology of Amorphous SiO_2', ed. R.Devine, Plenum Press (1988).

WOLTERS,D.R., ZEGERS-van DUYNHOVEN,A.T.A. : Phil. Mag. B 55, 669 (1987); J. Appl. Phys. 65, 5126 (1989); ibidem 65, 5134 (1989).

WONG,H., CHENG,Y.C. : J. Appl. Phys. 64, 893 (1988).

YING,Z., HO,W. : Phys. Rev. Lett. 60, 57 (1987).

YOUNG,E.M. : Appl. Phys. A 47, 259 (1988).

YOUNG,E.M., TILLER,W.A. : Appl. Phys. Lett. 42, 63 (1983); ibidem 50, 80 (1987); ibidem 50, 46 (1987); J. Appl. Phys. 62, 2086 (1987).

YU,C.F., SCHMIDT,M.T., PODELESNIK,D.V., OSGOOD,R.M. : J. Vac. Sci. Technol. 5, 1087 (1987).

YU,C.F., SCHMIDT,M.T., PODELESNIK,D.V., YANG,E.S., OSGOOD,R.M. : J. Vac. Sci. Technol. 6, 754 (1988).

YU,Y.Z., HUNG,K.K., CHENG,Y.C. : Extended Abstracts of the 18th Conference on Solid State Devices and Materials, Tokyo, 459 (1986).

ZACHARIASEN,W.H. : J. Am. Chem. Soc. 54, 3841 (1932).

ZOLLER,A., BOOS,M., HERRMANN,R., KLUG,W., LEHNERT,W.: Proc. SPIE, Hamburg, 1988.

LIST OF PUBLICATIONS

Articles:

MICHELI,F., BOYD,I.W.: 'Laser microfabrication of thin films: Part one', Optics and Laser Technol. 18, 313 (1986); ''Laser microfabrication of thin films: Part two', ibidem 19,19 (1987); 'Laser microfabrication of thin films: Part three', ibidem 19, 75 (1987).

BOYD,I.W., MICHELI,F. : 'Wavelength dependence of optical oxidation of silicon', Electron. Lett. 23, 298 (1987).

MICHELI,F., BOYD,I.W. : 'Photon-controlled oxidation of silicon', Appl. Phys. Lett. 51, 1149 (1987).

MICHELI,F., BOYD,I.W. : 'In-situ monitoring of laser-induced silicon oxidation', Appl. Phys. A 47, 249 (1988).

BOYD,I.W., NOLAN,A.J., NAYAR,V., MICHELI,F., OVERBURY,A., DAVIDSON, A., SWANSON,G., GEORGE,S.: 'Laser repair of faulty packaged VLSI chips', Electron. Lett. 24, 1474 (1988).

Conferences and Seminars where I have presented the work:

MICHELI,F., BOYD,I.W.: 'Mechanisms of photon enhanced oxidation of Si', IEE Colloquium on Laser Processing of Materials, London 1986.

MICHELI,F., BOYD,I.W. : 'Wavelength dependence to the photon-initiated silicon-oxygen reaction', Secon Photochemical Processing Workshop (BACG), Oxford 1987.

MICHELI,F., BOYD,I.W. : 'Growth and structure of argon laser grown SiO_2', Proc. of Symp. on the The Physics and Technology of Amorphous SiO_2, Les Arcs, France, 1987 (ed. R.A.B.Devine, Plenum Press, New York, 1988).